

KIT SCIENTIFIC REPORTS 7655

# Annual Report 2012

Institute for Nuclear Waste Disposal  
Institut für Nukleare Entsorgung

H. Geckeis, M. Altmaier, P. Kaden (eds.)



H. Geckeis, M. Altmaier, P. Kaden (eds.)

## **Annual Report 2012**

Institute for Nuclear Waste Disposal  
Institut für Nukleare Entsorgung

### **Cover illustration**

*left:* Detail of a spent nuclear fuel pellet showing radial cracks and the adjacent Zircaloy cladding.

*middle:* Quantum chemical calculation of the incorporation of selenite into the calcite (104) surface.

*right:* SEM image of  $Y(OH)_3$  nanoparticles precipitated on a calcite cleavage surface.

Karlsruhe Institute of Technology  
**KIT SCIENTIFIC REPORTS 7655**

# Annual Report 2012

Institute for Nuclear Waste Disposal  
Institut für Nukleare Entsorgung

by  
H. Geckeis, M. Altmaier, P. Kaden (eds.)

## Report-Nr. KIT-SR 7655

The Institute for Nuclear Waste Disposal, INE, (Institut für Nukleare Entsorgung) belongs to the KIT Energy Center. The KIT Energy Center with its 1100 employees is one of the largest energy research centers in Europe. It bundles the energy research activities of the KIT, the merger of the former Forschungszentrum Karlsruhe and Universität Karlsruhe and reknown cooperation partners. By this, it crosses the lines between disciplines and combines fundamental and applied research in all relevant energies for industry, household, service and mobility. The involved institutes and research groups conduct the research work on their own authority. The joining of subjects, the interdisciplinary collaboration of scientists, and the common use of high-end devices and installations, develops a new quality of research and teaching. The KIT Energy Center develops solutions in energy technology from a single source and acts as a highly valuable consultancy institution for politics, business, and society in all questions of energy. (<http://www.energy.kit.edu/>)

### Impressum



Karlsruher Institut für Technologie (KIT)  
KIT Scientific Publishing  
Straße am Forum 2  
D-76131 Karlsruhe

KIT Scientific Publishing is a registered trademark of Karlsruhe Institute of Technology. Reprint using the book cover is not allowed.

[www.ksp.kit.edu](http://www.ksp.kit.edu)



*This document – excluding the cover – is licensed under the Creative Commons Attribution-Share Alike 3.0 DE License (CC BY-SA 3.0 DE): <http://creativecommons.org/licenses/by-sa/3.0/de/>*



*The cover page is licensed under the Creative Commons Attribution-No Derivatives 3.0 DE License (CC BY-ND 3.0 DE): <http://creativecommons.org/licenses/by-nd/3.0/de/>*

Print on Demand 2013

ISSN 1869-9669

## Table of contents

<b>1</b>	<b>Introduction to the Institute for Nuclear Waste Disposal (INE)</b> .....	<b>1</b>
<b>2</b>	<b>Highlights</b> .....	<b>5</b>
<b>3</b>	<b>Education and Training</b> .....	<b>7</b>
<b>4</b>	<b>National and international cooperation, conferences and workshops</b> .....	<b>9</b>
<b>5</b>	<b>Fundamental Studies: Process understanding on a molecular scale</b> .....	<b>15</b>
5.1	Chemistry and thermodynamics of actinides in aqueous solution.....	15
5.2	Sorption on Mineral Surfaces .....	22
5.3	Retention of radionuclides by secondary phase formation.....	31
<b>6</b>	<b>Applied studies: Radionuclide retention in the multi-barrier system</b> .....	<b>37</b>
6.1	Examination of highly radioactive waste forms.....	37
6.2	Non-heat producing waste forms and barrier materials .....	42
6.3	Colloid impact on radionuclide (RN) migration .....	47
6.4	Simulation of thermo hydro mechanic (THM) processes in the near-field of a HLW disposal in rock salt .....	52
6.5	Hydro-chemical modeling .....	54

<b>7</b>	<b>Separation of long-lived minor actinides.....</b>	<b>61</b>
<b>8</b>	<b>Vitrification of High-Level Radioactive Liquid Waste .....</b>	<b>67</b>
8.1	VPC Project.....	67
8.2	Structural investigations on the impact of increasing MoO <sub>3</sub> loadings in borosilicate glasses for the immobilization of Mo-rich nuclear wastes .....	73
<b>9</b>	<b>Development of actinide speciation methods .....</b>	<b>77</b>
9.1	R&D projects conducted at the INE-Beamline for Actinide Research at ANKA and at external SR sources .....	77
9.2	Laser spectroscopy.....	84
9.3	New instruments for surface analysis.....	88
9.4	NMR spectroscopy – first results from EURACT-NMR projects .....	92
9.5	Computational Chemistry .....	96
<b>10</b>	<b>Radiochemical and Elementary Analysis .....</b>	<b>103</b>
<b>11</b>	<b>Radiation Protection Research.....</b>	<b>109</b>
<b>12</b>	<b>Publications .....</b>	<b>115</b>

# 1 Introduction to the Institute for Nuclear Waste Disposal (INE)

The Institute for Nuclear Waste Disposal, **INE**, (Institut für Nukleare Entsorgung) at the Karlsruhe Institute of Technology **KIT** performs R&D focusing on

- (i) long term safety research for nuclear waste disposal,**
- (ii) immobilization of high level radioactive waste (HLW),**
- (iii) separation of minor actinides from HLW, and**
- (iv) radiation protection.**

All R&D activities of KIT-INE are integrated into the program Nuclear Safety Research within the KIT Energy Center. INE contributes to German provident research for the safety of nuclear waste disposal, which is the responsibility of the Federal Government.

Following the decision taken by Germany to phase out the use of nuclear energy, the safe disposal of long-lived nuclear waste remains as a key topic of highest priority. Projections based on scheduled operation times for nuclear power plants (Amendment to German Atomic Energy Act, August 2011) in Germany, indicate that about a total of 17,770 tons of spent nuclear fuel will be generated. About 6,670 tons have been shipped to France and the UK until 2005 for reprocessing, to recover plutonium and uranium. Consequently, two types of high level, heat producing radioactive waste have to be disposed of safely: spent fuel and vitrified high level waste from reprocessing (HLW glass). The disposal of low- and intermediate level waste present in much larger quantities likewise needs to be addressed.

Over the last decades, a consensus within the international scientific/technical community was established, clearly emphasizing that storage in deep geological formations is the safest way to dispose of high level, heat producing radioactive waste. Disposal concepts with strong inherent passive safety features ensure the effective protection of the population and the biosphere against radiation expo-

sure over very long periods of time. The isolation and immobilization of nuclear waste in a repository is ensured by the appropriate combination of redundant barriers (multi-barrier system).

**Long term safety research for nuclear waste disposal** at KIT-INE establishes geochemical expertise and models to be used in the disposal Safety Case, focusing primarily on the detailed scientific description of aquatic radionuclide chemistry in the geochemical environment of a repository. Work concentrates on the disposal of spent fuel and HLW-glass in the relevant potential host rock formations currently considered: rock salt, clays and crystalline rock formations. Actinides and long-lived fission products play a central role, as they dominate HLW radiotoxicity over long periods of time. Long-live anionic fission products are likewise investigated as significant long-term contributors to the maximum radiation dose projected for relevant scenarios.

Relevant long term scenarios for nuclear repositories in deep geological formations have to take into account possible radionuclide transport via the groundwater pathway. Thermomechanical studies are performed at INE, in order to describe the evolution of the constructed repository after closure. Possible groundwater intrusion into emplacement caverns is assumed to cause waste form corrosion and eventually radionuclide release. Radionuclide mobility is then determined by the various geochemical reactions in complex aquatic systems: i.e. dissolution of the nuclear waste form (HLW glass, spent fuel), radiolysis phenomena, redox reactions, complexation with inorganic and organic ligands, colloid formation, surface reactions at mineral surfaces, precipitation of solid phases and solid solutions.

Prediction and quantification of all these processes require fundamental thermodynamic data and comprehensive process understanding at the molecular scale. Radionuclide concentrations in relevant aqueous systems typi-

cally lie in the nano-molar range, which is exceedingly small in relation to main groundwater components. Quantification of chemical reactions occurring in these systems require the application and development of advanced sophisticated methods and experimental approaches, to provide insight into the chemical speciation of radionuclides at trace concentrations. Innovative laser and X-ray spectroscopic techniques are continuously developed and applied to this end. A specialized working group performing state-of-the-art theoretical quantum chemical calculations for actinide chemistry support both interpretation of experimental results and optimized experiment design.

The long-term safety of a nuclear waste repository must be demonstrated by application of modelling tools on real natural systems over geological time scales. Geochemical models and thermodynamic databases are developed at INE as basis for the description of radionuclide geochemical behaviour in complex natural aquatic systems. The prediction of radionuclide migration in the geosphere necessitates coupled modeling of geochemistry and transport. Transferability and applicability of model predictions are examined by designing dedicated laboratory experiments, field studies in underground laboratories and by studying natural analog systems. This strategy allows to identify and analyze key uncertainties and continuously optimize the developed models.

Within the R&D topic **immobilization of high level radioactive waste**, INE contributes to the decommissioning of nuclear facilities. The core process technology for the Vitrification Plant (VEK) on the site of the former Karlsruhe Reprocessing Plant (WAK; located at KIT Campus North) has been developed by INE. INE was involved in functional testing of process systems, as well as in the performance of the cold test operation and played a leading role in the highly successful hot operation of the VEK plant. The vitrification technology developed at INE is highly competitive on an international level. This is evidenced by the strong interest of countries like China or the Russian Federation in establishing technology transfer.

The Partitioning & Transmutation (P&T) strategy is pursued and developed in many international research programs. INE research activities in P&T are focused on the partitioning step, i.e. **separation of minor actinides from HLW**. The R&D aims to develop efficient separation processes for minor actinide for subsequent transmutation into short-lived or stable fission products. INE develops highly selective extracting agents and performs experiments to derive kinetic and thermodynamic data to assess and optimize extraction reactions. R&D spans experimental, analytical and theoretical work, dedicated to understanding extraction ligand selectivity on a molecular scale.

The R&D topic **radiation protection** at INE focuses on the assessment of radiation exposures of man by estimating doses either from external radiation fields or from incorporation of radionuclides. The strategy driving this work is to provide techniques and models for an individualized dosimetry, which goes beyond the current approach of applying reference models in dose assessments. Both the specific anatomical and physiological features of the exposed individual and the specific effective radiation fields are considered in the frame of an individualized dosimetry. Work is performed in close cooperation with the KIT safety management KSM.

**INE laboratories** are equipped with all necessary infrastructures to perform radionuclide/actinide research, including hot cells, alpha glove boxes, inert gas alpha glove boxes and radionuclide laboratories. State-of-the-art analytical instruments and methods are applied for analysis and speciation of radionuclides and radioactive materials. Advanced spectroscopic tools exist for the sensitive detection and analysis of radionuclides. Trace element and isotope analysis is made by instrumental analytical techniques such as X-ray fluorescence spectroscopy (XRF), atomic absorption spectroscopy (AAS), ICP-atomic emission spectroscopy (ICP-AES) and ICP-mass spectrometry (Quadrupole-ICP-MS and high resolution ICP-MS). Methods available for surface sensitive analysis and characterization of solid samples include X-ray diffraction (XRD), atomic force microscopy (AFM) and laser-

ablation coupled with ICP-MS. A modern X-ray photoelectron spectrometer (XPS) and an environmental scanning electron microscope (ESEM) are installed. INE has direct access to a TEM instrument on the KIT Campus North site (Institute of Applied Materials, IAM). Laser spectroscopic techniques are developed and applied for sensitive actinide and fission product speciation such as time-resolved laser fluorescence spectroscopy (TRLFS), laser photoacoustic spectroscopy (LPAS), laser-induced breakdown detection (LIBD) and Raman spectroscopy. A tuneable optical parametric oscillator (OPO) laser system with TRLFS-detection is used for high resolution spectroscopy at liquid helium temperature. Structural insight into actinide species is obtained by extended X-ray absorption fine structure (EXAFS) spectroscopy at the INE-Beamline at the Karlsruhe synchrotron source ANKA. The INE-Beamline, in the direct vicinity of INE hot laboratories and in combination with the other analytic methods, represents a world-wide unique experimental and analytic infrastructure, which both profits from and contributes to INE's leading expertise in the field of actinide chemistry and spectroscopy. Quantum chemical calculations

are performed on INE's computing cluster which is equipped with 17 nodes and 76 processors. A 400 MHz NMR spectrometer adapted to measuring radioactive liquid samples adds to the analytical and speciation portfolio of INE. Additional facilities at INE include a non-radioactive vitrification test facility (PVA) used to investigate and to simulate vitrification processes for hot plants. The INE CAD workstations enable construction and planning of hardware components, process layout and flow sheets. The institute workshop is equipped with modern machine tools to manufacture components for specific experimental and analytical devices in hot laboratories.

In 2012 the **Institute for Nuclear Waste Disposal** had **115 employees** working in the seven departments, which reflect the R & D and organizational tasks of the institute (Fig. 1): (i) safety of nuclear waste disposal, (ii) geochemistry, (iii) radiochemistry, (iv) actinide speciation, (v) vitrification of high level waste, (vi) radiation protection research and (vii) scientific/ technical coordination and analytical chemistry.

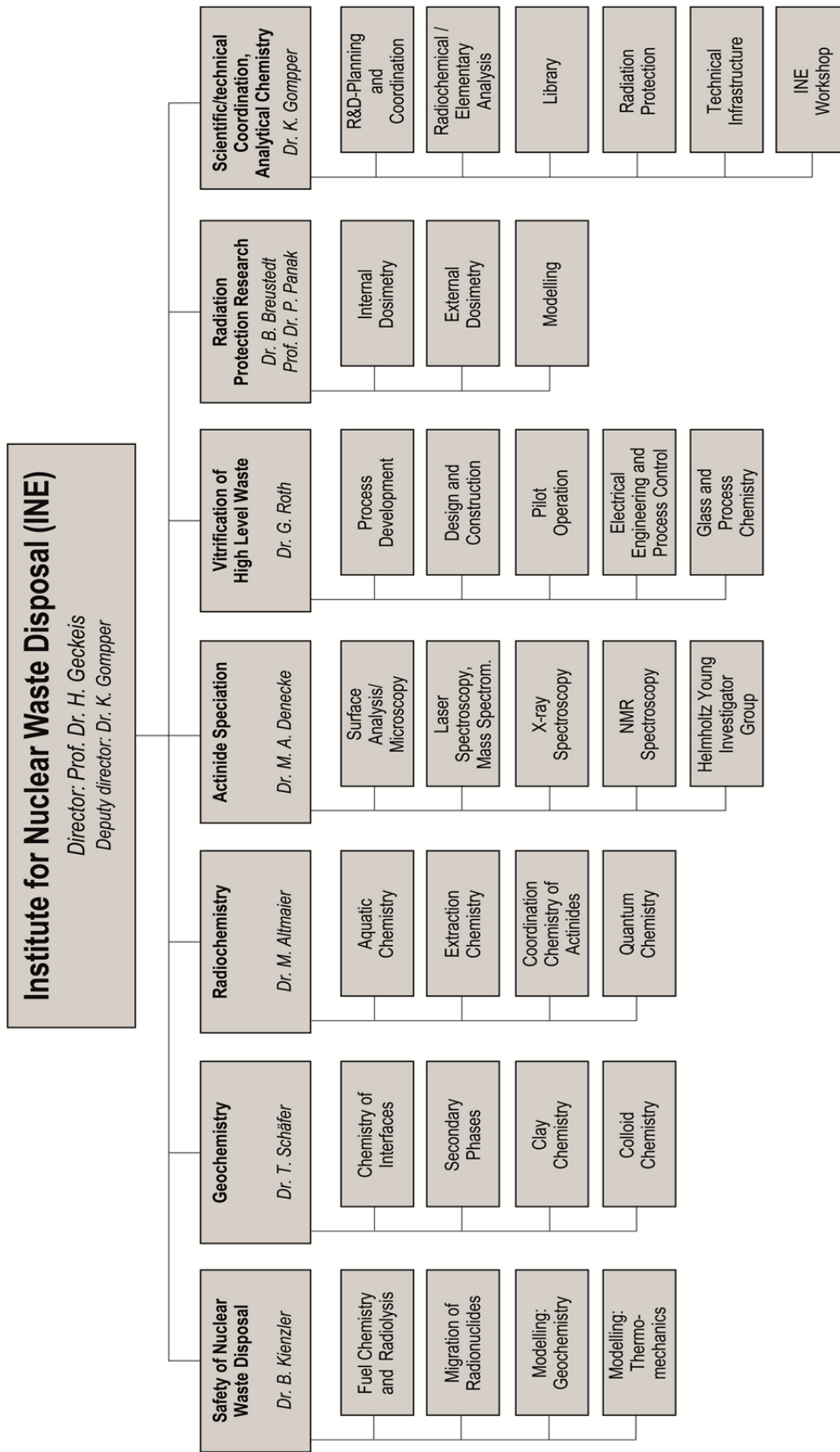


Fig. 1: Organisational chart of the Institute for Nuclear Waste Disposal (INE).

## 2 Highlights

The research and development activities (R&D) performed at INE are summarized in this report aiming to provide a representative overview of the scientific progress generated in 2012. Studies of particular interest and relevance are highlighted in the following, also exemplifying the experimental and conceptual approach adopted by INE.

INE researchers were involved in a project funded by the German Federal Ministry for the Environment (BMU) to perform a **Preliminary Safety Assessment for Gorleben** (Vorläufige Sicherheitsanalyse Gorleben, **VSG**). INE derived radionuclide source terms for specific waste forms and evolution scenarios. In 2012, work has focused upon several different waste forms with negligible heat generation (Chapter 6.2). Based upon analysis of the expected geochemical conditions, solubility limits were determined for relevant radionuclides. Following a generic scientific approach and using present state-of-art science, methodology and data, a robust approach to determine radionuclide source terms was established which is also applicable to other potential repository sites and geochemical conditions. INE has further analyzed and systematized specific features, events and processes (FEPs), thus contributing to the FEP catalog derived within VSG. The Preliminary Safety Assessment for Gorleben has highlighted the need for coupling fundamental scientific research and application oriented studies for the step-wise development of a future nuclear waste disposal safety case.

In order to improve understanding of basic actinide chemistry and solubility phenomena, **studies on actinide-borate interactions** were performed (Chapter 5.1). The studies were based upon systematic solubility experiments in combination with complementary analytical techniques available at INE (TRLFS, NMR, XRD, XPS). Experimental evidence shows that actinide(III)-borate complexation reactions are rather weak and do not significantly enhance An(III) solubility. Moreover, solubility studies show a pronounced solubility decrease under

certain experimental conditions related to a transformation of the solid An(III)-oxyhydroxide phase into a less soluble An(III)-borate phase. This mechanism constitutes a potential new actinide retention process not considered before. The comprehensive studies are partly performed in cooperation with HZDR and the Los Alamos National Laboratories, Carlsbad Office (USA).

Detailed investigation of radionuclide retention processes on mineral surfaces has been a continued focus of INE research activities and the international scientific community. As a large variety of minerals, surfaces and radionuclides have been investigated in dilute groundwater conditions both from an applied and fundamental perspective, no systematic studies have been performed at high ionic strength systems. In order to establish adequate process understanding, comprehensive investigations to assess **trivalent actinide and lanthanide sorption on clay minerals under saline conditions** were conducted (Chapter 5.2). Experiments were performed under systematic variation of ionic strength, also extending to near saturated NaCl, MgCl<sub>2</sub> and CaCl<sub>2</sub> solutions. Using batch sorption experiments and TRLFS spectroscopy it is clearly demonstrated that clay minerals represent strong retardation barriers for trivalent metal ions even under highly saline conditions. Quantitative models valid from dilute solutions to salt brine systems are assessed based upon the thermodynamic Pitzer model.

The retention of anionic Se(IV) species by structural incorporation in mineral phases and solid solution formation has been investigated (Chapter 5.3). Significant progress has been made by establishing a **thermodynamic entrapment model for the quantitative description of selenium(IV) coprecipitation with calcite**. The development of advanced chemical understanding and the subsequent thermodynamic analysis are based upon detailed experimental evidence and supported by **density functional theory (DFT) calculations** (Chapter 9.5). Selenite incorporation into the calcite

surface represents an intermediate reaction step in the incorporation process which is subsequently proceeding by adding consecutive crystal layers during solid solution growth.

Among the many important R&D projects conducted at the **INE-Beamline for Actinide Research at ANKA**, the studies using **High-temperature XAFS** (Chapter 9.1) are of particular interest in view of fundamental research activities at INE focusing on radionuclide chemistry at elevated temperature conditions. Combining TRLS and High-Temperature EXAFS using a custom build high temperature cell, the **complexation of Cm(III) and Am(III) with chloride in aqueous solution at 25 to 200°C** was investigated (Chapter 5.1). The tendency of An(III) towards chloride complexation is found to increase with increasing temperature, indicating that An(III)-chloride complexation may play an important role at elevated temperature conditions especially at high chloride concentrations. A thermodynamic description based upon the SIT model consistent with the NEA-TDB approach has been derived, yielding fundamental thermodynamic constants like complex formation constants,  $\Delta_r H_m^0$  and  $\Delta_r S_m^0$ .

INE's work program focusing on the **separation of long-lived minor actinides and lanthanides by liquid-liquid extraction** has been successfully continued (Chapter 7). The studies are well integrated into European research projects and cover both fundamental scientific questions related to liquid-liquid extraction processes and several more specific process related aspects. The **complexation of Cm(III) and Eu(III) with TODGA derivatives** was investigated using liquid-liquid extraction and TRLS techniques. Modified diglycolamide extracting agents were assessed, showing that the extraction efficiency for Am(III) and Eu(III) is TODGA > Me-TODGA > Me<sub>2</sub>-TODGA.

Time resolved laser fluorescence spectroscopy (TRLFS) is a powerful spectroscopic tool for studying the **coordination chemistry of f-ions (Cm(III) and Eu(III)) with aq-BTP molecules** (Chapter 9.2). In order to extract reliable quantitative information from fluorescence spectroscopy, establish the respective species

concentrations and derive reliable thermodynamic data, relative fluorescence intensity factors were derived. It is essential to account for the strong sensitization of the Cm(III) and Eu(III) luminescence due to distinct antenna effects of the extended aromatic ligand system. This work is of high relevance for spectroscopic studies of the coordination chemistry of f-ions with BTP type molecules.

The studies related to separation chemistry at INE were also supported by **<sup>1</sup>H, <sup>13</sup>C and <sup>31</sup>P NMR experiments**. Am(III) and Pu(IV) complexes with BTBP derivatives were analyzed, employing 1D and 2D NMR techniques (Chapter 9.4). The active NMR instrument installed in the INE controlled area is part of the "Karlsruhe Actinide NMR Centre of Excellence" and successfully integrated in the EURATOM FP7 funded EURACT-NMR transnational access project.

For the vitrification of High Level Waste, chemical mechanisms controlling the immobilization of particular waste components in the glass matrix were investigated. **Structural investigations on the impact of increasing MoO<sub>3</sub> loadings in borosilicate glasses for the immobilization of Mo-rich nuclear wastes** were performed at INE (Chapter 8.2). High resolution X-ray absorption near edge structure (HR-XANES) and magic angle spinning nuclear magnetic resonance (MAS NMR) techniques were applied to characterize glass network structure and molybdenum local atomic environment, respectively. Understanding the factors favoring or disfavoring the formation of soluble crystalline Mo(VI) phases in borosilicate glasses allows development of glass compositions capable of incorporating high Mo loadings.

The R&D performed at INE by young **PhD and Post-Doc researchers** at the highest international level is reflected by a total of **12 prizes awarded to young INE researcher in 2012**. The prizes include PhD awards from renowned scientific bodies, i.e. the Nuclear Chemistry Division of the German Chemical Society, as well as specific prizes for outstanding oral or poster presentations at leading national and international conferences.

### 3 Education and Training

Teaching of students and promotion of young scientists is of fundamental importance to ensure high level competence and to maintain a leading international position in the fields of nuclear and radiochemistry. INE scientists are strongly involved in teaching at KIT Campus South and the Universities of Heidelberg, Berlin, Jena and Mainz.

Prof. Dr. **Horst Geckeis**, director of INE, holds a professorship for radiochemistry at KIT Campus South, Department of Chemistry and Biosciences. He teaches fundamental and applied radiochemistry for chemistry students in bachelor, master and diploma courses. A radiochemistry module consisting of basic and advanced lectures on nuclear chemistry topics and laboratory courses has been set up for diploma and master students in Karlsruhe.

Prof. Dr. **Petra Panak**, heading a working group on actinide speciation at INE, holds a professorship of radiochemistry at the University of Heidelberg. A basic course in radiochemistry is offered for bachelor and/or master students. An advanced course comprised of chemistry of f-elements and medical applications of radionuclides is also offered. The advanced radiochemistry lectures are supplemented by scientific internships at the INE radioactive laboratories.

Nearly 35 students from Karlsruhe and Heidelberg participated in two 3-week radiochemistry laboratory courses in 2012 held at KIT-CN in the FTU radiochemistry and hot laboratories at INE. Some students are intensifying their knowledge in nuclear/radiochemistry topics during scientific internships at INE. Obviously students became interested in nuclear chemistry topics and appreciate the various semester courses.

Dr. **Andreas Bauer** is lecturing Clay Mineralogy at the University of Jena. His lecture deals with mineralogical characterization of these fine materials and the importance of quantifying surface reactions. In the second part of the lectures sound, practical advice on powder

X-ray diffraction in general is provided, as well as a useful set of step-by-step instructions for the novice.

Lectures and practical units taught by Dr. **Thorsten Schäfer** at the Freie Universität Berlin, Institute of Geological Sciences, Department of Earth Sciences, focused in 2012 on a master degree course on laboratory and field methods in hydrogeology, including performance and analysis of tracer tests using conservative, weakly sorbing tracers and colloids, pumping tests and determination of hydraulic parameters (Applied Hydrogeology III).

Dr. **Thorsten Stumpf** gave lectures at the KIT Campus South, Department Chemistry and Biosciences, in the field of chemistry of f-elements and inorganic chemistry. The seminar portion of the inorganic course was assisted by Dr. **Tonya Vitova**.

Dr. **Bastian Breustedt** gave a lecture on biokinetics of radionuclides and physiology and anatomy for engineers at KIT Campus South, Department Electrical Engineering and Information Technology.

Dr. **Frank Becker** gave lectures at the Baden-Wuerttemberg Cooperative State University (DHBW). The lectures comprised principles of statistics and measurements, atomic physics and nuclear physics.

#### **Others:**

- **Frank Heberling, Johannes Lützenkirchen** (INE), Phreeqc-Kurs, KIT, March 5-9, 2012
- **Volker Metz, Thorsten Schäfer** (INE) & Philipp Blum (KIT-AGW). Nukleare Tiefenlagerung, KIT, April 3-4, 2012
- **Bernd Schimmelpfennig, Robert Polly, Peter Kaden** (INE), Michael Patzscke (University of Helsinki), ACTINET-13: The ThUL School in Actinide Chemistry, KIT, April 26-30, 2012

- **Johannes Lützenkirchen** (INE),  
FIMIN – Workshop Modelling of surface reactions of ferric (hydr)oxides, Bayreuth, October 8-12, 2012

Through this close cooperation with universities, students are educated in the field of nuclear and actinide chemistry, which most universities can no longer offer. Hence, INE makes a vital contribution to the intermediate and long-perspective of maintaining nuclear science competence.

### **PhD-students**

In 2012 21 students worked at INE on their doctoral dissertations; seven of them were awarded their doctorate. Topics of the theses are:

- Simulation of the partial body dose during handling scenarios in inhomogeneous, time variant beta-/photon radiation fields
- Investigation of solubility and redox chemistry of Neptunium and Plutonium
- Complexation of partitioning relevant N-donor ligands – water soluble BTP ligands for the i-SANEX process
- Influence of pore clogging on the diffusion properties of porous media during geochemical perturbations: experiments and modeling
- Development of anthropomorphic models for in vivo measurements in radiation protection.
- Incorporation of elements with low solubility in alkaline borosilicate glasses for the immobilization of high-radioactive liquid waste
- Comparative NMR-Studies of extraction agents for the separation of trivalent actinides
- Interaction of human serum transferrin with actinides and lanthanides
- Structural study on Cm(III) and Eu(III) complexes with ligands relevant to partitioning
- Sorption of trivalent actinides on iron oxides
- Technetium mobility in natural systems, influence of ferrous iron speciation
- Technetium redox processes and Tc(IV) solubility studies in dilute to highly saline systems
- Redox-speciation of repository relevant and redox-sensitive elements in aqueous solutions by capillary electrophoresis coupled to ICP-MS
- Release and speciation of actinides by the fabrication and dissolution of Mo- and Zr-based nuclear fuel oxides
- Study of repository relevant carbon compounds and their influence on the <sup>14</sup>C- respectively actinide immobilization
- Investigation of the solubility and complexation of trivalent actinides: hydrolysis and complexation with organic ligands
- Influence of anions on the lanthanide/actinide interaction with mineral surfaces
- Characterization of actinide species in systems relevant for safety assessment of a nuclear waste repository by high-resolution X-ray emission/absorption spectroscopy
- Characterization of bonding differences by high-resolution X-ray emission and inelastic X-ray scattering techniques
- Description of radionuclide sorption at high ionic strength
- Effect of supersaturation index and precipitation kinetics on the incorporation of trivalent actinides/lanthanides in sulfate/carbonate minerals and CSH phases
- The effects of Porosity Clogging on Transport Properties of Porous Materials under Geochemical Perturbation
- Study on the complexation behaviour of actinides by ESI-MS

## 4 National and international cooperation, conferences and workshops

INE R&D involves numerous national and international cooperations and projects. These are described in the following.

### **National**

INE is involved in various bi- and multilateral cooperations with national research centers, universities and industrial partners on different topics. The projects are partly supported by the German Federal Ministry for Economics and Technology (BMWi), the Federal Ministry for Education and Research (BMBF), the Federal Ministry for the Environment, Nature Conservation and Nuclear Safety (BMU), the German Research Foundation (DFG) and the Helmholtz Association (HGF).

Primary goal within the collaborative project **VESPA** with partners GRS, HZDR-IRE and FZJ-IEF is to reduce the conservatism in the assumptions currently made in performance assessment calculations concerning the radionuclides  $^{14}\text{C}$ ,  $^{79}\text{Se}$ ,  $^{129}\text{I}$  and  $^{99}\text{Tc}$ . There is reasonable evidence that sorption values for radionuclides on organics, clay surfaces, layered double hydroxides or steel corrosion products are significantly higher than currently used in modeling approaches. This could, in “what if” scenarios, lead to significantly lower radionuclide release rates than currently predicted. The project VESPA focuses on the reduction of these uncertainties.

Within the **THEREDA** project, INE generates a centrally managed and administered database of evaluated thermodynamic parameters in cooperation with the Gesellschaft für Anlagen- und Reaktorsicherheit (GRS) mbH, Braunschweig, Helmholtzzentrum Dresden-Rossendorf, Institut für Ressourcenökologie (HZDR-IRE), Technische Universität Bergakademie Freiberg, Institut für Anorganische Chemie (TU-BAF) and AF-Colenco AG, Baden (Schweiz). Thermodynamic data are required for environmental applications in general and radiochemical issues in particular. This database is to be developed to a national (reference) standard and will be the basis for per-

formance assessment calculations for a national nuclear waste repository.

The **HATT** project focus is on the migration of radionuclides in natural clay formations and in bentonite, considered as technical barrier. Within this project not only the mechanism of radionuclide sorption onto clay is studied, but also the influence of organic matter naturally occurring in the clay stone on the radionuclide migration. Parallel to the characterization of clay organic compounds, the interaction of actinides with humic substances, kerogen-like compounds and small organic molecules are examined. Besides INE, the members of this collaborative project are GRS, HZDR-IRE, University of Mainz, University of Potsdam, University of Munich and University of Saarland.

The bilateral GRS-INE project **KOLLORADO-2** started mid-2009 as successor of the KOLLORADO project, focusing on the erosion stability of compacted bentonite barriers as a function of the contact water chemistry/hydraulics and the formation of near-field colloids/nanoparticles as potential carriers for actinides/radionuclides. Both a detailed experimental program investigating the influence of surface roughness/charge heterogeneity on nanoparticle mobility and actinide bentonite nanoparticle sorption reversibility, as well as approaches to implement the acquired process understanding in reactive transport modeling codes comprise the project activities.

In the BMBF/DFG funded joint research project **RECAWA** with partners from KIT (Institute of Reinforced Concrete Structure and Building Materials; KIT-IfMB, Institute of Mineralogy and Geochemistry; KIT-IMG), the University of Frankfurt (Institute of Geoscience, UniFaM-IfG) and industrial partners (Rheinkalk Akdolit, Lafarge Cement and Schäfer Kalk), basic understanding of processes with regard to the reactivity and dynamics of calcite mineral surfaces during crystal growth in aquatic systems are being developed. INE focuses on the immobilization of environmentally relevant ani-

onic trace elements (e.g., Se) on calcite surfaces using an integrated approach on the basis of batch sorption and co-precipitation experiments with molecular calculations and spectro-microscopic information.

The BMBF project funded in the framework of the funding concept „Basic research Energy 2020+“ entitled "**Grundlegende Untersuchungen zur Entwicklung und Optimierung von Prozessen zur Abtrennung langlebiger Radionuklide** (Partitioning)" continued in 2012. This is a cooperative project between KIT (both Campus North and South), Forschungszentrum Jülich and the Universities of Erlangen and Heidelberg and aims at understanding the differing reactivity between 4f and 5f elements with the ultimate goal of using this information to optimize their separation in partitioning.

The general aim of the BMWi Joint Project on the **Comparison of Constitutive Models III** is to check the ability of numerical models to describe correctly relevant deformation phenomena in rock salt under various influences, and thus increase confidence in numerical simulations and thereby enhance acceptance of results. Another aim is to identify possibilities for further model development and improvement.

In the BMBF-project **Radiation and Environment II**, INE is responsible for the work package "Efficiency calibration of *in-vivo* counters with anthropomorphic models adapted to individuals". In this work package, the influence of different anatomies on the calibration of *in-vivo* counters and subsequent dosimetry measurements are studied and quantified. By modifying the models, a better agreement between the geometries of measurement and calibration shall be reached. Different biometric parameters of the individual are measured and used in the adaption of the models.

The BMBF funded joint research project **ImmoRad** ("Fundamental investigations for the immobilization of long-lived radionuclides through interaction with secondary mineral phases in deep geological nuclear waste repositories" started in February 2012.

ImmoRad concentrates on application-based fundamental research on retention processes in deep geological environments. Within this project, structural incorporation/entrapment or formation of solid solutions of radionuclides into host minerals in aquatic environments is studied. National (KIT-INE, HZDR, University of Frankfurt) and international partners (PSI-LES; Switzerland and University of Oviedo; Spain) collaborate within this project.

The project "**Untersuchungen zum grundlegenden Verständnis der selektiven Komplexierung von f-Elementen (f-Kom)**" funded by the German Federal Ministry of Research and Education in the field of Basic Energy Research 2020+ aims at establishing a fundamental understanding of the separation of long-lived radionuclides from nuclear waste. The participating project partners from KIT-INE, KIT-CS, Universität Erlangen, Universität Heidelberg and Forschungszentrum Jülich are combining their expertise and activities in synthesis, spectroscopy, technology and theory, in order to be able to describe and ultimately predict and optimize liquid-liquid extraction processes for actinides at the molecular scale. The project includes a strong component of education and training of young scientists in research topics related to nuclear waste disposal and promotes their networking in the European research landscape.

In the framework of the **preliminary safety analysis for Gorleben (vSG)** radionuclide source terms were elaborated for high level waste glass, spent nuclear fuel, CSD-C wastes and for a variety of wastes with lower radionuclide inventories. However, some of these wastes represent significant volumes. The source terms comprise fuel elements from pilot and research reactors, reactor graphite wastes, structural materials, tails from uranium enrichment as well as cemented waste forms with negligible heat generation.

The Virtual Institute (VI) "**Advanced Solid-Aqueous Radio-Geochemistry**", supported by the HGF and coordinated by INE, began in March 2008. The work is focused on the elucidation of reaction mechanisms, which are re-

sponsible for the migration and/or retardation of radionuclides. The investigations cover a broad scale of complexity, from thorough study of model systems for solid solution formation (calcite, powellite), up to monitoring the complex interaction of cations and anions with cementitious material under repository conditions. Experimental work, modern spectroscopy and Monte Carlo simulations, as well as quantum mechanical calculations are performed to achieve a process understanding on a molecular level. Members of the VI are KIT, the Universities of Frankfurt (Germany) and Oviedo (Spain), the Research Center Jülich and the Paul Scherrer Institute (PSI) in Switzerland.

The Helmholtz young investigator group (HYIG) “**Advanced synchrotron-based systematic investigations of actinide (An) and lanthanide (Ln) systems to understand and predict their reactivity**” started July 2011 and will systematically investigate *in-situ* the electronic and coordination structure of actinides and chemical homologue lanthanide systems with novel synchrotron-based high resolution X-ray emission/inelastic scattering techniques. The experimental results are supported by theoretical calculations and simulations with quantum chemical codes. These investigations will improve our understanding of actinide/lanthanide reactivity in repository systems and waste matrices on a molecular scale and thereby support the reliability of evaluation of repository long-term safety. The elucidation of electronic and coordination structures of, e.g., actinide/lanthanide extraction ligand complexes will find application in optimization of separation technologies of lanthanide cations from minor actinides (partitioning), while at the same time provide basic insight into structure-reactivity relationships of actinide elements, which is a present scientific frontier.

### **International**

Two international projects focus on the stability of the bentonite buffer/backfill in contact with water conducting features and the influence of colloids on radionuclide migration in crystalline host rock: the Colloid Formation and Migration (**CFM**) experiment, coordinated by NAGRA (National Cooperative for the Disposal of Radioactive Waste, Switzerland), and

the Colloid Project, initiated by SKB (Swedish Nuclear Fuel and Waste Management Co., Sweden). Both projects are currently jointly working together using the experimental set-up at the Grimsel Test Site (Switzerland). Additional partners involved are from Japan (JAEA, AIST, CRIEPI), South Korea (KAERI), Finland (POSIVA Oy), Switzerland (NAGRA, PSI-LES), Spain (CIEMAT) and United States (LANL). INE plays a decisive role in the laboratory program of both projects and is also mainly carrying out the field activities.

### **EURATOM 7<sup>th</sup> Framework Program**

The Collaborative Project (CP) “Redox Controlling Systems” (**ReCosy**) started in April 2008. Main objectives of ReCosy are the sound understanding of redox phenomena controlling the long-term release/retention of radionuclides in nuclear waste disposal and providing tools to apply the results to performance assessment/safety case. The project is coordinated by INE, with Amphos 21 as the coordination secretariat and 32 institutions from 13 European countries contributing over the four-year duration of this CP. The international interest in ReCosy is large and organizations from Finland, Japan, Korea, UK and USA have signed associated group agreements.

An additional CP continued this year, namely “Cation diffusion in clayrocks” (**CatClay**), which began in June 2010. The aim of CatClay is to improve understanding of the phenomena governing migration of radionuclides in clayrocks as potential host rocks for the deep geological disposal of nuclear waste. The project focuses on the diffusion-driven transport of cationic species,  $\text{Sr}^{2+}$ ,  $\text{Zn}^{2+}$  and  $\text{Eu}^{3+}$ , which are more or less strongly sorbed on clay mineral surfaces. CatClay, coordinated by CEA, combines model and experimental developments from the partners ANDRA, BRGM, CEA, SCK-CEN, PSI-LES, Appelo Hydrochemical Consultant and KIT-INE.

The CP “Actinide Recycling by Separation and Transmutation” (**ACSEPT**) is dedicated to the development of actinide separation processes. It is a four year project (2008-2012) coordinated by CEA. KIT-INE leads the “hydrometallurgy” domain. The consortium consists of

34 members from Europe, Japan and Australia. ACSEPT is a continuation of previous FP4, FP5 and FP6 partitioning projects in which KIT-INE also participated.

INE continues to be a core member in **ACTINET-I3**, the follow-up project to the European "Network of Excellence for Actinide Sciences" (ACTINET-6, with EC FP6 and ended in 2008). ACTINET-I3 is an Integrated Infrastructure Initiative and commenced in January 2010. In contrast to the former ACTINET, the present consortium has only eight members. These are the leading European actinide laboratories: CEA, JRC-ITU and KIT-INE, as well as HZDR, PSI, CNRS, KTH and UNIMAN. The objectives of ACTINET-I3 are: (i) to establish and strengthen a network of actinide facilities across the EU and to foster their joint development in terms of capacity and performance; (ii) to support and manage jointly a program of access to appropriate infrastructures for training and associated research projects making use of the proposed facilities; (iii) to conduct on a limited scale a set of Joint Research Activities (JRA) involving consortium member organizations, with an objective to improve the performance of infrastructures by developing new relevant instrumentations and/or data of common interest; (iv) to provide open access to the actinide laboratories and the integrated beamlines for outside scientists to perform experimental work within well-defined joint research projects. Further, these activities are complemented by a virtual infrastructure, the Theoretical User Lab, providing support in theoretical and computational chemistry and modeling, with a focus on the complementarities between theory and experiment.

The **EURACT-NMR** project is a new 32 month coordination and support action starting February 2011 and is established to provide transnational access to the Karlsruhe Actinide NMR Centre of Excellence with state-of-the-art nuclear magnetic resonance facilities at the KIT-INE and JRC Institute for Transuranium Elements (ITU). These institutes have two 400 MHz NMR spectrometers, which have been adapted to allow advanced nuclear magnetic resonance experiments on radioac-

tive solid and liquid materials. The aim of EURACT-NMR is to open up unique and newly available actinide nuclear magnetic resonance facilities to nuclear researchers across Europe and EC associated countries. Additionally it will help to nurture nuclear magnetic resonance expertise and awareness amongst the European nuclear research community, in order to develop new experimental validation methods for complex models of the behavior in nuclear materials and processes.

Activities of the collaborative project **SKIN** (Slow processes in close-to-equilibrium conditions for radionuclides in water/solid systems of relevance to nuclear waste management) began upon its establishment in February 2011. Solid/liquid chemical equilibrium hypotheses (sorption, solubility, solid-solution formation) are key concepts in the assessment of nuclear waste safety. The project intends to assess the effect of surface properties on apparent solubility, as well as the kinetics of incorporation of radionuclides in the structure of a solid phase, and the associated reaction mechanisms for various solids in a systematic manner, using isotope exchange under close-to-equilibrium conditions.

The collaborative project **CROCK** (crystalline rock retention processes) aims at improving the safety case for crystalline rock far-field as a radionuclide migration barrier. Uncertainty and associated conservatism are the key problems in including radionuclide retention for improving safety prognoses. The overall CROCK objective is to develop a methodology for decreasing the uncertainty in the long-term prediction of the radionuclide migration in the crystalline rock far-field. Key aspects of radionuclide retention in this case are regarded, i.e. chemical processes and enhanced residence time in stagnant flow-system regions (matrix diffusion). The project started on January 1, 2011 and will last 30 months.

The **BOOSTER** project (BiO-dOSimetric Tools for triagE to Responders) addresses the requirement of effective management of an incident involving exposure of large numbers of people to radioactive material. BOOSTER is a capability project designed to research and

develop new bio-dosimetric tools, in order to quickly evaluate the level of potential casualties, determine by appropriate sensors their consequences, allow an efficient triage of exposed people, integrate a useful and usable toolbox, train civil protection operators and define commercial exploitation potentialities.

Within the EURATOM 7<sup>th</sup> FP, INE coordinates the Collaborative Project “Fast / Instant Release of Safety Relevant Radionuclides from Spent Nuclear Fuel (CP **FIRST-Nuclides**)”. The CP was started in January 2012. Quantification and understanding of the release mechanisms of gaseous and readily soluble radionuclides from high burn-up UO<sub>2</sub> fuel is investigated experimentally. Furthermore, models will be developed to predict the time-dependent mobilization of the different radionuclides on the fuel rod/fuel element scale as function of the time period between disposal and canister failure.

**ASGARD** (Advanced fuelS for Generation IV reActors: Reprocessing and Dissolution; 1/2012–12/2015) is a EURATOM FP7 Large Scale Integrated Project focusing on advanced/novel nuclear fuels fabrication and their respective reprocessing issues. ASGARD seeks integration between reactor, fuel and recycling communities, which today is lacking. In some cases this results in discrepancies between the reactor design on one hand, and the technological feasibility of fabricating, dissolving and reprocessing the selected fuel on the other hand. ASGARD is an integrated effort of 16 institutions from 9 European countries. It is coordinated by Chalmers Technical University.

Recent safety assessments of nuclear waste repositories in crystalline formations have shown that the formation and stability of colloids may have a direct impact on the overall performance of the repository. The main aim of the 7<sup>th</sup> framework collaborative project **BELBaR** is to increase the mechanistic understanding of the processes that control bentonite erosion, clay colloid stability, and ability to transport radionuclides. The final outcome is

to assess how colloids and related phenomena can be considered in the long-term safety case. Recommendations should be made on the quantitative and qualitative approaches that a safety case could pursue to adequately address this potentially very significant issue. BELBaR coordinated by SKB consists of a consortium of 14 partners from Sweden, Finland, Spain, Czech Republic, Great Britain, Russia and Germany with KIT-INE leading WP3 on “Colloid radionuclide & host rock interaction”.

**Conferences and workshops** INE has organized a series of workshops and conferences or has contributed significantly to the organization:

- **ReCosy 4<sup>th</sup> and final annual project workshop**, January 23-26, 2012 in Karlsruhe, Germany
- **Fast/Instant Release of Safety Relevant Radionuclides from Spent Nuclear Fuel (FIRST-Nuclides) - Kick-off meeting**, February 8-10, 2012 in Barcelona, Spain
- **Fourth Annual ACSEPT Meeting**, March 20-23, 2012 in Karlsruhe, Germany
- **Goldschmidt 2012** Conference, June 24-29, 2012 in Montréal, Canada, “**Interfacial geochemistry: From nano-scale processes to meso-scale results**”
- **Goldschmidt 2012** Conference, June, 24-29, 2012 in Montréal, Canada, Session 8c: “**Structural incorporation of heavy metals/radionuclides into mineral phases in aqueous environment**”
- **EUROSOIL 2012** Conference, July 2-6, 2012 in Bari, Italy, **Special session “Synchrotron radiation in soil science: applications and method development”**
- **Fast/Instant Release of Safety Relevant Radionuclides from Spent Nuclear Fuel (FIRST-Nuclides) - 1<sup>st</sup> Annual Workshop**, October 8-11, 2012 in Budapest, Hungary



## 5 Fundamental Studies: Process understanding on a molecular scale

The following section describes recent scientific advances in the field of fundamental radionuclide chemistry in aqueous solution relevant to nuclear waste disposal. A detailed understanding and reliable quantitative prediction of aqueous chemistry is relevant to assess the potential migration of actinides and long-lived fission products in the near- and far-field of a nuclear repository in deep geological formations. The investigated aqueous systems cover from dilute solutions to highly saline salt brine systems and establish essential site-independent data and process understanding.

Research activities at KIT-INE include the experimental investigation and systematic evaluation of radionuclide solubility and speciation, development of reliable chemical models and subsequent determination of consistent thermodynamic data. The studies reported in this section also include the contributions from highly successful research activities at KIT-INE investigating the interaction of radionuclides with mineral/water interfaces and the formation of radionuclide containing solid solution phases. Both topics are targeting the identification of radionuclide retention/retardation mechanisms on a molecular level and their robust thermodynamic quantification. The fundamental studies on aqueous radionuclide chemistry are strongly linked to the applied studies described in Chapter 6 on natural systems relevant for safety assessment.

### 5.1 Chemistry and thermodynamics of actinides in aqueous solution

*M. Altmaier, N. L. Banik, M. Böttle, K. Dardenne, D. Fellhauer, D. R. Fröhlich, X. Gaona, M. Herm, K. Hinz, T. Kobayashi<sup>a</sup>, P. Lindqvist-Reis, R. Marsac, P.J. Panak, J. Rothe, A. Skerencak-Frech, E. Yalcintas*

*In co-operation with:*

*C. Apostolidis<sup>b</sup>, Th. Fanghänel<sup>b,c</sup>, S. Kalmykov<sup>d</sup>, V. Petrov<sup>d</sup>, M. Skripkin<sup>e</sup>, O. Walter<sup>b</sup>*

*<sup>a</sup> Research Reactor Institute, Kyoto University, Osaka, Japan; <sup>b</sup> JRC-ITU, European Commission, Karlsruhe, Germany; <sup>c</sup> Heidelberg University, Heidelberg, Germany; <sup>d</sup> Moscow State University, Moscow, Russia; <sup>e</sup> St. Petersburg University, St. Petersburg, Russia*

#### Introduction

Fundamental research on the aquatic chemistry and thermodynamics of actinides and fission products is a challenging but rewarding research field with close links to the safe disposal of nuclear waste. Solubility and complexation studies provide the basis for the thermodynamic description of actinide systems, and further represent a key input for the estimation of the source term in performance assessment studies (PA) of repositories for radioactive waste disposal. Redox processes, effect of high ionic strength and influence of elevated temperatures on the chemistry of actinide and fission products were targeted in 2012 as main research activities within this field at KIT-INE.

The topics above were tackled with experimentally oriented investigations aiming at a

comprehensive thermodynamic description of actinide solubility and speciation. The direct access to advanced spectroscopic techniques available at KIT-INE (TRLFS, XAFS, LIBD, Raman, etc.) importantly contributes to the correct definition of chemical models, key milestone in the development of accurate thermodynamic and activity models. In the final step of this bottom-up approach, complete and consistent sets of thermodynamic data are published in peer reviewed journals and contributed to thermodynamic databases, e.g. THEREDA or NEA-TDB. Reflecting the expertise and commitment of KIT-INE in this field, the “Recent advances in aqueous actinide chemistry and thermodynamics” were summarized by M. Altmaier and co-workers for the special issue of Chemical Reviews dedicated to Nuclear Chemistry [1].

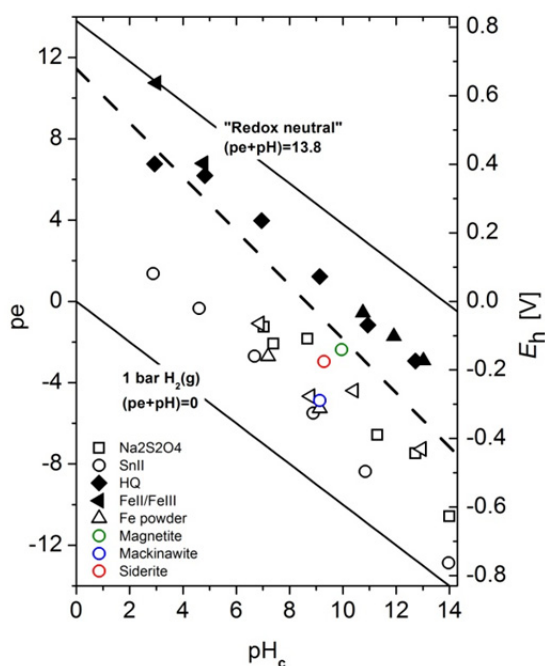


Fig. 1: Experimental data for the reduction of Tc(VII) at  $[TcO_4^-]_0 = 10^{-5}$  M in 5.0 M NaCl. Open symbols indicating reduction to Tc(IV); solid symbols corresponding to samples with no reduction of Tc(VII). Dashed line indicates the Tc(VII)/Tc(IV) borderline calculated according with the NEA–TDB [4].

### Redox chemistry and solubility of Tc in NaCl and MgCl<sub>2</sub> solutions

Technetium–99 is a  $\beta$ -emitting fission product highly relevant in the safety case for nuclear waste disposal due to its high yield in radioactive waste, long half-life ( $t_{1/2} \sim 211,000$  a) and redox sensitivity. An appropriate knowledge of the Tc(VII/IV) redox chemistry and Tc(IV) solubility in concentrated NaCl and MgCl<sub>2</sub> solutions is required in the context of nuclear waste disposal in rock-salt formations. This study continues the successful work on Tc redox chemistry in dilute systems initiated at KIT–INE in 2010 [2].

Redox experiments with Tc(VII) and  $[Tc]_0 = 10^{-5}$  M were conducted in dilute to concentrated NaCl (0.5 M–5.0 M) and MgCl<sub>2</sub> (0.25 M–4.5 M) solutions, in the presence of different reducing chemicals (Na<sub>2</sub>S<sub>2</sub>O<sub>4</sub>, SnCl<sub>2</sub>, hydroquinone (HQ), Fe(II)–Fe(III) and Fe powder). The reduction of Tc(VII) to Tc(IV) was followed by the decrease of Tc concentration in solution, and further confirmed by solvent extraction with TPPC in chloroform [3].

In the case of solubility experiments,  $\sim 200$  mg of Tc(VII) were electrochemically reduced to Tc(IV) in 1.0 M HCl, and precipitated as TcO<sub>2</sub>·xH<sub>2</sub>O at pH  $\sim 12$  in 5 mM Na<sub>2</sub>S<sub>2</sub>O<sub>4</sub>. The resulting solid was divided in two series of independent batch experiments ( $\sim 5$  mg Tc(IV) per sample) with NaCl 0.5 M and 5.0 M and  $4 \leq pH_c \leq 14$ . Reducing conditions were maintained with Na<sub>2</sub>S<sub>2</sub>O<sub>4</sub> or SnCl<sub>2</sub>. Tc concentration, pH<sub>c</sub> and  $E_h$  were monitored with time.

The reduction of Tc(VII) to Tc(IV) observed experimentally was in good agreement with thermodynamic predictions, represented by the borderline calculated according with the NEA–TDB [4] for the chemical reaction  $TcO_4^- + 4 H^+ + 3 e^- \rightleftharpoons TcO_2 \cdot xH_2O(s) + (2-x) H_2O$  (Fig. 1).

The reduction of Tc(VII) was found to be independent of the reducing system and could be properly characterized based on the pe+pH conditions of the experiment.

Preliminary Tc(IV) solubility data obtained in 0.5 M and 5.0 M NaCl revealed an increased solubility at  $4 \leq pH_c \leq 10$ . This observation likely indicates the predominance of TcOOH<sup>+</sup> and TcO(OH)<sub>3</sub><sup>-</sup> species, respectively, in good agreement with the current hydrolysis scheme selected in the NEA–TDB [4]. The pH-independent solubility reaction  $TcO_2 \cdot xH_2O(am) \rightleftharpoons TcO(OH)_2(aq) + 1-x H_2O$  is proposed for the solubility control within  $4 \leq pH_c \leq 10$ . The on-going studies in NaCl solutions will be further extended to dilute to concentrated CaCl<sub>2</sub> and MgCl<sub>2</sub> systems. In all cases, exhaustive solid phase characterization by XRD, SEM–EDS, XAFS and chemical analysis is foreseen to derive/confirm the proposed chemical model. SIT and Pitzer approaches will be used to gain the corresponding thermodynamic and activity models.

### Solubility and hydrolysis of Np(V) in alkaline NaCl solutions

The hydrolysis of Np(V) has been motive of debate in the last years due to the experimental shortcomings affecting the available solubility studies (lack of solid phase characterization) and to the known sensitivity of Np(V) to carbonate impurities. In this context,

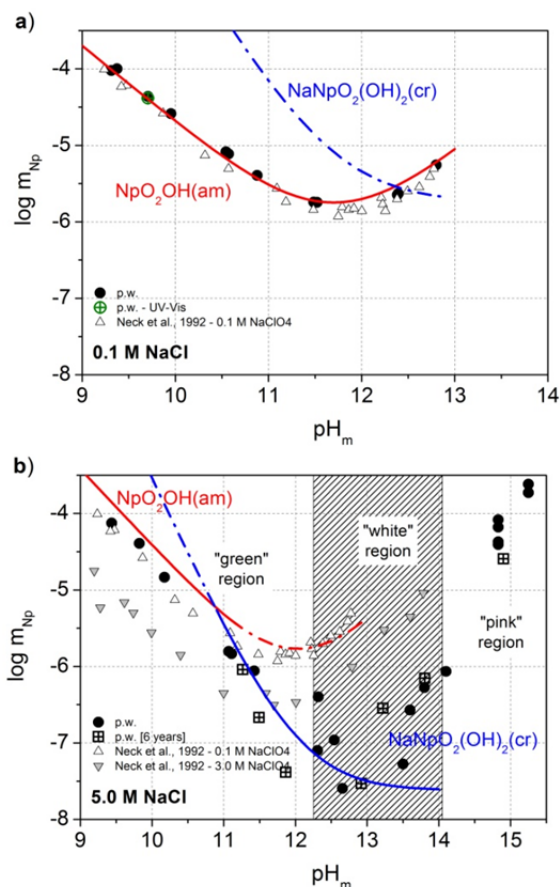


Fig. 2: Solubility of Np(V) in 0.1 M (a) and 5.0 M (b) NaCl [6] and NaClO<sub>4</sub> [5]. Solid lines corresponding to NpO<sub>2</sub>OH(am, fresh) and NaNpO<sub>2</sub>(OH)<sub>2</sub>(cr) solubility as calculated with the current NEA–TDB [4] and reported in [6].

the solubility and hydrolysis of Np(V) were re-investigated by a series of solubility experiments with <sup>237</sup>Np(V) in dilute to concentrated carbonate-free NaCl solutions (0.1 M ≤ *I* ≤ 5.0 M) under inert gas atmosphere. Special attention was dedicated to the accurate characterization of the solid phases controlling the solubility in each system (XRD, quantitative chemical analysis, SEM–EDS, XAFS).

In 0.1 M NaCl, the solubility of the initial NpO<sub>2</sub>OH(am) solid phase was in good agreement with previous experimental results obtained in NaClO<sub>4</sub> solutions [5] (Figure 2a), thus reinforcing the current NEA–TDB selection for Np(V) hydrolysis species (NpO<sub>2</sub>OH(aq) and NpO<sub>2</sub>(OH)<sub>2</sub><sup>−</sup>) and solubility product of the freshly precipitated NpO<sub>2</sub>OH(am). No ageing of this solid phase was observed below pH<sub>m</sub> ~11.5 (even in 5.0 M NaCl) during the

timeframe of the study (2 years). In concentrated NaCl solutions (*I* ≥ 1.0 M) and above pH<sub>m</sub> ~11.5, the greenish NpO<sub>2</sub>OH(am) transformed into a white solid phase (and further to a pinkish material), accompanied by a drop in Np(V) solubility of 0.5–1.5 log-units (depending upon NaCl concentration) (Figure 2b).

Chemical analyses and SEM–EDS indicated a clear Na–enrichment in the white and pink phases, with Np:Na ~1 not reported before in solubility studies. The presence of structural Na in these solids was further confirmed by EXAFS. XRD patterns obtained for the pink solid phase were found in good agreement with data reported for NaNpO<sub>2</sub>(OH)<sub>2</sub>(cr). A log \*K<sub>s,0</sub> for this solid phase was determined based on Np(V) solubility data at pH<sub>m</sub> ≥ 11.5 and *I* ≥ 1.0 M NaCl [6].

### Structure and spectroscopy of Np(VI)–nitrate complexes in solution

The neptunyl ion, Np<sup>VI</sup>O<sub>2</sub><sup>2+</sup>, is relatively stable in nitric acid solutions at oxidic conditions. This enhanced stability of the hexavalent state is related to the complexation between NpO<sub>2</sub><sup>2+</sup> and NO<sub>3</sub><sup>−</sup>, despite that nitrate is a rather weak ligand. As ligand in complexes the nitrate ion is either mono- or bidentately bound. Bidentate coordination is often found in solid complexes [7, 8], while monodentate coordination is likely to occur in dilute aqueous solution.

Because the coordination chemistry of AnO<sub>2</sub><sup>2+</sup> ions is similar, published equilibrium constants for U(VI)-nitrate complexation may be used for Np(VI) and Pu(VI) as such data is scarce or missing for the latter two. However, according to the NEA–TDB data base [4], the equilibrium

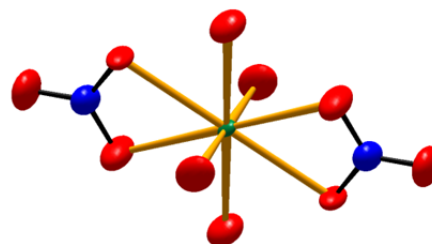


Fig. 3: X-ray structure of [NpO<sub>2</sub>(NO<sub>3</sub>)<sub>2</sub>(H<sub>2</sub>O)<sub>2</sub>] in **1** at 200 K (thermal ellipsoids at 90% probability).

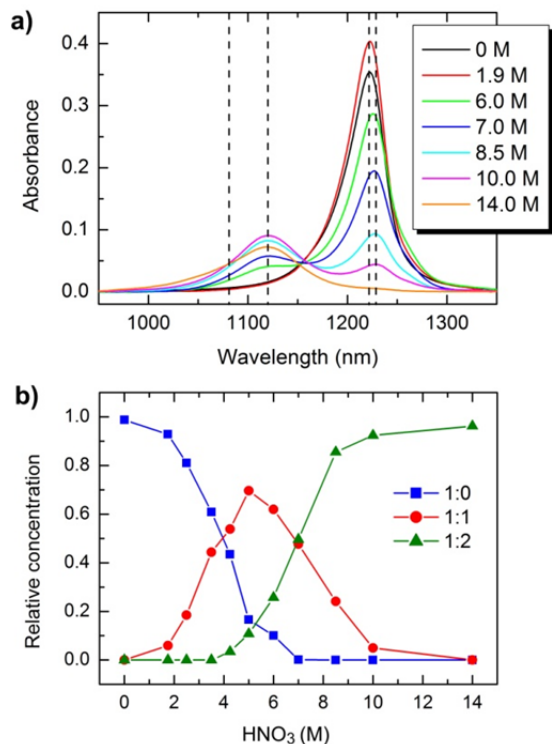


Fig. 4: a) vis-NIR absorption spectra of an 8 mM Np(VI) solution at different HNO<sub>3</sub> concentrations from 0 to 14 M (0 M is represented by a triflate solution) and b) distribution diagram of NpO<sub>2</sub><sup>2+</sup>, NpO<sub>2</sub>NO<sub>3</sub><sup>+</sup>, and NpO<sub>2</sub>(NO<sub>3</sub>)<sub>2</sub>(aq) species derived from the spectra in a).

constant for the mononitrate complex is reliable, while those for the di- and trinitrate complexes are not. To bridge these gaps, we have initiated structural and spectroscopic studies on Np(VI) in nitric acid, combined with thermodynamic modelling.

Single-crystals of [NpO<sub>2</sub>(NO<sub>3</sub>)<sub>2</sub>(H<sub>2</sub>O)<sub>2</sub>].H<sub>2</sub>O (**1**) were grown from a concentrated Np(VI) nitrate solution in 14 M HNO<sub>3</sub>. X-ray analysis showed that **1** is isotopic with those of U and Pu [7-8], all of which crystallize in the *P*-1 space group, with two structurally independent complexes of [AnO<sub>2</sub>(NO<sub>3</sub>)<sub>2</sub>(H<sub>2</sub>O)<sub>2</sub>], linked via hydrogen bonds to a lattice water (Figure 3). A central question is whether the [NpO<sub>2</sub>(NO<sub>3</sub>)<sub>2</sub>(H<sub>2</sub>O)<sub>2</sub>] complex also occurs in solution. Vis-NIR absorption, EXAFS, IR, and Raman studies on **1** and its mother liquid suggested that this was indeed the case. We found no evidence of a trinitrate complex in this solution, even after addition of ammonium nitrate, whereas upon evaporation crystals of NH<sub>4</sub>[NpO<sub>2</sub>(NO<sub>3</sub>)<sub>3</sub>] were formed. To obtain a

more complete picture about the different Np(VI)–nitrate complexes in solution, we recorded vis-NIR absorption spectra of dilute Np(VI) solutions at different nitric acid concentrations between 0 and 14 M (Figure 4a). As shown by peak deconvolution and factor analysis, the spectra consist of three key component bands with peak positions at 1222, 1228, and 1120 nm, assigned to the hydrated NpO<sub>2</sub><sup>2+</sup>, NpO<sub>2</sub>NO<sub>3</sub><sup>+</sup>, and NpO<sub>2</sub>(NO<sub>3</sub>)<sub>2</sub>(aq) species, respectively.

Figure 4b shows the distribution of the aqua, the mono- and dinitrate species as a function of the nitric acid concentration. This distribution is in agreement with that from a time-resolved laser fluorescence spectroscopic study of U(VI) in nitric acid solution [9]. However, our results are in contradiction to those presented in a recent paper on Pu(VI) in nitric acid solution, claiming that mononitrate species dominates in 15 M HNO<sub>3</sub> [8]. The discrepancies identified within the series U(VI)–Np(VI)–Pu(VI) will be assessed in further studies.

The development of thermodynamic and activity models based on the chemical model proposed above using both SIT and Pitzer approaches is underway.

### Complexation of Cm(III) with borate in alkaline NaCl, MgCl<sub>2</sub> and CaCl<sub>2</sub> solutions

Borate can be present in a repository for the disposal of radioactive waste as part of the emplaced waste inventory and as a component of intruding brines in the case of rock-salt formations (relict borate phases). A slight increase of Nd(III) solubility was recently reported at pH<sub>c</sub> = 8.59 and [B]<sub>tot</sub> = 160 mM [10]. In the present work, the interaction of borate with Nd(III) and Cm(III) was studied with a series of solubility and TRLFS experiments, respectively, in dilute to concentrated NaCl, MgCl<sub>2</sub> and CaCl<sub>2</sub> solutions.

Experiments were conducted inside an inert gas (Ar) glovebox. Samples were prepared in 0.1 – 5.0 M NaCl, 0.25 – 3.5 M MgCl<sub>2</sub> and 0.25 – 3.5 M CaCl<sub>2</sub>, with 4 mM ≤ [B]<sub>tot</sub> ≤ 400 mM and 7 ≤ pH<sub>c</sub> ≤ 13. Nd(III) solubility

experiments were performed from undersaturation with  $\text{Nd}(\text{OH})_3(\text{am})$  (~10 mg per independent batch experiment). Samples were monitored for  $[\text{Nd}]$  and  $\text{pH}_m$  up to 142 days. TRLFS experiments were performed with  $1 \times 10^{-7}$  M  $\text{Cm}(\text{III})$  per sample. Single emission spectra and fluorescence lifetimes were collected with a Nd:YAG pumped dye laser system (Surelite II Laser, Continuum).

The solubility of Nd(III) in 3.5 M  $\text{MgCl}_2$  solutions in the absence and presence of borate is shown in Figure 5. No increase in Nd(III) concentration was observed in  $\text{MgCl}_2$  solutions with  $[\text{B}]_{\text{tot}}$  up to 400 mM. On the contrary, a clear decrease in solubility occurred at  $\text{pH}_c \leq 9$  and  $[\text{B}]_{\text{tot}} \geq 40$  mM. Similar observations were obtained in NaCl and  $\text{MgCl}_2$  solutions.

The decrease of Nd(III) solubility with increasing  $[\text{B}]_{\text{tot}}$  as well as the clear change of the slope of the solubility curve indicated the likely formation of a new Nd(III) solid phase containing borate. Further investigations are ongoing to accurately characterize this newly formed solid phase (XRD, SEM-EDS, XPS).

$\text{Cm}(\text{III})$ -TRLFS spectra collected at  $\text{pH}_c = 8$  and  $4 \text{ mM} \leq [\text{B}]_{\text{tot}} \leq 400 \text{ mM}$  showed a red shift with increasing  $[\text{B}]_{\text{tot}}$ . This observation indicates a weak but clear complexation of  $\text{Cm}(\text{III})$

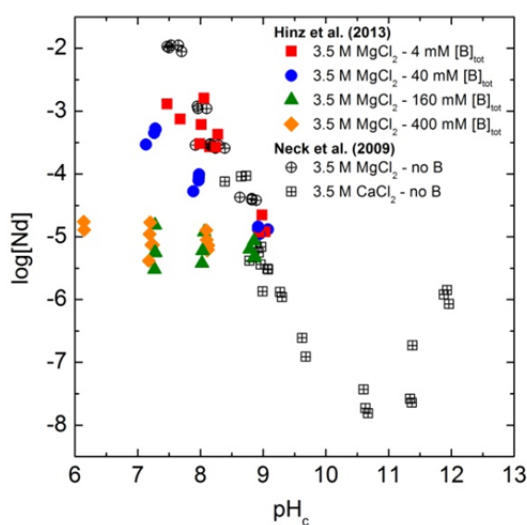


Fig. 5: Solubility of Nd(III) in 3.5 M  $\text{MgCl}_2$  and  $\text{CaCl}_2$  in the absence [11] and presence [12] of borate (4 to 400 mM).

with borate, which does not have a significant impact on the solubility (see Figure 5). Any quantitative interpretation of the TRLFS spectra is (so far) hindered by the very complex borate aqueous speciation.  $^{11}\text{B}$ -NMR studies in NaCl and  $\text{MgCl}_2$  solutions are on-going with the aim of obtaining a more accurate description of boron speciation in brine solutions

### Complexation of $\text{Cm}(\text{III})$ with $\text{Cl}^-$ at $T = 25 - 200^\circ\text{C}$

Chloride is abundant in the pore water of certain clay rocks as well as brines of deep salt formations. At  $25^\circ\text{C}$ ,  $\text{Cl}^-$  is a weak ligand for the complexation of trivalent actinides.  $\log \beta_n^0$  values are given by the NEA-TDB ( $\log \beta_{1,25^\circ\text{C}}^0 = 0.24 \pm 0.03$ ;  $\log \beta_{2,25^\circ\text{C}}^0 = -0.74 \pm 0.05$ ) [4]. Several studies on the interaction of Ln(III) with  $\text{Cl}^-$  show a strong increase of the stability constants with increasing temperature [13, 14]. Due to the radioactive decay and the associated heat release, temperatures of up to  $200^\circ\text{C}$  are expected in the near field of a nuclear waste repository. No studies on the interaction of An(III) with  $\text{Cl}^-$  are available under such conditions. Thus, we apply TRLFS and EXAFS in combination with a custom build high temperature cell to study the complexation of  $\text{Cm}(\text{III})/\text{Am}(\text{III})$  with  $\text{Cl}^-$  in aqueous solution at  $T = 25$  to  $200^\circ\text{C}$ .

Details on the experimental setup are given elsewhere [15]. The TRLFS samples were prepared at  $[\text{H}^+] = 0.1 \text{ m}$ ,  $[\text{Cm}(\text{III})] = 10^{-7} \text{ m}$  and  $[\text{Cl}^-] = 0.1 - 4.0 \text{ m}$ . The EXAFS sample contained  $[\text{Am}(\text{III})] = 10^{-3} \text{ m}$ ,  $[\text{H}^+] = 0.1 \text{ m}$ , and  $[\text{Cl}^-] = 3.0 \text{ m}$ .

A comparison of the emission spectra of  $\text{Cm}(\text{III})$  in  $\text{NaClO}_4$  (1.0 m) and NaCl (0.1 and 4.0 m) solution is displayed in Figure 6. At  $25^\circ\text{C}$ , only the  $\text{Cm}^{3+}$  aquoion is present in all samples. However, the spectra show significant differences at increased temperatures. Lindqvist-Reis et al. showed that  $\text{Cm}(\text{III})$  does not form any complexes with  $\text{ClO}_4^-$  up to  $200^\circ\text{C}$  under the present experimental conditions [15]. Thus, the observed differences are attributed to the formation of  $\text{Cm}(\text{Cl})_n^{3-n}$  complexes at increased temperatures.

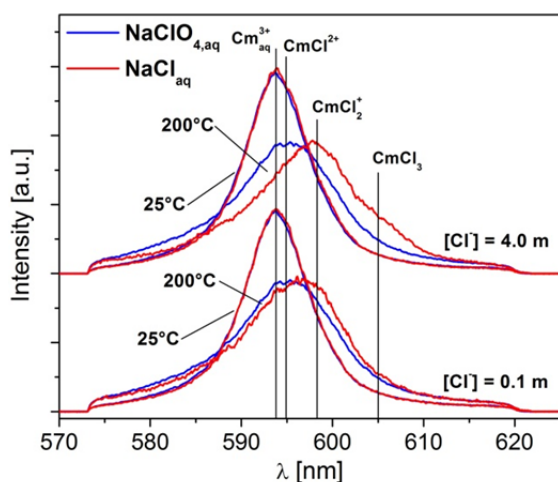


Fig. 6: Emission spectra of Cm(III) at  $[\text{NaClO}_4] = 1.0 \text{ m}$ ,  $[\text{NaCl}] = 0.1$  and  $4.0 \text{ m}$ ,  $T = 25$  and  $200^\circ\text{C}$ .

The spectra are analyzed by peak deconvolution at every studied temperature. Therefore, the single component spectra of the  $\text{CmCl}_n^{3-n}$  complexes are determined. The peak positions of the yielded emission bands are in very good agreement with the literature data at  $25^\circ\text{C}$  [16]. The emission bands are shifted slightly to higher wavelengths with increasing temperature. Thus, and due to the small shift of the band of the  $\text{CmCl}_2^+$  complex, this species cannot be quantified with acceptable accuracy at increased temperatures. The band of the  $\text{Cm}(\text{Cl})_2^+$  complex is shifted distinctly stronger to higher wavelengths, which enables the quantification of its molar fraction as a function of  $[\text{Cl}^-]$  and  $T$ . Furthermore, the  $\text{Cm}(\text{Cl})_3(\text{aq})$  complex is formed at  $T \geq 180^\circ\text{C}$ , but remains below 5%.

The results show a considerable increase of the  $\text{Cm}(\text{Cl})_2^+$  complex with increasing  $[\text{Cl}^-]$  and  $T$ . The determined  $\log \beta'_2(T)$  values are extrapolated to  $I_m = 0$  with the SIT [4]. The  $\log \beta'_2(T)$  increases linearly by almost 3 orders of magnitude in the studied temperature range. The temperature dependency is fitted by the integrated van't Hoff equation, yielding  $\Delta_r H_m^0$  and  $\Delta_r S_m^0$ . The results are summarized in Table 1.

The EXAFS spectra at 25 and  $100^\circ\text{C}$  are well described considering 9-10 oxygen neighbours at a distance of  $\sim 2.45 \text{ \AA}$ . At  $200^\circ\text{C}$  a second oscillation is present at  $k \approx 5 \text{ \AA}^{-1}$ . This results in a

Table 1: Thermodynamic data of the formation of the  $\text{Cm}(\text{Cl})_2^+$  complex.

$\log \beta'_2(25^\circ\text{C})$	$\log \beta'_2(200^\circ\text{C})$	$\Delta_r H_m^0$	$\Delta_r S_m^0$
$-0.12 \pm 0.39$	$2.80 \pm 0.07$	$53.4 \pm 4.4$ kJ/mol	$164.8 \pm 8.6$ J/mol·K

broadening of the peak in the pseudo-radial distribution in the related Fourier Transform. This effect is attributed to the presence of  $\text{Cl}^-$  in the inner coordination sphere of Am(III). 2-3 chloride ligands have to be included in the fit. These results are in excellent agreement with the TRLFS data.

The present work shows, that An(III)-chloride complexes may play an important role at elevated temperatures and thus have to be considered within a comprehensive long term safety assessment of a nuclear waste repository.

## References

- [1] Altmaier, M. et al., Chem. Reviews, 113: 901 (2013).
- [2] Kobayashi, T. et al., Radiochim. Acta, DOI:10.1524/ract.2013.2040 (2013).
- [3] Kopunec, R. et al., J. Radioanal. Nucl. Chem., 230: 51 (1998).
- [4] Guillaumont, R. et al., Chemical Thermodynamics Vol. 5, Elsevier, Amsterdam, (2003).
- [5] Neck, V. et al., Radiochim. Acta, 56: 25 (1992).
- [6] Petrov, V. et al., Geochim. et Cosmochim. Acta, (2013, submitted)
- [7] Hughes, K. A. et al., Acta Cryst., C59: 7 (2003)
- [8] Gaunt, A. J. et al., Inorg. Chem., 50: 4244 (2012)
- [9] Moulin, C. et al., Anal. Chem., 68: 3204 (1996)
- [10] Borkowski, M. et al., Radiochim. Acta, 98: 577 (2010)
- [11] Neck, V. et al., Pure Appl. Chem., 81: 1555 (2009)
- [12] Hinz, K. et al., Radiochim. Acta, (2013, in preparation)

- [13] Gammons, C. H. et al., *Geochim. Cosmochim. Acta*, 60: 4615 (1996).
- [14] Stepanchikova, S. A. et al., *Russ. J. Coord. Chem.*, 31: 193 (2005)

- [15] Lindqvist-Reis, P. et al., *J. Phys. Chem. B*, 109: 3077 (2005)
- [16] Fanghänel, Th. et al., *J. Alloys Compds.*, 225: 308 (1995).

## 5.2 Sorption on Mineral Surfaces

*M. Altmaier, N.L. Banik, H. Geckeis, T. Kupcik, J. Lützenkirchen, C. Marquardt, R. Marsac, T. Rabung, T. Schäfer, D. Schild, A. Schnurr, J. Rothe*

### Introduction

Radionuclide sorption onto mineral surfaces is a key aspect which has to be considered in performance assessment calculations for nuclear waste repositories. In this respect fundamental studies are essential to understand the (sorption) reactions and mechanisms at the mineral-water interface.

Besides pure and well defined laboratory systems also natural and site specific samples have to be studied. By combination of a top down / bottom up approach and a quantitative description of sorption reactions by the means of thermodynamic constants relevant sorption data can be provided for PA.

### Silica surface charge – influences on the occurrence of the hydrophobic site

Previous studies on Eu adsorption on quartz and the concomitant acid-base titration on the quartz sample up to high ionic strength have indicated that common surface complexation models calibrated at low ionic strength may allow the description of surface chemical equilibria up to highly saline conditions, by keeping all thermodynamic parameters the same as at low ionic strength and involving the Pitzer formalism to calculate aqueous species and water activities. However, one consistent observation in the quartz titrations was that deprotonation of the quartz sample was clearly measurable at  $\text{pH} < 5$ . Such behavior is very rare corresponding to maybe 5% of the overall available silica surface titration data that have been published. However, such behavior has been reported in spectroscopic work [1], and has spiked some recent interest [2,3,4]. The site at which the first deprotonation step occurs has been termed the hydrophobic site. Interestingly it exhibits cation specificity that is different from its hydrophilic counterpart [2,3]. Furthermore, the hydrophobic site has been observed to exhibit anion specificity [4],

which is not common for negatively charged oxide surfaces. The hydrophilic site with an intrinsic  $\text{pK}_a$  value of about 7.5 to 8.5 has been involved in the interpretation of the common silica and quartz charging curves with only one deprotonation reaction. Another obvious but rarely discussed problem related to the 95% “normal” silica titrations is that although visible deprotonation does not occur before  $\text{pH}$  is above 6 or 7 or even higher, zeta-potentials are strongly negative at  $\text{pH}$  values  $> 3$ . The usually reported range of isoelectric points for quartz and silica is between  $\text{pH}$  2 and 3. Consequently, it is important to find out what causes the appearance of the hydrophobic site. To this end acid-base titrations were carried out on two quartz samples and an amorphous silica sample. Results in 600 mM NaCl with starting points of the titrations at  $\text{pH} < 3$  are shown in Figure 1. Known amounts of the samples were added to a known volume of electrolyte solution. Then the same aliquot of HCl solution was added to all three systems and the suspensions were allowed to equilibrate for 2 hours at the initial  $\text{pH}$ . Subsequently the suspension was titrated by 50 mM NaOH. The surface charge was calculated from the consumption of hydroxide ions in the suspension corrected for the theoretical consumption in a corresponding system without solid. The zero level was arbitrarily set to zero at  $\text{pH}$  3, because titrations cannot be carried out to the expected point of zero charge (which is at  $\text{pH}$  1 for the amorphous silica, as discussed later). Figure 1 shows a clear two step deprotonation for the two quartz samples, which is more pronounced for the MINUSIL (Minusil 15, quartz) sample. The amorphous silica sample does not show this two-step protonation, but some deprotonation occurs at low  $\text{pH}$  for this sample as well. The apparent strongly negative charge at high  $\text{pH}$  is due to dissolution of the  $\text{SiO}_2$  samples, which results in aqueous species that release protons at this  $\text{pH}$ . No attempt has been made to correct for this. At lower  $\text{pH}$  values, no  $\text{pH}$ -

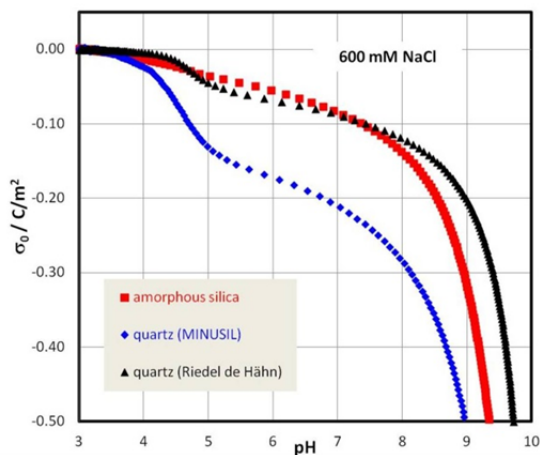


Fig. 1: Surface charge density of three silica samples as a function of pH in 600 mM NaCl solution.

dependent equilibrium solubility of  $\text{SiO}_2$  is expected. It is this pH-range that is of interest for the present work.

In a second series of experiments the titrations were started at the suspension pH, i.e. without extra addition of acid to the medium solution. Results for 1 mM NaCl medium are shown in Figure 2 for MINUSIL and amorphous silica. The amorphous silica sample (red dots) in this case does not show any deprotonation in the pH range between 5 and 7, whereas when started at low pH there is noticeable negative charge at pH 5 (Figure 1, in 600 mM NaCl).

When starting the titration from pH 5, the resulting behavior shown in Figure 2 for amorphous silica actually agrees with the huge majority of data published in the literature. The observation that the initial deprotonation at low pH does not occur when the titration starts at higher pH is also confirmed by the data shown for MINUSIL in Figure 2. A MINUSIL titration started from low pH shows the build-up of negative charge below pH 5 (open blue diamonds). This is not observed when the titration is started at about pH 5 (full blue diamonds). If the reaction causing the deprotonation below pH 5 also occurred in the titration started at pH 5, there should be a concomitant decrease in pH due to proton release and the initial charge at the start of the titration would be that observed in the titration started at low pH. The results therefore suggest that the first

deprotonation reaction needs to be activated at low pH. Furthermore, titrations started at pH 5 in different sodium media do not reveal any anion specificity that was reported elsewhere in experiments started at lower pH [4]. The absence of such effects concurs with the inactivity of the hydrophobic site if experiments are not started at low pH. Together with the fact that amorphous silica does not show enhanced deprotonation at low pH a number of conclusions can be drawn:

The hydrophobic site appears to be more pronounced on quartz samples. There is some deprotonation at low pH on amorphous silica, but it does not show the same two-step behavior observed for quartz. However, there is a clear difference between data sets obtained from low and high pH also on amorphous silica.

Whether or not both sites on silica samples are observed appears to depend on whether the more acidic (hydrophobic) site is activated or not. The acidic site will always be activated in electrokinetic measurements that attempt to attain the isoelectric point, which is below pH 3 (for our sample it is at about pH 1 as shown in Figure 3). It could also be a kinetic effect, i.e. the waiting time before the first addition of hydroxide might be too short.

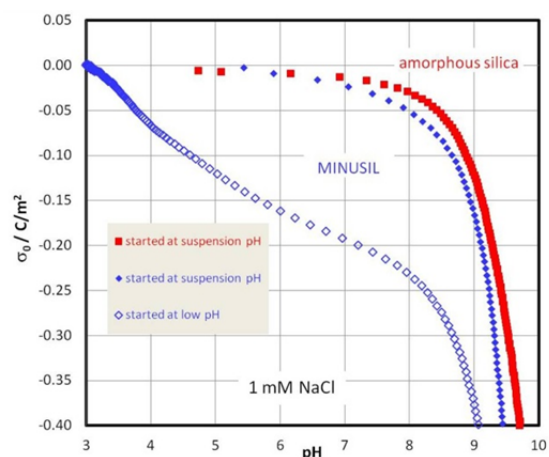


Fig. 2: Surface charge density of amorphous silica (red symbols) and MINUSIL (full blue symbols) as a function of pH in 1 mM NaCl solution, started at pH 5. Open blue symbols show a titration for MINUSIL (quartz) started at low pH in a 1 mM NaCl medium (nominal).

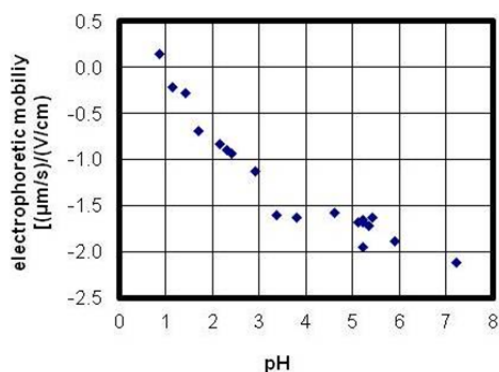


Fig. 3: Electrophoretic mobility of amorphous silica as a function of pH.

The very low isoelectric point makes it impossible to correctly fix the zero-level of the titration curves in Figures 1 and 2, if the acid site is to be included, because no reasonable titration data can be obtained at pH 1. Fixing the zero level can only be done via a model. At present the zero-level in Figures 1 and 2 is fixed at pH 3 arbitrarily.

If the acidic site is activated in an adsorption experiment, the onset of cation adsorption may be at lower pH than in experiments that are started at say pH 5. This explains rather strong and unexpected adsorption of Am on some samples [5] at low pH.

It is known that on quartz a gel-like (amorphous) layer starts to form, which explains the relatively high solubility of bulk quartz [6]. With time the surface properties of amorphous silica are retrieved on quartz and concomitant changes of adsorption behavior with time is to be expected. This has been observed in a study on Am-adsorption (Petrov et al., unpublished data), where strong shifts of adsorption edges occurred with time for Am on quartz (Minusil). The Minusil used originally for the adsorption experiments showed titration behavior similar to the curves shown in Figure 1.

Interestingly the hydrophobic site is hardly affected by ionic strength based on the presently available data in NaCl (not shown). Even more interestingly specific ion effects occur in this system. The acid (hydrophobic) site behaves as a structure breaker, i.e. it tends to attract more strongly the structure breaking cat-

ions (like Cs [2]) and surprisingly there are significant anion effects [4], while the common site has structure making properties and structure making cations are preferably adsorbed [2] and no preference in the anion series has been reported.

Finally the observations made here may also relate to the uncommon stability of silica close to its isoelectric point, in particular if ion adsorption shows uncommon features in the low pH range.

## References

- [1] Ong, S., Zhao, X., Eisenthal, K.B., Chem. Phys. Lett. 191: 327 (1992).
- [2] Morag, J., et al., Langmuir, 29: 6317 (2013).
- [3] Azam, M.S., et al., J. Phys. Chem. Lett. 3: 1269 (2012).
- [4] Gibbs-Davis, J.M., et al., GEOC-104, ACS conference, San Diego, 27.03.2013.
- [5] Stumpf, S., et al., J. Colloid Interface Sci. 318: 4 (2008).
- [6] Huber, F., Lützenkirchen, J., Aquatic Geoch. 15: 443 (2009).

## Trivalent actinide and lanthanide sorption on clay minerals under saline conditions

The final disposal in deep geological formations is considered as the safest way to keep high level radioactive waste isolated from the biosphere. Due to their high sorption capacity, their swelling properties and their low water permeability, clay minerals are of great interest as suitable components of geotechnical and geological barriers. Therefore, several countries have selected clay formations for their deep geological disposal projects e.g. Opalinus clay (Switzerland), Callovo-Oxfordian (France) or Boom clay (Belgium). In other concepts compacted clays have been proposed as backfill and sealing materials. For the safety assessment of nuclear waste concepts, the potential contact of waste forms with groundwater has to be considered. Sedimentary clay formations discussed as potential repository host rocks can be in contact

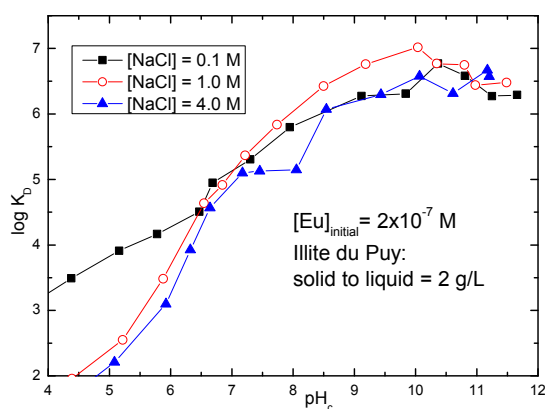


Fig. 1: Eu(III) sorption onto illite as the logarithm of the distribution coefficient vs.  $\text{pH}_c$  at different ionic strengths.

with highly saline (up to 5 molal) groundwater [1]. Only a few studies so far addressed radionuclide sorption under high ionic strength conditions [2]. The non-electrostatic 2SPNE SC/CE sorption model developed by Bradbury and Baeyens to describe sorption onto illite and smectite is only valid for relatively low ionic strength systems ( $I < 1 \text{ M}$ ) [3]. The present work focuses therefore on the sorption of trivalent metal cations (Eu(III)/Cm(III)) and hexavalent uranium onto different natural relevant clay minerals (illite, smectite and kaolinite) under saline conditions and exclusion of  $\text{CO}_2$ .

Batch sorption edge experiments were carried out with three different background electrolytes (NaCl,  $\text{CaCl}_2$  and  $\text{MgCl}_2$ ) at different ionic strengths ( $[\text{NaCl}]$  up to 4 M,  $[\text{CaCl}_2]$  and  $[\text{MgCl}_2]$  up to 2 M), at fixed metal concentration ( $[\text{Eu}]_{\text{total}} = 2 \times 10^{-7} \text{ M}$ , labeled with  $^{152}\text{Eu}$  for g-counting or  $[\text{U(VI)}]_{\text{total}} = 4 \times 10^{-7} \text{ M}$ ) and at constant solid to liquid ratios (S:L = 2 g/L) over a wide  $\text{pH}_c$  range (3-12). The extent of metal ion adsorption onto the different clay minerals approaches 100% at  $\text{pH}_c > 7$  for all investigated electrolyte solutions. In general, sorption edges shift to higher  $\text{pH}_c$ -values with increasing ionic strength (confirmed for Eu(III), first hints for U(VI)). In presence of divalent cations, however, actinide/lanthanide sorption is much stronger suppressed than observed for NaCl solutions. This is explained by the stronger competition of divalent cations with

actinide/lanthanide sorption to cation exchange sites but also to inner sphere sorption sites at the edges of the clay particles.

The applicability of the 2SPNE SC/CE model [3] was tested to describe Eu(III) sorption at high ionic strength. A good agreement of experimental data and model prediction was achieved in the NaCl systems at  $\text{pH}_c < 7$  where metal ion activities were calculated using the Pitzer approach. However, the model underestimates sorption at higher  $\text{pH}_c$ . Agreement for Ca/ $\text{MgCl}_2$  systems at higher pH and up to 0.6 M is much better. Deviations might be due to uncertainties in the Pitzer parameter data set for An(III) in NaCl solutions.

Time resolved laser fluorescence spectroscopy (TRLFS) studies confirm the existence of three distinguished Cm(III) surface complexes which have been described already earlier for low ionic strength conditions [4] also at high salinity. This finding demonstrates that the coordination of adsorbed actinide species does not change noticeably under highly saline conditions and validates speciation assumptions underlying the 2SPNE SC/CE model. However, with an improved detection system, an additional fourth inner-sphere surface species could be identified at higher wavelengths ( $\lambda \sim 610 \text{ nm}$ ) being comparable to the findings of a previous study on curium interaction with kaolinite. This species was interpreted as a clay/curium/silicate ternary complex [5].

The present work clearly demonstrates that clay minerals represent strong retardation barriers for tri- and hexavalent metal ions even under highly saline conditions.

## References

- [1] Brewitz, W., Eignungsprüfung der Schachanlage Konrad für die Endlagerung radioaktiver Abfälle. GSF-T136, Neuherberg (1982).
- [2] Vilks, P., Sorption of Selected Radionuclides on Sedimentary Rocks in Saline Conditions – Literature Review. Technical Report NWMO TR-2011-12 (2011).
- [3] Bradbury, M.H., Baeyens, B., Geochim. Cosmochim. Acta, 66: 2325 (2002).

- [4] Rabung, Th., et al., *Geochim. Cosmochim. Acta*, 69: 5393 (2005).
- [5] Huittinen, N., et al., *Geochim. Cosmochim. Acta*, 99: 100 (2012).

### Eu sorption onto natural illite; a batch- and TRLFS study

Clay mineral dominated geological formations (e.g. claystones) are being investigated by several countries as potential host rock formations for a high-level nuclear waste repository. Clay minerals such as kaolinite, montmorillonite, or illite generally form the main constituent in these sedimentary rock formations and are being investigated thoroughly by means of their sorption properties [1-3]. In case of illite, the studies dealing with radionuclide sorption have been performed only with the pure, purified mineral [4-6]. However, accessory mineral phases initially present in the natural clays such as calcite or iron (hydr)oxides are also known to be effective sorbents for actinides [7,8]. In natural waters, where tri- and tetravalent actinides are expected to be in low concentrations due to solubility limitations, such mineral phases may influence the radionuclide retardation sorption or might even dominate the sorption properties [9].

In the present study the sorption properties of an unpurified illite sample have been investigated by both batch sorption and time resolved laser fluorescence spectroscopy (TRLFS) experiments.

The illite material is derived from the basin near Le Puy en Velay. Besides illite, also kaolinite, quartz and well crystallised calcite are present as minor constituents in varying amounts. Separation of the < 63µm size fraction was performed by crushing and sieving of the natural material. The surface area was determined to be 113.7 m<sup>2</sup>/g by means of N<sub>2</sub>-BET. This raw, natural material was not being treated further, especially no acid treatment and size fractioning procedures [10] were performed. The unpurified illite is compared to two purified Na-illite batches. The first sample was obtained during the CatClay

project ([www.catclay.org](http://www.catclay.org)) and only an acidic treatment step (pH 3.5) was applied as a purification procedure, resulting in a Na-illite with a < 63 µm size fraction. A further sedimentation procedure was performed in the second case, giving the < 0.5 µm size fraction. A thorough description on the latter purification procedure can be found in the literature [11,12]. The surface areas were determined to be 132.1 m<sup>2</sup>/g and 129 m<sup>2</sup>/g for the < 63 µm and < 0.5 µm size fraction, respectively.

The batch sorption experiments, both sorption edges and sorption isotherms, with Eu were performed in a glove box (O<sub>2</sub> < 1ppm) performed in 0.1 M and 0.5 NaCl solutions with a solid-to-liquid ratio of 2 g/L. For the sorption edge experiments [Eu] was varied between 6.6×10<sup>-8</sup> and 6.6×10<sup>-6</sup> M and the pH was adjusted in a range between 3 < pH < 11 (no buffer added). The sorption isotherms were recorded at two fixed pH values (5.5 and 7.0; 5×10<sup>-3</sup> M MES and TRIS/TRIS-HCl buffer, respectively) with [Eu] ranging from 2.8×10<sup>-11</sup> M and 2×10<sup>-4</sup> M. After labelling the suspensions with <sup>152</sup>Eu, the samples were mixed end-over-end for 7 days. After this, the pH was checked and phase separation was performed by ultracentrifugation (90,000 rpm). The Eu content in the supernatants was analysed by ICP-MS and LSC, respectively. A reference specimen was used as an internal standard and measured simultaneously. The pH dependent Eu uptake is presented as distribution ratios, K<sub>d</sub> (L/kg), defined as:

$$K_d = \frac{C_{tot} - C_{eq}}{C_{eq}} \cdot \frac{V}{m} \quad (1)$$

with C<sub>tot</sub> the initial aqueous metal ion concentration (mol/L), C<sub>eq</sub> the measured Eu in the supernatant (mol/L), V the volume of the liquid phase (L) and m the mass of the solid phase (kg). Surface normalized K<sub>D</sub> values (L/m<sup>2</sup>) are used to compare different illite samples with different surface areas.

For the TRLFS investigations three parallel samples were prepared with a mineral concentration of 0.25 g/L illite and 2×10<sup>-7</sup> M of Cm(III) in 0.1 M NaClO<sub>4</sub>. The pH was increased from 2.9 to 6.6 in small steps (no buffer add-

ed). After 2-3 days the pH was checked and the samples were transferred into quartz cuvettes and investigated by TRLFS. For detail on the experimental setup see [3].

The pH dependent Eu sorption onto natural illite in 0.1 M and 0.5 M NaCl at three different Eu(III) concentration ( $6.6 \times 10^{-8}$  M -  $6.6 \times 10^{-6}$  M) is depicted in Figure 1a. At low pH the  $K_D$  values for 0.1 M NaCl are 1.5 log units higher than for 0.5 M NaCl indicating an uptake mechanism dominated mainly by cation exchange (CE) processes [3]. With increasing pH the sorption increases and at  $\text{pH} > 5$  the sorption data are not significantly different for both ionic strengths, pointing to an uptake by surface complexation. As the position of the sorption edge is not significantly influenced by different Eu concentrations, an ideal sorption behaviour in the investigated Eu concentration range can be deduced. The present data are in accordance with Eu sorption data obtained for the purified Na-illite samples. Thus, the minor mineral phases present in the unpu-

rified illite material tend not to have a significant influence on the pH dependent Eu uptake.

In Figure 1c and d the Eu sorption isotherms at two pH values are depicted. For all the three systems and  $\text{Eu}_{\text{equilibrium}} < 10^{-7}$  M a slope  $\sim 1$  indicates a linear sorption behaviour and the Eu surface complexation through only one type of reactive surface site. This result is consistent with the sorption edge data with an ideal sorption behaviour for  $6.6 \times 10^{-8}$  M  $<$  [Eu]  $<$   $6.6 \times 10^{-6}$  M. At higher Eu concentrations, the slope of the different sorption isotherms tends to decrease in a different manner, which can be attributed to saturation effects and/or a sorption onto an additional surface site. A relatively high Eu uptake at pH 5.5 in a narrow  $[\text{Eu}_{\text{equilibrium}}]$  range at  $\sim 10^{-7}$  M, for both the unpurified illite and purified illite with  $< 63 \mu\text{m}$  is obvious, whereas this feature is missing for the  $< 0.5 \mu\text{m}$  size fraction. This result is not yet understood in detail, but possible explanations may include the presence of

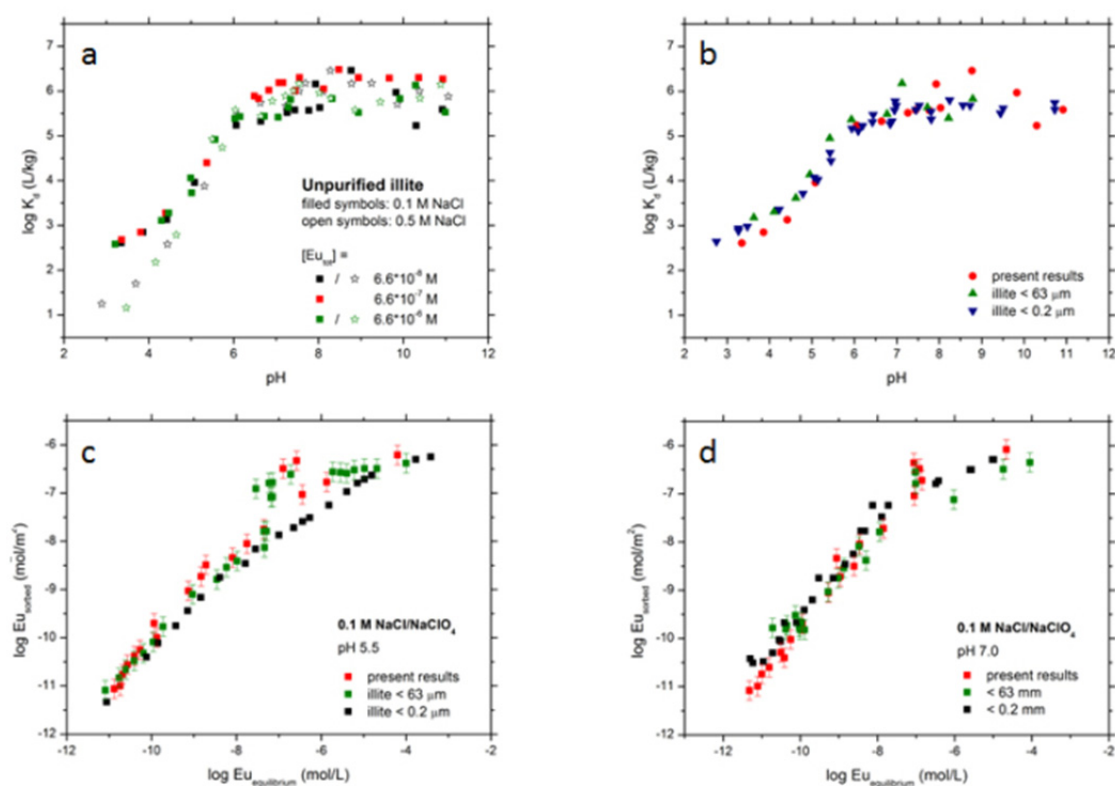


Fig. 1: Sorption edge (a+b) and sorption isotherm (c+d) results on the interaction of Eu with natural and purified Na-illite [11,12].

another sorption active phases (smectite/illite mixed layers) or the precipitation of an Eu bearing phase.

However, both the sorption edge and - isotherm results show, especially at low Eu concentrations, a good correlation between the natural and purified illite samples, indicating only minor effects of the additional mineral phases (i.e. calcite, Fe-phases) on the Eu uptake.

Figure 2 shows the evolution of the fluorescence emission spectra between pH 2.9 and 6.6. For pH < 4.7 the emission spectra resembles the one for the  $\text{Cm}^{3+}_{\text{aq}}$  ion with an emission peak maximum at 593.8 nm. This is in accordance with the results of the batch sorption experiments, where the sorption below pH 5 is dominated by cation exchange processes, where the metal ion retains its complete hydration sphere (outer-sphere complexation). At pH ~ 5 a shoulder at higher wavelengths appears in the emission spectra,

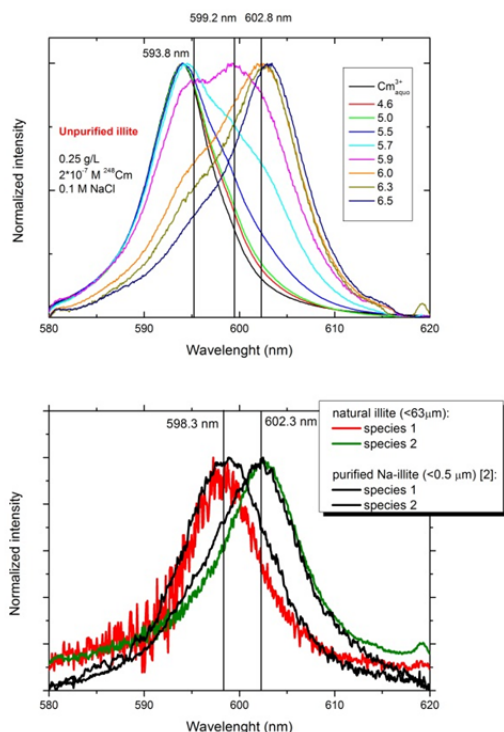


Fig. 2: TRLFS spectra on the interaction of Cm with natural, unpurified illite at different pH values (above) and single component emission spectra for inner-sphere surface species (below) together with data on a purified Na-illite [2].

indicating a change in the first Cm coordination sphere and pointing to the formation of surface sorbed Cm(III) complex. With increasing pH the intensity of this shoulder increases. When the pH is increased further (pH ~ 6), the Cm fluorescence is dominated by an emission spectrum with a peak maximum ~ 602 nm. Along with the red shift of the emission spectra, the curium fluorescence lifetime increases from  $\tau = 64 \mu\text{s}$  to  $115 \mu\text{s}$ . As  $\tau$  can be correlated to the number of  $\text{H}_2\text{O}$  and/or  $\text{OH}^-$  units in the first Cm coordination sphere by means of a linear relationship [13], 5  $\text{H}_2\text{O}/\text{OH}^-$  entities can be calculated for the surface sorbed Cm. Given the fact, that the metal ion loses ~ 4 water ligands by complexation, this result confirms an inner-sphere complexation. From peak deconvolution two single component emission spectra, i.e. two surface sorbed Cm species with emission peak maxima at  $\lambda_{\text{max}} = 598.3 \text{ nm}$  and  $602.3 \text{ nm}$  can be distinguished. As the first curium species appears at low pH (pH > 4.1), the formation of a Cm(III) complex  $\equiv\text{SO}-\text{Cm}(\text{H}_2\text{O})_5$  is most likely [2]. As the second Cm species is being formed with increasing pH, the second Cm species can be assigned to the a hydrolyzed Cm surface complex, i.e.  $\equiv\text{SO}-\text{Cm}(\text{OH})(\text{H}_2\text{O})_4$ .

The positions of the emission bands of the Cm species as well as the fluorescence lifetime is in perfect agreement with finding of Rabung et al. [2] for the sorption of Cm onto a purified Na-illite (size fraction <math> < 0.2 \mu\text{m}</math>). Together with the batch sorption, the TRLFS show, that the Cm sorption on the unpurified illite material is dominated by the pure illite mineral phase, whereas impurities have no or only minor effects on the Cm complexation.

## References

- [1] Bradbury, M.H. and B. Baeyens, *Geochim. Cosmochim. Acta*, 66(13): 2325 (2002).
- [2] Rabung, T., et al., *Geochim. Cosmochim. Acta*, 69(23): 5393 (2005).
- [3] Huittinen, N., et al., *Radiochim. Acta*, 98: 613 (2010).
- [4] Bradbury, M.H., et al., *Geochim. Cosmochim. Acta*, 69(23): 5403 (2005).
- [5] Bradbury, M.H., Baeyens, B., *Geochim. Cosmochim. Acta*, 73(4): 990 (2009).

- [6] Bradbury, M.H., Baeyens, B., *Geochim. Cosmochim. Acta*, 73(4): 1004 (2009).
- [7] Stumpf, T., Fanghänel, T., *Colloid Interface Sci*, 249(1): 119 (2002).
- [8] Li, D. and D.I. Kaplan, *Journal of Hazardous Materials*, 243(0): 1 (2012).
- [9] Payne, T.E., et al., *Applied Clay Science*, 26(1–4): 151 (2004).
- [10] Baeyens, B., Bradbury, M. H., *Contaminant Hydrology*, 27(3–4): 199 (1997).
- [11] Bradbury, M.H., Baeyens, B., NAGRA Technical Report (2005).
- [12] Poinssot, C., et al., Experimental studies of Cs, Sr, Ni, and Eu sorption on na-illite and the modelling of Cs sorption, in PSI Bericht (1999).
- [13] Kimura, T., Choppin, G. R., *Journal of Alloys and Compounds*, 213: 313 (1994).

### Pu and Np interaction with Opalinus clay (OPA) and Callovo-Oxfordian argillite (COx)

Np and Pu speciation in OPA- and COx-synthetic porewater system (i.e. pH = 7.5; total ionic strength = 0.3 M) under 1% CO<sub>2</sub> was investigated as a function of the solid to liquid ratio (10 g/L < S/L < 200 g/L) and contact time (6 weeks and 4 months), at low total Np/Pu concentrations (~10<sup>-7</sup> M) for batch experiments (liquid-liquid extraction and CE-ICP-MS for concentration and oxidation state determination) and higher concentration (10<sup>-4</sup> M) for spectroscopy: UV-Vis/NIR, XAFS and XPS. Phase separation was performed by ultrafiltration at 10 kDa. The pH and Eh measurements were performed over time for all samples. Geochemical speciation modeling was performed with PHREEQC, where the 2SPNE SC/CE model [1] was introduced to consider Np/Pu(IV,V) sorption to clay minerals, and Geochemist's Workbench to plot Pourbaix diagrams (redox speciation as function of pH and Eh). Np(V) and Pu(V) were introduced in the sample but thermodynamic calculations suggest that Np(V)/Pu(V) are reduced to the +IV oxidation state.

Fig. 1 presents the sorption data of the present work and a comparison with literature data. After 6 weeks contact time, Np(V) is the

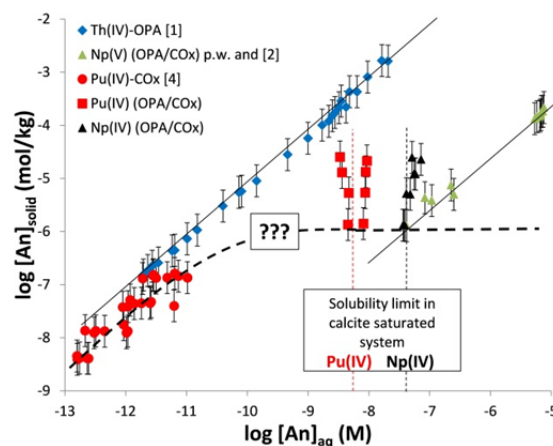


Fig. 1: Amount of Np and Pu present on the solid phases (i.e. sorbed to OPA and COx or precipitated) versus aqueous concentration. The present results are compared with literature data for Pu(IV), Th(IV) and Np(V). Np(V) data are obtained for a contact time ≤ 6 weeks.

dominant species both in solution and in the solid as deduced from liquid-liquid extraction and EXAFS, respectively. Our sorption data (green triangles) are consistent both with [2] and surface complexation modeling. After 4 months contact time, Eh decreased and Np(V) is reduced to Np(IV) as evidenced by the higher amount of Np on the solid phase. Such reduction was not observed by spectroscopy at higher Np concentration, showing the limited amount of reducing species on the solid. Pu(V) reduction to Pu(IV) is fast. Sorption data remain constant between 6 weeks and 4 months. At higher Pu concentration, spectroscopic (XAFS and XPS) studies show the formation of PuO<sub>2(s)</sub> with a structure similar to Pu(IV)-colloids.

Final concentrations of the tetravalent actinides in solution ([An(IV)]<sub>aq</sub>) are consistent with aqueous speciation modeling and show that the formation of An(IV) hydroxycarbonato complexes [3] can enhance An(IV) solubility in calcite saturated systems (e.g. log [Pu(IV)]<sub>aq</sub> increase from -10.2 to -8.3 at pH ~ 7.5 without and with calcite, respectively). In the present work, all the [An(IV)]<sub>aq</sub> data are equal to the solubility limit and show that An(IV)-(hydr)oxides precipitate.

However, the present observations are neither consistent with literature data for Pu(IV) [4] and Th(IV) [1] (see Fig. 1) nor with surface

complexation modeling (not shown). Indeed, at such low loading ( $10^{-6}$  mol/kg), sorption is expected to be linear as is the case for Th(IV). Therefore,  $[\text{An(IV)}]_{\text{aq}}$  should theoretically be controlled by surface complexation and should also be several orders of magnitude below the solubility limit. Conversely, the high consistency between the present Np(IV) and Pu(IV) data show that this surprising behavior is not an experimental artifact but points to more complex chemical mechanisms.

The present Np and Pu studies have in common that the observed aqueous solution concentrations  $[\text{An(IV)}]_{\text{aq}}$  are similar to the corresponding calculated An(IV) solubility limit in calcite saturated system. This contrasts with literature data for Pu(IV) [4] and Th(IV) [1]. At low  $[\text{An(IV)}]_{\text{aq}}$ , monomeric An(IV) is expected to dominate the aqueous speciation and, probably, surface speciation. Close to the solubility limit, the occurrence of different process might explain our observations. First, we note that Pu(IV) colloids have been shown to be stabilized by mineral surfaces [5] and might block surface binding sites for monomeric species, explaining the deviation from the sorption results reported in the literature [4]. Second, under acidic conditions polymeric Pu(IV) species have been shown to dominate aqueous speciation when  $[\text{Pu(IV)}]_{\text{aq}}$  is slightly below the solubility limit [6]. Np(IV) might have a comparable behavior to Pu(IV). If com-

parable species were relevant at pH = 7.5 in the presence of carbonates, the apparently lower sorption (or maybe a sorption plateau at  $10^{-6}$  mol/kg) might reflect a different sorption behavior than for monomeric An(IV) species. Therefore, our present results show the limits to understanding such complex natural system, that cause complex and difficult to control complexation reactions, without concomitant spectroscopic results for all relevant elements (including inorganic carbon in the present case) AND for the concomitant conditions. Further studies have to be dedicated to more simple systems, namely, An(IV) sorption to purified clay and An(IV) aqueous speciation in the presence of carbonates.

## References

- [1] Bradbury and Baeyens, *Applied Clay Sci.* 52: 27 (2011).
- [2] Wu et al., *Environ. Sci. Technol.* 43: 6567 (2009).
- [3] Zavarin et al., *Radiochim. Acta* 93: 93 (2005).
- [4] Latrille et al., *Radiochim. Acta* 94 : 421 (2006).
- [5] Powell et al., *Environ. Sci. Technol.* 45 : 2698 (2011).
- [6] Walther et al., *Radiochim. Acta* 97: 199 (2009)

### 5.3 Retention of radionuclides by secondary phase formation

N. Finck, L. Temgoua, A. Chagneau, F. Heberling, S. Hofmann, T. Stumpf, R. Polly, K. Dardenne, S. Heck, T. Schäfer, H. Geckeis

In co-operation with:

V. L. Vinograd<sup>a,b</sup>, K. Voïtchovsky<sup>c</sup>

<sup>a</sup> Institute of Geoscience, Goethe Universität Frankfurt (Germany), <sup>b</sup> Institute for Energy and Climate Research 6, Forschungszentrum Jülich (Germany), <sup>c</sup> École Polytechnique Fédérale de Lausanne (EPFL), Lausanne (Switzerland).

#### Introduction

The contact of the High Level nuclear Waste (HLW) matrix with ground water may lead to the formation of secondary phases over geological time scales. The formation of such alteration phases represents a significant retention potential for the radiotoxic and long-lived radionuclides (RNs). The presence of RN released from the corroding waste matrix during the (co)precipitation of such phases opens the possibility to structurally incorporate them in the bulk solid. The formation of such solid solutions may result in effective long-term immobilization. The molecular scale mechanism of RN incorporation in selected mineral phases is currently investigated at INE. The combination of various complementary spectroscopic techniques provides such molecular scale information. Most of the activities focus on the actinides, but the retention of long-lived fission products is also investigated.

#### Precipitation kinetics of celestite from supersaturated solutions of strontium sulfate in mixed flow reactors

The precipitation of strontium sulfate (SrSO<sub>4</sub>, celestite) from supersaturated aqueous solutions is of concern in a wide variety of fields such as oceanography, sedimentology, petroleum industry and nuclear waste disposal [1]. Impurities play a crucial role in the theory of crystallization in supersaturated solutions and the exclusion of foreign particles is of major importance in the study of precipitation kinetics. <sup>90</sup>Sr is one of the fission products from the <sup>235</sup>U decay series that is responsible for most of the heat and penetrating radiation in high-level waste. In order to predict interactions such as incorporation or adsorption of radionuclides in the most abundant strontium salt

celestite, it is necessary to explore both the kinetics and mechanism of precipitation. In this study, heterogeneous formation of celestite from supersaturated strontium sulfate solutions at near neutral pH and 20 ± 2°C has been studied in mixed flow reactor (MFR) experiments. The precipitation of celestite was investigated using stable supersaturated solutions seeded with SrSO<sub>4</sub> crystals and the rates of precipitation were measured from the concentration-time profiles.

#### Experimental and results

A MFR is a stirred reactor allowing continuous addition of reactants and removal of products. The tank is stirred to ensure a homogeneous suspension of the seed crystals within the reactor by using Teflon coated floating magnetic stirrer. Chemical analysis of the outlet solution gives information about the composition of the solution in the reactor tank.

In this work, the MFRs (45 mL volume) were first filled with seed crystals of celestite (SrSO<sub>4</sub>, puratronic, Alfa Aesar, Kandel). Before use, the seed crystals were sieved through a 50 µm sieve and their surface area was determined by N<sub>2</sub>-BET (0.99 m<sup>2</sup>/g). Aqueous strontium chloride and sodium sulfate with different saturation indexes (SI) were prepared from the corresponding salts. Sodium chloride (0.1 mol/L) was used to increase the ionic strength of the solutions. The solutions

Table 1: Results of MFR-experiments.

SI	R [10 <sup>-9</sup> mol m <sup>-2</sup> s <sup>-1</sup> ]
0.20	3.11
0.60	3.56
0.76	3.52
0.80	5.94
0.90	6.70
1.00	12.49
1.38	19.85

were fed in the reactor tank through different inlets with a flow rate of approx. 0.3 mL/min. Aliquots of the outlet solution were taken every day and analyzed by IC (anions) or ICP-OES (cations). Steady state was reached when the concentration of different species in the outlet solution was constant over 24 h. The determined precipitation rates as a function of the SI are presented in Table 1.

It was reported [2] that the strontium sulfate precipitation obeys a second-order rate equation at small and moderate supersaturations, whereas it may follow a first-order dependence at very low supersaturations. The rates determined in this study seem to follow a second order dependence. Additional experiments are needed to confirm this trend. The major difficulties related to MFR-experiments are the control of the flow rate and an accurate determination of the yield of precipitates at the end of the experiments. Future investigations will overcome these difficulties by collection and chemical analysis of the outlet solutions. From the volume and concentration of the effluent, the total amount of precipitated celestite will be calculated gravimetrically. Additional MFR-experiments will be performed in the presence of sea sand as seeding material to have a look at the effect of seeding surface chemistry. All these experiments will also be performed for the strontium carbonate system.

### **A thermodynamic entrapment model for the quantitative description of selenium(IV) coprecipitation with calcite.**

Selenium-79 is a long-lived fission product with a half-life of  $3.27 \cdot 10^5$  a [3]. It is formed e.g. by nuclear fission of  $^{235}\text{U}$ . Especially the oxidized Se species show only weak interactions with most common mineral surfaces and  $^{79}\text{Se}$  is usually expected to migrate unretarded through aquifer systems. Therefore  $^{79}\text{Se}$  is often considered a critical RN for the safe disposal of nuclear waste.

Calcite is a common mineral in many formations considered as potential host rocks for a nuclear waste disposal e.g. as component of clay stones (up to 20%) or as fracture filling

material in granitic rocks. Furthermore, it is a corrosion product of concrete based materials. Numerous studies have shown that especially Se(IV), in aqueous solution present as selenite anion ( $\text{Se(IV)O}_3^{2-}$ ), which is chemically and structurally similar to carbonate, interacts with calcite and may adsorb at the calcite surface or be incorporated into the calcite structure [4-8].

In last years' annual report [9] we reported coprecipitation experiments of Se(IV) with calcite and the corresponding X-ray spectroscopic investigation of the selenite incorporation species. Previous investigations showed that selenite is structurally incorporated into calcite, which leads to the formation of a  $\text{Ca}(\text{SeO}_3)_x(\text{CO}_3)_{(1-x)}$  solid solution. The constant partition coefficient,  $D_{\text{exp}} = 0.016 \pm 0.012$ , observed in coprecipitation experiments over a large range of selenite concentration ( $10^{-13}$  –  $10^{-4}$  mol/L) indicates that selenite incorporation into calcite can be described as an ideal solid solution between a virtual  $\text{CaSeO}_3$  endmember ( $\log_{10}K_{\text{exp}} = -6.7 \pm 0.4$ ) and calcite [9]. This year we focus on the comparison of experimental and theoretical results on selenite incorporation into calcite and the development of a consistent thermodynamic concept to describe the incorporation process. Additional batch adsorption and aragonite recrystallization experiments support the suggested entrapment model.

### **Experiments**

Batch type adsorption experiments are performed in pre-equilibrated calcite suspensions at pH 7.5, 8.3 and 9.8 containing 0.1 mol/L NaCl and 25 g/L calcite (0.51 m<sup>2</sup>/g, BET). The initial selenite concentration is  $3.4 \cdot 10^{-13}$  mol/L ( $^{75}\text{Se(IV)}$ ). Aragonite recrystallization experiments are performed starting from suspensions of 20 g/L self-synthesized aragonite (97% pure, XRD) containing 0.1 mol/L NaCl. The aragonite to calcite recrystallization rates of a pure and a  $10^{-4}$  mol/L selenite containing experiment are compared.

### **Atomistic calculations**

Density functional theory (DFT) calculations are applied to calculate the reaction enthalpy

of the substitution of selenite for carbonate in the bulk calcite structure, at the calcite (104) surface and at the calcite (104) surface in the presence of water. Empirical potential lattice dynamics calculations are used to estimate the effect of entropy on the bulk substitution.

### Results and discussion

Comparison of theoretical and experimental results for selenite incorporation into bulk calcite reveals a puzzling picture. While the calculated structural environment of selenium in calcite (Figure 1) is in perfect agreement with experimental observations [9], the thermodynamic interpretation of the substitution could hardly be more unlike. According to theory incorporation should be quasi impossible. The calculated partition coefficient is  $D_{\text{bulk}} = 5.2 \cdot 10^{-10}$ , and the corresponding endmember stability is  $\log_{10}K_{\text{bulk}} = 0.81$  (compared to experimental values:  $D = 0.016$  and  $\log_{10}K = -6.7$ ).

This discrepancy can be overcome by considering selenite incorporation into the calcite surface as an intermediate reaction step in the incorporation process. Surface incorporation, or ion exchange, has been shown previously to be the relevant process in selenite-calcite adsorption experiments [5,6].

Indeed, DFT results qualitatively confirm that incorporation into the calcite (104) surface is energetically much more favorable than incorporation into the bulk calcite structure. The

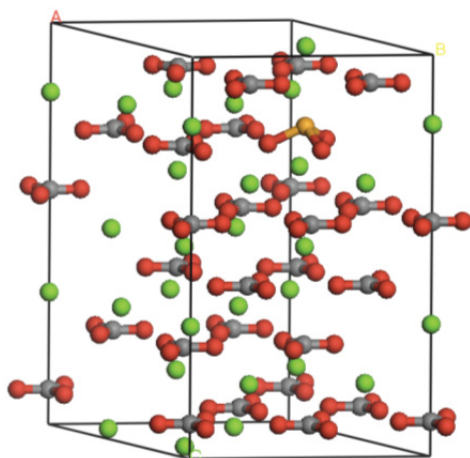


Fig. 1: 2x2x1 supercell of calcite with a single selenite (orange) substitution.

corresponding  $\log_{10}K_{\text{surface}}$  values of the  $\text{CaSeO}_3$  surface endmember being -8.23 or -3.74, depending on whether a calcite-vacuum- or a calcite-water-interface is considered. It's important to note that the surface  $\text{CaSeO}_3$  endmember is not a bulk phase and correspondingly its solubility product  $\log_{10}K = -6.7$ , which is taken from the experimental results, is not a bulk thermodynamic property. It can only be used to calculate the composition of the calcite surface in contact with a selenite containing solution. To accomplish entrapment it is assumed that a surface solid solution, with a composition corresponding to the surface endmember stability, is entrapped by consecutive crystal layers upon solid solution growth. This implies an analogy between adsorption and coprecipitation, and indeed if we use the results from adsorption experiments at pH 7.5 and 8.3 (pH in coprecipitation experiments is 7.6 to 8) and interpret them in terms of a surface monolayer partition coefficient, the results:  $D = 0.002 \pm 0.0015$  and  $D = 0.02 \pm 0.015$  are within uncertainty equal to the partition coefficient observed in coprecipitation experiments,  $D_{\text{exp}} = 0.016 \pm 0.012$ .

A consequence of the suggested entrapment model is that a certain amount of energy is required to accomplish entrapment, i.e. to transform an energetically favorable surface solid solution into an energetically unfavorable bulk solid solution. This entrapment energy can be calculated from the Gibbs free energies of the surface and the bulk endmember, and the molefraction X of selenite in calcite:

$$\Delta G_{\text{entrap}} = X[G(\text{CaSeO}_3_{\text{bulk}}) - G(\text{CaSeO}_3_{\text{surface}})]$$

In the aragonite recrystallization experiment, calcite is due to the stabilities of aragonite and calcite, intrinsically supersaturated at  $SI(\text{calcite}) = 0.14$ . Consequently, aragonite dissolves in the favor of the more stable calcite. In the selenite containing experiment ( $10^{-4}$  mol/L) the supersaturation is not sufficient to overcompensate the entrapment energy, and indeed, during the 420 days experimental period of the recrystallization experiment a quasi-complete inhibition of calcite growth has been observed (Figure 2).

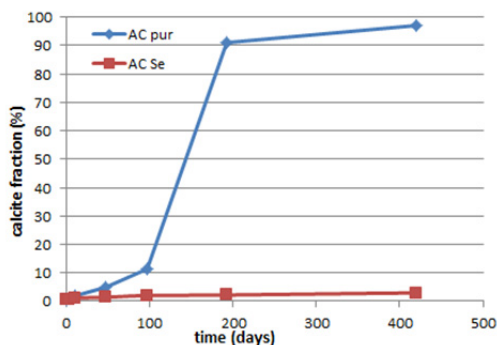


Fig. 2: Aragonite to calcite recrystallization experiments. While in the pure system (AC pur) aragonite dissolves in favor of the more stable calcite, calcite growth is inhibited in the selenite containing ( $10^{-4}$  mol/L) system (AC Se).

### The influence of nitrate on the Eu(III)/calcite system

The long term safety of nuclear waste repositories is mainly governed by the retardation potential of the host rock formation. Therefore, the knowledge of interactions of primary and secondary mineral phases with radionuclides on a molecular scale is essential for safety assessments. Calcite is present up to high amounts in clay formations and is also generated by the degradation of cementitious material as a secondary phase [10,11]. In geological environments, ground and pore waters contain considerable amounts of inorganic and organic anions like  $\text{NO}_3^-$ ,  $\text{CO}_3^{2-}$ ,  $\text{SO}_4^{2-}$ ,  $\text{Cl}^-$ , propionate or lactate [12,13]. The presence of these ligands strongly affects the speciation and mobility of metal ions and other RNs in solution and hence their interactions with mineral phases. Likewise, anions can influence mineral interfaces, e.g. by surface coverage or charge balancing. For this study, nitrate was chosen since it is an isostructural analogue to carbonate and also a contaminant of nuclear waste forms resulting from various waste treatment processes.

#### *Ln(III) and An(III) uptake by calcite*

Earlier studies [14,15] showed that trivalent Eu, Cm and Am can be incorporated into the crystal structure of calcite. For Eu, three distinct sites could be determined (Figure 3). By measurement of luminescence lifetimes, one inner-sphere sorbed species ( $2 \text{H}_2\text{O}$ ) and two bulk incorporated Eu(III) ions were identified.

The aim of this work was to study the influence of nitrate on the formation of solid solutions. For this, site-selective time-resolved laser fluorescence spectroscopy (TRLFS) and high resolution atomic force microscopy (AFM) were used.

#### *Site-selective TRLFS*

The Figure 4 presents the spectra of Eu-doped calcite samples prepared in the presence of nitrate. The spectra of both the coprecipitation and the recrystallization samples are very similar, exhibiting one single excitation peak at  $\lambda_{\text{exc}} = 579.95$  nm. By direct excitation, the  ${}^7\text{F}_1$  emission band was found to be maximum split, while the  ${}^7\text{F}_2$  shows 4-fold splitting, both indicating a tetragonal or less symmetric environment [16] of the metal ion. The mean lifetime of this species was determined as  $\tau = 629 \pm 47 \mu\text{s}$ , i.e. one water molecule is left in the first hydration sphere of Eu(III).

#### *Atomic force microscopy*

High resolution AFM imaging was carried out with image size ranging from  $5 \times 5 \mu\text{m}$  to  $10 \times 10 \text{ nm}$  to visualize surface modifications of calcite caused by nitrate. Freshly cleaved calcite single crystals exhibit a smooth surface with step edges of straight lined shape and oxygen atoms protruding out the (104) plane. In contact with  $\text{NaNO}_3$ , major changes in the appearance can be observed. At low concentrations ( $10^{-7}$  to  $10^{-6}$  mol/L) of nitrate, areas of soft consistency arise on the crystals with different chemical compositions regarding their phase. An increase of nitrate concentration to  $10^{-5}$  mol/L results in a gel-like layer which is

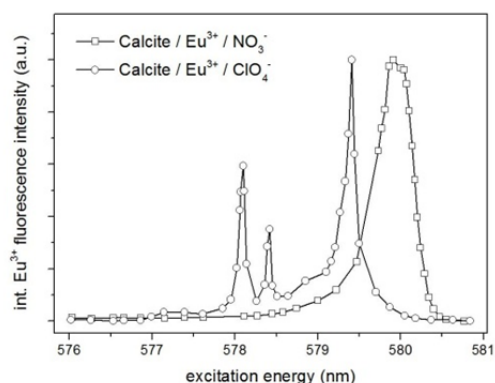


Fig. 3: TRLFS excitation spectra of the Eu(III)/calcite system in the presence and in the absence of nitrate.

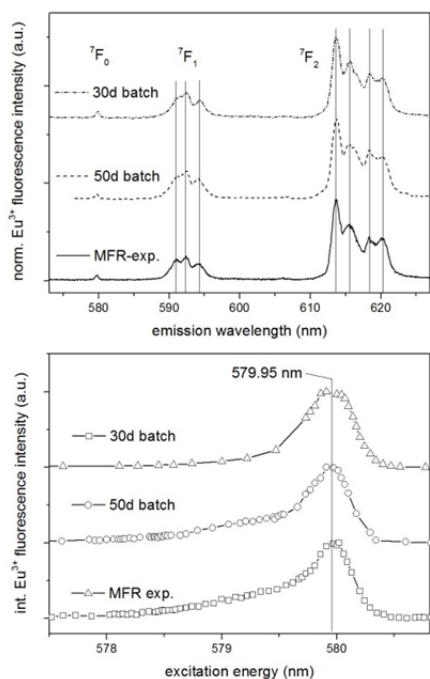


Fig. 4: Excitation spectra of nitrate-experiments with one peak at 579.95 nm (top) and emission spectra of the respective Eu-nitrate species (bottom).

easily scratched away by the tip of the cantilever, making the harder calcite surface beneath reappear. At even higher concentration ( $10^{-3}$  mol/L), also the step edges become rounded and frayed. In accordance with TRLFS, Eu(III) seems to be incorporated into that layer.

### Clay mineral coprecipitation with Zr(IV)

In HLW repositories hosted by clay rock, reducing conditions are expected to prevail so that the long-lived and radiotoxic actinides (e.g., Pu) may also be present in tetravalent oxidation state [17]. The retention of trivalent actinides (e.g., Am, Cm) by surface reaction and by structural incorporation has been documented in the literature, but the retention of tetravalent cations deserved less attention. Clay minerals can form by corrosion of HLW glass in contact ground water. These minerals are known to have a high affinity for trivalent *f*-elements. Furthermore, it was shown that trivalent lanthanides [18] (non-radioactive chemical surrogates for actinides) can occupy octahedral lattice sites in hectorite, a magnesian smectite identified in glass corrosion experiments [19]. The present study reports on

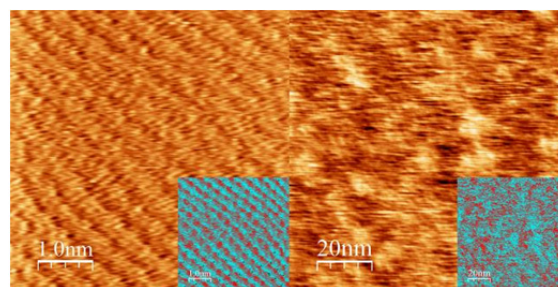


Fig. 5: Unaltered calcite (104) face with protruding oxygen atoms (left) and calcite surface after 20 h contact with 1 mmol/L  $\text{NaNO}_3$  (right).

the tetravalent cation Zr(IV) incorporation in hectorite by coprecipitation.

### Experimental

Hectorite was synthesized in the presence of Zr(IV) (sample ZrCopHec) following a multi-step synthesis procedure [18]. A freshly precipitated Zr(IV)-containing brucite precursor was aged in the presence of LiF and a silica sol for three days. Separately, a Zr(IV)-containing brucite (ZrCopBru) was prepared under identical conditions.

### Results and discussion

The structure of both compounds was characterized by XRD. The samples consist either of brucite (ZrCopBru) or of clay mineral (ZrCopHec), no other separate phase could be detected. SEM micrographs (data not shown) showed that the samples consist of crystallites of small size having a layered structure.

Zirconium *K*-edge XAS data were collected at the INE-Beamline. The XANES regions of the data collected for  $\text{ZrO}_2$ , the Zr(IV) aqueous ions (sample  $\text{Zr(IV)}_{\text{aq}}$ ), ZrCopBru and ZrCopHec are presented in Figure 6. The white line (WL) features are different in each sample, pointing to different local chemical environments. Furthermore, the WL in ZrCopBru and ZrCopHec are broad and split. These features are attributed to degenerate levels in the valence band, the broadness and splitting increasing for decreasing Zr site symmetry [19]. Obviously, the Zr(IV) chemical environment is different in all samples, meaning that Zr(IV) is sequentially occluded in different phases during the hectorite synthesis procedure.

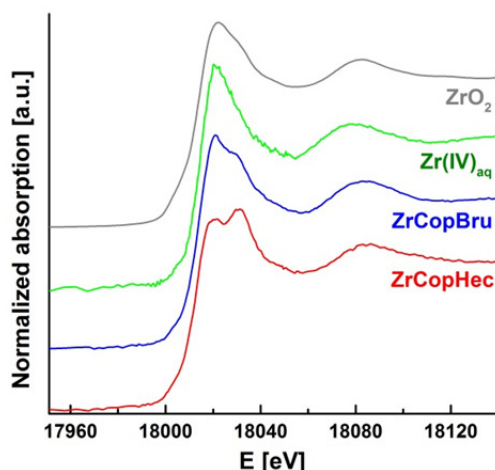


Fig. 6: XANES region of the X-ray absorption spectroscopy data collected for ZrCopBru and ZrCopHec and the references compounds.

Information on the chemical environment was obtained by fitting the EXAFS region data (Figure 7). Zirconium is ligated to O atoms located at  $d(\text{Zr-O}) = 2.18 \text{ \AA}$  in ZrCopBru. Next nearest neighbors consist of 2 Mg subshells. These results can be interpreted as Zr located in a brucite-like environment where the Zr and Mg polyhedra share faces and edges. The Zr local chemical environment changed upon hectorite crystallization. The O shell is located at shorter distance ( $d(\text{Zr-O}) = 2.07 \text{ \AA}$ ) and next nearest neighbors consist of Mg ( $d(\text{Zr-Mg}) = 3.04 \text{ \AA}$ ) and Si ( $d(\text{Zr-Si}) = 3.22 \text{ \AA}$ ) shells. All three shells are located at identical distances reported for octahedral Mg in hectorite, with almost identical coordination numbers [20]. Zirconium is thus very likely

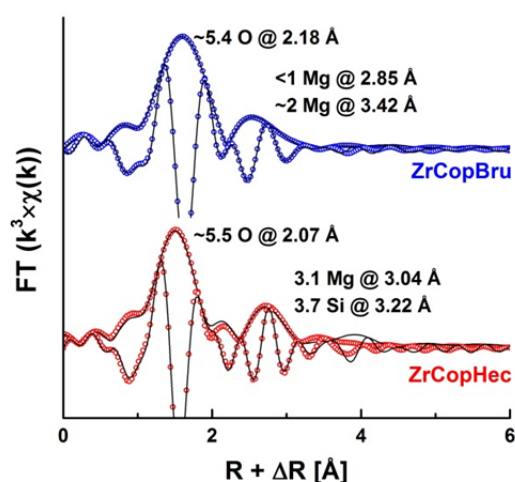


Fig. 7: Fourier transforms and the corresponding fit of the EXAFS data collected for the samples ZrCopBru and ZrCopHec.

substituting for Mg at the same position in hectorite. These results show the possibility to incorporate tetravalent elements at clay octahedral site, but do not allow to conclude about thermodynamic stability. Further studies are needed to address this issue.

## References

- [1] Hamdona, S. K. et al., Desalin. Water Treat., 24: 55 (2010).
- [2] Yeboah, Y. D. et al., J. Crystal Growth, 135: 323 (1994).
- [3] Jörg, G. et al., Appl. Radiat. Isot., 68: 2339 (2010).
- [4] Aurelio, G. et al., Chem. Geol., 270: 249 (2010).
- [5] Cheng, L. W. et al., Surf. Sci., 382: L690 (1997).
- [6] Cowan, C. E. et al., Geochim. Cosmochim. Acta, 54: 2223 (1990).
- [7] Montes-Hernandez, G. et al., Chem. Geol., 290: 109 (2011).
- [8] Wang, X. K. et al., Appl. Radiat. Isot., 62: 1 (2005).
- [9] Finck, N. et al., In: Annual Report 2011, Institute for Nuclear Waste Disposal, Geckes H., Stumpf T., Eds KIT Scientific Publishing, Karlsruhe (2012).
- [10] Hartmann, E. et al., Radiochim. Acta, 96: 699 (2008).
- [11] Glasser, F. P. et al., Cem. Concr. Res., 38: 226 (2008).
- [12] Leroy, P. et al., Geochim. Cosmochim. Acta, 71: 1087 (2007).
- [13] Courdouan, A. et al., Appl. Geochem., 22: 2926 (2007).
- [14] Stumpf, T. et al., Geochim. Cosmochim. Acta, 73: A1286 (2009).
- [15] Schmidt, M. et al., Angew. Chem. Int. Ed., 47: 5846 (2008).
- [16] Hemmila, I. and Laitala, V. J., Fluoresc., 15: 529 (2008).
- [17] Runde, W., Los Alamos Science, 26: 392 (2000).
- [18] Finck, N. et al., Environ. Sci. Technol., 43: 8807 (2009).
- [19] Jollivet, P. et al., J. Nucl. Mater., 420: 508 (2012).
- [19] Li, P. et al., Phys. Rev., B48: 10063 (1993).
- [20] Seidl, W. and Breu, J., Z. Kristallogr., 220: 169 (2005).

## 6 Applied studies: Radionuclide retention in the multi-barrier system

Long-term safety of a nuclear waste disposal depends on the multi-barrier system which consists of technical and geo-technical barriers such as the waste forms, canisters, backfill and sealing of the mined openings as well as on the natural barrier function of the host rock. A series of applied studies on subsystems of the multi-barrier system are performed, which cover a variety of components with specific characteristics and properties. The investigations and quantifications of their respective retention functions require specific approaches, methods, analytical techniques and models. Achievements presented in this chapter cover the mobilization of radionuclides from spent nuclear fuel in high pH solutions under the conditions of the Belgian “Supercontainer Design”. Measurements of the fission gas release from an irradiated PWR fuel rod segment are presented. These measurements contribute to the 7<sup>th</sup> FP project FIRST-Nuclides, dealing with the fraction of radionuclides rapidly released from spent nuclear fuel. With respect to non-heat producing wastes, the thermodynamic data of long-term metastable magnesium hydroxo (chloro-) carbonates and the retention of Cm(III) and Eu(III) on stable solid phases in the system Mg-Na-Cl-H<sub>2</sub>O have been quantified. Application of basic research on disposal safety is shown in the context of the “Preliminary Safety Analysis Gorleben (vSG)” project and the database project “THEREDA” which provides consistent and reliable thermodynamic reference data for all potential German host rocks (salt, clay, crystalline rocks). Migration studies cover the colloid-associated RN transport under near-natural flow conditions in the scope of the Colloid Formation and Migration (CFM) project at the Grimsel Test Site and the influence of the mineral/fracture surface roughness on the colloid retention investigated by atomic force microscopy (AFM). Modelling includes the simulation of thermo hydro mechanic (THM) processes in the near-field of a HLW disposal in rock salt as well as the simulation of flow and transport phenomena in crystalline host rocks. The THM and some specific transport studies rely on the ADINA code, whereas for reactive transport modelling the codes FASTREACT and PHREEQC / PHAST are used. Simulations are presented for Np(V) migration in a single fracture using FASTREACT and leaching of cemented waste forms with PHREEQC.

### 6.1 Examination of highly radioactive waste forms

*E. Bohnert, E. González-Robles Corrales, B. Kienzler, A. Loida, V. Metz, and N. Müller*

#### Corrosion behaviour of spent nuclear fuel in high pH solutions

Assessing the performance of spent nuclear fuel (SNF) in a geological disposal system requires the understanding and quantification of the radionuclide release. The release of the radionuclides into water will be constituted by two main processes:

- i) short term release of the so-called instant release fraction (IRF).
- ii) long term release dominated by the dissolution of the UO<sub>2</sub> grains, which is referred as matrix contribution.

In Belgium, Boom clay is considered as host rock for disposal of high level wastes. The

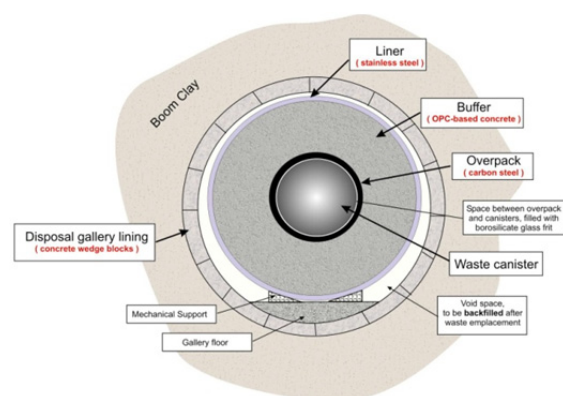


Fig. 1: Belgian Supercontainer design (after [2]).

thermomechanical, hydraulic as well as geochemical properties of this host rock are under investigation since 30 years in the HADES underground laboratory.

For SNF, a specific concept was developed, the so-called, Belgian "Supercontainer Design", see Fig. 1. It comprises the encapsulation of the waste in carbon steel overpacks surrounded by a concrete buffer called "supercontainer" [1,2].

After re-saturation of the engineered barriers, the pore water composition will be altered by interactions with concrete. The altered pore water is simulated by a "young cement water with calcium (YCWCa)" solution (pH of 13.5) that represents a certain degree of concrete alteration. The YCWCa is composed mainly by KOH and NaOH, and in a minor concentration by Na<sub>2</sub>SO<sub>4</sub>, Ca(OH)<sub>2</sub> and CaCO<sub>3</sub>.

Due to the slow corrosion rate of the canister materials [3] under highly alkaline conditions, the SNF could come in contact with the evolved highly alkaline solution.

The aim of the experimental work is to study the corrosion behaviour of the UO<sub>2</sub> matrix in YCWCa in presence of externally applied H<sub>2</sub> overpressure. In these experiments, the contributions from the gap between SNF pellets and the Zircaloy cladding, contributions of fracture surfaces and grain boundaries should not dominate the radionuclide release processes. This is achieved by using single SNF fragments, enabling an effective contact between the UO<sub>2</sub> matrix and the solution. Specific objectives of the investigations are the quantification of the:

- evolution of pH and the redox potential in the YCWCa – SNF system;
- dissolution rate of the SNF matrix;
- the associated release and / or retention of radionuclides as function of time and specific surface properties.

## Experimental

Five corrosion experiments with SNF fragments are performed in YCWCa solutions (pH of 13.5) under H<sub>2</sub> overpressure up to 3.2 bars in 250 mL Ti lined stainless steel autoclaves.

The composition of the YCWCa was defined by SCK-CEN [4], see Table 1:

Table 1: Composition of YCWCa.

Compound	Composition (mM)
KOH	370
NaOH	136
Na <sub>2</sub> SO <sub>4</sub>	2.0
Ca(OH) <sub>2</sub>	0.4
CaCO <sub>3</sub>	0.3

The experiments started after a 4 days cleaning procedure with DIW and wash cycles over 21 days with YCWCa. The release of radionuclides was measured by sampling and subsequent analyse of the free gas phases and the solutions during the cleaning and wash cycles. This procedure will be repeated after finishing the experiment under H<sub>2</sub> overpressure that have a duration time of and 58, 181, 253, 343 and 426 days. Detailed descriptions of the sampling and analytical procedures are given elsewhere [5].

## Material

A commercial PWR UO<sub>2</sub> SNF irradiated during four cycles in Gösgen power plant (Switzerland) and achieving a mean average burnup of 50.4 MWd/kg<sub>HM</sub> was selected to be used in the experiments. The SNF was discharged on May 23, 1989 that implies a cooling time period of 23 years. More details about the SNF can be found elsewhere [6].

Two cladded SNF segment, named 2K11a and 2K11b, were used to provide the fragments necessities to carry out the experiment. Both pellets were already corroded during the first (2007-2008) and the second phase (2009-2010) of this project.

The cladded SNF segment was fixed in a sample holder to be decladded. The Zircaloy cladding was cut by means of a manipulator hand operated metal saw. Afterwards, the selected fragments were isolated to characterise them. Fig. 2 shows the complete procedure followed.

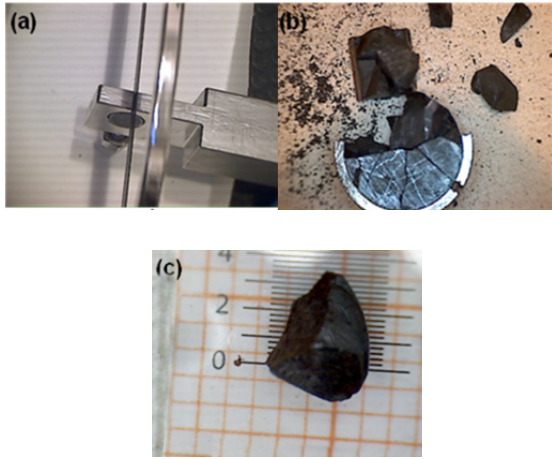


Fig. 2: Different steps performed to obtain a fragment from a pellet. (a) Device for decladding the SNF segment 2K11a by means of a metal saw and an adapted sample holder. (b) SNF segment after cutting of the Zry-cladding and released particles. (c) One of the selected SNF fragments to be used in the experiments.

## Characterisation

A total of 5 individual fragments were selected and denoted as following: K11 F1, K11 F2, K11 F3, K11 F4 and K11 F5.

The fragments were weighted and their volume was calculated considering their weight as well as the density of the  $\text{UO}_2$  pellet after fabrication ( $d = 10.41 \text{ g/cm}^3$ ). The results are reported in Table 2.

The geometric surface area,  $S_{GEO}$ , of the fragments was determined using five to nine images of each fragment made in different positions with the help of an optical microscope. Then, the different faces observed on the images, were delimited and their surface area values were calculated, see Fig 3. Finally, the  $S_{GEO}$  was the sum of all faces surface area.

The surface of the SNF presents some irregularities as porous or fractures that will increase the  $S_{GEO}$  obtaining the specific surface area,  $S_{spec}$ . The images obtained by optical microscopy did not allow to differentiate and determine the surface area of these pores or/and fractures.  $\text{N}_2$ -BET surface area analysis technique is not available at INE's shielded box-line.

Taking a look in the bibliography, there are publications in which the  $S_{GEO}$  is correlated with the  $S_{spec}$  (obtained by  $\text{N}_2$ -BET method) by using a, so-called, roughness factor ( $R$ ), see eq. 1:

$$S_{spec} = R \times S_{GEO} \quad (1)$$

Gray and Wilson [7] proposed a roughness factor of 3 for SNF. In a recent study carried out by Iglesias et al. [8] taking into account SNF samples as well as analogous of SNF, they proposed a roughness factor of 3.5.

The specific surface area of each fragment was calculated by applying both roughness factor of 3 and 3.5. The results are summarized in Table 2.

Table 2: Physical characterisation of SNF fragments.

Sample	K11 F1	K11 F2	K11 F3	K11 F4	K11 F5
W (g)	0.136	0.225	0.174	0.169	0.205
V ( $\text{cm}^3$ )	0.013	0.022	0.017	0.016	0.020
$S_{GEO}$ ( $\text{m}^2$ )	$2 \cdot 10^{-5}$	$3 \cdot 10^{-5}$	$2 \cdot 10^{-4}$	$3 \cdot 10^{-5}$	$2 \cdot 10^{-5}$
* $S_{spec}$ ( $\text{m}^2/\text{g}$ )	$4 \cdot 10^{-4}$	$4 \cdot 10^{-4}$	$4 \cdot 10^{-4}$	$5 \cdot 10^{-4}$	$3 \cdot 10^{-4}$
** $S_{spec}$ ( $\text{m}^2/\text{g}$ )	$5 \cdot 10^{-4}$	$5 \cdot 10^{-4}$	$4 \cdot 10^{-4}$	$6 \cdot 10^{-4}$	$4 \cdot 10^{-4}$

\*corresponds to  $R=3$ .

\*\*corresponds to  $R=3.5$ .

## Fission gas measurements of irradiated PWR fuel rod segment.

The IRF is due to the segregation of a part of the radionuclide inventory to the gap interface between the cladding and the pellet, the fractures as well as to grain boundaries. The radionuclides that will be segregated are: fission gases (Kr and Xe), volatiles elements ( $^{129}\text{I}$ ,  $^{137}\text{Cs}$ ,  $^{135}\text{Cs}$ ,  $^{36}\text{Cl}$  and  $^{79}\text{Se}$ ) and segregated metals ( $^{99}\text{Tc}$  and  $^{126}\text{Sn}$ ) [9].

The degree of segregation of the various radionuclides is highly dependent on in-reactor fuel operating parameters such as linear power rating, fuel temperature, burn-up, ramping processes, and interim storage time.

In the case of the fission gases, the gas release occurs by diffusion to grain boundaries, grain growth accompanied by grain boundary sweeping, gas bubble interlinkage and intersection of gas bubbles by cracks in the fuel. The fission gas release is more correlated to the linear heat rating, which is also correlated to fuel temperature, than to the burn-up of the SNF [9]. The conditions during irradiation ensure that linear heat ratings are kept low and the fission gas release is minimised. The radionuclides located in the gap interface will be released after some weeks, whereas a complete release of the radionuclides segregated in the grain boundaries will take several months or even years.

During the last decade three European projects, SFS [10], NF-PRO [11] and MICADO [12] were carried out, in which, the IRF concept was revised and redefined as the radionuclide inventory located within microstructures with low confinement properties: fuel plenum, gap zone, fracture surfaces, the rim zone with high burn-ups structures and grain boundaries [11].

The present work aims to analyse the fission gases (Xe and Kr) released into the plenum of a  $UO_2$  fuel rod segment, which was irradiated during four cycles in Gösgen power plant and achieved a mean average burnup of 50.4 MWd/kg<sub>HM</sub>.

## Experimental procedure

The necessary device to perform the puncturing of the fuel rod was not available at INE. Therefore, the fuel rod segment was transported to the Joint Research Centre - Institute for Transuranium Elements (JRC-ITU) to do the puncturing inside a hot cell.

Once the puncturing of the fuel rod segment was performed, the pressure was measured and the gases were collected in stainless steel single-ended miniature sampling cylinders. The SS-4CS-TW-50 Swagelok gas sampling cylinders were characterised by a volume of 50 mL, a length of 159 mm, an outer diameter for tube fitting of 9.5 mm and an inner diameter for tube socket weld connection of 6.4 mm, see Fig. 3a. Since the volume of the



Fig. 3: a) stainless steel single-ended miniature sampling cylinder used to collect gas samples; b) GAM400 quadrupole gas mass spectrometer.

tubes is known, the total amount of gas can be calculated.

The cylinders were carried back to KIT-INE, where the gases were analysed by means of a quadrupole gas mass spectrometer (gas MS).

The gas MS (GAM400, In Process Instruments, Bremen, Germany) was equipped with a Faraday and SEV detector and a batch inlet system, see Fig. 4b. The batch-type gas inlet system was optimised for low gas sample consumption. Within the gas dosage and inlet system, the total gas pressure was controlled at four successive positions. It applied three different expansion-volumes to charge relatively low gas contents in the desired pressure range. Ten scans of each gas sample were measured, using the SEV-detector, and the mean value was taken. Calibration of the gas MS analysis was performed in the same pressure range as the respective range for analyses of the sample aliquots.

## Results

The average values of gases measured in the samples taken from the puncturing test of the fuel rod segment are presented in Table 3.

Table 3: Physical characterisation of SNF fragments.

Gas	Concentration (vol.%)	Volume (cm <sup>3</sup> )
Ar	0.28	0.40
CO <sub>2</sub>	0.13	0.18
N <sub>2</sub>	1.3	1.87
O <sub>2</sub>	0.31	0.44
Kr	1.5	2.1
Xe	18	26
He	78	111

The contents of O<sub>2</sub> and N<sub>2</sub> in the gas composition (0.31 and 1.3 vol%, respectively) are related to air contamination during the sampling of the cylinders. The gas released from the plenum of the punctured fuel rod segment contains a certain amount of CO<sub>2</sub>. In the past, similar CO<sub>2</sub> contents were observed in various fuel rod puncturing tests performed by different institutes, i.e. JRC-ITU (Germany), PSI (Switzerland), SCK-CEN (Belgium) and Studsvik (Sweden). The measured contents of Kr and Xe will be compared to their calculated total inventory in the 50.4 MWd/kg<sub>HM</sub> fuel rod segment, in order to determine the percentage of the fission gas released into the plenum.

## References

- [1] Gens, R. et al., *Journal de Physique IV (Proceedings)*, 136: 13 (2006).
- [2] van Humbeeck, H., *ESDRED International Technical Conference on Practical Aspects of Deep Radioactive Waste Disposal*, Czech Technical University, Prague (2008).
- [3] Kursten, B. et al., *Sixth International Conference on the Management and Disposal of Radioactive Waste*, Luxembourg, 428 (2004).
- [4] Cachoir, C., *Preparation of Evolved Cement Water (ECW) and Young Cement Waters (YCW and YCWCa) for the Super-container experiments*, SCK-CEN Work Instruction IW.W&D.0009 (2006).
- [5] Grambow, B. et al., *Forschungszentrum FZKA report 5702* (1996).
- [6] Loida, A. et al., *Mat. Res. Soc. Symp. Proc.*, 1193: 597 (2010).
- [7] Gray, W. J., Wilson, C. N., *Spent fuel dissolution studies FY 1991 to 1994*. Richland, Washington, USA: Pacific Northwest National Laboratory. Technical Report, PNL-10540 (1995).
- [8] Iglesias, E., Quiñones, J., *Analogous materials for studying spent nuclear fuel: The influence of particle size distribution on the specific surface area of irradiated nuclear fuel*. *Applied Surface Science*, 254: 6890 (2008).
- [9] Johnson, L. et al., *Spent fuel source-term model for assessing spent fuel performance in geological disposal. Part I: Assessment of the instant release fraction*, *Journal of Nuclear Materials*, 346: 56 (2005).
- [10] Poinssot, C. et al., *Final report of the European project Spent Fuel Stability under repository conditions*, vol. CEA-R-6093, Saclay, France. (2005).
- [11] Grambow, B. et al., *Final Synthesis Report for NF-PRO: "Understanding and Physical and Numerical Modelling of the Key Processes in the Near-Field and their Coupling for Different Host Rocks and Repository Strategies"*. RTD Component 1: *Dissolution and release from the waste matrix*, F16W-CT-2003-02389, European Commission, Brussels, Belgium (2008).
- [12] Grambow, B. et al., *MICADO, Model uncertainty for the mechanism of dissolution of spent fuel in nuclear waste repository*, *Final activity report*, European Commission, Brussels, Belgium, (2010).

## 6.2 Non-heat producing waste forms and barrier materials

M. Altmaier, E. Bohnert, C. Bube, S. Hilpp, B. Kienzler, V. Metz, M. Plaschke, T. Rabung, D. Schild, M. Schlieker, E. Soballa and M. Wiedemann.

### Retention of Cm(III) and Eu(III) on Stable Solid Phases in the System Mg-Na-Cl-H<sub>2</sub>O

Retention of actinides in the near field is critical for the long-term disposal and storage of radioactive waste in geological salt deposits. Under reducing conditions, which develop after closure of deep underground repositories for nuclear waste, actinides are expected to prevail in tri- and tetravalent redox states. There is currently a strong interest in developing backfill materials which provide favorable chemical conditions with respect to low actinide solubility and significant actinide retention capacities. For decades, a combination of Mg-oxychloride ( $\text{Mg}_2(\text{OH})_3\text{Cl}\cdot 4\text{H}_2\text{O}(\text{s})$ , so-called Sorel phase) and brucite ( $\text{Mg}(\text{OH})_2(\text{s})$ ) is used as building material in conventional salt mines and currently discussed in concepts for sealing of radioactive waste repositories in rock salt [1,2]. At 25° C, brucite and Mg-oxychloride are the thermodynamically stable solid phases in the system Mg-Na-Cl-H<sub>2</sub>O, besides halite ( $\text{NaCl}(\text{s})$ ) and bischofite ( $\text{MgCl}_2\cdot 6\text{H}_2\text{O}(\text{s})$ ) [2,3] (Fig. 1). For the Asse II salt mine (Lower Saxony, Germany) and the Waste Isolation Pilot Plant (New Mexico, USA), where low level and intermediate level radioactive waste products are emplaced, brucite / Sorel based materials and MgO are used as sealing material and engineered buffer, respectively. In contact with NaCl or MgCl<sub>2</sub> dominated salt brines, these materials buffer the pH at 8 – 9, and scavenges CO<sub>2</sub> potentially produced by microbial degradation of organic waste constituents [1].

We studied the retention of a trivalent actinide (Cm(III)) and a trivalent lanthanide (Eu(III)) by brucite and Mg-oxychloride, at room temperature. Various batch experiments were prepared with pure MgCl<sub>2</sub> and mixed NaCl–MgCl<sub>2</sub> solutions as background electrolytes. In the brucite experiments, the ionic strength was adjusted to 0.15, 1.2 and 5.2 mol·(kg H<sub>2</sub>O)<sup>-1</sup>, and in the experiments with Mg-oxychloride it was adjusted to 9.9,

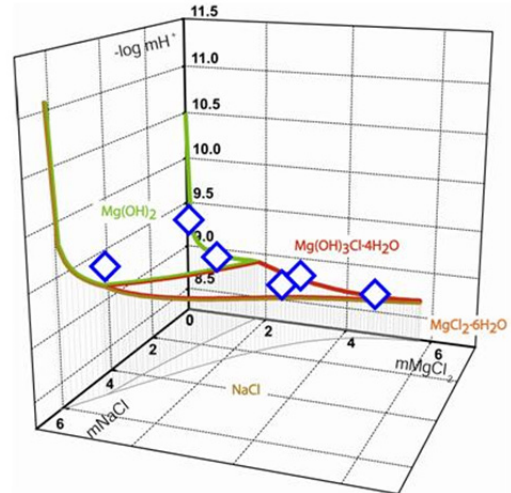


Fig. 1: Studied sorption systems, indicated by diamonds, in the stability fields of brucite ( $\text{Mg}(\text{OH})_2(\text{s})$ ) and Mg-oxychloride ( $\text{Mg}_2(\text{OH})_3\text{Cl}\cdot 4\text{H}_2\text{O}(\text{s})$ ) at 25°C.

10.0 and 15.0 mol·(kg H<sub>2</sub>O)<sup>-1</sup>, respectively. In presence of brucite and Mg-oxychloride, the specific pH<sub>c</sub> values were fixed in a disposal relevant range of 8.7 < pH<sub>m</sub> < 9.4 (Fig. 1). After a pre-equilibration of at least two weeks, the suspensions were doped with Eu(III). Brucite experiments were doped with  $\leq 7\cdot 10^{-9}$  mol·(kg H<sub>2</sub>O)<sup>-1</sup>, Mg-oxychloride experiments with  $\leq 7\cdot 10^{-7}$  mol·(kg H<sub>2</sub>O)<sup>-1</sup> per batch, to ensure Eu(III) concentrations considerably below the solubility of  $(\text{Eu})(\text{OH})_3(\text{c})$ . For the different MgCl<sub>2</sub> and NaCl–MgCl<sub>2</sub> solutions, three sorption experiments and one blank experiment were prepared and sampled continuously for each V/m ratio ( $10 \leq \text{V}/\text{m} \leq 10000 \text{ mL}\cdot\text{g}^{-1}$ ) and doping concentration. All experiments were prepared and stored in Ar gloveboxes under exclusion of CO<sub>2</sub> and O<sub>2</sub>. To determine sorption species and the aqueous speciation of the studied systems, time-resolved laser fluorescence (TRLFS) measurements were performed with  $1\cdot 10^{-7}$  mol·(kg H<sub>2</sub>O)<sup>-1</sup> Cm(III) per sample.

Brucite (BioUltra >99%) was purchased from Fluka and Mg-oxychloride was synthesized by transformation of brucite in concentrated

MgCl<sub>2</sub> solution. Brucite and Mg-oxychloride were characterized using DTA-TG (Netzsch STA409C/CD), Raman spectroscopy (Bruker Senterra), SEM-EDX (Quanta 650 FEG, FEI), XPS (ULVAC-PHI) and XRD (D8 Advance diffractometer, Bruker AXS). The molal H<sup>+</sup> concentration (pH<sub>m</sub>) of the suspensions was determined with combination pH electrodes (type Orion Ross, Thermo Scientific). To convert the operational “measured pH<sub>exp</sub>” values, the approach of Altmaier et al. [3] was applied. Eu(III) concentrations were determined by ICP-MS (X-Series II, Thermo Scientific). Cm(III) fluorescence spectra were collected using a Nd:YAG laser (Continuum Surelite II 10 Hz) pumping a dye laser (Narrowscan Dye Laser, Radiant Dyes).

In the macroscopic sorption experiments and in the TRFLS measurements a strong retention of Eu(III) and Cm(III) of ≥ 95.5% (Rs >> 210 mL·g<sup>-1</sup>) and ≥ 99.5% is determined, respectively. Since the Eu(III) concentration decreased to below the ICP-MS detection limit of 3·10<sup>-10</sup> mol·(kg H<sub>2</sub>O)<sup>-1</sup> within less than a week, the reported Rs value represents a lower limit for the retention by brucite. A less pronounced retention of Eu(III) and Cm(III) is observed in the experiments with Mg-oxychloride (Rs = 24 – 30 ± 10 mL·g<sup>-1</sup>). Laser fluorescence spectra of Cm(III) / brucite / brine suspensions show a significantly shifted emission band at 609 nm (Fig. 2). Peak deconvolution of the spectra reveals the formation of two sorption species. The considerable red shift in relation to the Cm(H<sub>2</sub>O)<sub>9</sub><sup>3+</sup> and the relatively long fluorescence life times of the spe-

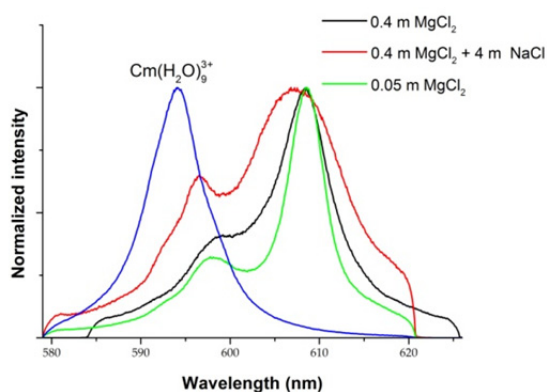


Fig. 2: Laser fluorescence spectra of Cm(III) / brucite / MgCl<sub>2</sub> and NaCl-MgCl<sub>2</sub> suspensions in comparison to the spectrum of the hydrated Cm<sup>3+</sup> ion.

cies (> 198 ± 25 μs first species, > 67 ± 5 μs second species) indicate incorporation of Cm(III) into the brucite structure. Measured spectra of Cm(III) / Mg-oxychloride / brine suspensions do not allow an unambiguous determination of Cm(III) sorption species.

The observed retention of Cm(III) and Eu(III) by brucite at I = 0.15 to 5.2 mol·(kg H<sub>2</sub>O)<sup>-1</sup> and Mg-oxychloride at I = 9.9 to 15 mol·(kg H<sub>2</sub>O)<sup>-1</sup> demonstrates the suitability of brucite / Sorel based materials as engineered buffer with respect to retention of trivalent actinides under a wide range of saline conditions. In experimental studies in diluted solutions, an incorporation of Eu(III) and Am(III) into the octahedral brucite structure was determined (Finck et al. [4]). Ongoing TRFLS studies with Cm(III) / brucite / brine suspensions focus on the ionic strength effect of Cm(III) incorporation into brucite.

### Sorption Studies onto Technical Sorel Based Construction Materials

In the scope of contingency plans for the Asse II salt mine, safety analyses are performed which demonstrate the effects of specific emergency measures. The analyses cover the behaviour of radionuclides in contact with Mg(OH)<sub>2</sub> / Sorel based construction materials with respect to the resulting geochemical environment as well as sorption of radionuclides onto these materials. In previous safety assessments, these materials have not yet been considered with respect to their radionuclide retention. The Sorel concrete used to backfill the roof gap of chambers in the mine is fractured and penetration of solutions and radionuclides into these materials were considered to be negligible.

To provide more information on the retention properties of these materials, batch and diffusion experiments were performed. The batch experiments used Eu(III) as tracer, diffusion experiments used tritiated water and the anion <sup>129</sup>I<sup>-</sup>. The Sorel concrete for batch and diffusion tests was provided by the BfS, in the batch experiments, additionally crushed rock-salt used as backfill material and mixtures of crushed salt with Sorel concrete were investi-

gated. Slightly under-saturated  $MgCl_2$  solution was used for both types of experiments.

The materials were analyzed with respect to chemical and mineralogical composition, DTA-TG, SEM-EDX and XRD. Solids for batch experiments were crushed and the surface size determined by the  $N_2$ -BET method. For the diffusion test, cubic samples of 40 mm edge length were cut and embedded in epoxy resin, keeping one side open.

For the Eu(III) sorption experiments, a V/m ratio of  $10 \text{ mL}\cdot\text{g}^{-1}$  was selected. After equilibration of the solids, the tracers were added. The Eu concentration was kept below  $1 \mu\text{mol}\cdot\text{L}^{-1}$  which is below the solubility of  $(Eu)(OH)_3(c)$  under the studied conditions. The results are shown in Fig. 3. The highest sorption coefficient was found surprisingly for crushed rock salt. This strong retention could not be observed for pure NaCl, therefore minor accessory phases in the crushed rocksalt seem to control the sorption properties. After 90 days, following sorption coefficients were determined: Sorel concrete:  $70 \pm 10 \text{ mL}\cdot\text{g}^{-1}$ , crushed rocksalt:  $212 \pm 43 \text{ mL}\cdot\text{g}^{-1}$  and the mixture of Sorel concrete and crushed rocksalt:  $105 \pm 5 \text{ mL}\cdot\text{g}^{-1}$ .

Diffusion profiles were measured by abrasion from the cubic samples at different times.

$D_{\text{eff}}$  is a macroscopic diffusion coefficient relevant for the complete pore system. This system is represented by a connected porosity ( $\epsilon$ ), the tortuosity ( $\delta$ ) and the constrictivity ( $\tau$ ).

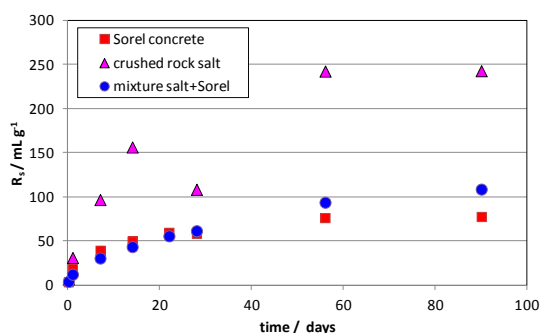


Fig. 3: Sorption coefficients  $R_s$  as function of time for the investigated systems.

$$D_{\text{eff}} = \frac{D \cdot \epsilon \cdot \delta}{\tau}$$

The apparent diffusion coefficient  $D_{\text{app}}$  takes sorption into account. In the case of a linear sorption isotherm ( $K_D$ ), following equation can be applied:

$$D_{\text{app}} = \frac{D_{\text{eff}}}{R_d}$$

using a retardation coefficient  $R_d$  which is defined as follows:

$$R_d = 1 + \frac{(1-\epsilon)}{\epsilon} K_D \cdot \rho$$

For the diffusion of HTO and  $^{129}\text{I}^-$  in Sorel concrete following results were obtained:

	HTO	$^{129}\text{I}^-$	unit
$D_{\text{eff}}$	$8.0 \times 10^{-11}$	$4.0 \times 10^{-11}$	$\text{m}^2 \text{ s}^{-1}$
$K_D$	0.9	0.2	$\text{mL g}^{-1}$
$R_d$	14.1	3.9	-
$D_{\text{app}}$	$5.6 \times 10^{-12}$	$1.0 \times 10^{-11}$	$\text{m}^2 \text{ s}^{-1}$

In both cases, a “rock capacity factor” could not be found.

### Thermodynamics of long-term metastable magnesium hydroxo (chloro-) carbonates

Though magnesite ( $MgCO_3$ ) is the thermodynamically stable solid in the system  $Mg\text{-Cl-HCO}_3\text{-CO}_3\text{-H-OH-H}_2\text{O}$  at room temperature, even in long-term laboratory experiments its precipitation is hardly observed. Instead, long-term metastable magnesium hydroxo (chloro-) carbonates are formed in  $MgCl_2$  solutions in the presence of carbonate. With respect to radionuclide retention, it is of fundamental importance to accurately describe the geochemical conditions and processes that control aqueous carbonate chemistry.

Therefore, the system  $Mg\text{-Cl-HCO}_3\text{-CO}_3\text{-H-OH-H}_2\text{O}$  was studied in a series of batch experiments performed in Ar glove boxes by adding 0.05 M  $Na_2CO_3$  to  $MgCl_2$ -solutions of different concentrations (0.25 to 4.5 M).

The  $pH_c$  was monitored over more than three years. The precipitated solids were analysed by different methods (Raman spectroscopy, XRD, SEM-EDX, XPS). In the solutions with  $MgCl_2$  concentrations lower than 2.8 M, hydromagnesite  $Mg_5(CO_3)_4(OH)_2 \cdot 4H_2O(s)$  was found to be the long-term metastable solid present, while chlorartinite  $Mg_2CO_3OHCl \cdot 3H_2O(s)$  was found in  $MgCl_2$  solutions with higher concentrations ( $\geq 2.8$  M  $MgCl_2$ ). At phase transition, both solids coexist in a solution with specific carbonate concentration and activity. Using measured  $pH_c$  and  $MgCl_2$  concentration of the solution at the observed phase transition, activity coefficients calculated with the Pitzer database of Harvie et al. [5] and published solubility data for hydromagnesite [6,7], the equilibrium constant of chlorartinite can be calculated:

$$\log K^{\circ}_{(\text{chlorartinite})} = 13.15 \pm 0.36 \text{ for the reaction } Mg_2CO_3OHCl \cdot 3H_2O(s) + 2 H^+ \rightleftharpoons 2 Mg^{2+} + HCO_3^- + Cl^- + 4 H_2O.$$

Introducing this new constant together with the literature data for hydromagnesite [6,7], into the dataset of Harvie et al. [5], the system at metastable state can be described thermodynamically (see Fig. 4). This significantly improves the description of geochemical pro-

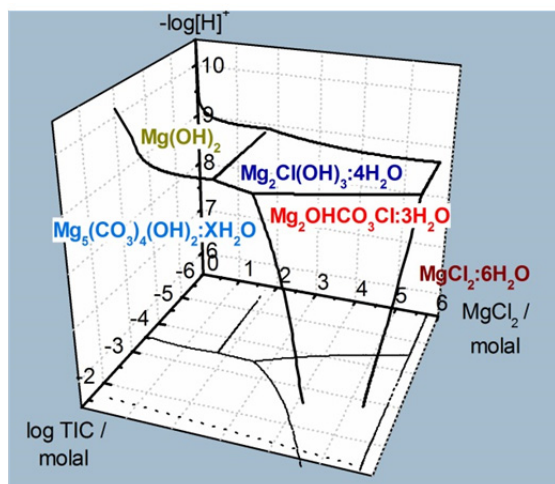


Fig. 4: Phase diagram of the stable and long-term metastable phases in the system Mg-Cl-HCO<sub>3</sub>-CO<sub>3</sub>-H-OH-H<sub>2</sub>O at room temperature (formation of MgCO<sub>3</sub>(s) suppressed).

cesses in  $MgCl_2$  brines relevant for nuclear waste disposal in rock salt.

### Radionuclide Source Term for Non Heat-producing Wastes in the scope of the “vSG” Project

On behalf of the German Federal Environment Ministry (BMU) a preliminary safety analysis for the Gorleben site was performed which summarized all available information on the salt dome and the results of exploration activities to date. After providing the radionuclide source term for high level wastes (see Annual Report 2011) the source terms for a variety of wastes, such as fuel elements from the pilot reactors AVR/THTR, from the research reactors KNK II and NS Otto Hahn, and from the research and material test reactors BER II and FRM II. Further, graphite wastes, compacted structural materials from conditioning of spent LWR fuel elements, the tails from uranium enrichment and other wastes with negligible heat generation were elaborated.

The boundary conditions were deduced for several disposal concepts developed within the project: A - emplacement of wastes with negligible heat generation, B1 and B2 - emplacement in horizontal galleries, and C - emplacement in vertical boreholes. The boundary conditions include the evolution of the geochemical conditions, the generation of a H<sub>2</sub> atmosphere in LLW emplacement rooms in the presence of steel containers as well as microbial degradation processes. The geochemical performance of containers of the Konrad type IV and type VI was evaluated including self-shielded concrete and steel containers. Some of the materials contain also wastes solidified in bitumen and in plastics.

The source terms considered the kinetics of radionuclide release and the maximum radionuclide concentrations in the different emplacement rooms under the expected geochemical boundary conditions. Three different geochemical boundary conditions were defined as follows:

Reference system	NaCl system 5.6 m NaCl	MgCl <sub>2</sub> system 4.0 m MgCl <sub>2</sub>	CaCl <sub>2</sub> system 2.0 m CaCl <sub>2</sub>
Carbonate	calcite saturation: $4 \times 10^{-6}$ mol/L	calcite saturation $2 \times 10^{-4}$ mol/L	calcite saturation $3 \times 10^{-6}$ mol/L
Sulfate	Gypsum saturation: $5 \times 10^{-2}$ mol/L	Gypsum saturation $2 \times 10^{-2}$ mol/L	Gypsum saturation $3 \times 10^{-3}$ mol/L
pH <sub>c</sub>	$-\log [H^+] = 12.8$	$-\log [H^+] = 9$	$-\log [H^+] = 12$
Redox conditions	reducing	reducing	reducing

The maximum radionuclide concentrations are assessed based on the concept of thermodynamic solubilities assuming that concentrations are limited by solubility-controlling solids only. Solubility-controlled element concentrations (in units of mol·kg H<sub>2</sub>O) in NaCl, MgCl<sub>2</sub> and CaCl<sub>2</sub>-rich brines are provided for Am(III), Th(IV), U(IV), Np(IV), Pu(III), Pu(IV), Tc(IV) and for Zr(IV) for the different emplacement rooms with wastes of negligible heat generation.

	NaCl system	MgCl <sub>2</sub> system	CaCl <sub>2</sub> system
Am(III)	$10^{-7}$	$10^{-4.5}$	$10^{-6}$
Th(IV)	$10^{-6}$	$10^{-6}$	$> 10^{-3}$
U(IV)	$10^{-6}$	$10^{-6}$	$10^{-6}$
U(VI)	$10^{-6}$	$10^{-5.5}$	$10^{-6}$
Np(IV)	$10^{-6}$	$10^{-6}$	$10^{-6}$
Np(V)	$10^{-4}$	$10^{-3}$	$10^{-6}$
Pu(III)	$10^{-7}$	$10^{-8}$	$10^{-8}$
Pu(IV)	$10^{-8}$	$10^{-8}$	$10^{-8}$
Zr(IV)	$10^{-6}$	$10^{-6}$	$> 10^{-2}$
Tc(IV)	$10^{-6}$	$10^{-6}$	$10^{-6}$
Tc(VII)	$> 10^{-1}$	$> 10^{-1}$	$> 10^{-1}$

Finally, sorption of radionuclides onto Zircaloy compounds, iron phases, corroded cement products and rock salt were described.

Open questions concerned (i) the numerous different components which may affect the radionuclide concentrations, such as fluorides, artificial complexing agents and some waste degradation products (iso-saccharinic acid), (ii) potential effect of temperature increase by the nearby HLW, (iii) lack of sorption database under saline conditions, and (iv) the potential microbial interactions. Due to the complexity of the different waste components, it is highly recommended to keep the different waste materials separated, especially from the high level waste disposal site.

## References

- [1] Metz, V. et al., *Radiochim. Acta*, 92: 819 (2004).
- [2] Freyer, D., *Proceed. Int'l Workshops ABC-Salt(II) and HiTAC 2011*. KIT Scientific Reports 7625, Karlsruhe, p. 29 (2012).
- [3] Altmaier, M. et al., *Geochim. Cosmochim. Acta*, 67: 3595 (2003).
- [4] Finck, N. et al., *J. Contam. Hydrol.*, 102: 253 (2008).
- [5] Harvie, C. E. et al., *Geochim. Cosmochim. Acta*, 48: 723 (1984).
- [6] Königsberger, E. et al., *Geochim. Cosmochim. Acta*, 63: 3105 (1999).
- [7] Robie, R. A. et al., *U.S. Geol. Survey Bull.* 2131 (1995).

## 6.3 Colloid impact on radionuclide (RN) migration

N. Banik, M. Bouby, S. Büchner, G. Darbha, N. Finck, H. Geckeis, R. Götz, W. Hauser, S. Heck, P. Höss, F. Huber, T. Kupcik, M. Lagos, C. Marquardt, J. Lützenkirchen, T. Schäfer

In co-operation with:

I. Blechschmidt<sup>a</sup>, J. Brendlé<sup>b</sup>, J. Eikenberg<sup>c</sup>, C. Fischer<sup>d</sup>, A. Martin<sup>a</sup>

<sup>a</sup> NAGRA Natl. Cooperat. Disposal Radioact. Waste, Wetingen, Switzerland; <sup>b</sup> Lab. Mat. Mineraux, UMR CNRS 7016, Univ. Haute Alsace, Mulhouse, France; <sup>c</sup> Paul Scherrer Institut (PSI-LES), Villigen, Switzerland; <sup>d</sup> MARUM / FB Geowissenschaften, Universität Bremen, Bremen, Germany

### Introduction

The influence of colloidal/nano-scale phases on the radionuclide (RNs) solubility and migration behaviour is still one of the uncertainties of the repository safety assessment [1,2]. In our work, we aim to 1) identify the presence and the formation of relevant colloids in repository specific areas, 2) determine their stability as a function of geochemical parameters, 3) elucidate the thermodynamics and kinetics of the colloid interaction with radionuclides, 4) perform laboratory and field experiments to quantify the colloid mobility and their interaction with surfaces. The final goal is to state on the relevance of the nanoparticles (NPs) / colloids for the radionuclides migration in natural geochemical conditions.

This year, in this chapter, we report on the progress concerning a) the colloid migration under near natural hydraulic conditions at the Grimsel Test Site, b) the influence of mineral/fracture surface roughness on colloid retention probed by atomic force microscopy (AFM) colloid probe technique, c) a bentonite erosion test under quasi stagnant flow conditions.

#### a) Colloid-associated RN transport under near-natural flow conditions

Within the Colloid Formation and Migration project (CFM) at the Grimsel Test Site (GTS Switzerland, [www.grimsel.com](http://www.grimsel.com)) a huge geo-technical effort was taken to isolate hydraulically a shear-zone from the artificially introduced hydraulic gradient due to the tunnel construction (see Fig. 1). The construction is based on a polymer resin impregnation of the tunnel surface operating as surface sealing and a steel cylinder. The steel cylinder with re-

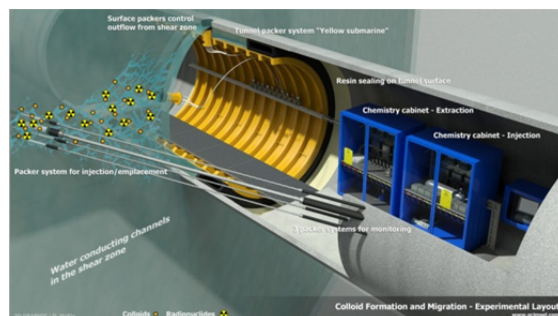


Fig. 1: Schematic overview of the current Donut packer design to establish near-natural flow conditions at the CFM site.

inforcement rings is sealed on both ends with rubber based hydraulic “donut” packers and the annulus between resin and steel ring filled and pressurized with water to counteract the hydrostatic pressure of the water conducting feature giving mechanical support to the resin. Natural outflow points of the shearzone were localized at the tunnel wall prior to the construction and sealed by surface packers. This design gives the opportunity by outflow regulation to adjust the flow velocity in the fracture. The hydraulic heads are well controlled with this “Donut Packer” system essentially stable at level of natural variations due to lake level changes of the local hydropower con-

Table 1: Isotope list of the CFM Run 12-02 injection cocktail with the total activities given for 2.25 L volume and the initial colloid association differentiated by ultracentrifugation (1 hour at 90,000 rpm).

Tracer	concentration (mol/L)/ Total activity	Colloid association (min-max values)
<sup>22</sup> Na	1.0-1.1·10 <sup>-10</sup> (1.17 MBq)	0 - 3.5%
<sup>133</sup> Ba	6.8-7.0·10 <sup>-10</sup> (1.97 MBq)	24 - 34%
<sup>137</sup> Cs	7.9-8.0·10 <sup>-10</sup> (785 kBq)	97 - 98%
<sup>232</sup> Th	5.3-5.6·10 <sup>-9</sup> (8 mBq)	94 - 97%
<sup>237</sup> Np	9.3-9.4·10 <sup>-9</sup> (119 Bq)	0 - 1%
<sup>243</sup> Am	7.0-7.4·10 <sup>-11</sup> (290 Bq)	99 - 100%
<sup>242</sup> Pu	3.0-3.2·10 <sup>-9</sup> (190 Bq)	99 - 100%

structions (~tenths of cm over months) and earth tides (~tenths of mm 12/24 cycles).

After optimization of the experimental setup and injection procedure through a number of conservative tracer tests using fluorescence dyes (Uranine, Amino-G Acid (AGA)) and so-called “homologue” tracer tests performed by injecting a suspension of Febex bentonite colloids associated Eu, Tb, Hf in addition to the conservative tracer the license was granted in January 2012 by the Swiss regulatory (BAG) to perform the first radionuclide tracer test under these low-flow conditions.

The injection cocktail of 2.25 L volume was prepared at INE. A total colloid concentration of  $101.4 \pm 2.5$  mg/L montmorillonite clay colloids were used, whereas  $8.9 \pm 0.4$  mg/L were present as synthetic montmorillonite with structural incorporated Ni. For details on the structural characterization of the Ni-montmorillonite phyllosilicate, see [3]. Beside the colloids and the conservative tracer AGA ( $1646 \pm 8$  ppb) the radioisotopes as listed in Table 1 were injected.

The trivalent and tetravalent actinides were quantitatively associated with the colloids present as well as Cs, whereas Np(V) and Na are not bentonite colloid bond.

The injection of the radionuclide bentonite colloid cocktail was performed through borehole CFM 06.002-i2 into the shearzone and the water extracted under a constant flow rate of approx. 25 mL/min from the “Pinkel” surface packer (dipole distance 6.08 m). The tracer cocktail was recirculated in the injection loop to monitor the fluorescence decrease of the conservative tracer (AGA) and therefore providing an injection function for consequent transport modeling. It has been shown through prior migration tests that the local transmissivity of borehole CFM 06.002 is very heterogeneous and under the low flow conditions established an almost stagnant zone around the borehole exists. Therefore, in Run 12-02 an injection with 0.25 mL/min during recirculation has been used.



Fig. 2: (left) Transfer of LIBD bus via cable car to the Grimsel Test Site (GTS), (right) LIBD with flow through cuvette for colloid in-line monitoring during Run 12-02.

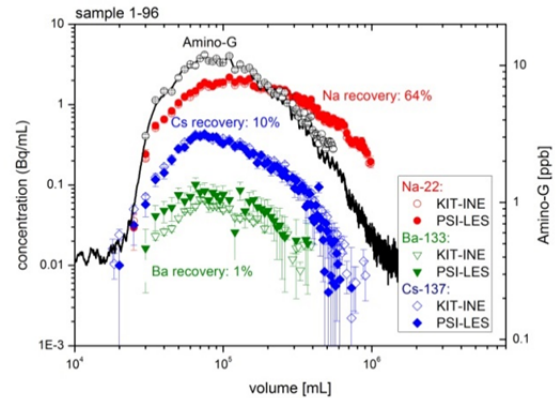


Fig. 3: BTC's of colloids via LIBD and mass spectrometry (Al, Ni).

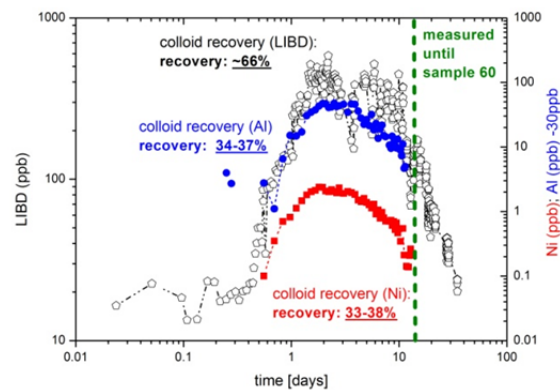


Fig. 4: BTC's of colloids via LIBD and mass spectrometry (Al, Ni).

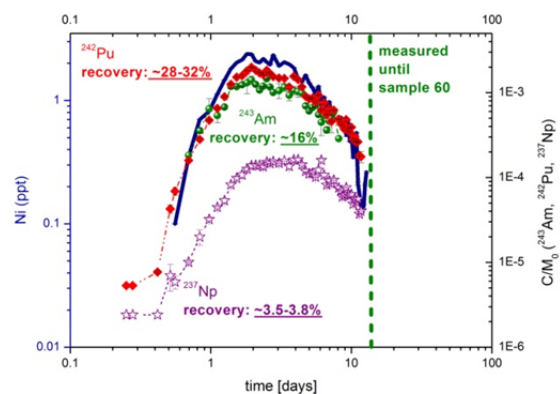


Fig. 5: BTC's of Pu, Am and Np in comparison to colloids (Ni) for the first 60 samples.

For on-site colloid analysis a mobile Laser- Induced Breakdown Detection (LIBD) system similar to the one used in the CRR experiments [4] was transferred to Grimsel and installed in-line at the “Pinkel” outlet to directly monitor the mobile colloid fraction throughout the experiment (see Fig. 2)

The results of the tracer breakthrough curves (BTC’s) are shown in Fig. 3 to 5 and the data are summarized in Table 2. The conservative tracer AGA was recovered quantitatively both by on site inline and off-site fluorescence detection.

Sinusoidal oscillations on top of the AGA BTC both seen in the in-line and off-site analysis can be interpreted as tidal effects (earth-moon cycles).

This is a consequence of the very low gradients established at the CFM site. Analysis of the weakly sorbing tracers by  $\gamma$ -spectrometry performed by PSI-LES and INE showed very good conformity and revealed recoveries for  $^{22}\text{Na}$ ,  $^{137}\text{Cs}$  and  $^{133}\text{Ba}$  of 64%, 10% and 1%, respectively. These data are confirmed in addition by analysis of sample aliquots taken from the waste tanks, where the complete eluted water volume was collected (see Table 2).

Table 2: Summary of recoveries (CFM Run 12-02)

Colloid/ Tracer	Recovery (%)	Sample region/ time
<i>Colloids</i>		
LIBD on site	66%	up to 34.7 d
Al signal	34-37%	Sample 1-60 (11.4 d)
Ni signal	33-38%	Sample 1-60 (11.4 d)
Amino-G	100% (in line)	Sample 1-96 (27.3. d)
$^{22}\text{Na}$	64% (68.7%)*	Sample 1-96 (27.3. d)
$^{133}\text{Ba}$	1% (0.6%)*	Sample 1-96 (27.3. d)
$^{137}\text{Cs}$	10% (8.4%)*	Sample 1-96 (27.3. d)
$^{232}\text{Th}$		Sample 1-60 (11.4 d)
$^{237}\text{Np}$	3-4%	Sample 1-60 (11.4 d)
$^{243}\text{Am}$	16%	Sample 1-60 (11.4 d)
$^{242}\text{Pu}$	28-32%	Sample 1-60 (11.4 d)

The on-site LIBD analysis could also detect the colloid concentration changes due to tidal effects, which was hardly observable in the samples taken by the auto-sampler due to the low sampling frequency. LIBD determined recovery was quantified to be ~66%, whereas for the structural components Al and Ni detected by high resolution HR-ICP-MS up to sample 60 (integration until 11.4 days) a recovery of 33-38% was quantified. The analysis of the full sample set is still ongoing. The Al/Ni ratio in the injection cocktail was determined to be 21.6 and an average ratio of  $20.4 \pm 0.5$  was found over the samples analyzed providing clear evidence that a mobilization of Al containing phases as an additional colloid source from the fracture can be excluded.

Based on a number of colloid migration experiments performed in the MI shearzone under variation of flow velocity and subsequent residence time a colloid attachment/filtration rate  $K_2$  of  $(6.0 \pm 0.6) \cdot 10^{-3}$  can be estimated, which is considerably lower than the value of  $2 \cdot 10^{-2}$  estimated by filtration theory [5].

All injected radionuclides could be detected in the effluent. Np recovery is significantly reduced to ~4% in comparison to the CRR experiment of  $82 \pm 4\%$ , which is in line with the time dependent sorption increase observed in batch-type studies [2]. For the initial colloid associated actinides Am(III) and Pu(IV) a recovery of at least 16% and 28-32%, respectively, could be determined.

The data of Run 12-02 obtained so far clearly show the mobility of bentonite derived montmorillonite colloids under near-natural flow conditions in the MI shearzone of the Grimsel Test Site. A full analysis of the data presented is currently in progress. In the next phase it is planned to install a compacted bentonite source labeled with radionuclides and monitor bentonite buffer erosion in this fracture proven to be permeable for bentonite derived montmorillonite colloids.

## b) The influence of mineral/fracture surface roughness on colloid retention probed by atomic force microscopy (AFM) colloid probe technique.

Understanding the sorption processes at the interface of colloids and mineral surfaces where both the colloids and mineral surfaces are negatively charged is important to answer key questions related to transport and retardation of colloids in the nuclear waste repository [6-8]. In the current study the sorption of colloids onto minerals as a function of surface heterogeneity and metal ion (Eu(III)) concentration is studied. The colloid sorption results obtained from flow-through experiments are verified by measuring the actual forces applying AFM colloid probe technique.

Colloidal suspension of carboxylated polystyrene particle (latex, diameter =  $1000 \pm 25$  nm and concentration =  $48 \times 10^6$  particles / mL, NaCl =  $10^{-3}$  M) was exposed to the main mineral constituents of granodiorite surface (quartz, plagioclase, K-feldspar, biotite) possessing varying surface roughness in a fluid cell (velocity =  $4.7 \times 10^{-7}$  m/sec) for 1 h (at pH = 5). Vertical Scanning Interferometry (VSI) is applied for surface topography characterization and colloid quantification. AFM cantilevers modified with carboxylated latex spheres were used to obtain force-volume measurements under the similar chemical conditions. The data from VSI and AFM was processed using SPIP software (Image Metrology, Denmark).

At pH = 5, all minerals are negatively charged leading to unfavorable deposition conditions. At Eu(III) = 0 M and for a surface roughness range of 250 nm, colloid deposition is ranked as quartz  $\approx$  K-feldspar > plagioclase > biotite while, at high Eu concentrations ( $10^{-6}$  M) the order of sorption reactivity becomes quartz > plagioclase > K-feldspar > biotite. In general, increasing Eu(III) concentration from zero to  $10^{-6}$  M increased the colloid deposition rate. The increase is by a factor of 4.5 for plagioclase, 1.8 for biotite, 2.7 for K-feldspar and 3.4 for quartz (Fig. 6a). Colloid deposition efficiencies on feldspars and quartz minerals were nearly 2 to 4 times higher than biotite. From

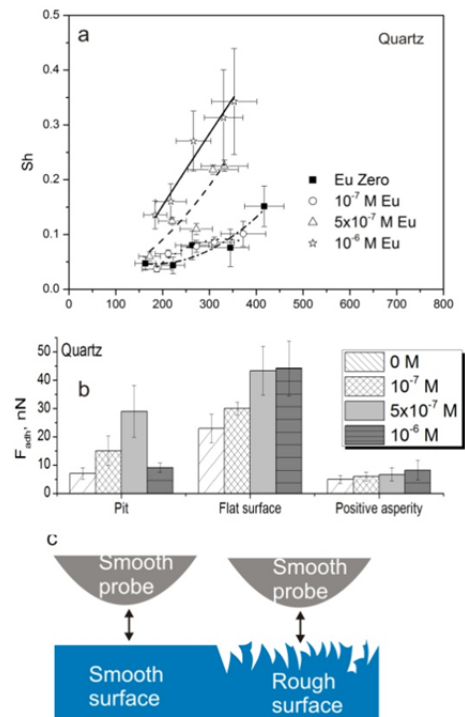


Fig.6: a. colloid deposition density (Sh) as a function of surface roughness and [Eu(III)] on quartz substrate, b. adhesion forces on quartz surface at varying [Eu(III)] as a function of surface heterogeneity, c. scheme to explain the reduced local contact area between colloid and surface with an increase in the surface roughness.

the measured forces (snap-in and adhesion) using colloid probe technique, the adhesion forces explain well the observed sorption results better than snap-in forces. Interestingly, the force-volume measurements along the rough mineral surfaces predict a higher adhesion forces for flat surface sections compared to pits or positive asperities towards colloid retention highlighting the differences in reactivity with respect to surface heterogeneity (Fig. 6b). The differences in measured forces could be due to the decreased local contact area at the interface of colloid-rough surface (Fig. 6c) or differences in the distribution of Eu on rock surface with respect to physical heterogeneity.

## c) Bentonite erosion/destabilisation under quasi-stagnant flow conditions.

The erosion process in compacted bentonite is tested by using a reactor as designed in [5] (see Fig. 7.).

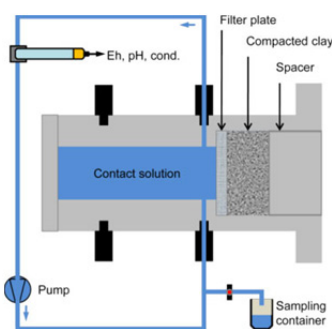


Fig.7: Experimental set-up for the erosion experiment (here the contact solution is not re-circulated).

As contact solution, we used a synthetic carbonated ground water containing  $\text{Na}^+$  (28.4 mg/L),  $\text{Ca}^{2+}$  (1.49 mg/L),  $\text{F}^-$  (2.8 mg/L),  $\text{Cl}^-$  (2.64 mg/L),  $\text{SO}_4^{2-}$  (4.13 mg/L) and Si (7 mg/L),  $\text{HCO}_3^-$ :  $10^{-3}$  M. The ionic strength was  $1.3 \cdot 10^{-3}$  M, the initial pH was 8.4 and remained constant during this first experiment. A filter plate (20  $\mu\text{m}$  pore size, stainless steel) was inserted in front of the compacted clay pellet (raw FEBEX bentonite,  $\phi = 19$  mm,  $h = 10$  mm,  $1.6 \text{ g}\cdot\text{cm}^{-3}$ ) and blocked inside the reactor by a PEEK spacer. The flow rate was fixed and controlled at  $(2.8 \pm 0.2) \mu\text{L}/\text{min}$ . The water composition evolution and the colloid production

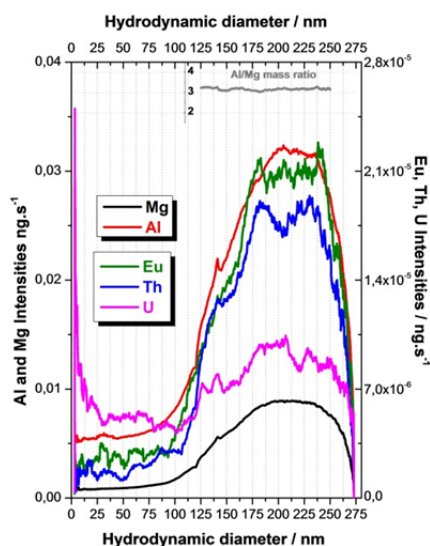


Fig.8: AsFIFFF-ICP-MS fractograms of the colloidal suspension collected after 1 month erosion time and spiked with Eu, Th and U elements. Mean of two measurements.

were monitored. The  $[\text{Cl}^-]$  and  $[\text{SO}_4^{2-}]$  concentrations increased while the  $[\text{F}^-]$  remained constant. The clay colloids concentration produced increased slowly over one month to reach a value of  $193 \text{ g}/\text{L}/\text{m}^2$  in agreement with [5]. This colloidal suspension has been spiked with a RNs cocktail and analysed by AsFIFFF/ICP-MS. The fractograms are presented in the Fig. 8. The colloid size determined from the peak maxima positions is  $(210 \pm 10) \text{ nm}$ , in agreement with values usually reported. The colloidal recovery is  $(61 \pm 5)\%$ . The Al/Mg mass ratio determined in the size range [125-250] nm is  $(3.17 \pm 0.05)$  in agreement with the theoretical structural formula which gives an Al/Mg molar ratio of  $(2.85 \pm 0.05)$  for FEBEX bentonite. Under the present experimental conditions, the sorption percentages appear much lower than usually observed: 3.7% for Eu, 15.5% for Th and only 1% for U. This has to be validated by new experiments.

## References:

- [1] Schäfer, T. et al., *Appl. Geochem.*, 27: 390 (2012).
- [2] Geckeis, H. et al., *Actinide Nanoparticle Research*, Springer Verlag, Berlin, Heidelberg, pp. 1-33 (2011).
- [3] Reinholdt, M. et al., *Nanomat.*, 3: 48 (2013).
- [4] Geckeis, H. et al., *Radiochim. Acta*, 92: 765 (2004).
- [5] Schäfer, T. et al., *Project KOLLORADO; Final report*, Forschungszentrum Karlsruhe FZKA report 7515 (2010).
- [6] Darbha, G. K. et al., *Env. Sci. Technol.*, 46: 9378 (2012).
- [7] Darbha, G. K. et al., *Langmuir*, 28: 6606 (2012).
- [8] Fischer, C. et al., *Am. J. Sci.*, 312: 885 (2012).

## 6.4 Simulation of thermo hydro mechanic (THM) processes in the near-field of a HLW disposal in rock salt

A. Pudewills

### Benchmark Calculations of the Thermo-Mechanical Behavior of Rock Salt

Within the frame of a national joint research project, five participants performed benchmark like calculations on in-situ tests in a heated borehole in the Asse salt-mine in Northern Germany. The well documented and published Netherlands Energy Foundation (ECN) borehole experiments [1] were chosen by the partners as subjects for the benchmark analyses.

The aim of the project was to evaluate the ability of the models to correctly describe the relevant deformation phenomena in rock salt under various influences, (i.e. transient and steady-state creep, the evolution of dilatancy and damage) and to increase confidence in the results of numerical simulations and enhance the acceptance of the results.

In our institute the finite element (FE) code ADINA was used to study the coupled thermo-mechanical behavior of rock salt [2]. A new viscoplastic constitutive model for rock salt that can describe the volumetric strain (dilatancy) and the damage of the rock salt has been proposed and implemented in this code [3]. The parameters determination for the

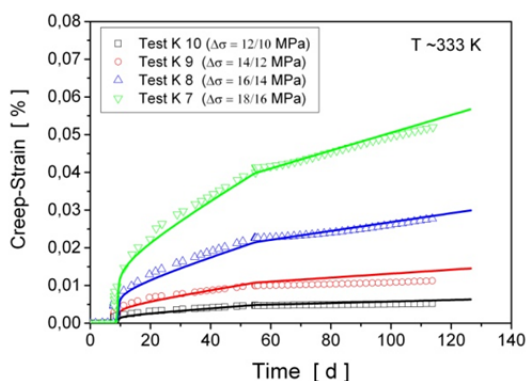


Fig. 1: Simulation (continuum lines) with a unique set of parameter values of a series of two-stage creep tests at ~333 K on Asse-Salt.

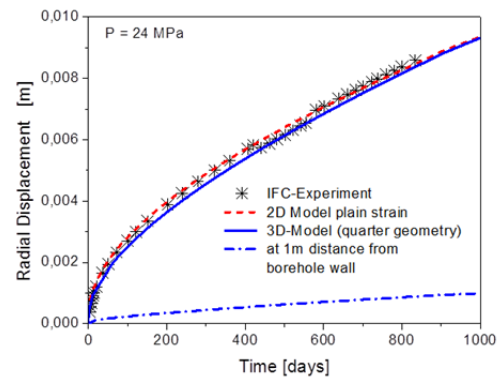


Fig. 2: Comparison of simulation results and measured borehole convergence for different geometric models.

rock salt type in vicinity of borehole tests is based on recalculation of new laboratory experiments. The modeling of a number of two-stage laboratory creep tests at ~60°C was performed to adjust the steady-state creep parameters (Fig. 1).

The benchmark calculations for the thermo-mechanical behavior of rock salt were performed on the 300 m deep borehole, drilled from the 750 m level downwards. The ECN performed the Isothermal Free Convergence (IFC) at a depth of 292 m (i.e. 1042 m below ground). The measurements were continued

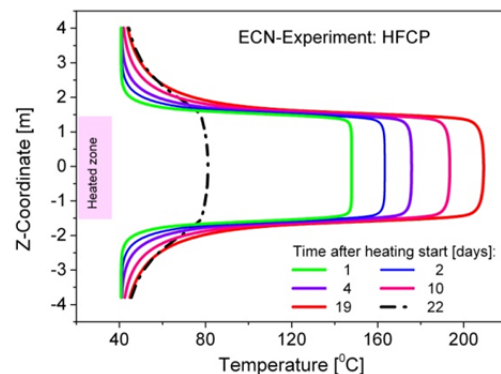


Fig. 3: Development of the temperatures along the borehole wall for different time points. After 19 days the electrical heater was switched off and the free cooling temperature at the wall was calculated until 22 days.

over 830 days. Later, the Heated Free Convergence Probe (HFCEP) – Experiment was conducted at 231 m level with a heater power of 6000 Watt over 19 days. The heated length was 3 meters.

The temperature at the borehole wall and the convergence were measured. The predicted isothermal convergence over about 900 days together with measurements is presented in Figure 2. The development of thermal induced convergence along the vertical direction in the borehole is plotted in Figure 3.

The benchmark results and the comparison of several results with in situ measurements have shown that the considered constitutive models are able to describe reliably the various relevant deformation phenomena in rock salt including the temperature dependence of transient and steady-state creep. A comparison of calculation results from five project partners was already performed and will be described in [4] [in print].

The simulation results of IFC and HFCEP in situ tests have shown that the constitutive rela-

tions are an important source for uncertainties in the prediction of the thermo-mechanical behavior of rock salt. There is also an uncertainty with respect to the lithostatic rock pressure at the test location. Finally, it must be further pointed out that in the final comparison of numerical predictions and experimental results the uncertainties in the measurements have to be considered.

## References

- [1] Vons, L. H., Progress report covering the period 1-1-1984–31-12-1984, Petten: Netherlands Energy Research Foundation ECN (1984).
- [2] Adina R & D Inc., Report ARD 01-9, Woburn, MA, USA (2011).
- [3] Pudewills, A., FZKA-7314 (2007).
- [4] Hampel, A. et al., in Proc. of the 47<sup>th</sup> US Rock Mechanics Symposium (ARMA-13), San Francisco, 22-26 June 2013, American Rock Mechanics Association, (2013) in print.

## 6.5 Hydro-chemical modeling

### Application of the numerical framework FASTREACT for reactive transport modeling of Np(V) migration in a single fracture from Äspö, Sweden.

F. Huber, T. Schäfer

In co-operation with:

P. Trincherio,<sup>a</sup> J. Molinero<sup>a</sup>

<sup>a</sup> Amphos 21 Consulting S.L., Spain

#### Introduction

In the context of nuclear waste disposal reactive transport modeling represents an important tool for long-term predictions of radio-nuclide migration. In this work, the Lagrangian-based framework FASTREACT (FrAmework for STochastic REACTIVE Transport) [1] is applied which is able to solve for multicomponent reactive transport. This approach is tested to model experimental data on Np(V) migration through a natural fracture in an Äspö diorite drill core.

#### Theoretical background and methodological approach

The FASTREACT approach is founded on the theory of Stochastic-Convective (SC) models [2] assuming steady state fluid flow and neglecting local-scale dispersion. Under these assumptions, a complex 3D transport problem can be reduced to a set of streamlines which can be treated independently. Disregarding local-scale dispersion assumes that no mass is exchanged between adjacent streamlines consequently limiting this approach to advection dominated systems (high Peclet numbers). The stream tube approach based on the stochastic models makes them attractive for the solution of reactive transport problems since it is computationally less expensive to solve for a set of 1D models than for a single multi-dimensional model.

The application of FASTREACT involves a step-wise process described in the following:

- Infer travel time probability density functions (PDF) at given control locations. This

is usually done using particle tracking simulations on existing flow fields

- Parameterization and calculation of a reference 1D reactive transport simulation
- Coupling between the reference simulation and the set of streamlines

Ideally, results of particle tracking simulations on an existing flow field should be equivalent to the experimental conservative tracer breakthrough curve. The available 3D fracture flow model of the Äspö diorite core migration experiments [3] was used in the particle tracking simulations but failed in reproducing the tracer breakthrough due to difference in the boundary conditions (e.g. unknown spatial distribution of tracer injection at the fracture inlet) of the experiment and the model, respectively. It was thus decided to fit a PDF to the conservative tracer breakthrough curve to obtain a travel time distribution of the particles needed in the next step. For the reference 1D reactive transport simulation the geochemical code PhreeqC [4] was used. In the last step the results of the 1D reference simulation and the travel time PDF are coupled to obtain the temporal evolution of the geochemical parameter of interest (in this case the Np concentration and thus the Np breakthrough curve) at the desired reference plane (here the outlet of the fracture).

#### Conceptual geochemical models

To model the Np reactive transport we tested different approaches with increasing complexity ranging from simplified Kd based sorption models (first order reversible sorption/desorption kinetics) to more complex, mechanistically based surface complexation

models [5] for sorption of  $\text{NpO}_2^+$  onto one ( $\text{Fe}_2\text{O}_3 \cdot 2\text{H}_2\text{O}$  (HFO)), two (HFO and biotite (Bt)) and three (HFO, Bt and kaolinite) different mineral phases. First, the surface distribution coefficient  $K_a$  is derived using eq. 1 [6]:

$$R_f = 1 + a_w K_a \quad (\text{eq. 1})$$

here  $a_w$  is the flow wetted surface area [ $\text{m}^2/\text{m}^3$ ] and  $K_a$  is the surface distribution coefficient [m]. The flow-wetted surface area describes the ratio of total surface area of the fracture [ $\text{m}^2$ ] to the total volume of the fracture [ $\text{m}^3$ ]. Both the fracture surface area ( $0.01165 \text{ m}^2$ ) and fracture volume ( $2.7 \text{ ml}$ ) are obtained by the 3D model based on the  $\mu\text{CT}$  characterization of the drill core [3] yielding a value of  $4307 \text{ [m]}$ . By rearranging eq. 1 a  $K_a$  value of  $0.18 \text{ [l/m}^2\text{]}$  is obtained. Next, PhreeqC batch models have been set-up reproducing the experimental  $K_a$ . Since the  $K_a$  value calculated using the surface area given by the  $\mu\text{CT}$  data is too low (the actual reactive surface area of the fracture is unknown) it was decided to use it as fitting parameter by coupling FASTREACT to the parameter estimation code PEST [7]. These batch models have then been used to simulate the reactive transport. In case of the first-order reversible sorption/desorption kinetics model, the sorption and desorption rate was fitted as well.

### Migration experiments

Migration experiments have been conducted on the single fractured drill core (length  $13.5 \text{ cm}$ ; diameter  $5.048 \text{ cm}$ ) from Äspö, Sweden using a radionuclide cocktail on basis of natural Grimsel ground water to mimic the influence of glacial melt water intrusion into a repository. Here, only the results of the conservative tracer (Tritium (HTO)) and of  $^{237}\text{Np(V)}$  ( $[\text{Np}]\text{TOT} = \sim 1.25 \times 10^{-6} \text{ M}$ ) are presented. For more information on the drill core and the experimental setup it is referred to the literature [3].

### Results

Figure 1 depicts the experimental breakthrough curves for HTO and Np. Np shows a retardation (retardation factor ( $R_f = 1.8$ )) and a pronounced tailing indica-

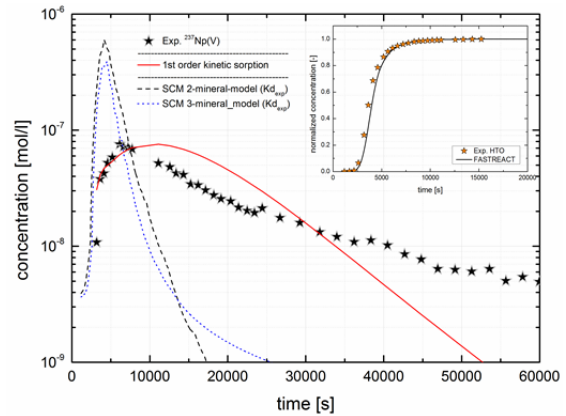


Fig. 1: Comparison between experimental Np breakthrough curve and model results using the experimentally derived  $K_d$ .

tive of an interaction with the fracture surfaces. Np recovery is  $\sim 76\%$  at the end of the experiment, but the tailing seems to be still ongoing thus a quantitative Np recovery is reasonable to expect. The high Np recovery is in line with measured Eh values ( $\sim +200 \text{ mV}$ ) and thermodynamic modeling yielding no Np reduction and  $\text{NpO}_2^+$  as dominating species which is known to sorb only weakly. Results of the FASTREACT modeling exercise are shown in Fig. 1 for both HTO (inset) and Np. The experimental HTO BTC is captured well by FASTREACT due to the fitting of the PDF verifying the correctness of the coupling of PhreeqC and FASTREACT. It is obvious that by using the  $K_a$  derived from the migration experiments ( $K_a = 0.18$ ) in the different SCM models, it is not at all possible to adequately describe the Np BTC. While the peak position is captured relatively

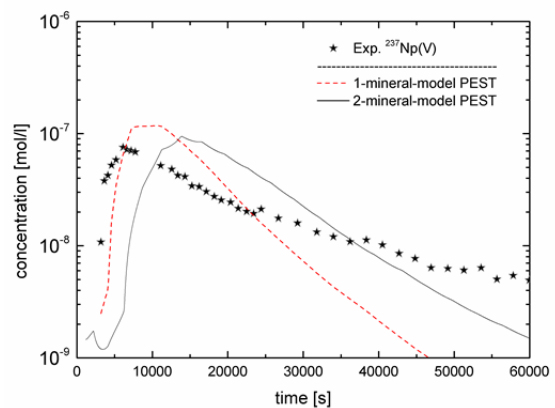


Fig.2: Results of the FASTREACT/PEST fitting exercise for the 1- and 2-mineral-model, respectively.

good the models completely fail both in describing the Np BTC peak concentration and tailing. In case of the 1<sup>st</sup> order kinetic model, the model fit describes the ascending part of the curve quite well, and also shows a pronounced tailing, but the overall fit is again not satisfactory. Moreover, no process understanding may be gained by this approach. Since the actual reactive surface area of the core is unknown PEST is used to fit the surface area (which correlates to the total number of sorption sites) trying to improve the SCM model results. Fig. 2 depicts the first results of the fitting exercise for the 1-, and 2-mineral model, respectively. The results are fitting better compared to the results without the adjustment of the surface area but are still not matching the exp. BTC satisfactorily. The final 3-mineral-model will further increase the results based on preliminary results but is still in progress. Further options to be tested in the modeling exercise are (i) the possibility of matrix diffusion which may not be neglected a priori [8] and (ii) the coupling of FASTREACT to the reactive transport code HBGC123D with which the SCM can be used to model a kinetic sorption and desorption processes rather than an equilib-

rium SCM sorption/desorption approach as used so far. To sum up, the FASTREACT approach coupled to PhreeqC has been shown to represent an effective computational framework for the solution of complex reactive transport simulations taking into account real fracture geometry.

### **References**

- [1] Trinchero, P. et al., SKB R-10-45, Svensk Kärnbränslehantering AB (to be published).
- [2] Shapiro, A. M. and Cvetkovic, V. D., *W. Res. Res.*, 24(10): 1711 (1988).
- [3] Huber, F. et al., *J. Con. Hydr.*, 133(0): 40 (2012).
- [4] Parkhurst, D. L. and Appelo, C. A. J., *Water-Resources Investigations Report 99-4259*, U.S. G. S. (1999).
- [5] Wang, P. M. et al., *Ind. Eng. Chem. Res.*, 40(20): 4428 (2001).
- [6] Wels, C. et al., *Wat. Res. Res.*, 32(7): 1943 (1996).
- [7] Gallagher, M., Doherty, J., *Environ. Model. Soft.*, 22(7): 1000 (2007).
- [8] Neretnieks, I., *J. Geo. Res.*, 85(NB8): 4379 (1980).

## THEREDA project

M. Altmaier, C. Bube, X. Gaona, C. M. Marquardt

In cooperation with:

F. Bok<sup>a</sup>, V. Brendler<sup>a</sup>, H. Moog<sup>b</sup>, A. Muñoz<sup>b</sup>, A. Richter<sup>a</sup>, T. Scharge<sup>b</sup>, D. Sukhanov<sup>c</sup>, W. Voigt<sup>c</sup>, S. Wilhelm<sup>d</sup>

<sup>a</sup>IRE-HZDR, Dresden, Germany, <sup>b</sup>GRS, Braunschweig, Germany, <sup>c</sup>TU-BAF, Freiberg, Germany, <sup>d</sup>AFC, Baden, Switzerland

The THEREDA project was initiated to establish a thermodynamic reference database providing consistent and reliable data for all repository host rock formations (salt, clay, granite) that are under discussion for disposal of radioactive waste in Germany. The currently running second project phase ends in March 2013 and focuses on Pitzer consistent data.

### Web interfaces for databases

In spring 2012, the web interface for the database was activated. It contains different modules for basis species, solubility and thermochemistry data as well as ion interaction parameters (e.g. Pitzer). The interface allows the editors within the project to enter, edit and view data and in addition, it contains all tools required for the auditing – an internal review process. Several control functions ensure data consistency, identify gaps in the data and produce error messages for the editor, e.g. missing entry in a mandatory field, entry incompatible with previous entries.

### Benchmark calculations

Before new thermodynamic data is uploaded in the THEREDA database and released to the scientific community, benchmark calculations are performed to guaranty correctness of the data in the database and the generated output files. These calculations are done by different THEREDA project partners using the geochemical codes PhreeqC, ChemApp, EQ3/6 and the Geochemist's Workbench<sup>®</sup> (GWB). The results obtained with the different codes should be the same within error and are documented in the benchmark papers that can be downloaded together with parameter and input files by everyone who has registered on the THEREDA website. In some cases, the

results of the benchmark calculations are also compared to experimental results.

Several released datasets are available for registered users: The first release comprises the carbonate-free oceanic salt system (Na, K, Mg, Ca, Cl, SO<sub>4</sub> and H<sub>2</sub>O at 0 to 250°C). The second release includes the trivalent actinides Am and Cm (+Nd) in NaCl, MgCl<sub>2</sub> and CaCl<sub>2</sub> solutions (Na, Mg, Ca, Cl, Am(III), Nd(III), Cm(III) and H<sub>2</sub>O at 25°C). The third release added carbonate to the data for the oceanic salt system at 25°C. The fourth release contains data for the Np(V)-hydrolysis in NaCl solutions (Na, Cl, Np(V) and H<sub>2</sub>O at 25°C). Parameter files can be generated directly from the database via export programs for GWB, ChemApp, PhreeqC and EQ3/6. The benchmark calculations with EQ3/6 as well as the main editorial work for

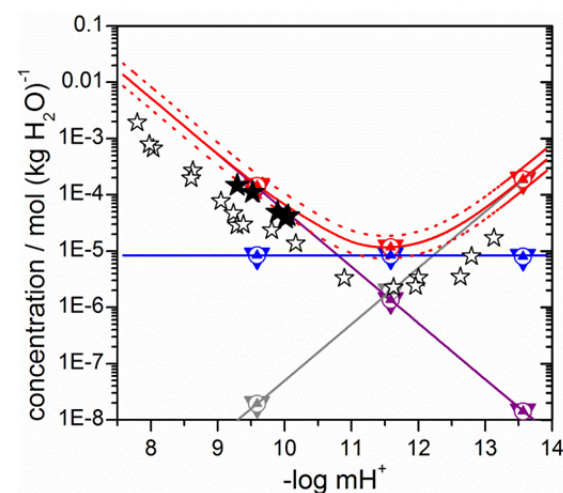


Fig. 1: Example of a benchmark calculation with the THEREDA database: Solubility and speciation of NpO<sub>2</sub>(OH)(fresh,am) in 5 M NaCl solution compared to experimental data; filled stars: fresh solid NpO<sub>2</sub>(OH)(fresh,am) [1], closed stars: aged solid NpO<sub>2</sub>(OH)(fresh,aged) [2], solid lines: calculated with GWB, open circles, down- and upward triangles: results with ChemApp, Phreeqc and EQ3/6.

the fourth release were done at INE. The selected test systems were 1 and 5 M NaCl solutions, in which the solubility of amorphous  $\text{NpO}_2(\text{OH})$ (fresh,am) was calculated at different  $\text{pH}_m$  ( $-\log[\text{H}^+]$ ) values.

The results generated by different geochemical codes were compared and validated against experimental data [1,2]. The calculated values were identical within numerical inaccuracies, and the code specific parameter files proved to work correctly (cf. Fig. 1). It can be seen that the experimental data is de-

scribed well within the experimental error. More details on the calculations can be found in the benchmark documents on the THEREDA homepage ([www.thereda.de](http://www.thereda.de)).

Data selections for An(IV), Pu(III) and U are planned to be released within the first half of 2013.

- [1] Neck, V., FZK-INE 004/97 (1997).
- [2] Runde, W., Kim, J. I., Report RCM 01094 (1994).

## Leaching of cemented wastes

V. Montoya, C. Bube, B. Kienzler

### Introduction

Cementitious materials are commonly used to solidify/stabilize low/intermediate level liquid and solid nuclear waste prior to be disposed in a geological repository. The degradation of these cement-based materials exposed to water solutions depends on many factors, such as the cement composition, liquid/solid volume ratio, time, temperature, pH and contacting solution composition.

The present work focuses on the reactive transport modeling of leaching experiments performed with cemented waste products in tap water for more than 30 years in a specific drift of the Asse II salt mine.

### Experimental approach

Simulated cemented waste has been produced using Ordinary Portland Cement (i.e. CEM I 42.5R) with a water/cement ratio of 0.24 and a load of chemicals with similar composition to those resulting from the reprocessing of spent fuel by the Purex process (mainly  $\text{NaNO}_3$  but also Na-citrate, Na-tartrate,  $\text{Na}_2\text{HPO}_4 \cdot 12\text{H}_2\text{O}$  and Na-oxalate) The cemented simulated waste studied in this work has a mass of 192 kg and is doped with tracer concentrations of inactive Cs. After complete hydration, the waste is immersed

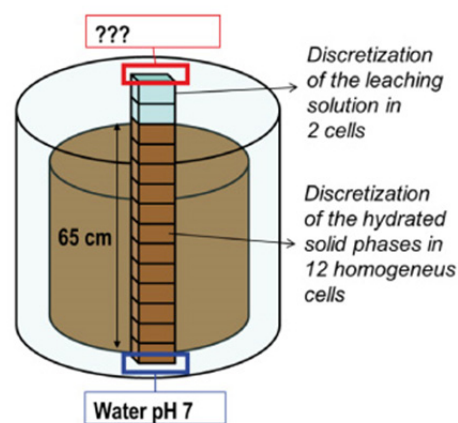


Fig. 1: Schematic conceptual model used in the calculations. Initial conditions: leaching solution  $\text{pH} = 7$  and cement porewater composition in equilibrium with hydrated cement phases.

in 400 L steel cylindrical canister filled with 239 L of tap water. The initial composition of the leachant in  $\text{mol L}^{-1}$  is  $\text{Mg}^{2+}$ : 0.001;  $\text{Ca}^{2+}$ : 0.002;  $\text{Na}^+$ : 0.013;  $\text{K}^+$ : 0.013;  $\text{Cl}^-$ : 0.025 and  $\text{SO}_4^{2-}$ : 0.001 and  $\text{pH} 7$  [1].

Solution composition and pH were monitored for more than 30 years. Different analytical methods, e.g. SEM-EDX, XRD, XRF and Ra-man  $\mu$ -spectrometry were used for solid phase analyses after termination of the experiments.

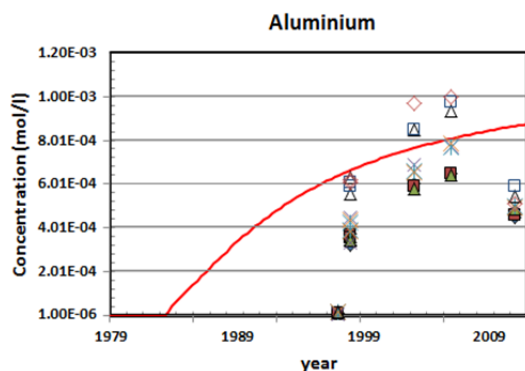


Fig. 2: Variation of the concentration of Al in the leaching solution as a function of time. Different symbols correspond to measured concentration at different position levels of the cylindrical canister.

### Reactive transport modeling

The reactive transport code PHREEQC v3.0 [2] has been used to simulate the dynamic leaching tests taking into account diffusive transport of solutes in 1D and different chemical processes (i.e. dissolution, precipitation). The thermodynamic database used in the calculations is THERMODDEM, developed by BRGM [3], and the ionic strength correction has been done using the Debye-Hückel equation. In Fig. 1 the conceptual model taken into account in the calculations is represented schematically.

The concentration gradients between the pore solution (calculated composition with PHREEQC taking into account equilibrium with the hydrated solid phases) and the leaching solution cause diffusion of chemical species

from the pore solution to the surrounding diluted water. The high concentration gradient between the pore and the leaching solutions, pH ~13 and 7, respectively, leads to the diffusion of hydroxyl ions from the pore solution to the tap water observing an increase of pH with time. The dissolution of the solid phases present in the cement, mainly portlandite, CSH phases, and ettringite, increase the concentration of aluminium, calcium, and silica in the tap water (see Fig 2). The release of nitrate to the leaching solution has also been observed with a constant increase of  $\text{NO}_3^-$ . The possible precipitation of secondary phases has also been taken into account in the model (i.e. monosulphoaluminate, and CSH phases with different Ca:Si ratio). Although, precipitation and dissolution of solid phases can modify the porosity on the cement system, a constant porosity has been taken into account in the calculations.

According to the obtained results it can be concluded that the geochemical code PHREEQC v3.0 is appropriate and capable of simulating the wide range of transport and chemical processes occurring in the leaching experiments of the studied cemented wastes.

### References

- [1] Kienzler, B. et al., FZKA 6716 (2002).
- [2] Parkhurst, D. L., Appelo, C. A. J. U.S. Geological Survey Techniques and Methods, book 6, chap. A43, 497 p. (2013).
- [3] Blanc, P. et al. (2012) BRGM (Orléans, France). <http://thermoddem.brgm.fr>



## 7 Separation of long-lived minor actinides

B. B. Beele, A. Bremer, A. Geist, D. Magnusson, R. Malmbeck,<sup>1</sup> G. Modolo,<sup>2</sup> U. Müllich, P. J. Panak, C. M. Ruff, A. Wilden<sup>2</sup>

<sup>1</sup>European Commission, Joint Research Centre, Institute for Transuranium Elements, Karlsruhe, Germany

<sup>2</sup>Forschungszentrum Jülich GmbH (FZJ), IEK-6, Jülich, Germany

### Background

Recycling transuranium elements (TRU = Np, Pu, Am, Cm) from irradiated nuclear fuel may provide advantages over the direct disposal of used nuclear fuel [1]. This would require separating the actinides from fission products and re-using them as nuclear fuel.

Actinide separation schemes are being considered in Europe, involving the PUREX process to remove uranium and plutonium (plus neptunium after slight process modification), then routing the raffinate through a minor actinide and lanthanide co-extraction process (DIAMEX) followed by An(III)/Ln(III) separation (SANEX) [2, 3, 4]. Several new process options have been developed recently in France and in the framework of European research projects:

- 1c-SANEX [5] and i-SANEX [6] processes for extracting An(III) directly from the PUREX raffinate (i.e., without a prior DIAMEX process);
- GANEX processes for the co-separation of all TRU [7, 8];
- processes for extracting only Am(III) from the PUREX raffinate, e.g., the French EXAm process [9].

INE's work programme covers all above processes (except the PUREX process), integrating our participation to EURATOM (ACSEPT [10], ASGARD, and ACTINET-I3) and BMBF-funded (02NUK012 and 02NUK020) projects. Both fundamental and process related aspects are studied. Examples are given below; further related studies are presented in the laser spectroscopy, NMR, and X-ray spectroscopy sections of this report.

### Basic Studies

The challenging separation of An(III) from chemically similar Ln(III) is possible using *N*-donor (lipophilic) extracting or (hydrophilic) complexing agents such as bis-triazinyl-pyridines (BTP, Fig. 1 left) [6, 11, 12] and bis-triazinyl-bipyridines (BTBP, Fig. 1 right) [13, 14]. These extract An(III) with excellent selectivity over Ln(III).

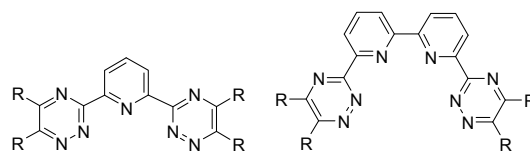


Fig. 1: BTP and BTBP.

Their extraction and complexation properties have extensively been studied over the past 15 years [15]. An appreciable fraction of this work consisted of fundamental studies dedicated to understanding how BT(B)P work on a molecular scale. By combining TRLFS studies on Cm(III) and Eu(III) complexes prepared in monophasic solution and prepared by biphasic extraction, the inner sphere composition of several extracted *N*-donor complexes was identified [16, 17, 18, 19]. This procedure has recently been applied to several new TODGA derivatives, see below.

#### Complexation of Cm(III) and Eu(III) with TODGA derivatives

TODGA (*N,N,N',N'*-tetra-*n*-octyl diglycolamide) [20] is used as an extracting agent for the co-extraction of An(III) and Ln(III) from PUREX raffinate in a DIAMEX process. To fine tune extraction properties, modified diglycolamide extracting agents (Fig. 2) were synthesized and assessed [21]. It was shown that the ex-

traction efficiency for Am(III) and Eu(III) was TODGA > Me-TODGA > Me<sub>2</sub>-TODGA.

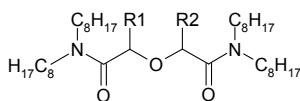


Fig. 2: TODGA (R1 = R2 = H), Me-TODGA (R1 = H, R2 = CH<sub>3</sub>), and Me<sub>2</sub>-TODGA (R1 = R2 = CH<sub>3</sub>).

The complexation of Cm(III) and Eu(III) in ethanol with these TODGA derivatives was studied by TRLFS [22]. The formation of the respective 1:1 and 1:3 complexes (as confirmed by slope analysis) was identified, the speciation was determined (two examples are shown in Fig. 3), and stability constants were determined (cf. Table 1 for the log β<sub>03</sub> values).

Table 1: Conditional stability constants for the formation of [Cm(L)<sub>3</sub>]<sup>3+</sup> (L = TODGA, Me-TODGA, Me<sub>2</sub>-TODGA) complexes in ethanol.

	log β <sub>03</sub> Cm(III)	log β <sub>03</sub> Eu(III)
TODGA	14.9 ± 0.3	15.7 ± 0.2
Me-TODGA	14.8 ± 0.3	15.5 ± 0.2
Me <sub>2</sub> -TODGA	12.7 ± 0.3	15.5 ± 0.2

The three TODGA compounds studied form stable 1:3 complexes with Cm(III) and Eu(III). The stability of the Eu(III) complexes does not vary significantly. Stability constants of the Cm(III) complexes with TODGA and Me-TODGA are lower by 0.7–0.8 log units, which is in good agreement with TODGA's selectivity in liquid-liquid extraction ( $SF_{Eu(III)/Cm(III)} \approx 5$  [6]). However, the stability constant of the 1:3 Cm(III)-Me<sub>2</sub>-TODGA complex is approx. two log units lower than those for TODGA and Me-TODGA.

Unexpectedly and in contrast to findings with BT(B)P [15], the stability constants of the 1:3 TODGA complexes do not mirror the trends found in liquid-liquid extraction experiments [21]: Am(III) and Eu(III) distribution ratios decrease by more than four orders of magnitude in the order TODGA > Me-TODGA > Me<sub>2</sub>-TODGA.

This apparent disagreement is explained by taking a closer look at the liquid-liquid extraction data [21]: Under extraction conditions, the dependency of distribution ratios on the extracting agent concentration slightly varies between the TODGA derivatives and also between Cm(III) and Eu(III). Extrapolating these data to the much lower concentrations used in the TRLFS complexation study yields extraction efficiencies and selectivity in good agreement with the 1:3 complex stability constants.

## Process Development

In the framework of the ACSEPT project, several processes for separating actinides have been developed. Final aim is to develop continuous counter-current separation processes and testing them in a small lab-scale centrifugal contactor setup.

Before such a process test is performed a suitable flow-sheet must be calculated. This is done using dedicated software codes. The

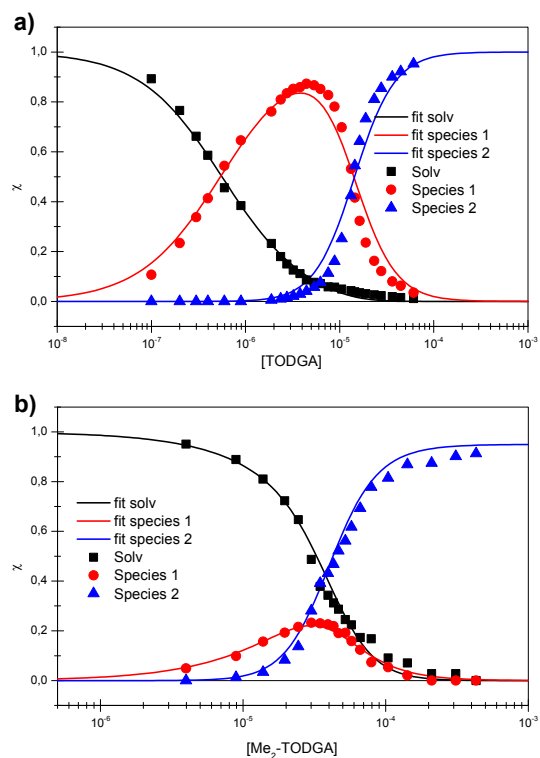


Fig. 3: Speciation of Cm(III) titrated with TODGA (a), and Me<sub>2</sub>-TODGA (b) in ethanol; [Cm(III)]<sub>ini</sub> = 1.0·10<sup>-7</sup> mol/L; lines calculated with log β<sub>01</sub> and log β<sub>03</sub> given in [22].

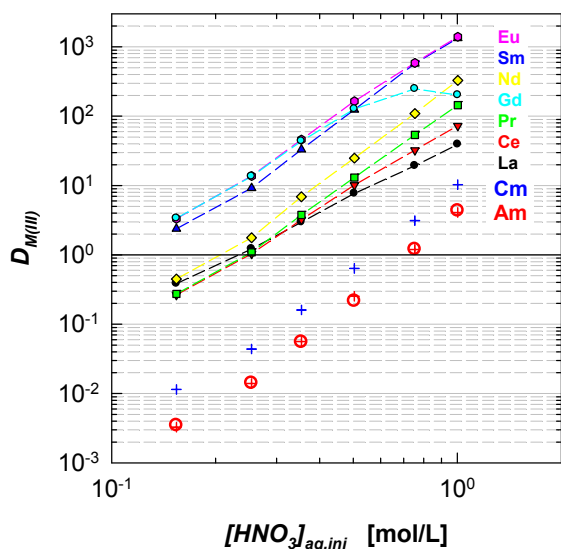


Fig. 4: Effect of  $\text{SO}_3\text{-Ph-BTBP}$  on the extraction of Am(III), Cm(III) and Ln(III) into TODGA. Organic phase, 0.2 mol/L TODGA + 5 % vol. 1-octanol in TPH. Aqueous phase, 18 mmol/L  $\text{SO}_3\text{-Ph-BTBP}$  +  $^{241}\text{Am(III)}$  +  $^{244}\text{Cm(III)}$  (1 kBq/mL each) + Ln(III) (20 mg/L each) in  $\text{HNO}_3$ . A/O = 1, T =  $(293 \pm 0.5)$  K.

*SX Process* code [23] was developed and further improved for this task, see below.

Development of new processes is sometimes based on the suitable combination of compounds originally intended for a different application: By combining the selectivity of an organic extracting agent and an aqueous complexing agent a new system for separating Am(III) from Cm(III) (and the fission lanthanides) was developed.

### AmSel process

Recycling curium in a reactor would not result in a significant reduction of long-term radio-toxicity and thermal power of the HLW to be disposed of. However, its presence would complicate fuel fabrication due to its high neutron dose rate and short-term thermal

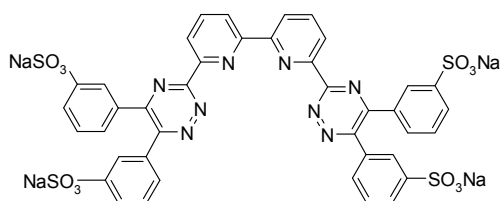


Fig. 5:  $\text{SO}_3\text{-Ph-BTBP}$ .

power. To take this into account, processes are developed which only extract americium from the PUREX raffinate, routing curium to the HLW. The French CEA have developed and successfully tested the EXAm process [24], making use of chemistry based on the TALSPEAK process [25].

Based on the experience with the water soluble  $\text{SO}_3\text{-Ph-BTP}$  [6] and taking into account the reverse Am(III)/Cm(III) selectivity of BTBP [14] compared to BTP [26] an americium-only extraction system was developed. TODGA (Fig. 2) is used to co-extract actinides(III) and lanthanides(III) from HAR. The loaded TODGA phase is then contacted with an aqueous phase containing  $\text{SO}_3\text{-Ph-BTBP}$  [27] (Fig. 5) in  $\text{HNO}_3$  to strip actinides(III).

In the range of  $0.25 \text{ mol/L} < [\text{HNO}_3] < 0.55 \text{ mol/L}$ , actinides(III) are separated from lanthanides(III) (i.e.,  $D_{\text{An(III)}} < 1$  and  $D_{\text{Ln(III)}} > 1$ , see Fig. 4).

More importantly, Am(III) and (Cm(III) + Ln(III)) are separated in the range of  $0.55 \text{ mol/L} < [\text{HNO}_3] < 0.7 \text{ mol/L}$ . Although the separation factor  $SF_{\text{Cm(III)/Am(III)}} \approx 2.5$  is not large it is nevertheless sufficient to achieve good separation in a multi-stage counter-current process.

A separation process based on the TODGA/ $\text{SO}_3\text{-Ph-BTBP}$  process is currently under development.

### SX Process software code

The software code *SX Process* [23] (initially developed at JRC-ITU) is useful for calculating flow sheets for continuous counter-current solvent extraction separation processes. Transient and steady-state concentration profiles and outlet concentrations can be calculated.

*SX Process* was further developed and optimised in several aspects. Initially, equilibrium distribution ratios were described by polynomial fits to experimental distribution data. The code was modified to alternatively use equilibrium functions based on equilibrium constants. Furthermore, a new kinetic model was implemented. By using a flow-rate independent stage efficiency the prediction capability

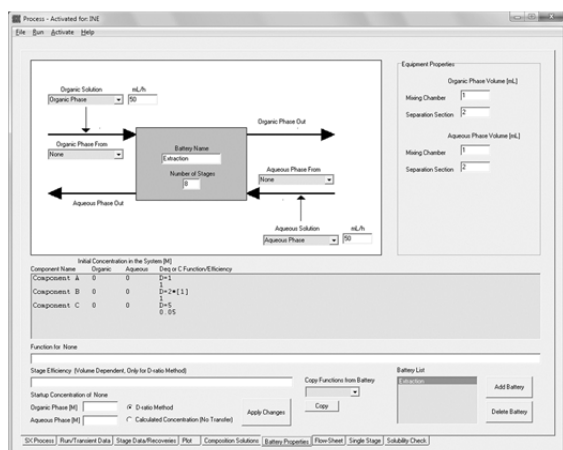


Fig. 6: Interface of the SX Process code showing the page defining the properties of a given section.

was improved. Also, the computing speed could be improved [28].

While it is obvious that loading of the organic phase lowers distribution ratios its effect on kinetics is often overlooked. Experiments were run in a single-stage centrifugal contactor, loading BTBP-based organic phases with millimolar concentrations of  $^{241}\text{Am}(\text{III})$ . Combining the results with results from stirred cell kinetic measurements [29], a kinetic model responding to loading was implemented in the SX Process code [30].

## Acknowledgements

Financial support for this research was provided by the European Commission (projects ACSEPT, contract 211267, ASGARD, contract 295825, and ACTINET-13, contract 232631), by the German Federal Ministry of Education and Research (BMBF; contracts 02NUK012A, 02NUK012D, 02NUK020A, and 02NUK020D) and the Stiftung Energie Baden-Württemberg (EnBW-Stiftung).

## References

[1] NEA No. 6894, OECD, Nuclear Energy Agency (NEA), Paris, 2011.  
 [2] Magnusson, D. et al., Solvent Extr. Ion Exch., 27(2): 97 (2009).  
 [3] Modolo, G. et al, Radiochim. Acta, 101(3): 155 (2013).

[4] Modolo, G. et al., Radiochim. Acta, 100(8–9): 715 (2012).  
 [5] Wilden, A. et al., Solvent Extr. Ion Exch., 31: (2013). DOI:10.1080/07366299.2013.775890  
 [6] Geist, A. et al., Solvent Extr. Ion Exch., 30(5): 433 (2012).  
 [7] Aneheim, E. et al., Sep. Sci. Technol., 47(5): 663 (2012).  
 [8] Bell, K. et al., Procedia Chem., 7: 392 (2012).  
 [9] Rostaing, C. et al., Procedia Chem., 7: 367 (2012).  
 [10] Bourg, S. et al., Nucl. Eng. Des., 241(9): 3427 (2011).  
 [11] Kolarik, Z., et al., Solvent Extr. Ion Exch., 17(5): 1155 (1999).  
 [12] Trumm, S. et al., Solvent Extr. Ion Exch., 29(2): 213 (2011).  
 [13] Hudson, M. J. et al., Dalton Trans., (9): 1675 (2003).  
 [14] Geist, A. et al., Solvent Extr. Ion Exch., 24(4): 463 (2006).  
 [15] Panak, P. J. and Geist, A., Chem. Rev., 113(2): 1199 (2013).  
 [16] Bremer, A. et al., Dalton Trans., 41(25): 7582 (2012).  
 [17] Bremer, A. et al., Inorg. Chem., 51(9): 5199 (2012).  
 [18] Bremer, A. et al., Radiochim. Acta, (accepted): (2013).  
 [19] Beele, B. B. et al., Procedia Chem., 7: 146 (2012).  
 [20] Sasaki, Y. et al., Solvent Extr. Ion Exch., 19(1): 91 (2001).  
 [21] Iqbal, M. et al., Supramol. Chem., 22(11/12): 827 (2010).  
 [22] Wilden, A. et al., Solvent Extr. Ion Exch., (2013), submitted.  
 [23] Magnusson, D., Malmbeck, R., Solvent Extr. Ion Exch., 30(2): 115 (2012).  
 [24] Bollesteros, M.-J. et al., Procedia Chem., 7: 178 (2012).  
 [25] Weaver B., Kappelmann F. A., USAEC report ORNL-3559, (1964).  
 [26] Banik, N. L. et al., Inorg. Chem. Commun., 29: 172 (2013).  
 [27] Müllich, U. et al., EP2377861 (2011).  
 [28] Magnusson, D. et al., Chem. Eng. Sci., 99: 292 (2013).

[29] Geist, A. et al., 12th Information Exchange Meeting on P&T, Prague, Czech Republic, 24–27 September 2012.

[30] Magnusson, D. et al., Solvent Extr. Ion Exch., (2013), accepted.



## 8 Vitrification of High-Level Radioactive Liquid Waste

### 8.1 VPC Project

*G. Roth, W. Grünwald, W. Tobie, S. Weisenburger, A. Salimi, J. Knobloch, K.-H. Weiß, K. Hardock, K. Meyer, H. Braun, U. Weiler*

The German-Chinese VPC (Vitrification Plant China) project has been established in November 2009 to construct an HLLW vitrification plant in the Sichuan province of China on the basis of the process technology developed by KIT-INE. From German side the project is executed by an industry consortium (STEAG Energy Services, WAK GmbH, Kraftanlagen Heidelberg GmbH) with KIT-INE as nominated subcontractor responsible for design of the core process technique and components like the waste glass melter and for input of process-chemical and glass-chemical knowhow and expertise. Besides the design work a main part of the contract also includes the delivery of core process components as well as of mechanical and remote handling equipment.

The Project is divided into three main phases: design phase (2009-2013), supply phase (2013/2014) and technical service (from 2014 on). In 2010 the main part of the project was dedicated to elaboration of the basic design of the vitrification plant and the intermediate storage building to be used for waste glass canisters. The subsequent Detailed Design (DD) of the parts to be supplied by the German side started in 2011 and will be finished in 2013.

#### 1. Detailed Design (DD)

The execution of the DD has been underway since 2011. The DD documentation includes dimensioning calculations, 2D/3D design drawings, data sheets and diverse lists for each part of a component as well as its 3D presentation. The DD documentation serves as detailed information to a potential manufacturer as basis for calculation of an offer price as well as a basis for the subsequent manufacturing procedure. All DD documents have to be checked by an independent quality assurance step before release to the manufac-

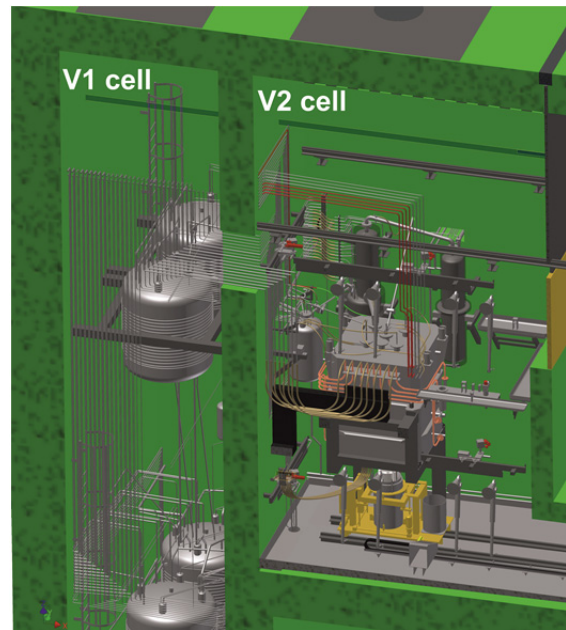


Fig. 1: 3D image of the HLLW receipt cell V1 and the cell V2 containing melter (center), feeding vessel (left), dust scrubber (rear, left) and condenser (rear, right).

turer. The QA procedure follows a well-defined control sequence plan. The DD created by INE mainly comprehends components inside the V2 cell being the waste glass melter, the HLLW feeding vessel, the dust scrubber and the condenser as well as the remote jumpers for the glass frit feeding line and the HLLW feeding line. Fig. 1 shows in a simplified manner the 3D-arrangement of the core process components in the V2 cell and parts of the HLLW receipt cell V1, additionally.

The glass melter as the key component of the vitrification process is composed of 19 sub-component groups. As shown in Fig. 2 it is composed of firmly integrated parts (group 1-6) like melt tank ceramic refractories, plenum ceramics, power electrodes, bottom electrode, stainless steel containment and remotely exchangeable parts (group 7-17) like bottom drain housing, HLLW and glass frit feeding pipe, off-gas pipe, thermo-well for

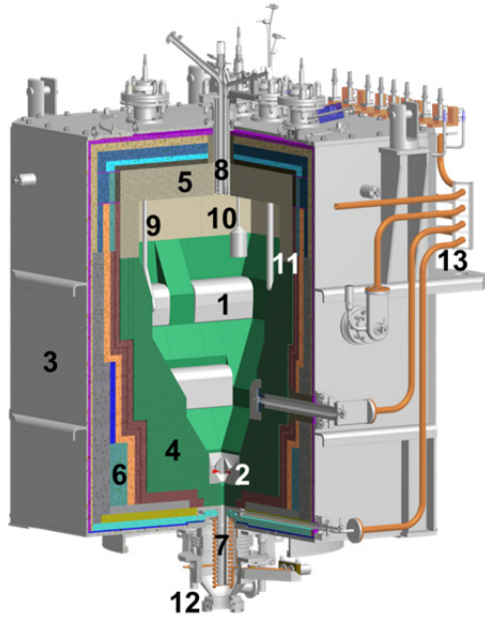


Fig. 2: Main structure of the VPC glass melter. Firmly integrated subcomponents: 1 Power electrodes, 2 bottom electrode, 3 stainless steel containment, 4 melt tank ceramic refractory, 5 melter plenum ceramics, 6 thermal insulation, 7 glass pouring pipe, Remote subcomponents: 8 feed inlet tube, 9 air bubbler, 10 glass level detection system, 11 thermo-well, 12 bottom drain housing, 13 copper tubes for power supply.

monitoring process temperatures, glass level detection system, and two air bubblers. The off-gas pipe had to undergo a completely new design being necessary due to the insufficient experience gained from the VEK operation [1]. The remaining subcomponent groups (18,19) are composed of service parts and tools for assembly and transportation of the melter. The bulk of the melter DD has been created in 2012 and will be completed until end of March 2013. The DD of the other process components was finished in 2012.

As consequence of changes in the design occurring as a result of elaboration of the DD the P+ID flow sheets had to be modified. The most severe modification was caused by the new design of the melter off-gas pipe.

## 2. Manufacturing of melter subcomponents

With respect to the assembly of the melter in 2013, the manufacturing of melter parts has been started in 2012 as one of the major tasks

of KIT. The manufacturing procedure includes the control and coordination of the working progress, of the time schedule and also the compliance with the QA control sequence plan. In the first manufacturing phase the fabrication of the firmly integrated melter sub-components was started. At first the high-temperature ceramic refractory for the melt tank was fabricated until mid of 2012 by company SEPR/France. In a next step the metallic glass-contacting subcomponents (power electrodes, glass pouring channel etc.) were manufactured by INE in cooperation with the mechanical workshop of KIT Campus North (TID). Parallel to these activities the manufacturing of the stainless steel containment of the melter by a specialized company was initiated. Figure 3 as an example shows subcomponents to be firmly integrated in the melter which are ready for melter assembly.

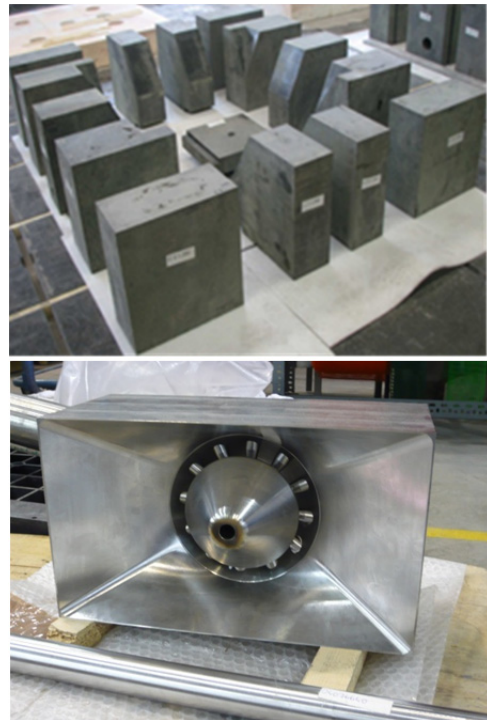


Fig. 3: Melter subcomponents manufactured for the VPC melter assembly (melt tank ceramic refractory-upper photo, bottom electrode).

## 3. Test of RFD Fluidic Pumps

The RFD (Reverse Flow Diverter) fluidic pumps will be used in the VPC plant for periodic transfer of HLLW batches of 4.9 m<sup>3</sup> from the

intermediate tank 841 BB 01 (which receives the HLLW solution from the storage building) to the receipt tanks 841 BB 02/03 (Fig. 1, V1 cell). The RFD fluidic pump has been selected as transfer system to replace the formerly used double-stage vacuum-supported airlift system as the airlift system could not cope with the required transfer height of about 10 m. Designer and supplier of the RFD fluidic pump element is the NuVision Engineering company located in Charlotte, Virginia, US. The design of application of RFD has been made by INE (P+ID flow diagrams

Prior to supply of the RFD fluidic pump and associated equipment to the VPC facility in China as well as for the purpose of carrying out the final part of the factory acceptance test, the items and the functions were tested in the PVA facility at INE under most representative operating conditions using one of two ordered pump systems. The test arrangement approaches as much as possible the operating conditions in the receipt cell V1 of the future VPC facility. The purpose of the testing was

- (1) to demonstrate and confirm the correct function according to specified operation parameters
- (2) to proof the reliability of long-term operation of the RFD fluidic pump and in particular the reliability of the associated control equipment

The RFD fluidic pump unit consists of the following major items:

- RFD pump element
- Charge vessel
- Delivery line
- Jet pump pair (JPP)
- Several control valves including the drive and suction valves
- PRESCON controller

Fig. 4 shows a simplified arrangement of the RFD pump system along with a scheme and photo of the RFD. The RFD together with the Charge Vessel is installed inside the tank. The RFD is connected to the Charge Vessel and via Delivery Line to the target tank. The Charge

vessel is connected to the Jet Pump Pair (JPP), which in turn is connected to a compressed air supply line. The working cycle of the RFD pump system is divided into three phases:

- Suction Phase: The jet pump pair generates a partial vacuum in the charge vessel sucking liquid through the RFD into the vessel
- Drive Phase: The jet pump pair pressurizes the charge vessel to drive the liquid through the RFD pump element into the delivery tank
- Vent Phase: When the charge vessel is nearly emptied it is depressurized through the jet pump pair into the tank ventilation system

The suction jet provides the suction of the liquid from the waste tank into the charge vessel during the suction phase. The drive jet is used to press the liquid out from the charge vessel into the delivery line which delivers the fluid to the target tank (e.g. the receipt tanks). The PRESCON controller is the central unit for control of the different working phases of the RFD fluidic pump.

The RFD fluidic pump unit had to be tested in the PVA facility of KIT-INE using equipment supplied by NuVision Engineering Inc. which will be used later in the VPC plant (RFD pumping element, PRESCON II controller, valve skid, pressure measurement devices). Other equipment had to be additionally supplied and installed to enable PVA's infrastructure for the performance of the test (delivery line air, vent line etc.). The charge vessel as part of the receipt tank to be shipped to China had been manufactured by a German supplier.

The arrangement of the test equipment in the PVA facility is shown in Fig. 5. The charge vessel with the RFD pump unit has been arranged in the existing PVA simulate tank (capacity 5.5 m<sup>3</sup>) located in the PVA basement. From there the transfer was performed via the delivery line and a break pot into the PVA receipt tank 01 which is connected to the receipt tank

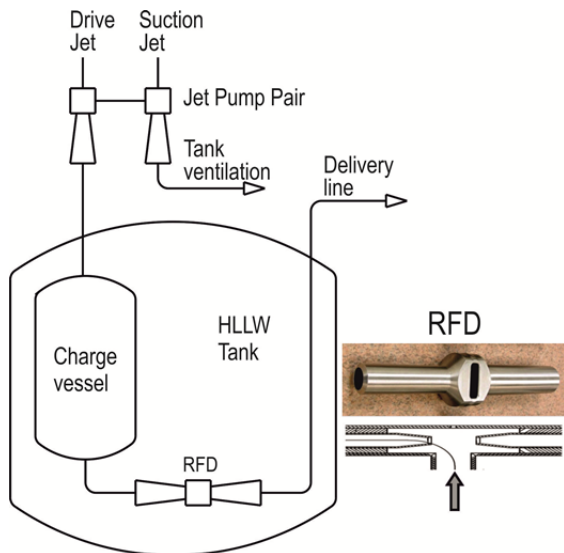


Fig. 4: Simplified arrangement of the RFD fluidic pump system.

02 by an overflow. As the volume capacity of each of the two PVA receipt tanks is  $3.2 \text{ m}^3$  the total volume capacity of the two tanks is  $6.4 \text{ m}^3$  which was sufficient for demonstration of the required transfer batch volume of  $4.9 \text{ m}^3$ . All three tanks (PVA simulate tank, PVA receipt tanks 01 and 02) were equipped with level measurement devices which allowed to monitor the fluidic pumping action and to calculate the RFD fluidic pump flow rate capacity. The liquid collected in the PVA receipt tanks 01 and 02 during a batch transfer operation of  $4.9 \text{ m}^3$  should be recycled into the PVA simulate tank for start of a new batch transfer by the RFD fluidic pump.

The height position of the RFD fluidic pump unit 841 PA 01 in the PVA simulate tank has been arranged at  $-2.65 \text{ m}$ . The upper end of the delivery line was placed in a height of  $+7.85 \text{ m}$ . Thus the effective pumping height for the liquid was  $+10.5 \text{ m}$  which is in compliance with the required value in the future VPC plant.

The test was carried out in three phases:

(1) Experimental arrangement of the RFD fluidic pump including modification of PVA infrastructure

(2) Basic function tests of the RFD fluidic pump (using water)

(3) Long-term reliability test using water and  $\text{NaNO}_3$ , alternatively, to simulate the higher density of the HLLW solution. Demonstration of the reliability of periodic transfers of  $4.9 \text{ m}^3$  batches from PVA simulate tank in the basement into the PVA receipt tanks 841 BB 01/02.

The test performed under the supervision of a representative of NuVision Engineering Inc. also served as final Factory Acceptance Test (FAT) for the RFD fluidic pump system to be supplied to China.

### Test results

The main purpose of the RFD test was to demonstrate the ability to overcome the pumping height of  $10.5 \text{ m}$  and to prove the transfer time of maximal  $3 \text{ h}$  for a  $4.9 \text{ m}^3$  HLLW batch. In the pre-test phase with water all the necessary installation and equipment was commissioned and the functions of measurement devices could be verified. During the long-term testing with water and sodium-nitrate 113 charge vessel cycles were performed in total (single cycle volume  $40\text{-}45 \text{ l}$ ) until the aspiration point of the RFD was reached. This point characterizes the lowest transfer level of the RFD in the tank. It appeared during the test that due to the aspiration point the actually transferred batch volume was limited to approximately  $4.5 \text{ m}^3$ .

The main results of the RFD testing were:

- Required pumping height achieved
- Transfer rate for a  $4.9 \text{ m}^3$  batch higher than required (extrapolated)
- Transfer time per batch of  $4.9 \text{ m}^3$  was approx.  $2.1 \text{ h}$  (extrapolated)
- Transfer rate for each charge vessel cycle is independent on the liquid level in the tank
- No influence of the density of the liquid on the transfer rate
- Transfer characteristics (volume in charge vessel, transfer rate) proved to be very uniform

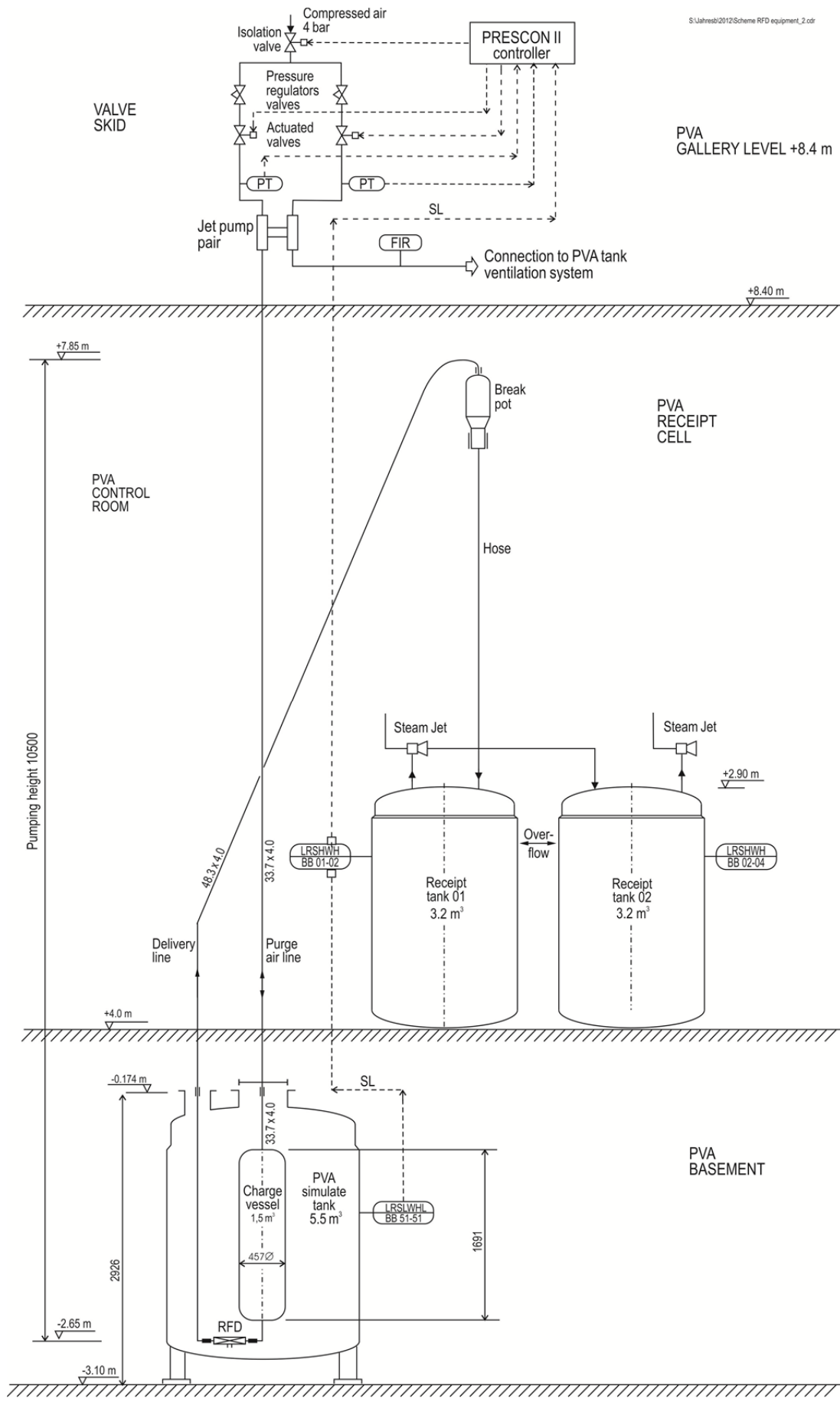


Fig. 5: Arrangement of the RFD fluidic pump system for testing in the PVA facility.

As a general result the suitability of the RFD system for the intended purpose in the VPC plant could be demonstrated. Moreover, the RFD system has successfully passed the Factory Acceptance Test necessary for application in the VPC plant in China.

#### **4. Outlook**

Detailed Design for the residual melter sub-components will be finished in spring 2013. Major activities are concentrated on final manufacturing of melter subcomponents and assembly of all subcomponents to the VPC melter ready for shipping to China. KIT-INE will be in charge of coordination and supervision of the assembly work to be carried out at INE. The total assembly time is estimated to last about 9 months.

In view of the installation, testing and commissioning of the core process components to

be supplied by the German consortium, functional test programs, commissioning programs and operation manuals will be created and shipped together with the respective core process component.

To ensure the production of a specified waste glass according to the contract, instructions for mass stream control and process control will be created as basis for implementation into the VPC process control system, supplied by the Chinese side.

#### **5. References**

- [1] Braun H., Grünwald W. et al., „Vitrification of High-level Liquid Waste“, published in Annual Report 2011, Institute for Nuclear Waste Disposal, Institut für Nukleare Entsorgung, H. Geckeis, T. Stumpf (eds.)

## 8.2 Structural investigations on the impact of increasing MoO<sub>3</sub> loadings in borosilicate glasses for the immobilization of Mo-rich nuclear wastes

A. Kutzer, T. Vitova, K. Kvashnina\*, T. Prüßmann, J. Rothe, C. Adam, P. Kaden, M. A. Denecke, S. Weisenburger, G. Roth, H. Geckeis

\* European Synchrotron Radiation Facility (ESRF), BP 220, 38043 Grenoble Cedex 9, France

### Introduction

Highly radioactive waste residual material remaining in HLLW storage tanks on the 'Karlsruhe Reprocessing Plant' (WAK) site following vitrification of the tanks' original liquid waste contains a high Mo(VI) content. This residual material can potentially be immobilized in a borosilicate glass matrix for ultimate disposal. Mo(VI) shows a low solubility in borosilicate glass, tending to separate out into molybdate-rich phases during the vitrification process [1]. These phases may crystallize during glass melt cooling and are able to incorporate significant amounts of radioactive isotopes within their crystal structure. However, the chemical composition of the formed phases is strongly dependent on borosilicate glass composition used, as well as the applied conditions in the vitrification process. If water soluble phases such as alkali molybdates are formed, the release of radioactivity into the environment will be facilitated in case of water intrusion into a deep geological repository. Understanding factors favoring or disfavoring the formation of soluble crystalline Mo(VI) phases in borosilicate glasses allows development of glass compositions capable of incorporating high Mo loadings, yet avoiding formation of such soluble phases.

In 2012 investigations on a nuclear waste simulate with varying MoO<sub>3</sub> concentrations vitrified in a multi-component borosilicate glass ('VPC' glass [2]) were performed. High resolution X-ray absorption near edge structure (HR-XANES) and magic angle spinning nuclear magnetic resonance (MAS NMR) techniques were applied to characterize glass network structure and molybdenum local atomic environment, respectively.

### Experimental

#### **Glass preparation:**

A glass frit was prepared from mixtures of stoichiometric amounts of SiO<sub>2</sub>, B<sub>2</sub>O<sub>3</sub>, Al(OH)<sub>3</sub>, Na<sub>2</sub>CO<sub>3</sub>, CaCO<sub>3</sub>, Li<sub>2</sub>CO<sub>3</sub>, MgO, BaCO<sub>3</sub>, V<sub>2</sub>O<sub>5</sub> and Sb<sub>2</sub>O<sub>5</sub>. The mixed powders were first decarbonized for 1 h at 800°C, in air, in a Pt crucible and then molten for 2 h at 1250°C. Subsequently, the glass melt was quenched as a cylinder on a stainless steel plate. To ensure homogeneity, the glass was ground and remelted for 2 h at 1250°C.

Respective amounts of the glass frit powder, the simulated waste composite containing an inactive mixture of 18 metallic and nonmetallic oxides and MoO<sub>3</sub> powder were mixed and then molten in a Pt crucible for 2 h at 1150, 1200 or 1250°C, depending on the MoO<sub>3</sub> content. Finally, the glass melts were quenched as cylinders on a stainless steel plate and ground to powders.

#### **MAS NMR:**

<sup>29</sup>Si MAS NMR spectra were recorded on a Bruker Avance III 400 spectrometer operating at 79.50 MHz. Powdered samples were spun at 15 kHz in a 4 mm MAS probe. A one pulse sequence with a 30 degree excitation pulse (7.8 μs) and a relaxation delay of 20 s was applied accumulating 15,360 scans for each experiment. Chemical shifts are reported relative to tetramethylsilane (with δ(<sup>29</sup>Si) = 0).

#### **HR-XANES spectroscopy:**

Mo K-edge HR-XANES spectra were recorded at the ID26 undulator beamline at the ESRF. Powdered glass samples and reference compounds, diluted with microcrystalline cellulose and pressed as pellets of 4 mm diameter, were prepared for measurements in fluores-

cence mode. The emitted Mo  $K_{\alpha}$  fluorescence was diffracted by a bent Ge(999) crystal at  $77.74^{\circ}$  Bragg angle and focused onto a Ketek silicon drift detector.

## Results and discussion

### MAS NMR studies:

All acquired  $^{29}\text{Si}$  MAS NMR spectra were modeled with Gaussian curves centered at  $\delta(^{29}\text{Si})$  values of 80.0, 92.2 and 103.6 ppm using the DMFit program [3]. These shift values model respective  $Q^2$ ,  $Q^3$  and  $Q^4$  environments ( $Q^n$  being tetrahedral  $[\text{SiO}_4]_n$  units with  $n = 0 - 4$  bridging oxygen atoms) [4]. Keeping the chemical shifts constant and varying individual Gaussian function intensities in fits to the  $^{29}\text{Si}$  spectrum (see Fig. 1) allows determination of the degree of silicon network polymerization as a function of glass  $\text{MoO}_3$  concentration (Fig. 2).

The evolution of the  $Q_n$  ratios in Fig. 2 reveals that  $[Q^2]$  decreases with increasing  $\text{MoO}_3$  content from 2 to 8 wt%, whereas  $[Q^3]$  increases.  $[Q^4]$  (framework  $(\text{SiO}_4)_n$ ) species are not present in any significant amount. These results suggest that the amount of crystalline phases in the glasses increases with increasing  $\text{MoO}_3$  concentration through formation of crystalline  $\text{CaMoO}_4$  and  $\text{BaMoO}_4$ . The formation of these phases removes the network modifiers  $\text{Ca}^{2+}$  and  $\text{Ba}^{2+}$  from the glassy network, and thereby creates higher ' $Q^n$ ' structures by replacing

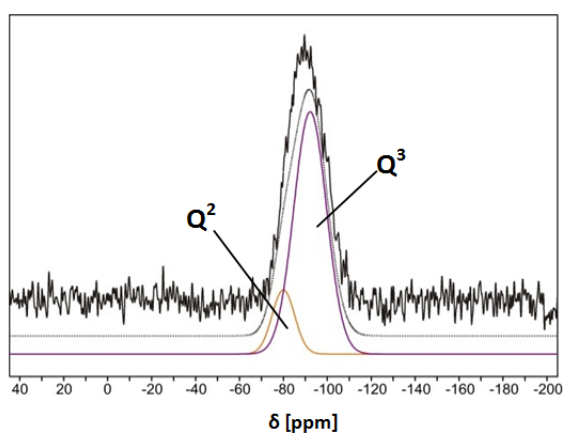


Fig. 1: A representative  $^{29}\text{Si}$  MAS NMR spectrum (black) fit result (narrow black line) and individual  $Q^n$  Gaussian fit curves (colored lines) for a model borosilicate glass containing 5 wt%  $\text{MoO}_3$ .

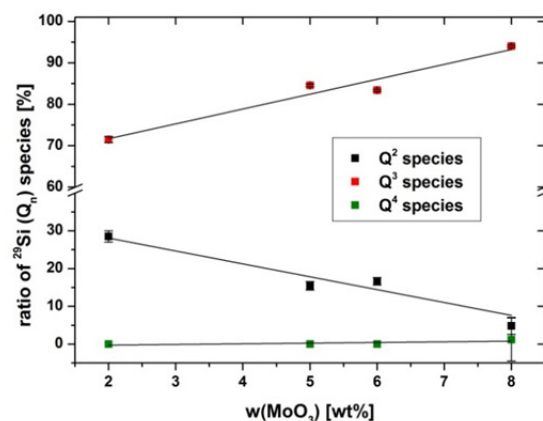


Fig. 2: Fit results of the  $^{29}\text{Si}$  MAS NMR spectra of the glass samples with increasing  $\text{MoO}_3$  content. The relative proportions of three different  $^{29}\text{Si}$  environments  $Q^2$  (black),  $Q^3$  (red) and  $Q^4$  (green) show a linear dependence as a function of the  $\text{MoO}_3$  loading in the glass.

non-bridging oxygen atoms with bridging ones (due to decreased need for modifier charge compensation in the glassy network).

### Mo K HR-XANES studies:

The Mo K-edge HR-XANES spectra of the borosilicate glasses containing varying  $\text{MoO}_3$  loadings are shown in Fig. 3 together with the spectra of crystalline  $\text{CaMoO}_4$ ,  $\text{BaMoO}_4$  and  $\text{Na}_2\text{MoO}_4$  as reference compounds. The shape of the spectral features in the glass spectra changes systematically as a function of the  $\text{MoO}_3$  concentration. Visual inspection shows that the spectrum of the glass with the highest  $\text{MoO}_3$  loading (12 wt%) resembles that of crystalline  $\text{CaMoO}_4$ . By modeling the HR-XANES spectra of the glasses by linear combination least squares fit analyses, the evolution of the Mo(VI) coordination structure with increasing glass  $\text{MoO}_3$  content was quantified. The  $\text{CaMoO}_4$ ,  $\text{BaMoO}_4$  reference HR-XANES and HR-XANES for three different borosilicate glasses, each containing low  $\text{MoO}_3$  content, one type of modifier cation ( $\text{Ca}^{2+}$ ,  $\text{Ba}^{2+}$  or  $\text{Na}^+$  designated as Ca-SiBMo, Na-SiBMo and Ba-SiBMo, respectively) and known to not contain crystalline molybdates (not shown in Fig. 3), were used in modeling the data. This choice of reference compounds for the fits was based on results obtained from SEM-EDX, powder X-ray diffraction (XRD) and Raman spectroscopic analyses. XRD and Raman studies confirmed formation of crystalline  $\text{CaMoO}_4$

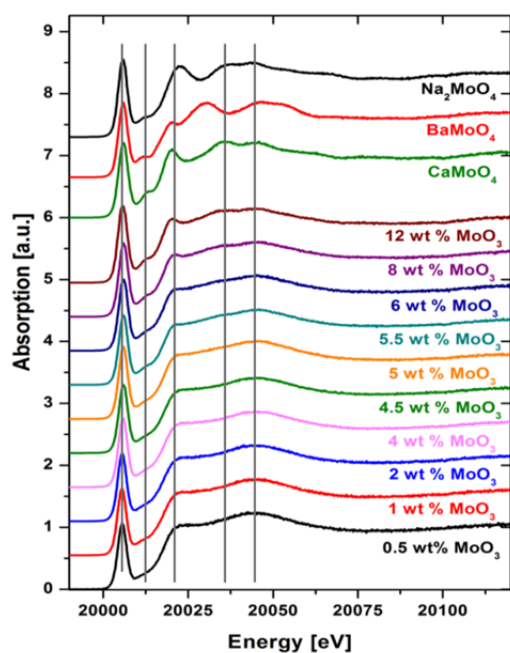


Fig. 3: Mo K-edge HR XANES spectra of glasses with increasing  $\text{MoO}_3$  concentration from bottom to top. The top spectra are from three crystalline reference compounds  $\text{Na}_2\text{MoO}_4$ ,  $\text{CaMoO}_4$  and  $\text{BaMoO}_4$ .

and  $\text{BaMoO}_4$  phases for  $\text{MoO}_3$  concentrations above 4 wt%. These phases are associated with spherically shaped regions on the glass surface, which increase in size with increasing  $\text{MoO}_3$  content, and shown in SEM-EDX to be rich in Ca, Ba, Mo and O.

The results of the HR-XANES fits are depicted in Fig. 4. For low  $\text{MoO}_3$  concentrations an amorphous environment dominates and  $\text{Na}^+$  cations preferably compensate molybdate

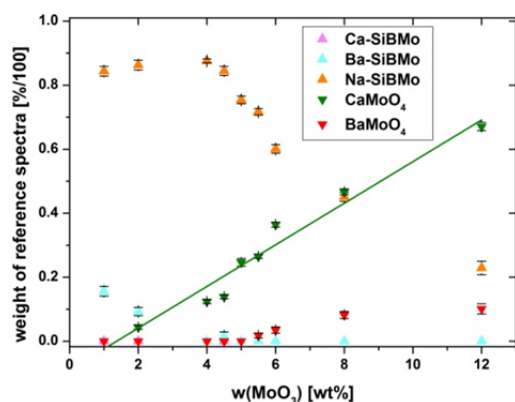


Fig. 4: Linear combination least squares fit results of Mo K-edge HR XANES spectra of glasses with increasing  $\text{MoO}_3$  concentration. See text for details.

charge over  $\text{Ba}^{2+}$  and  $\text{Ca}^{2+}$ . With increasing  $\text{MoO}_3$  concentration, the favored Mo atomic environment shifts from amorphous to crystalline and  $\text{CaMoO}_4$  and  $\text{BaMoO}_4$  phases form. At the highest  $\text{MoO}_3$  concentration crystalline  $\text{CaMoO}_4$  dominates, as expected from visual inspection of spectra. We find no evidence for the formation of water soluble crystalline alkali molybdates, indicating that the chemical composition of the glass used is favorable for immobilization of Mo-rich nuclear waste with this specific chemical composition.

## Outlook

Further work is underway to correlate observed HR-XANES spectral trends with cluster size by performing *ab initio* quantum chemical calculations using the multiple scattering approach (FEFF9 code). “Shell by shell” HR-XANES calculations might allow the estimation of the average cluster size of the crystalline particles formed in the glasses for  $\text{MoO}_3$  concentrations exceeding the solubility limit. In addition, Na, Ca and Ba K-edge XANES studies are planned in order to characterize the atomic environment of charge balancing cations as a function of  $\text{MoO}_3$  concentration.

## Acknowledgements

The authors gratefully thank the European Synchrotron Radiation Facility (ESRF) for beamtime and I. Pidchenko for support at the ID26 beamline. This work is financially supported by the WAK GmbH.

## References

- [1] Lutze, W., Ewing, R. C. (Hrsg.), Radioactive Wasteforms for the Future, North Holland, Amsterdam (1988).
- [2] Grünewald, W. et al., Proceedings of Global 2009, Paris, (2009).
- [3] Massiot, D. et al., Magn. Reson. Chem., 40: 70 (2002).
- [4] Caurant, D. et al., J. Nucl. Mater., 396(1): 94 (2010).



## 9 Development of actinide speciation methods

Maintaining a state-of-the-art analytical/instrumental portfolio at INE is an important R&D activity, as this is critical for advancing discovery and understanding of actinide and lanthanide (geo)chemistry. The new environmental SEM and XPS instruments at INE are examples, which better serve the surface analytical research needs. In 2012 progress in laser-based instrumentation include development of the first portable commercial LIBD system for field experiments and the use of confocal fluorescence microspectroscopy for Eu speciation. In the synchrotron-based R&D work, first applications of recent developments have been successfully performed, such as studies of Am(III) complexation with nitrate, chloride and lactate at elevated temperatures using a version of the high-T / high-pressure cell developed for TRLFS adapted for XAFS and characterization of corroded cement matrices from the Asse II salt mine using  $\mu$ -XAFS,  $\mu$ -XRF and  $\mu$ -XRD. In addition, significant progress in the multi-analyzer crystal spectrometer for high energy resolution X-ray emission spectroscopy (HRXES) was made this year. HREXS development has been supported by experimental and theoretical efforts. The NMR instrument at INE is being increasingly used for in-house research and is also part of the "Actinide NMR Centre of Excellence", which is accessible through highly competitive (five-fold over-subscription) application to the European EURACT-NMR project. Much of the inhouse developmental work is supported by theoretical quantum chemical calculations, some of which are developmental activities themselves, e.g., the new ansatz to parameterize the actinide – water interaction potential, and its implementation into the POLARIS MD-software package.

### 9.1 R&D projects conducted at the INE-Beamline for Actinide Research at ANKA and at external SR sources

*C. Bube, K. Dardenne, M. A. Denecke, D. R. Fröhlich, B. Kienzler, V. Metz, P. J. Panak, T. Prüßmann, J. Rothe, D. Schild, A. Skerencak, E. Soballa, T. Vitova*

#### Introduction

Continuous development and adaption of *in situ* speciation methods capable of providing molecular-scale information on key parameters determining radionuclide mobility in the barrier system surrounding a future HAW repository is necessary, with emphasis on methods applicable for long-lived actinide elements and fission products. The INE-Beamline for actinide science [1] at the KIT synchrotron radiation (SR) source ANKA was designed, constructed, and is operated as a flexible experimental station for spectroscopic investigation of these elements. The INE-Beamline is the only facility of its kind in Europe offering access to radiochemistry laboratories with state-of-the-art analytical and microscopy equipment in direct proximity to a SR experimental station dedicated to X-ray spectroscopic radionuclide characterization on the same research campus. Although its design is optimized for X-ray absorption spectroscopy

(XAS) applications, because of this unique constellation the INE-Beamline makes continual efforts to increase the portfolio of available methods to meet users' needs, in addition to user support in planning, performing and evaluating experiments, including addressing all relevant radiation safety and personal security clearance issues. INE scientists also conduct various experiments at external SR sources offering capabilities not – or not yet – available at KIT.

#### INE-Beamline user operation in 2012

In 2012 a total of 28 INE in-house and external projects were hosted at the INE-Beamline. The time available for INE internal research amounted to ~29% of all available shifts (32 days). Ten days were spent for maintenance, development and pilot experiments. As in the previous years, the majority of beamtime shifts in 2012 was given to external projects with (52 days) and without (7 days) PRC

(ANKA Peer Review Committee) ranking. INE projects at the beamline covered a broad range of topics related to safe disposal of HAW, with emphasis on actinide complexation and surface sorption phenomena, and alternative disposal strategies, e.g., reduction of HAW radiotoxicity. Many of these studies are presented in more detail elsewhere in this report or the recent ANKA Annual Report [2]. In-house projects in 2012 included studies of molybdate phases in simulated nuclear waste glasses, high temperature investigations of Am(III) complexation by sulphate and lactate, polarized XAFS measurements of lanthanide and Th(IV) doped brucite and hectorite, investigations of Np cation complexation by propionate, nitrate and fulvate ligands, studies of tetravalent actinide complexation by BTP extraction ligands, structural characterization of trivalent metal complexes of transferrin and measurements on sorption and redox speciation of Np(V) on Illite mineral phases.

General user research projects receive beamtime following PRC evaluation (biannually in January and June), as approved ACTINET-i3 Joint Research Projects (both together comprising at least 30% of all available shifts) or through direct cooperation with KIT-INE. In 2012 scientists from the 12 German and European research institutions listed below conducted experiments at the INE-Beamline:

- JRC - Institute for Transuranium Elements, Karlsruhe, EU;
- Institut für Kernchemie, Universität Mainz, Germany;
- Universität Heidelberg, Fakultät für Chemie und Geowissenschaften, Germany;
- Physics and Astronomy Department, Uppsala University, Sweden;
- University of Manchester, SEAES, Williamson Research Centre, United Kingdom;
- Cambridge University, Department of Earth Sciences, United Kingdom;
- KIT Institut für Nanotechnologie, Karlsruhe, Germany;
- CEA Cadarache, Saint Paul Lez Durance, France;
- CEA Marcoule, Bagnols-sur-Cèze, France
- Amphos<sup>21</sup>, Barcelona, Spain;

- Paul Scherrer Institut, Bereich Nukleare Energie und Sicherheit (NES), Villingen, Switzerland;
- Institut für Energie- und Klimaforschung 6, Forschungszentrum Jülich, Germany.

Seven projects in 2012 received beamtime and were funded as ACTINET-i3 Joint Research Projects.

As in previous years, a significant percentage of in-house and PRC beamtime was used by PhD students to perform experiments in the framework of their theses (a total of 7 projects, corresponding to ~20% of all available shifts).

### **Microfocus ( $\mu$ ) measurements at the INE-Beamline**

Since 2008 considerable effort has been undertaken at the INE-Beamline to implement spatial resolution in the  $\mu\text{m}$  regime for investigation of radioactive samples with heterogeneous elemental or phase distributions (cf. Annual Report 2009). In this context,  $\mu$ -XAFS ( $\mu$ -XANES/ $\mu$ -EXAFS),  $\mu$ -XRF and  $\mu$ -XRD have been combined to characterize U-rich regions in thin section samples of corroded cement matrices retrieved from the Asse II salt mine after long-term exposure (17 years) to salt (NaCl, MgCl<sub>2</sub>) brines [3,4]. Regions of interest were pre-selected from SEM backscattering images, showing high contrast for U-rich aggregates (hot spots) embedded in the corroded cement matrix (Fig. 1, left). A polycapillary optic mounted on a hexapod positioning unit was used to focus monochromatic radiation delivered by the double crystal monochromator to a beam spot-size of 25-30  $\mu\text{m}$  for  $\mu$ -XRF and  $\mu$ -XAFS measurements. Thin section samples mounted on quartz slides were placed on a three-axis positioning stage with the sample surface at a 45° angle to the incident beam for 2D scanning. A silicon drift detector was used for collecting X-ray fluorescence radiation. Uranium hot spots identified in element distribution maps reconstructed from the scanning  $\mu$ -XRF data were selected for  $\mu$ -XAFS and  $\mu$ -XRD analysis. Diffraction patterns were collected in Laue transmission mode on erasable X-ray sensitive films, mounted perpendicular

to the beam, downstream from the sample. In this case, a single bounce capillary was used to deliver a low divergent  $\sim 35\ \mu\text{m}$  focused beam.

Uranium-rich hot spots generally exhibit U L3-XANES energy positions characteristic for U(VI), in accordance with previous U speciation results based on bulk XAFS spectra [3], thus clearly confirming preservation of the hexavalent uranium state in the cement after long-time exposure to brine.  $\mu$ -XANES features obtained for most U hot spots and in more dif-

fuse U distributions located nearby are nearly indistinguishable from each other, obviously representing a prevalent U(VI) species formed throughout the corroded cement matrices. A representative  $\mu$ -XANES is shown in Fig. 1 (red curve marked F33-B1-50). These spectra exhibit features significantly different from those typical for U(VI) uranyl dioxo-moieties (e.g.,  $\beta$ -uranophane, Fig. 1, upper green curve) and resemble more a diuranate type phase (Fig. 1, upper red curve), characterized by elongated axial and reduced average equato-

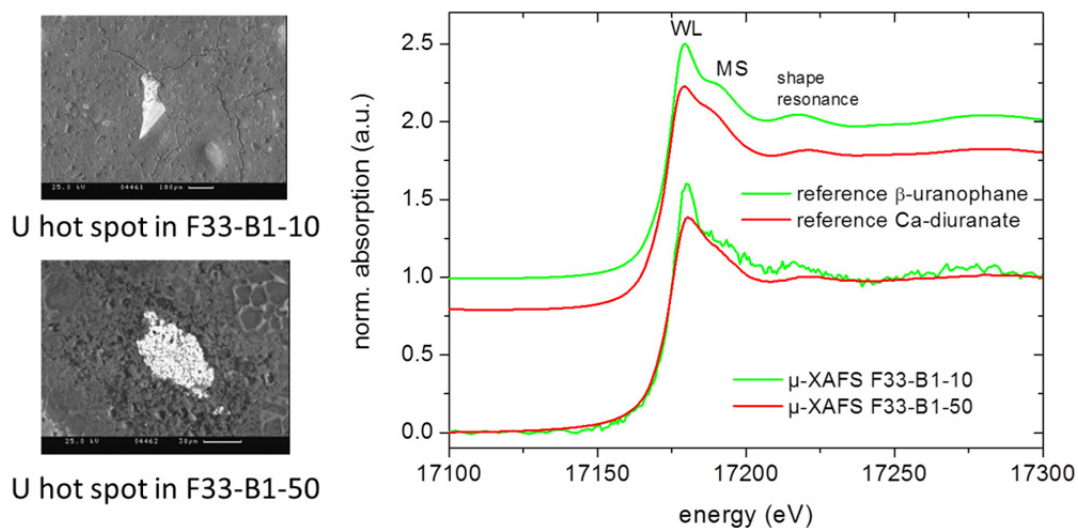


Fig. 1: left – SEM images of U-rich hot spots in corroded cement samples F33-B1-10 (top) and F33-B1-50 (bottom), taken from different core depths ( $\text{MgCl}_2$  system, cf. text for details); right – U L3  $\mu$ -XANES spectra recorded at these spots compared to bulk XANES of crystalline U(VI) references Ca-diuranate and  $\beta$ -uranophane (spectra vertically shifted for clarity).

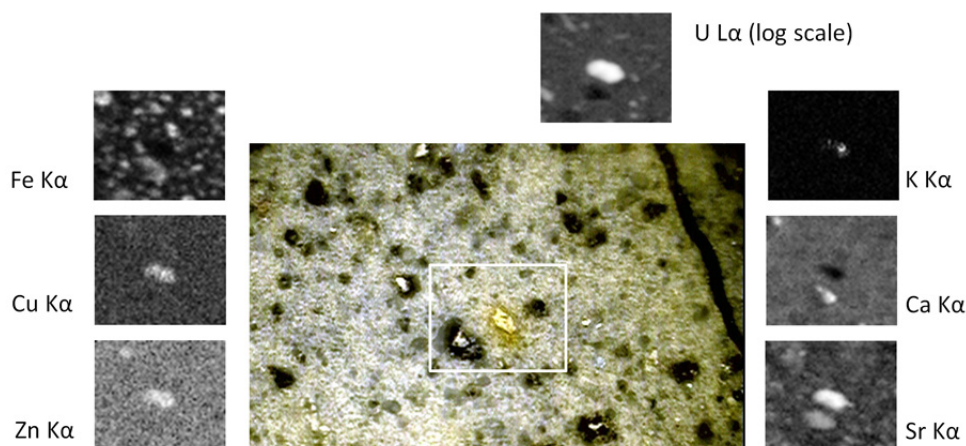


Fig. 2: VLM image of area around U hot spot in F33-B1-50 (same hot spot as depicted in SEM image, Fig. 1 bottom left) and  $\mu$ -XRF element distribution maps recorded for the marked area (scan area  $600\ \mu\text{m} \times 500\ \mu\text{m}$ ,  $10\ \mu\text{m} \times 10\ \mu\text{m}$  steps, beam spot size  $\sim 25\ \mu\text{m}$ ).

rial U-O distances compared to those typical for uranyl coordination polyhedra. This diuranate coordination geometry results in dampening of the U L3 white line (WL) intensity and a decrease in the energy difference between the WL and axial oxygen multiple scattering (MS) feature compared to that observed for uranyl containing materials. Nevertheless, at least one U-rich area in a MgCl<sub>2</sub> brine corroded sample having distinct XANES features similar to a uranophane-like U(VI) phase was found. These findings are in agreement with thermodynamic solubility calculations performed for the U-doped cement/MgCl<sub>2</sub> brine systems, suggesting that both diuranates and uranophane are possible solubility limiting phases in this cement/salt system. In contrast, measured U(VI) concentrations in the cement/NaCl brine system are only in agreement with a diuranate solubility limiting phase. In agreement, only diuranate-type  $\mu$ -XANES were observed for analogous cement samples corroded in NaCl (data not shown).

In addition to U-rich hot spots and uranium ubiquitously present in diffuse distributions throughout the thin section samples, a number of other elements associated with the cement and its additives are identified in  $\mu$ -XRF distribution maps. As a general trend, Fe shows a clear anti-correlation with U enriched areas, whereas K, Sr and Rb (not shown) show areas with distributions correlated to U-rich areas. Other transition metals (Ti, Mn, Cu, Zn) show either no or a U correlation to only limited sample areas (Fig. 2).  $\mu$ -XRD measurements of numerous U-rich hot spots, including those depicted in Fig. 1, show these to be generally X-ray amorphous; no evidence is obtained for the presence of any crystalline uranium phase. Weak diffraction patterns identified for some of these hot spots can be attributed to cement corrosion products.

### High-temperature XAFS

Due to the decay heat of high-level nuclear waste stored in a deep geological formation, the temperature in the repository near-field will increase significantly ( $T_{\max} = 100^{\circ}\text{C}$  (clay), or  $200^{\circ}\text{C}$  (salt)). In a possible failure scenario,

the increased temperature will change the chemical properties of radionuclides dissolved after groundwater influx and container / waste matrix dissolution. To investigate the complexation behaviour of actinides at elevated temperatures, a custom built high-T / high-pressure cell already successfully used in time-resolved laser fluorescence spectroscopy (TRLFS) studies [5] has been adapted for XAS measurements at the INE-Beamline (cf. Annual Report 2010). This set-up was used to study the interaction of Am(III) with different (in)organic ligands (i.e., nitrate, chloride, lactate) as a function of temperature. As an example, Am L3-EXAFS spectra of 1 mM Am(III) in the presence of 5 mM lactate at 20 and 90°C are depicted in Fig. 3 (solid lines). Their best fits to the EXAFS equation are shown as symbols and related structural parameters given in Tab. 1. EXAFS analysis shows that the amount of complex formed is reduced with increasing temperature, indicated by a decrease in number of carbon neighbours in the second coordination sphere at 90°C. Hence, the related complex formation reaction is an exothermic process. Furthermore,

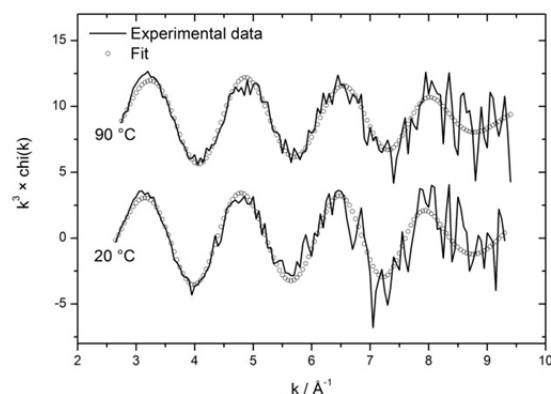


Fig. 3:  $k^3$ -weighted high-temperature EXAFS spectra of 1 mM Am(III) in 0.1 M NaCl solution in the presence of 5 mM lactate at 20 and 90°C.

Table 1: Structural parameters related to the fit curves in Fig. 3.

T / °C	Am-O			Am-C*		$\Delta E_0$ / eV
	N	R / Å	$\sigma^2$ / Å <sup>2</sup>	N	R / Å	
20	10.5	2.46	0.010	2.8	3.40	-2.2
90	10.0	2.45	0.012	1.8	3.35	-0.6

Errors of N  $\approx$  1, R  $\approx$  0.01 (Am-O) and 0.04 Å (Am-C),  $\sigma^2 \approx$  0.001 Å<sup>2</sup> (Am-O),  $\Delta E_0 \approx$  1 eV, \* $\sigma^2$  set to 0.003

the Am-C distance of 3.35 - 3.40 Å clearly indicates that lactate is bound through its carboxyl- and  $\alpha$ -hydroxyl-function, forming a chelate complex with Am(III).

### High resolution X-ray emission spectroscopy (HRXES)

In 2012 the design and manufacture of the multi-analyzer crystal (MAC) spectrometer for high energy resolution X-ray emission spectroscopy (HRXES) have been completed (Fig. 4). The spectrometer assembly comprises a mobile and a stationary positioning unit, both supplied by HUBER Diffraktionstechnik GmbH (Rimsting, Germany). The five analyzer crystal positioning stages possess four degrees of freedom each. The crystal stages are mounted on a common granite block, which is installed on a mobile rack, hosting power supplies and motion controllers for all 23 spectrometer motors. The stationary detector positioning unit comprises three degrees of freedom (a long and a short linear stage and a rotation stage), which allow the detector to be moved along the Rowland circle. Initial mechanical spectrometer performance tests and adaption of the control software were started in the 2012/2013 ANKA winter shutdown.

In 2012 benchmark calculations of lanthanide (Ln) and actinide (An) L3 edge high energy resolution X-ray absorption near edge structure (L3-HR-XANES) and Ln L3 edge core-to-core resonant inelastic X-ray scattering (L3-CC-RIXS) spectra have been performed with the *ab initio* quantum chemical code *FEFF9.5* in collaboration with the group of Prof. John Rehr, Washington State University, USA [6,7]. Both a  $4f$  ( $\text{Yb}_2\text{O}_3$ ) and a  $5f$  system (the natural mineral schroeckingerite) were considered. The experimental and calculated Yb L3-HR-XANES spectra of  $\text{Yb}_2\text{O}_3$  and the corresponding experimental and calculated Yb L3-CC-RIXS, are plotted in Fig. 5a & 5b, respectively. The *FEFF9.5* code successfully reproduces all spectral features at energies differing only a few eV from the experimental values for Yb; some intensity differences are also observed.

$\text{Yb}_2\text{O}_3$  is characterized by Yb1 and Yb2 sites in octahedral and distorted octahedral coordina-

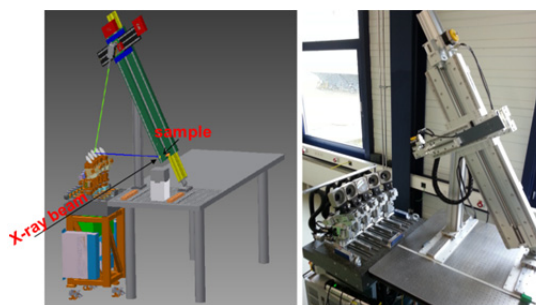


Fig. 4: 3D CAD model (left) and photo of the MAC spectrometer during initial mechanical performance tests (right).

tion, respectively. The weighted Yb1 and Yb2 calculated spectra including only dipole or quadrupole transitions are shown in Fig. 5a. The Yb L3-HR-XANES spectrum is a linear combination of the two calculated spectra ( $1/4 \times \text{Yb1} + 3/4 \times \text{Yb2}$ ). The A1 (Yb2) and A2 (Yb1) regions in the pre-edge feature originate mainly from  $2p_{3/2} \rightarrow 4f$  electronic transitions. In contrast,  $2p_{3/2} \rightarrow 5d$  transitions lead to broadening of the A1 peak (Yb2). The calculated energy difference between features A1 and B2 (15.7 eV) and B1 and B2 (4 eV) is larger, whereas the distance between B2 and C (12.1 eV) is smaller, compared to the experimental spectrum (B2-A1=13.4 eV, B2-B1=3.3 eV, B2-C= 16.7 eV). In Fig. 5b the Yb  $L\alpha_1$  emission is plotted on the energy transfer scale as a function of the excitation energy (Yb L3-CC-RIXS). The Yb L3-CC-RIXS of  $\text{Yb}_2\text{O}_3$  displays an intense pre-edge structure at about 8935 eV and a double structure in the WL region. The left RIXS plot shows the *FEFF9.5* calculation result using only dipole transitions ( $2p_{3/2} \rightarrow 5d$ ), the middle plot the result obtained including quadrupole transitions ( $2p_{3/2} \rightarrow 4f$ ). The pre-edge absorption resonance is weak in the left plot but the middle plot has much stronger intensity and both have positions comparable to the experimental spectrum (right), thus suggesting  $2p_{3/2} \rightarrow 4f$  transitions dominate this part of the spectrum, with an admixture of  $2p_{3/2} \rightarrow 5d$  transitions. This interpretation is in accordance with previous atomic multiplet calculations restricted to the pre-edge region [8], attributing the pre-edge feature to  $2p_{3/2} \rightarrow 4f$  electronic transitions. The experimental and theoretically calculated U L3-HR-XANES, as well as the U unoccupied  $f$  and  $d$  angular mo-

mentum projected density of states (*d*- and *f*-DOS) for the mineral schroekingite are depicted in Fig. 5c. In this case the FEFF9.5 code successfully reproduces spectral features at correct energy positions. The results reveal that  $2p_{3/2}$  electronic transitions to  $5f$  valence states contribute to the pre-edge region at  $\sim 9$  eV relative energy, indicated by the pronounced calculated U *f*-DOS maximum in this energy region. The WL and post-edge regions

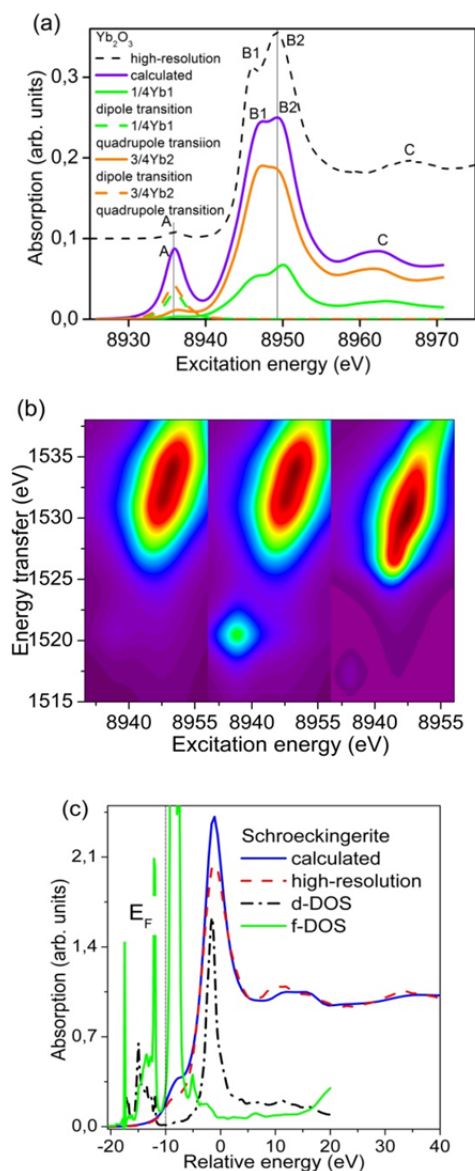


Fig. 5: (a) experimental Yb L3-HR-XANES of  $\text{Yb}_2\text{O}_3$  compared to FEFF9.5 calculation; (b) FEFF9.5 calculation of Yb L3-CC-RIXS for  $\text{Yb}_2\text{O}_3$  including dipole (left) or dipole and quadrupole transitions (middle) compared to the experimental Yb L3-CC-RIXS (right); (c) experimental U L3-HR-XANES of schroekingite compared to FEFF9.5 calculation and the calculated *d*- and *f*-DOS.

of the U L3-HR-XANES spectrum are well described by dipole  $2p_{3/2} \rightarrow 6d$  transitions and resemble the U *d*-DOS as expected.

The capability of the HR-XANES and RIXS techniques to measure the relative energy difference between An/Ln *f* and *d* states in materials with small structural variations is extremely valuable for fine-tuning theoretical approaches. These techniques will also shed light onto the degree of stabilization of the An  $5f$  valence orbitals across the actinide series and onto the amount of orbital mixing between An/Ln valence and ligand molecular orbitals.

## Outlook

The MAC spectrometer will be commissioned and exhaustively tested in various pilot experiments at the INE-Beamline in 2013. In addition, further milestones towards realization of the new high-energy / high-flux CAT-ACT beamline at ANKA (cf. Annual Report 2011) will be achieved. After finishing the necessary ANKA hall east extension in 2012, construction of the control cabin has commenced. Once the beamline front-end and optics design is finalized, ordering of all components and the radiation protection hutch will follow (summer 2013). Fabrication of the wiggler source began in November 2011. Its delivery and installation, along with the front-end section, is planned for the 2013/14 ANKA winter shut-down.

## Acknowledgement

Many thanks to H. Blank (Bonn University), A. Neumann, V. Krepper, J. Thomas, A. Bauer and C. Marquardt (all INE), T. Hoffmann and G. Christill (both KSM) for invaluable technical and logistic support.

## References

- [1] Rothe, J. et al., Rev. Sci. Instrum., 83: 043105 (2012).
- [2] ANKA Annual Report 2010/2011, KIT (2012).
- [3] Kienzler, B. et al., Radiochim. Acta, 98: 675 (2010).

- [4] Rothe, J. et al., Journal of Physics: Conference Series, 2013 (in print).
- [5] Skerencak, A. et al., Radiochim. Acta, 97: 385 (2009).
- [6] Prüßmann, T. et al., Journal of Physics: Conference Series, 2013 (in print).
- [7] Vitova, T. et al., Journal of Physics: Conference Series, 2013 (in print).
- [8] Kvashnina, K. et al., J. Anal. At. Spectrom., 26: 1265 (2011).

## 9.2 Laser spectroscopy

S. Büchner, S. Eidner<sup>a</sup>, C. Garcia-Perez, H. Geckeis, A. Geist, R. Götz, W. Hauser, C. Hille<sup>a</sup>, M. Kumke<sup>a</sup>, T. Kupcik, J. Laber, U. Müllich, P. J. Panak, C. M. Ruff, T. Schäfer

<sup>a</sup>Universität Potsdam, Institut für Physikalische Chemie, UPPC, Karl-Liebknecht-Str. 24-25, 14476 Golm, Germany

### Introduction

Development of new and existing analytical/instrumental methods is crucial in endeavours to understand the environmental behaviour of actinide and lanthanide elements. Development of laser spectroscopic methods, including laser induced breakdown detection (LIBD) and time-resolved laser fluorescence spectroscopy (TRLFS), play an important role in the INE R&D program. Recent efforts are devoted to improve LIBD capabilities for detection of colloidal nanoparticles. Building upon years of experience of INE scientists both in the laboratory and infield experiments, the first portable commercial LIBD system is currently under development. Recent TRLFS activities at INE include use of confocal fluorescence microspectroscopy for Eu speciation in highly compacted clay systems and fundamental studies devoted to identifying reasons for selectivity in complexation of An(III) over Ln(III) with partitioning relevant extraction ligands.

### Development of a commercial mobile nanoparticle analyzer

In a technology transfer project between KIT-INE, KIT-IMA (Innovation Management) and the industrial partner Cordouan Technologies (Bordeaux, France), a nanoparticle analyzer named MAGELLAN has been designed and a prototype assembled. The aim of the project is to develop a commercially available, mobile instrument, which is robust enough to be used for colloid detection under field conditions.

MAGELLAN uses LIBD to measure the size distribution (size range: 10 nm to 1  $\mu$ m) and concentration of colloids with high sensitivity (ng/L). The complete nanoparticle analyzer prototype with its cover plate removed is shown in Fig. 1 showing the upper portion of the instrument containing optical compo-



Fig. 1: First prototype of a commercially available nanoparticle analyzer. Inset: close-up of the sample cuvette. The photoacoustic sensor head is seen at the lower left.

nents: a diode-pumped solid-state laser, a pulse-energy setting polarizer, two 90 degree mirrors, an energy detector and lenses to focus the laser beam into a standard flow-through cuvette. The breakdowns are detected with a photoacoustic sensor developed at INE. The 19'' module contains the complete instrument, including the electronic components in the bottom portion of the instrument; only the controlling computer is an external part.

The next steps of the project are calibration of the prototype, optimization of the evaluation software and assembly of further instruments.

### Eu speciation in a compacted Na-illite sample: a confocal microscopy study

Clay mineral-rich sedimentary formations are currently under investigation as host formations for disposal facilities for high-level nuclear waste in several countries (e.g., Boom Clay (BE), Opalinus Clay (CH) and Callovo-Oxfordian argillite (FR), see [1] and reference therein). In addition, compacted bentonites, mainly composed of smectite-type clay miner-

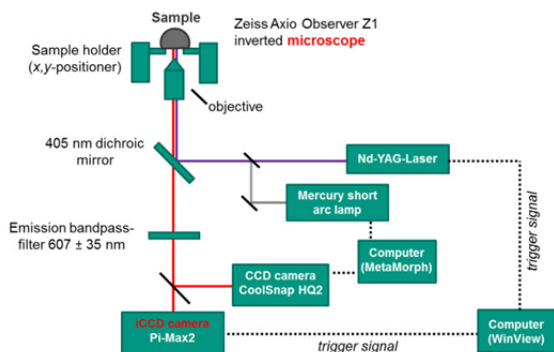


Fig. 2: Experimental setup for the confocal microscopy experiments.

al montmorillonite, are proposed as geotechnical barriers. Thus, a thorough understanding of the migration processes of radionuclides in compacted clay systems is an important requirement for a quantitative assessment and a long-term safety analysis of such a repository in deep geological formations. In contrast to neutral (HTO) and anionic species (e.g., Cl<sup>-</sup>) [2] or cations sorbed by outer-sphere complexation (cation-exchange; e.g., Sr<sup>2+</sup>) [3], only little is known about the diffusion of cations sorbed by inner-sphere complexation (surface complexation; e.g., Zn<sup>2+</sup>, Eu<sup>3+</sup>).

In order to describe trivalent actinide/lanthanide speciation in highly compacted clay systems (here Na-illite), Eu speciation (i.e. its hydration state) of an illite-filled column following an in-diffusion experiment was investigated by confocal fluorescence microscopy.

### Experimental description and results

Illite de Puy used in this study was purified according to a procedure agreed on within the EC project CP CatClay ([www.catclay.org](http://www.catclay.org)). A Eu in-diffusion experiment with a compacted, cylindrical Na-illite sample Illite de Puy (8.18 g,  $d = 2.54$  mm,  $h = 10$  mm, compaction factor =  $1.61$  g/cm<sup>3</sup>) was performed at a background electrolyte concentration of 0.2 M NaCl. The experimental set-up comprises a diffusion cell made of PEEK material after the design of [2], a peristaltic pump and two reservoirs, one containing the Eu solution ( $10^{-6}$  M), the other the background electrolyte. The solutions were circulated through the end plates and

the Eu concentration was monitored in regular time intervals. While the Eu concentration decreased slowly for < 60 d, it dropped to almost zero for longer reaction times. This steep decrease can be attributed to an increase of pH from 5.3 to 6.4, as no additional buffer was added. After 150 days, the contact solution was exchanged by different methanol/water ratios, followed by epoxy resin (LRwhite<sup>®</sup>) impregnation. Analysis of the various alcohol/water mixtures and the epoxy resin revealed no mobilization of Eu during this preparation step. After drying, the clay core was cut and investigated by confocal microscopy (Fig. 2) at UPPC (Universität Potsdam, Institut für Physikalische Chemie). Images of the sample surface were recorded both in fluorescence, as well as in incident light mode.

In Figure 3a an image of the compacted Na-illite recorded in fluorescence mode is presented, showing the core edge in contact with the Eu containing reservoir. Eu fluorescence is detected near the sample edge, as well as inside the compacted Na-illite core. Fluorescence decay curves originating from two different areas (indicated in Fig. 3a) are presented in Fig. 3b. Both curves show biexponential decay behaviour, which can be approximated by two Eu fluorescence lifetimes,  $\tau_1 = 46$   $\mu$ s and  $\tau_2 = 200$   $\mu$ s. Based on [4] the latter lifetime corresponds to  $\sim 5$  bound H<sub>2</sub>O/OH<sup>-</sup> entities, indicating a surface sorbed, inner-sphere Eu, which has lost  $\sim 4$ -5 water ligands in the original hydrate sphere of the aquo ion. The relative short lifetime of 46  $\mu$ s points to fluorescence quenching processes, which can be due to Eu-Eu (short interatomic distances of surface sorbed Eu) or Eu-Fe interactions [5] (Fe is present at 6.8 wt.-% in the used Na-illite).

By comparing these results with studies on clay suspensions [6] and assuming a similar sorption behaviour of Eu and Cm [7], we conclude that two different Eu species exist in the compacted Na-illite sample under the given experimental conditions (i.e. between pH 5.3 and 6.4):  $\equiv\text{S}-\text{Eu}(\text{H}_2\text{O})_5$  and  $\equiv\text{S}-\text{Eu}(\text{OH})(\text{H}_2\text{O})_4$  ( $\equiv\text{S}$  denotes the clay surface). However, a clear diffusion profile was not obtained, which can mainly be attributed to a rough sample sur-

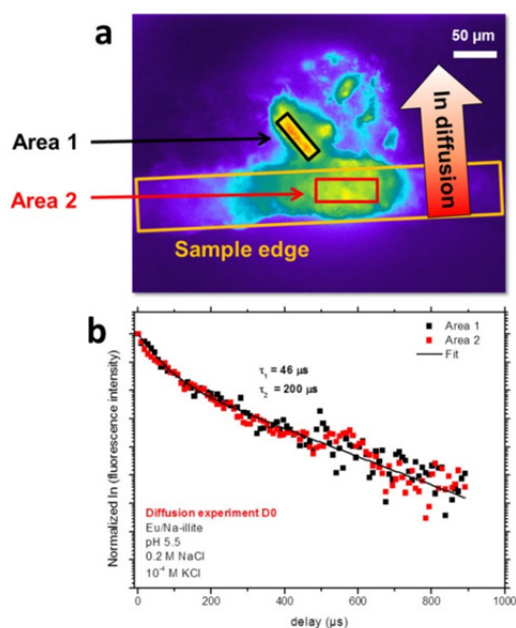


Fig.3: (a) Eu fluorescence in a compacted Na-illite sample. The sample edge as well as the Eu in-diffusion direction is indicated in the figure. (b) Eu fluorescence decay at increasing delay times originating from two different areas on the sample.

face and difficulties in focusing the emitted fluorescence light.

In summary, confocal fluorescence microscopy was successfully applied to investigate the Eu speciation in a compacted Na-illite. Comparing these Eu results with previous studies using Cm [7] indicates a comparable metal ion speciation for trivalent lanthanides and actinides in a compacted and dispersed Na-illite system, under the given experimental conditions. Future experimental optimization will reduce surface roughness (including microtome slicing or broad ion beam polishing).

### TRLFS for studying the coordination chemistry of f-ions (Cm(III) and Eu(III)) with aq-BTP molecules

The coordination chemistry and thermodynamic properties of trivalent actinides and lanthanides complexed with bis-triazinyl pyridine-type ligands (BTPs) are of particular interest to establish fundamental understanding of the An(III)/Ln(III) separation processes with BTP [8]. TRLFS can be applied to characterize

metal complexation associated with extraction processes on a molecular level.

In recent years a hydrophilic BTP molecule, 2,6-bis(5,6-di(sulfophenyl)-1,2,4-triazin-3-yl)-pyridine (aq-BTP) was developed to be used in the so called innovative SANEX process [9]. In addition to aq-BTP's excellent separation and complexation properties towards trivalent f-ions, aq-BTP also shows exceptionally strong sensitization of the Cm(III) and Eu(III) luminescence due to distinct antenna effects of the extended aromatic ligand system [10]. In order to calculate complex concentrations needed to determine thermodynamic data, these energy transfer processes in the sensitization must be quantified. This can be done by introducing relative fluorescence intensity factors,  $f^{rel}$ , which connect the spectroscopically determined peak areas  $\chi$  of the M(III) emission bands with the respective species concentrations.

$$[M(\text{III})\text{-complex } i] = \frac{\chi_i}{f_i^{rel}} \cdot [M(\text{III})]_{\text{tot}}$$

Since M(III) forms complexes with one, two and three aq-BTP-ligands [11], a linear regression of the relative fluorescence intensity  $I^{rel}$  according to the following equation was performed to determine the complex-specific factors.

$$I^{rel} = \sum_i f_i^{rel} \cdot \chi_i$$

The emission intensity of the solvated f-element ion (Cm(III), Eu(III)), which is the only species present in solution in absence of the ligand, is used as an internal reference by defining its fluorescence intensity factor to be 1.0. Figure 4 shows the spectroscopically determined and calculated evolution of the relative fluorescence intensity  $I^{rel}$  of Cm(III) with increasing [aq-BTP] in H<sub>2</sub>O (pH 3.0). The intensity contributions of the different [M(aq-BTP)<sub>n</sub>] (n = 0-3) complexes are also displayed. An identical regression procedure was also performed for the evaluation of the Eu(III) fluorescence intensities.

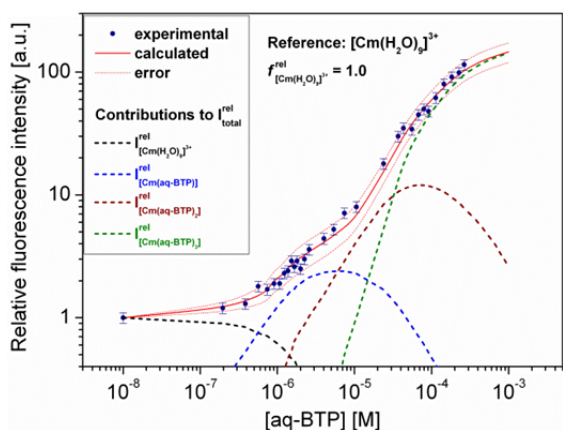


Fig. 4: Spectroscopically determined and calculated evolution of the relative fluorescence intensity of Cm(III) with increasing [aq-BTP] in H<sub>2</sub>O (pH 3.0).

The resulting fluorescence intensity factors of the [M(aq-BTP)<sub>n</sub>] (n = 0 - 3) complexes for M = Cm(III) and Eu(III) in H<sub>2</sub>O are summarized in Table 1. The sensitization of the f-ion luminescence increases with increasing number of coordinated aq-BTP ligands. Furthermore the energy transfer processes are more effective in the case of the Eu(III) ion compared to Cm(III). As a consequence of the magnitude of the FI factors, their consideration becomes crucial for the calculation of thermodynamic data.

Table 1: Relative fluorescence intensity factors of the [M(aq-BTP)<sub>n</sub>] (n = 0 - 3) complexes in H<sub>2</sub>O

Complex	FI-factor $f^{rel}$	
	Cm(III)	Eu(III)
[M(H <sub>2</sub> O) <sub>9</sub> ] <sup>3+</sup>	1.0	1.0
[M(aq-BTP)]	3.3 ± 1.0	9.0 ± 2.0
[M(aq-BTP) <sub>2</sub> ]	21.0 ± 4.0	96.5 ± 25.0
[M(aq-BTP) <sub>3</sub> ]	165.0 ± 30.0	1410 ± 300

These results clearly demonstrate the reliability and significance of considering fluorescence intensity factors, when sensitizing ligands such as aq-BTP are studied. Therefore, the present work is of high relevance for future spectroscopic studies of the coordination chemistry of f-ions with BTP type molecules.

## References

- [1] Altmann, S. et al., Appl. Geochem., 27(2): 463 (2012).
- [2] Van Loon, L. R. et al., J. Contam. Hydrol., 61: 73 (2003).
- [3] Van Loon, L. R. et al., Appl. Geochem., 20: 2351 (2005).
- [4] Horrocks, W. D. and Sudnick D. R., J. Am. Chem. Soc. 101(2): 334 (1979).
- [5] Hartmann, E. et al., Environ. Sci. Technol., 42(20): 7601 (2008).
- [6] Rabung, T. et al., Geochim. Cosmochim. Ac., 69(23): 5393 (2005).
- [7] Choppin, G. R., J. Alloy. Compd., 223(2): 174 (1995).
- [8] Panak, P. J. and Geist, A., Chem. Rev., 113: 1199 (2013).
- [9] Geist, A. et al., Solvent Extr. Ion Exch., 30: 433 (2012).
- [10] Weissman, S. I., J. Chem. Phys., 10: 212 (1942).
- [11] Ruff, C. M. et al., Dalton Trans., 41: 14594 (2012).

### 9.3 New instruments for surface analysis

*D. Bach, M.A. Denecke, H. Geckeis, D. Schild, E. Soballa*

#### Introduction

Surface analysis of minerals and solids comprising the multi-barriers of a nuclear waste repository is essential for microscopic description of chemical processes such as waste form corrosion, precipitation of secondary phases, redox-reactions of actinides at the solution-solid interface and actinide retention by incorporation into minerals. The scanning electron microscope (SEM) and X-ray photoelectron spectrometer (XPS) surface analytical instruments at INE were recently modernized to better serve the needs of present research activities and to provide new state-of-the-art analytical possibilities. The new SEM is a so-called environmental scanning electron microscope (ESEM), which enables analysis of wet samples by an adjustable water atmosphere inside the analytical chamber. Potential applications are analysis of gel layers on corroded glass, clay materials in their hydrated state, suspensions, hydration/dehydration phenomena and phase transformation. The new XPS is equipped with a scanning X-ray microprobe for analyses of small sample amounts such as radioactive particles. An argon glove-box is available (equipped with a sputter and carbon coater), which enables mounting of air-sensitive and/or radioactive samples and transfer to the instruments without air-contact.

#### Environmental Scanning Electron Microscopy (ESEM)

The ESEM of type FEI QUANTA 650 FEG (Figure 1) is equipped with a field emission gun to generate a fine focused electron beam, with ultimate resolution of 1.0 nm at 30 kV. Several detectors are installed to analyse the signals stemming from electron beam - sample interaction: a secondary electron detector for sample surface imaging (Figure 2), a backscattered electron detector for Z contrast imaging, a scanning transmission electron microscopy



Fig. 1: Environmental scanning electron microscope station in the surface analysis lab in INE active laboratories. The ESEM itself is to the right; top: electron source and column, middle: analytical chamber with docking station for transfer vessel at far right.

(STEM) detector with bright and dark field (Z contrast) imaging capabilities, a wet-STEM detector combining a cold stage with a STEM detector for observing thin liquid films in transmission mode, a thermoelectric cooled silicon drift X-ray detector for energy dispersive analysis of characteristic X-rays (EDX) excited by the electron beam and thereby providing elemental analysis of samples.

Differential pumping stages within the electron optics column provide a pressure gradient between the analytical chamber and the ultra-high vacuum at the field emission source of about 10 orders of magnitude. The pressure inside the analytical chamber can be selected in the range from high-vacuum, about  $6E-4$  Pa, to a maximum of 2600 Pa using water vapour (Figure 3). An oil-free pumping system and a plasma cleaner is applied to minimize the presence of adventitious hydrocarbon in the analytical chamber thus avoiding graphitization of the surface due to electron beam induced hydrocarbon cracking.



Fig. 2: Secondary electron image of a precipitate,  $\text{CaNpO}_2(\text{OH})_{2.6}\text{Cl}_{0.4} \cdot 2\text{H}_2\text{O}$ .

Low-vacuum, to 130 Pa, enables charge-free imaging and analysis of isolating samples without any need for conductive coating. However, under these conditions dehydration may occur. By regulation of water vapour pressure and temperature of the sample stage, the phase boundary of water between liquid and vapour can be achieved and samples can be analysed in wet state (ESEM mode).

Imaging of samples with high surface sensitivity is performed using low energy electron beams to minimize the electron penetration depth into the sample. A well-defined electron beam at low landing energy at the sample surface is attained by beam deceleration using a retarding potential up to 4 kV at the sample.

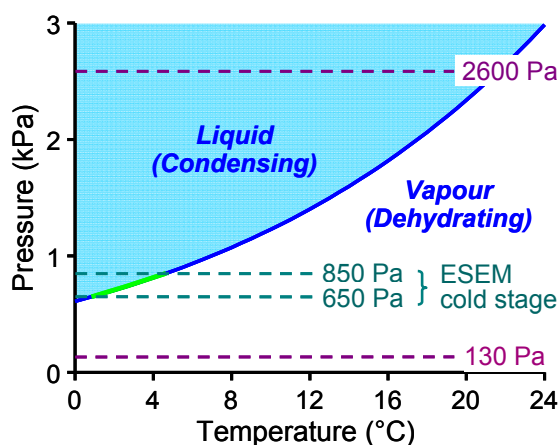


Fig. 3: Phase diagram of water in the range relevant for ESEM. Optimal pressure and temperature range for wet sample analysis is indicated by green colour.

## X-ray Photoelectron Spectroscopy

The new XPS (VersaProbe II, ULVAC-PHI Inc.) is a multi-technique instrument based on a scanning X-ray microprobe for spatially resolved elemental and chemical analysis of solid surfaces, Figure 4. The instrument can produce a focused, monochromatic X-ray beam that can be scanned over the sample surface. A point source of Al  $K\alpha$  X-rays (1486.6 eV) is created by a focused 15 keV electron beam from a  $\text{LaB}_6$  scanning electron gun impinging on an aluminum target. An ellipsoidal shaped quartz crystal monochromator on a Rowland circle collects the X-rays and focuses them onto the sample surface. When the electron beam is scanned over the aluminum target, the sample surface is scanned by an X-ray beam of similar spot size. The X-ray beam size can be computer controlled from less than 10  $\mu\text{m}$  diameter (for highest spatial resolution) to 200  $\mu\text{m}$  diameter for highest sensitivity. The field-of-view can be as large as 1300  $\mu\text{m}$  by 1300  $\mu\text{m}$ . Most of the X-ray induced photo- and Auger electrons are collected by the scanning input lens of the analyzer, following the scanning X-ray spot at the sample, using deflection plates. The electrons pass a ramped retardation field (spectral scanning) before entering the 180° hemispherical capacitor energy analyzer at constant pass energy, defining energy resolution. Finally, the electrons are detected by a multi-channel plate with 16 discrete anodes, providing high sensitivity and dynamic range. Because the analysed area is defined by the X-ray probe instead of analyzer apertures, potential X-ray induced sample damage is minimized as only the area being analysed is irradiated with X-rays. Multiple analyses of a single sample are thus possible by analysing fresh areas, previously not altered by X-rays, which is especially useful for sensitive samples.

## Sample transfer and sample navigation

Samples are transferred into and out of the analytical chamber via an introduction chamber evacuated with a turbomolecular pump. A magnetically coupled transfer rod guarantees leak-free movements. Inside the analytical chamber a differential ion pump and a titani-

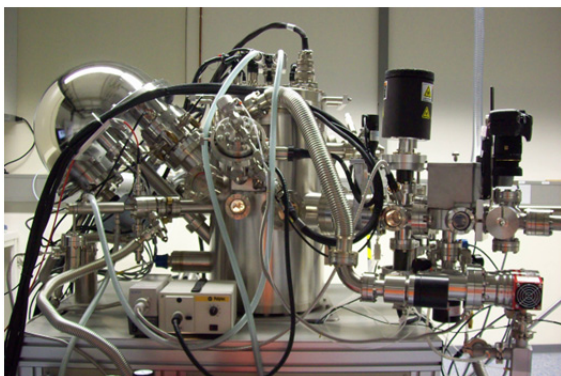


Fig. 4: X-ray photoelectron spectrometer. Right side: sample intro with camera, mini-fume hood and cooling/heating station. Middle: analytical chamber, ion gun, X-ray microprobe source mounted at top flange. Left side: VUV source and hemispherical analyzer.

um sublimation pump maintain an oil-free ultra-high vacuum. Air-sensitive or radioactive samples are mounted inside a glovebox on the sample holder, introduced into a vacuum-tight transfer vessel, and moved to the XPS where it is attached to the introduction chamber. After evacuation of the introduction chamber, the vessel is opened and the sample holder is introduced into the XPS using the transfer rod. A special sample holder with built-in heater and thermocouple is available for heating or cooling samples to  $-120^{\circ}\text{C}$  within the introduction and analytical chamber. A mini-fumehood around the attached transfer vessel enables safe venting of the introduction chamber after XPS study and detachment of the transfer vessel.

Sample navigation is enabled by combining a photograph of the sample in the sample holder and X-ray excited secondary electron imaging (SXI) with a raster scanned  $10\ \mu\text{m}$  diameter X-ray beam of the sample surface (in a manner analogous to SEM generation of secondary electron images and typically acquired in a few seconds). Calibration of the photograph by triangulation using SXI links the coordinates of the photograph to sample stage coordinates. This guarantees that spectroscopic data is collected from the selected feature of interest. SXI can be used for location of small sample features and definition of regions of interest for micro- and macro-area spectroscopy, Figure 5.

## Low voltage argon ion gun

A floating column argon ion gun integrated in the XPS instrument provides ion beams with energies from 5 eV to 5 keV. A beam bend within the ion gun removes neutrals from the beam for well-defined sputter rates, with beam current measured by a Faraday cup. Sputter depth-profiling of layered samples is performed by cycling alternate ion beam sputtering and XP spectroscopy. High sputter rates are attained at high ion energies, whereas good depth resolution is provided at low ion energies, typically at 500 eV. In addition, computerized sample rotation (Zalar rotation) around the defined analysis position during ion beam sputtering enhances depth resolution by uniform material removal.

## Surface charge compensation

A dual beam (electrons, argon ions) charge compensation technique is applied to compensate charging of isolating sample surfaces due to emission of photo- and Auger electrons. Without neutralization, the small X-ray spot at isolating surfaces generates a highly positively charged sample surface area. An

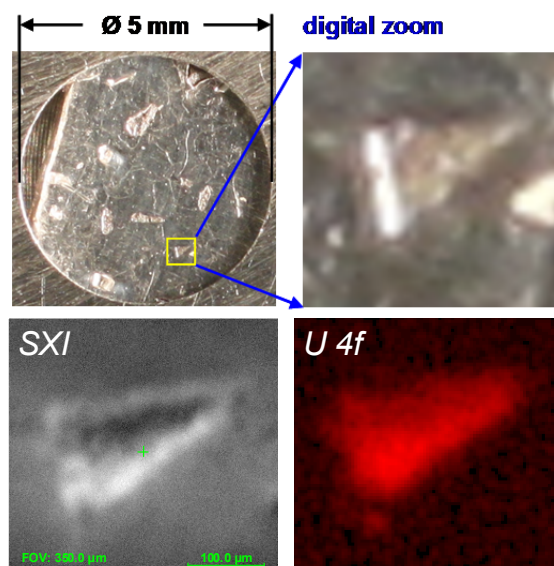


Fig. 5: (Top) Photograph of uranium-oxide particles pressed onto an indium foil and digital zoomed area of interest. (Bottom left) Scanning X-ray image (SXI, spot  $\varnothing\ 9\ \mu\text{m}$ ) and (bottom right) map of U 4f intensity (field-of-view  $350\ \mu\text{m}$ ) with entire single spectra stored at each pixel of the map (spot  $\varnothing\ 12\ \mu\text{m}$ ).

electron flood gun (1-2 eV) alone would negatively charge the sample surface around the X-ray spot deflecting subsequent electrons needed for charge compensation. Low energy argon ions (about 5-10 eV) are applied to compensate for this negative charging. The dual beam charge compensation, in combination with a fully automated five axis precision sample positioning stage, allows sequential, multiple analyses of insulating samples with no additional tuning using the queue function of the instrument control software.

### **Additional X-ray source**

A non-monochromatic standard twin-anode X-ray source providing either Mg K $\alpha$  (1253.6 eV) or Al K $\alpha$  (1486.6 eV) X-rays is attached to the analytical chamber. Spectra with Mg K $\alpha$  X-ray excitation are acquired if spectral superposition of Auger and photoelectron elemental lines occurs using Al K $\alpha$  X-ray excitation. In addition, Auger electron transitions involving core electron shells, which are not

accessible by Al K $\alpha$  X-rays, are ionized by the Bremsstrahlung of the non-monochromatic source and used for Auger parameter studies (e.g. kinetic energy of Si (KLL) 1610 eV, S (KLL) 2110 eV). The lateral analysis area is at minimum 300  $\mu\text{m}$  by 800  $\mu\text{m}$  and defined by the fixed aperture of the analyzer.

### **Ultraviolet photoelectron spectroscopy**

Ultraviolet photoelectron spectroscopy (UPS) for high-resolution, high-intensity valence band spectroscopy is performed using HeI (21.2 eV) and HeII (40.8 eV) vacuum ultraviolet (VUV) photons generated by continuous discharge (550 V, 80 mA) at about 5 Pa inside a glass capillary, diameter 1.2 mm. The relative photon intensities of either HeI or HeII depend on gas pressure and discharge current. By means of two differential pumping stages at the end of the window-less capillary, the vacuum inside the analytical chamber is maintained.

## 9.4 NMR spectroscopy – first results from EURACT-NMR projects

*P. Kaden, C. Adam, L. Natrajan<sup>a</sup>, S. Woodall<sup>a</sup>, D. Whittaker<sup>a</sup>, J.-F. Desreux<sup>b</sup>, N. L. Banik, C. M. Marquardt, A. Geist, M. A. Denecke*

<sup>a</sup> School of Chemistry, The University of Manchester, Brunswick Street, Manchester M13 9PL, United Kingdom; <sup>b</sup> Coordination and Radiochemistry, Department of Chemistry, University of Liège, Sart Tilman B16, Liège, B4000, Belgium.

### Introduction

Nuclear Magnetic Resonance spectroscopy (NMR) is one of the most commonly used spectroscopic methods in chemistry, providing valuable insight into the constitution, configuration and conformation of organic and inorganic compounds in solution and solid state. NMR also provides facile access to important dynamic information for molecules in solution by probing magnetic relaxation and diffusion behaviour. However, NMR has become available as a speciation method in nuclear/radiochemistry only in recent years. The NMR instrument at INE is used for in-house research of systems relevant for the safety assessment of a nuclear repository and for partitioning strategies, as well as for determining basic physical parameters of the actinide series. This instrument is also part of the “Actinide NMR Centre of Excellence”, access to which is possible through competitive application to the EURATOM FP7 funded EURACT-NMR transnational access project. In the first two EURACT-NMR calls, more than five times the available spectrometer time was requested, a strong attest to the impact of this newly available technique. Results of conducted research projects from these calls are described in the following.

### Basic physical properties of the actinides

Coordination bonds in complexes of the early actinide elements are thought to bear a significant degree of covalence. This is reflected in their water exchange times in aqueous solutions of the naked metal ions measured by relaxation experiments and induced paramagnetic shifts on <sup>17</sup>O nuclei of the solvent [1]. Thus, a covalence scale for the actinides, analogous to that scale available for the lanthanides [2-4], could be established. A different approach to access this scale is the measure-

ment of the <sup>1</sup>H relaxivity in similar samples in a range of different magnetic fields (nuclear magnetic relaxation dispersion, NMRD) [2, 5, 6]. A prerequisite for a reliable interpretation of these NMRD curves, however, is the knowledge of exact water exchange times of the naked ions determined in the aforementioned <sup>17</sup>O experiments. To obtain reliable T<sub>1</sub> (spin-lattice relaxation) and T<sub>2</sub> data (spin-spin relaxation) the effects of the nuclei's paramagnetism on the solvent have to be large enough. As paramagnetism is a metal ion intrinsic property, only the concentration in solution is left to scale the observed effects.

A 40 mM solution of NpO<sub>2</sub><sup>+</sup> in partially <sup>17</sup>O-enriched water was prepared to measure T<sub>1</sub> and T<sub>2</sub> relaxation times over a temperature range of 0°-100°C, whilst monitoring the <sup>17</sup>O chemical shift for correction purposes. The resulting data is in good agreement with data obtained at the University of Liège by Desreux and co-workers. An extension of these experiments to more concentrated samples (above 0.1 M) is planned for 2013 to obtain relaxation data with even higher precision. These experiments cannot be done elsewhere in Germany and hardly anywhere globally. Interpretation of previously acquired NMRD data based on the newly obtained water exchange data is in progress.

### Paramagnetism and symmetry

Solution NMR spectroscopy is a powerful tool in determining structural properties of axially symmetric paramagnetic lanthanide compounds (for example of DOTA, 1,4,7,10-tetraazacyclododecane-*N',N'',N''',N''''*-tetraacetic acid and its derivatives)[7], provided the origin of the chemical shift is purely dipolar in nature. However, when the donor set anisotropy changes or when the symmetry deviates from an axial point group, NMR spectra be-

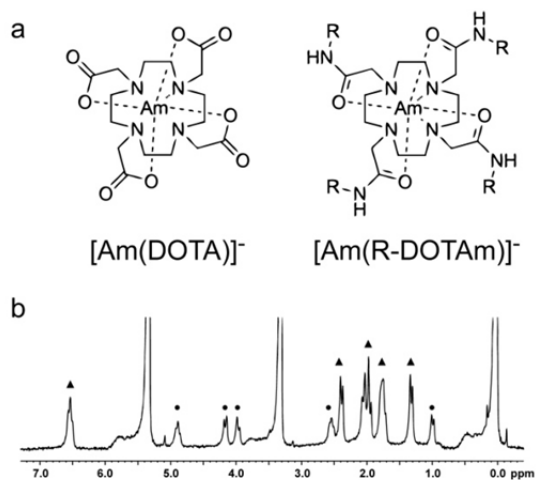


Fig. 1: a) Structure of DOTA and DOTAm-like ligands with Am(III). b) <sup>1</sup>H spectrum of [Am(DOTA)]<sup>-</sup> showing moderate signal dispersion and population of different isomers(▲●).

come more complicated, and hence difficult to interpret and predict. In the actinide series, reliable assignment of the NMR spectra is an even greater challenge, in part due to the possibility of a contact contribution to the bonding model.

In funded EURACT-NMR placements to INE, researchers from the University of Manchester commenced development of a working protocol to interpret paramagnetic NMR (pNMR) spectra of the f-elements, in tandem with luminescence spectroscopy and computational quantum chemistry. The long-term goal is to provide an information-rich tool, correlating experiment with theory in this area, thereby providing a means to predict NMR spectra of more geometrically complicated systems (lower symmetry) and systems involving the actinides in different oxidation states.

To date aqueous and methanolic solutions of Am(III) complexes of DOTA, Et<sub>2</sub>-DOTAm, Ph-DOTAm, DO3A and DTPA (see Fig. 1) were fully characterised by 1D and 2D NMR techniques, observing the nuclei <sup>1</sup>H, <sup>13</sup>C and <sup>15</sup>N. In the case of the Am(III)-Et<sub>2</sub>-DOTAm complex, 2D <sup>1</sup>H-<sup>15</sup>N spectroscopy showed a correlation peak, indicating a high coordination symmetry for this complex in solution (C<sub>4v</sub>). In contrast, either a deviation from averaged C<sub>4</sub> symmetry due to coordination isomerism between the

square antiprismatic and the twisted square antiprismatic isomer or relatively fast apical water exchange rates precluded observation of an analogous correlation for all the other tetra-substituted cases. The chemical shift of this correlated resonance is in the range typical for diamagnetic compounds. In all cases, variable temperature studies enabled observation of coordination isomerism exchange dynamics. Measurements of spin-lattice relaxation times (T<sub>1</sub>) of protons in the complexes corroborated complex formation. Comparison to data for yttrium(III) diamagnetic complexes indicates that at room temperature there is negligible excited state-ground state mixing of the Russell-Saunders spin orbit coupling terms that would result in an induced paramagnetic contribution to the observed NMR chemical shifts. Complementary time resolved laser induced fluorescence spectroscopic studies (TRLFS) on the Cm(III) derivatives, with a time-scale similar to the NMR experiments, confirmed the speciation inferred by NMR. Analysis of NMR data for analogous uranium(IV) complexes and estimation of relative contributions of Fermi contact shifts (covalent, through bond effect) versus pseudo-contact dipolar effects (through space) compared to the lanthanide(III) series are currently underway.

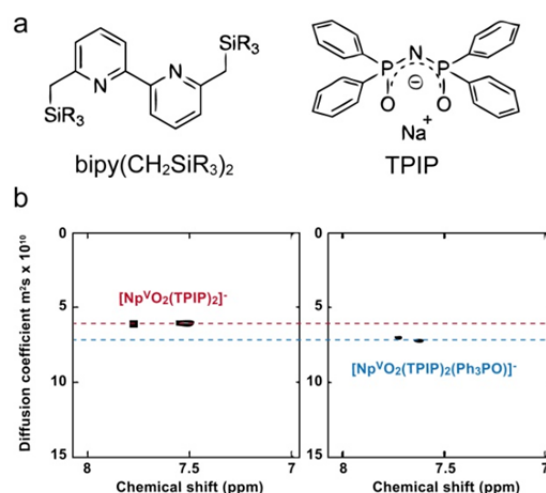


Fig 2 a) Basic structure of N- and O-donor ligands of the bipy(CH<sub>2</sub>SiR<sub>3</sub>)<sub>2</sub> class (left) and TPIP (tetraphenylimido-diphosphate, right); b) Pseudo 2D <sup>1</sup>H DOSY spectrum (diffusion ordered spectroscopy) of [Np<sup>V</sup>O<sub>2</sub>(TPIP)<sub>2</sub>]<sup>-</sup> and [Np<sup>V</sup>O<sub>2</sub>(TPIP)<sub>2</sub>(Ph<sub>3</sub>PO)]<sup>-</sup>.

Similar to the studies with aminocarboxylate DOTA and DOTAm-like ligands, the dynamic behaviour and symmetry of Am(III) and NpO<sub>2</sub>(V) complexes of N- and O-donor ligands TPIP and bipy(CH<sub>2</sub>SiR<sub>3</sub>)<sub>2</sub> (R = <sup>t</sup>BuMe<sub>2</sub>, <sup>i</sup>Pr<sub>3</sub>, <sup>t</sup>BuPh<sub>2</sub>, Fig 2a) was determined through full 1D and 2D NMR characterisation using the NMR active nuclei <sup>1</sup>H, <sup>13</sup>C, <sup>15</sup>N and <sup>31</sup>P. In the case of the ligand bipy(CH<sub>2</sub>Si<sup>t</sup>BuMe<sub>2</sub>)<sub>2</sub>, the presence of a correlation peak in the <sup>1</sup>H-<sup>15</sup>N 2D spectrum suggests that the complex possesses C<sub>3</sub>-symmetry, i.e. a 3:1 L:M complex. This is in agreement with previous reports on Eu(III) complexes [7] and TRLFS studies of the equivalent Cm(III) complexes performed at INE. NMR spectroscopic results on complexes with more sterically bulky ligands suggest only lower symmetry 2:1 M:L complexes form. <sup>1</sup>H and <sup>31</sup>P DOSY (diffusion ordered spectroscopy) NMR was used to investigate the coordination and nuclearity of the NpO<sub>2</sub>(V) congeners in solution. Previous work at Manchester showed that UO<sub>2</sub>(VI) forms monomers, dimers and trimers; in the case of the trinuclear species, the (O=U=O)<sup>2+</sup> ions are connected in an unusual fashion by uranyl-oxo-uranium orthogonal interactions, a coordination type more prevalent in actinyl(V) species. Addition of the strong donor ligand Ph<sub>3</sub>PO to solutions of TPIP and NpO<sub>2</sub>(V) showed formation of a smaller complex than for TPIP and NpO<sub>2</sub>(V) alone (Fig. 2b), indicating that NpO<sub>2</sub>(V) forms dimeric units with this ligand in solution. If cation-cation interactions are involved in this complex is currently being investigated. T<sub>1</sub> measurements were used to validate the oxidation state of Np as +V in all of these compounds; no reduction to Np(IV) was observed over a four month time period.

### NMR spectroscopy in separation chemistry

NMR studies related to separation chemistry of the SANEX/GANEX process [8] were performed and aimed at characterizing solution complexes of Am(III) and Pu(IV) with CyMe<sub>4</sub>-BTBP and CyMe<sub>4</sub>-BTPPhen with and without TBP as a modifier. Employing 1D and 2D NMR techniques involving <sup>1</sup>H, <sup>13</sup>C and <sup>31</sup>P nuclei allowed full characterization of all available resonances. Unfortunately, <sup>15</sup>N experiments were

not successful [9] due to its low natural abundance and the expected low symmetry of these complexes. <sup>1</sup>H and <sup>31</sup>P DOSY results reveal there is no interaction of TBP with Am(III) complexes. BTP and BTPPhen Pu(IV) complexes, synthesized in a monophasic medium, were titrated with increasing amounts of TBP and observed with <sup>1</sup>H NMR. No replacement of BTX ligands with added TBP was observed. This is in contrast to EXAFS measurements on these systems indicating that Pu<sup>4+</sup> is extracted as a Pu(NO<sub>3</sub>)<sub>4</sub> · 3.3 TBP complex. However, the NMR titration was performed in a monophasic (organic) solution and may not reflect the actual species extracted from a biphasic medium.

### Plans for 2013

Establishing a scale for paramagnetism in actinide containing systems and its effect on NMR spectra is of enormous importance to the establishment of this method in the field of nuclear and radio-chemistry. As mentioned above, relaxivity measurements on concentrated actinide solutions will continue in 2013. Results will be compared to those obtained at CEA Marcoule by Berthon and co-workers using a different approach of acquiring spectra following the Evans' NMR protocol [10-12] directly assessing the magnetic properties of the actinide series.

A EURACT-NMR funded workshop will be held in Karlsruhe (July 17-19, 2013), covering all aspects of solution and solid-state NMR in actinide research. This is the second in a series and directly precedes the ACTINIDES 2013 Conference, also in Karlsruhe. The EURACT-NMR workshop will highlight the potential of NMR to characterize structure and bonding in actinide materials through combination of experiment and theory.

### Acknowledgements:

This work is supported by the German Federal Ministry of Education and Research (BMBF) under contract numbers 02NUK020A and 02NUK012D. We are grateful for the generous financial support of the EURATOM FP7 funded EURACT-NMR project.

## References

- [1] Desreux, J. F., in *Advances in Inorganic Chemistry, Vol. Volume 57*, Academic Press, pp. 381 (2005).
- [2] Bertini, I. et al., *Solution NMR of paramagnetic molecules, Vol. Volume 2*, Elsevier, (2001).
- [3] Bleaney, B., *J. Magn. Reson.*, 8(1): 91 (1972).
- [4] Golding, R. M., Halton, M. P., *Aust. J. Chem.*, 25(12): 2577 (1972).
- [5] Banci, L. et al., *Nuclear and electron relaxation: the magnetic nucleus-unpaired electron coupling in solution*, Wiley-VCH, (1991).
- [6] Bertini, I. et al., in *Advances in Inorganic Chemistry, Vol. Volume 57*, Academic Press, pp. 105 (2005).
- [7] Aime, S. et al., *Inorg. Chem.*, 31(21): 4291 (1992).
- [8] Panak, P. J. and Geist, A., *Chem. Rev.*, 113(2): (2013).
- [9] Mason, J., in *Encyclopedia of Nuclear Magnetic Resonance* (Eds.: Grant, D. M., Harris, R. K.), John Wiley & Sons, Ltd, Chichester, (2007).
- [10] Evans, D. F., *J. Chem. Soc.*, 2003 (1959).
- [11] Loliger, J., Scheffold, R., *J. Chem. Educ.*, 49(9): (1972).
- [12] Piguet, C., *J. Chem. Educ.*, 74(7): (1997).

## 9.5 Computational Chemistry

*B. Schimmelpfennig, R. Polly, V. Vallet,<sup>a</sup> F. Real,<sup>a</sup> M. Masella,<sup>b</sup> S. Trumm, F. Heberling and N. Finck*

*a Université Lille 1 (Sciences et Technologies), Laboratoire PhLAM, CNRS UMR 8523, Bât P5, F-59655 Villeneuve d'Ascq Cedex, b Laboratoire de Chimie du Vivant, Service d'ingénierie moléculaire des protéines, Institut de biologie et de technologies de Saclay, CEA Saclay, F-91191 Gif sur Yvette Cedex, France*

### Introduction

Computational chemistry developed to an additional very powerful tool in many different areas of chemistry. At INE, computational chemistry has been used very successfully as a further predicting and supporting tool for experimental investigations in various different research areas such as studying chemical and physical properties of mineral surfaces [1], extraction chemistry [2], studies of oxo-hydroxo systems ranging in size from small solution species to nano-particles [3] and other aspects of actinide solution behavior.

Accurately describing actinide elements by means of quantum theory requires the inclusion of relativistic quantum chemistry. There are scalar-relativistic and spin-orbit effects. Additional difficulties are the complicated couplings in the open  $5f$ -shell, which require a balanced description of electron-electron correlation beyond the mean-field approach based on single-reference wave functions, such as Hartree-Fock (HF) or Density Functional Theory (DFT). We routinely apply DFT, but always assess the accuracy of this approach by doing benchmark calculations on small, but chemically similar, test systems with high-quality wave-function-based ab initio methods such as Møller Plesset perturbation theory (MP2) and Coupled Cluster Singles Doubles with triple corrections (CCSD(T)). Only, where good agreement with experimental data is found, we are able to provide important additional and reliable information such as structural parameters or reaction energies, which are experimentally not accessible.

There is a wide range of different computational tools utilized at INE, including high-level ab initio methods and DFT, which treat the electrons explicitly on a quantum-

mechanical level. More approximate classical Monte Carlo (MC) simulations and Molecular Dynamics (MD) based on classical mechanics complement the ab initio and first principle methods. The main results applying these tools to specific re-search activities at INE over the last year are described in the following.

### Interaction of selenite with the hydrated calcite (104) surface

Sorption reactions with surrounding mineral phases may have an essential impact on the mobility and bioavailability of the oxidized selenium species in soils and sediments. Both, incorporation and surface sorption, are important retardation mechanisms of the transport of radionuclides in ground water.

In the context of nuclear waste disposal, the radioisotope  $^{79}\text{Se}$  is of special concern due to its long half-life ( $1.1 \cdot 10^6$  a) and the expected high mobility. Selenite ( $\text{SeO}_3^{2-}$ ) and selenate ( $\text{SeO}_4^{2-}$ ) as anions interact only weakly with common mineral surfaces. Therefore they have been identified as crucial fission product species for long term safety of disposed nuclear waste. Calcite is the most common polymorph of calcium carbonate. In the surroundings of potential nuclear waste disposal sites calcite is e.g. present as a mineral constituent in clay formations (up to 20% in some cases), as fracture filling material in granitic rocks, or as a corrosion product of concrete based materials in the technical barrier. Recent studies showed that selenite can be incorporated into calcite.

We studied the incorporation of selenite into the bulk phase as well as into the first surface layer of calcite.

The DFT calculations are carried out with periodic boundary conditions and plane-wave ba-

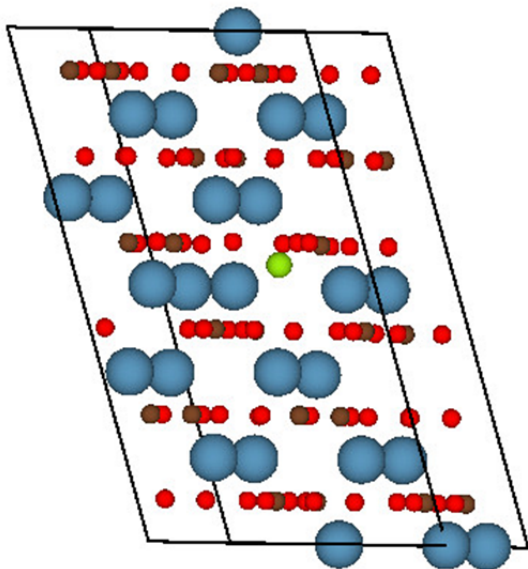


Fig. 1: Hexagonal 2x2x1 supercell used for the study of the incorporation of selenite into calcite. Blue spheres: calcium, red spheres: oxygen, white spheres: hydrogen, green sphere: selenium.

sis sets as implemented in the Vienna ab initio simulation package (VASP). Electron exchange and correlation are described using the Perdew-Burke-Ernzerhof (PBE) functional. The ion cores are dealt with by the projector augmented wave (PAW) method.

We employed an energy cut-off of 400 eV for the kinetic energy of the plane waves for all bulk and surface calculations. For these calculations we employed monoclinic and hexagonal unit cells.

For the study of the incorporation of selenite into calcite we had to use a 2x2x1 supercell based on the hexagonal unit cell of calcite. This was necessary to retain the three-fold axis. Fig. 1 shows the resulting structure.  $\text{SeO}_3^{2-}$  is not planar as  $\text{CO}_3^{2-}$ . Therefore the incorporation of  $\text{SeO}_3^{2-}$  into calcite leads to additional required space within the bulk phase of calcite. Compared to the gas phase ( $r_{\text{gas,Se-O}} = 176$  pm) the Se-O bond distance is shorter in the bulk phase  $r_{\text{bulk,Se-O}} = 173$  pm.

The incorporation of  $\text{SeO}_3^{2-}$  into the first surface layer of calcite replacing one  $\text{CO}_3^{2-}$  was studied with a 2x2x1 supercell based on the monoclinic unit cell and containing five layers of  $\text{Ca/CO}_3^{2-}$ . A vacuum gap of 150 pm was in-

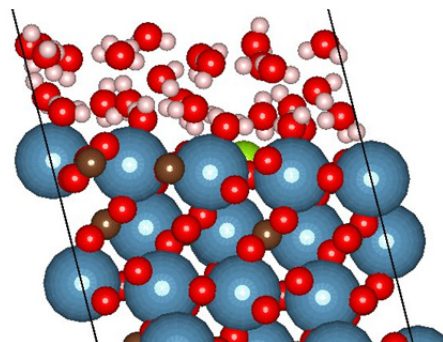


Fig. 2: Incorporation of selenite into the calcite (104) surface. Blue spheres: calcium, red spheres: oxygen, brown spheres: carbon, white spheres: hydrogen, green sphere: selenium.

roduced between the surfaces so the slabs are well isolated from their periodic images.

Here, of course, the spatial limitations do not hold anymore as in the case above and the Se can protrude from the surface into vacuum or the water phase (Fig. 2). The three calculated Se-O bond lengths are  $r_{\text{bulk,Se-O},1} = 170$  pm,  $r_{\text{bulk,Se-O},2,3} = 175$  pm. Slightly longer as in the bulk phase. Additionally the symmetry of the  $\text{SeO}_3^{2-}$  is reduced from  $C_{3v}$  to  $C_s$ .

Besides the structural characterization of the selenite incorporation species in calcite, the main focus of this study is the quantification of the selenite incorporation into calcite at standard conditions, and the phenomenological thermodynamic description of selenite

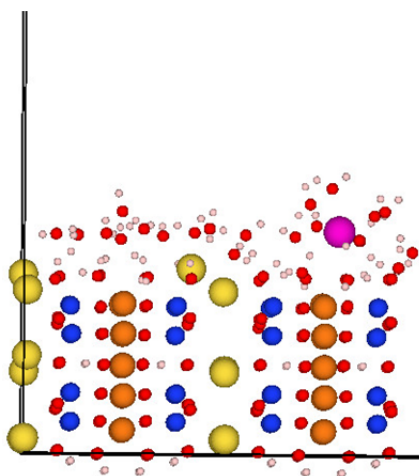


Fig. 3: Outer-sphere complex of  $\text{Eu}^{3+}$  at the hectorite edge site. Blue spheres: silicon, red spheres: oxygen, brown spheres: magnesium, white spheres: hydrogen, yellow spheres: sodium, magenta sphere: europium.

doped calcite, and of selenite coprecipitation with calcite. This was very successfully demonstrated in [5].

These calculations were carried out with the plane wave DFT programm VASP.

### Interaction of $\text{Eu}^{3+}$ with hectorite: theoretical considerations of sorption and incorporation

As described above, we used VASP for these calculations. The energy cut-off was set to 400 eV and the vacuum gap was 140 pm.

We investigated sorption at the edge surface of hectorite. In order to simulate neutral or higher pH values we saturated the dangling bonds of the oxygen's with hydrogen atoms.

The subjects of this investigation were outer-sphere complexes of  $\text{Eu}^{3+}$  at the edge site of hectorite, incorporation of  $\text{Eu}^{3+}$  into this surface by replacing one  $\text{Mg}^{2+}$  ion and incorporation of  $\text{Eu}^{3+}$  into the bulk phase of hectorite by replacing one  $\text{Mg}^{2+}$  ion, as well.

For the outer-sphere complex of  $\text{Eu}^{3+}$  we found nine water molecules in the first coordination sphere with  $r_{\text{Eu-O}}$  distances ranging from 233-369 pm. Most values are in the range 233-276 pm, but two distances are somewhat larger  $r_{\text{Eu-O},8} = 363$  and  $r_{\text{Eu-O},9} = 369$  pm. The optimized structure is shown in Fig. 3.

When an  $\text{Eu}^{3+}$  replaces an  $\text{Mg}^{2+}$  ion at the surface, the position of the  $\text{Eu}^{3+}$  ion is 33 pm above the  $\text{Mg}^{2+}$  surface plane because of the larger ionic radius of  $\text{Eu}^{3+}$  (Fig. 4).

Another possibility is the replacement of an  $\text{Mg}^{2+}$  ion by an  $\text{Eu}^{3+}$  ion in the bulk phase (Fig. 5). The  $\text{Mg}^{2+}$ - $\text{Mg}^{2+}$  distances are  $r_{\text{Mg-Mg}} = 308$ - $313$  pm and the  $\text{Mg}^{2+}$ -O distances  $r_{\text{Mg-O}} = 202$  pm. This compares very well with the experimental results of Seidle and Breu [6] ( $r_{\text{Mg-Mg}} = 304$ ,  $r_{\text{Mg-O}} = 208$  pm). Upon replacement of a  $\text{Mg}^{2+}$  ion by an  $\text{Eu}^{3+}$  ion the corresponding distances increase to  $r_{\text{Eu-Mg}} = 318$ - $326$  pm and  $r_{\text{Eu-O}} = 226$  pm. The reason for this is again the much larger ionic radius of  $\text{Eu}^{3+}$ .

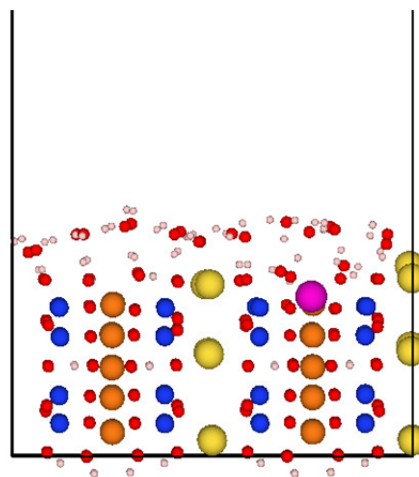


Fig. 4: Incorporation of  $\text{Eu}^{3+}$  at the hectorite edge surface. Blue spheres: silicon, red spheres: oxygen, brown spheres: magnesium, white spheres: hydrogen, yellow spheres: sodium, magenta sphere: europium.

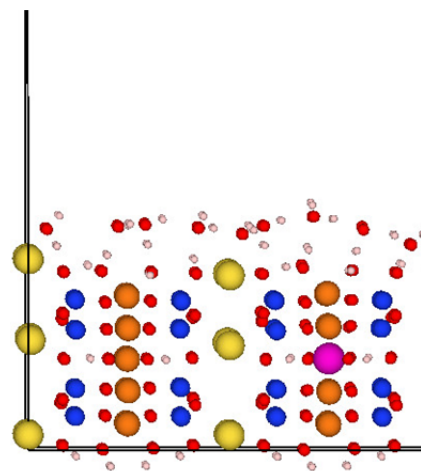


Fig. 5: Incorporation of  $\text{Eu}^{3+}$  into the hectorite bulk phase. Blue spheres: silicon, red spheres: oxygen, brown spheres: magnesium, white spheres: hydrogen, yellow spheres: sodium, magenta sphere: europium.

Again these results fit very well to experimental results of Finck *et al.* [7] ( $r_{\text{Eu-Mg}} = 326$  pm and  $r_{\text{Eu-O}} = 227$  pm).

These calculations were carried out with the plane wave DFT programm VASP.

### Molecular Dynamics for actinide complexes in aqueous solution

Detailed understanding of actinide complexes in solution, including dynamic processes, has been a key-topic of the theoretical work in the past year. In close international collaboration

with groups in France (Lille and CEA-Saclay), we have developed a new ansatz to parameterize the actinide – water interaction potential, including non-additive charge-transfer terms. These force fields are implemented in the POLARIS MD-software package. The main motivation for this approach is to avoid the limitations of static continuum models which are parameterized for room temperature only or Car-Parinello Molecular Dynamics (CPMD) which is based on DFT, thus lacking the accuracy required for actinide complexes and limited to simulations in the picoseconds range. A wide range of data, which is directly comparable to experiment, can be extracted from the trajectories, including

- coordination numbers,
- structural parameters,
- Gibbs Free energies,
- exchange rates and mechanisms,
- activation volumina,
- thermodynamic properties and
- diffusion coefficients
- EXAFS spectra.

The work in the last year focused mainly on technical issues as parallelization and general improvement of the POLARIS software as well as a detailed analysis of the force-fields developed for Th(IV) and Cm(III) in aqueous solution [8]. Our main goal was here to estimate the impact of the uncertainties and of the arbitrary choices made as building classical water/water and ion/water interaction models, on the MD simulation results of actinide ions in solution. In particular, we identify three main sources of uncertainties affecting the development ion/water classical models:

- (1) the quantum ab initio level, which may lead to uncertainties of few kcal mol<sup>-1</sup> in the ion/water BE;
- (2) the accuracy of the ion/water parameter adjustment process, which points out the limits of the chosen mathematical model to describe the interactions within the system of interest; and
- (3) errors in the description of water/water interactions, in particular for molecular structures corresponding to water mol-

ecules interacting in ion first hydration shells.

To estimate the impact of the latter two sources of uncertainties, we built four ion/water classical models, including a cooperative charge-transfer energy term. These models differ from the analytical form chosen to account for cooperative character of the charge-transfer term (the so-called models  $M_{\text{dens}}$  and  $M_{3\text{body}}$ ). They differ also from their parameter adjustment protocol. The parameter set of two models  $M_{\text{dens}}$  and  $M_{3\text{body}}$  are assigned using the common protocol, that is, their parameters are adjusted to reproduce the full BE of ion/water clusters in gas phase (the corresponding models are noted M). In that case, the possible drawbacks of the water model to accurately describe water/water interactions for water molecules interacting in ion first hydration shells are then tentatively corrected. The parameters of the remaining two models  $\sim M_{\text{dens}}$  and  $\sim M_{3\text{body}}$  are assigned to reproduce the latter BE, from which the water/water interaction energies are subtracted.

These models have been used to simulate, at the 10 ns scale, the actinide ions Cm(III) and Th(IV) in liquid water at ambient conditions (however, by omitting their counter ion cloud). The model predictions along the solvated MD trajectories are very close in terms of ion hydration pattern, temporal properties, and water electrostatic properties at the ion vicinity.

Our computed data usually match the available theoretical ones concerning these two ions. However, the spread in our theoretical results are smaller compared to the earlier ones, derived from molecular simulation protocols based on quantum or classical approaches (with the ion considered as solvated alone in a water box). Moreover, by comparing our model predictions to those derived from a model for which the cooperative effects affecting the ion/water charge-transfer term are neglected, we exhibit the latter effects to tend to reduce the coordination of both ions in solution, to strongly destabilize the ion/water interactions, and thus to weaken the mean residence time of water molecules in ion first hydration shell. Hence, these

effects appear to be pivotal for an accurate modeling of desolvation process at interfaces or of ligand competitive reactions involving the present two actinide ions, even if the influence of such effects vanishes as soon as the ion second hydration shell.

Lastly, our four cooperative charge-transfer models provide a very close picture for the solvation of Cm(III). In particular, its hydration pattern is predicted to be the result of a 1:1 equilibrium between 8- and 9-coordinated ion/water clusters. Concerning Th(IV), the models M and  $\sim$ M provide an overall similar picture for its solvation, however, these models predict either a 9- or an 8-coordination species in solution.

Additionally to this systematic study the water-water force field was systematically improved such that M and  $\sim$ M models can in future studies be treated as one model and the refinement of the model by including counter ions will be conceptually straightforward.

### An(III)/Ln(III) separation with heterocyclic ligands

For more than a decade heterocyclic N-donor ligands have been in the focus of international researchers involved with the partitioning of spent nuclear fuels. Since the discovery of BTPs' excellence in the separation of An(III)/Ln(III) [9], as required for efficient transmutation of An(III), numerous ligand classes have been derived from the BTP backbone, of which only few produced satisfactory separation factors [10]. With the 2,6-bis-pyrazolylpyridines (BPPs, see Fig. 6) one promising ligand class has recently been developed. As valid for all highly selective extractants for An(III)/Ln(III) separation, the molecular driving force of their selectivity is insufficiently understood yet, hampering their optimization with regard to process requisites and, hence, mandating intense research activities.

From extraction and spectroscopic data BPPs are known to form 1:3 complexes with both An(III) and Ln(III) ions [11]. It is understood that under acidic conditions both N-1 posi-

tions of the two pyrazolyl moieties remain protonated upon complex formation.

The protonation of free HBPP was investigated, in order to provide information on the prevailing ligand species and their conformation and, hence, shed light on the protons role on complex formation. Thus, structures of the various planar protonated species (HBPPH<sub>2</sub>, HBPPH<sup>-</sup> and HBPP<sup>2-</sup>) are calculated at MP2 level. For HBPP<sup>-</sup> the tt conformation is favored by -76.7 kJ/mol compared to the cc conformere, whereas a stabilization of -33.2 kJ/mol is found between tt and ct conformation. The energetic preference of the tt conformere is in line with the reduction of sterical hindrance between ring protons of pyridine and pyrazole. Three monoprotinated isomers HBPPH<sup>-</sup> (protonation at N-1, N-2 and pyridine) can be formed. The protonation of N-2 is favored in both cc (-68.2 kJ/mol) and tt (-9.3 kJ/mol) conformation over the respective N-1 protonated isomers, which is due to the pyridine nitrogen's vicinity (cc only) and resonance stabilization. For cc-HBPPH<sup>-</sup> protonated at the pyridine nitrogen, a 34.8 kJ/mol higher energy is obtained compared to N-2 protonation. The trend found for cc-HBPPH<sup>-</sup> is sustained for HBPPH<sub>2</sub> with N-2 protonation at both pyrazole moieties being favored by -33.0 kJ/mol and -45.5 kJ/mol over N-1/N-2 and N-2/N-2 protonation, respectively. However, lower energies are found for N-1/N-1 protonation in the tt conformation compared to N-2/N-1 (10.8 kJ/mol) and N-2/N-2 (26.0 kJ/mol), respectively, reflecting the sterical hindrance between both protons for the latter isomer. N-2/N-2 protonation in cc conformation renders the lowest energy. Hence,

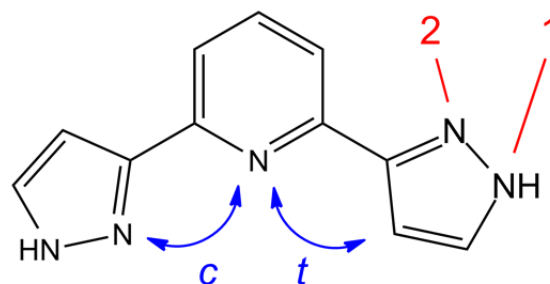


Fig. 6: Molecular structure of HBPP; cis (c) and trans (t) refer to the dihedral orientation of pyridine and pyrazole nitrogens.

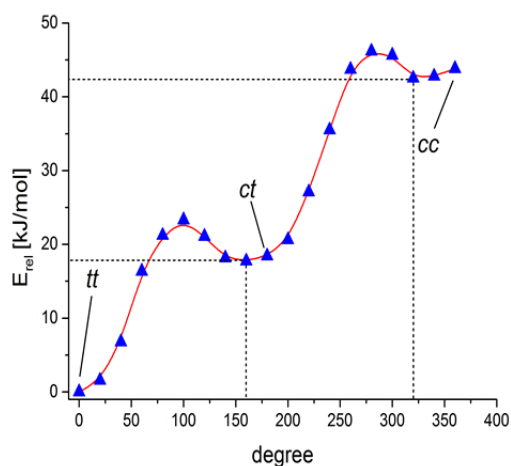


Fig. 7: Relative energies of *cc*-N-1/N-1-HBPP as a function of the dihedral angle between pyridine and pyrazole nitrogens (0-180°: ring 1; 181-360°: ring 2).

the highly acidic process solutions used for An(III)/Ln(III) separation shift the molecular equilibrium towards the preferential formation of *cc*-HBPPH<sub>2</sub>, which appears to be favorable for complex formation.

However, in *cc*-N-2/N-2-HBPP the protons might hamper bond formation between nitrogen an An(III)/Ln(III). The thermodynamically disfavored *cc*-N-1/N-1-HBPP isomer thus represents a reasonable alternative ligand species for complex formation with both protons bond as in the final complex and readily accessible nitrogen atoms. The previous results showed *tt* to be the favored conformation of N-1/N-1-HBPP. To investigate on the availability of the *cc* isomer, the rotational barriers of N-1/N-1-HBPP are calculated at MP2 level. Starting from the *tt* isomer, one pyrazole ring

is gradually rotated, while the two remaining rings are fixed in a planar conformation. Once the *ct* conformation is reached the second pyrazole ring is rotated as described before, to finally obtain *cc* conformation (Fig. 7). 17.7 kJ/mol and 24.8 kJ/mol, respectively, are required to converge *tt* to *ct* and subsequently obtain the *cc* conformation. The activation energies showed to be only less than 5 kJ/mol higher. Hence, the rotation of the cyclic fragments of HBPPH<sub>2</sub> is only moderately hindered and a significant concentration of *cc*-N-1/N-1-HBPP is available in equilibrium.

## References

- [1] Geckeis, H. et al., Chem. Rev., 113(2): 1016 (2013).
- [2] Banik, N. L. et al., Dalton Transactions, 39: 5117 (2010).
- [3] Walther, C. et al., Dalton Transactions, 41: 10941 (2012).
- [4] Heberling, F. et al., JCS, 354: 843 (2011).
- [5] Heberling, F. et al., in preparation.
- [6] Seidl, W., Brey, J., Z. Kristallogr., 220: 169 (2005).
- [7] Finck, N. et al., Min. Mag., 76: 2723 (2012).
- [8] Real, F. et al., J. Comp. Chem., 34: 707 (2013).
- [9] Kolarik, Z. et al., Solv. Extr. Ion Exch., 17(1): 23 (1999).
- [10] Panak, P. J. and Geist, A., Chem. Rev., 113(2): 1199 (2013).
- [11] Bremer, A. et al, Inorg. Chem., 51(9): 5199 (2012).



## 10 Radiochemical and Elementary Analysis

*N. Banik, K. Bender, M. Böttle, H. Geckeis, F. W. Geyer, C. H. Graser, K. Gompper, S. Heck, S. Hilpp, A. Kaufmann, T. Kisely, M. Lagos, Ch. Marquardt, M. Plaschke, T. Schäfer, A. Seither, C. Walschburger*

The main task of the INE analytical group is providing, operating and continuously improving (radio-) chemical and analytical methods. These activities largely contribute to the INE R&D projects. Additionally, analytical service is provided for various external clients. Routine samples are analysed for waste disposal technical facilities of WAK-HDB including samples from decommissioning of nuclear installations. Other external clients are in the fields of quality control of separation resins for radio-analytical applications and quality control of radiopharmaceuticals. Furthermore, analytical support and collaborations are provided for various partners inside and outside of KIT. For all these purposes analytical methods are developed and adapted. Advanced techniques are especially developed and improved for trace element analysis and speciation studies of actinides. Sector Field (SF)-ICP-MS and collision cell quadrupole CC-Q-ICP-MS are coupled to species sensitive methods, i.e. to capillary electrophoresis (CE-SF-ICP-MS) and field-flow field fractionation (FFF-Q-ICP-MS, cf. chapter 6.3). Furthermore, the analytical group supports the INE infrastructure, is involved in various educational activities and is responsible for teaching of chemical laboratory assistants.

### Routine Analysis

Several tens of thousands of samples are analysed each year providing data for the INE R&D projects and external clients. Both profits from a pool of advanced analytical techniques, well-developed procedures and competence in the fields of radiochemical sample preparation and separation techniques, elemental and isotope analysis, chromatographic methods and nuclear spectroscopic techniques. In addition, our personnel are trained in handling of nuclear samples and in the operation and maintenance of instruments adapted to glove boxes. Several analytical techniques listed in Table 1 are available both in inactive and radio-analytical labs in the INE controlled area.

### Analysis for External Clients

Radiochemical analysis is accomplished for various external clients on the basis of formal contract agreements. Data are recorded, documented and quality controlled according to the requirements of the clients.

### WAK-HDB

Samples delivered from the WAK-HDB (Wiederaufarbeitungsanlage Karlsruhe GmbH, Hauptabteilung Dekontaminationsbetriebe)

Table 1: Analytical techniques available at INE.

Elemental and Isotope Analysis
Quadrupol Inductively Coupled Mass Spectrometry (Q-ICP-MS)
Collision Cell Q-ICP-MS (CC-Q-ICP-MS)
Sector Field ICP-MS (SF-ICP-MS)
Inductively Coupled Optical Emission Spectrometry (ICP-OES)
Flame Atomic Emission Spectrometry (F-AES)
X-Ray Fluorescence Spectrometry (XRF)
Nuclear Spectroscopic Methods
Alphaspectrometry
Liquid Scintillation Counting (LSC, conventional and high sensitivity)
Gamma spectrometry (with auto-sampler)
Further Methods
Ion Chromatography (IC)
Gas Chromatography (GC)
Carbon Analysis (TOC, DOC, TIC)
Specific Surface Area Analysis (BET)
Differential Thermal Analysis (DTA)
Dilatometry
Fusion and Microwave Digestions
Gravimetry and Titrations

can be classified according to their origin in samples from the HDB incineration (ashes) or LAW evaporation plants (liquid concentrates), samples from decommissioning of nuclear facilities (e.g., KNK, MZFR, VEK) and special samples (e.g., samples taken from selected waste canisters). Samples are processed by

radio-analytical separation methods and then analysed using elemental, isotope and nuclear spectroscopic techniques. The nuclides routinely determined include (but are not limited to):  $^{238,239,240,241,242}\text{Pu}$ ,  $^{233,234,235,236,238}\text{U}$ ,  $^{55}\text{Fe}$ ,  $^{63}\text{Ni}$ ,  $^{90}\text{Sr}$ ,  $^{242,243+244}\text{Cm}$ ,  $^{241}\text{Am}$ . Around 80 samples are analysed this year with an upward trend.

### **Quality Control of Separation Resins**

INE is the first quality control lab of the TRIS-KEM Sr separation resin and the secondary lab for actinide separating TRU and TEVA resins. The analytical service comprise the determination of the capacity of the Sr resin, column tests (loading, washing, elution), determination of possible interferences and the determination of eluted organic material by carbon analysis. Around 50 samples are analysed this year.

### **Quality Control of Radiopharmaceuticals**

In a confidential collaboration a Ra containing alpha-radiopharmaceutical is regularly analysed with regard to the content of toxic heavy metal trace impurities. This pharmaceutical is developed for patients suffering from bone metastases. This year a method for the quantitative ICP-MS analysis of specified heavy metals and other elements of interest is developed and a batch of samples is measured approximately each week. Additionally, a method validation procedure adopting the guidelines of the USP (United States Pharmacopedia) is developed.

### **Projects**

The analytical group contributes to the organisation and development of analytical procedures for INE research projects.

The sorption behaviour of Sorel concrete based construction material and salt backfill material originating from the ASSE underground mining was investigated. The aim of this project is to get preliminary information concerning the retention potential of these materials for radionuclides. In batch sorption experiments Sorel concrete, salt backfill material and a mixture of Sorel concrete and salt

backfill were contacted with Eu(III) in under-saturated salt brine. From these experiments conducted over a period of 3 month sorption coefficients could be determined.

Similar radionuclide retention experiments with heat treated concrete were performed in simulated seawater. These batch type sorption experiments covered the nuclides I(-I), Cs(I), Co(II), and Eu(III). The concrete samples originate from the COMET-L1 experiment where the situation of basement attack by a simulated corium melt was investigated previously [1]. For more details concerning the concrete projects cf. chapter 6.2.

For the FIRST NUCLIDES project an experimental setup for the collection of the volatile radionuclide  $^{14}\text{C}$ , which is part of the inventory of instant release fractions of nuclear spent fuel, is designed. The development of analytical procedures for the sensitive determination of  $^{14}\text{C}$  from the gas phase and from leaching experiments is under way. For more details concerning the FIRST NUCLIDES project cf. chapter 6.

### **Development of Speciation Methods**

#### **Sector Field Inductively Coupled Plasma Mass Spectrometry (SF-ICP-MS) – High Selectivity and low Detection Limits**

Modern SF-ICP-MS, installed at the INE radioactive laboratories, is a very powerful and widely used tool for trace element and isotope ratio analysis with the benefit of relatively high sample throughputs requiring at the same time only relatively small sample volumes ( $\mu\text{L}$  to  $\text{mL}$  range). SF-ICP-MS offers very low detection limits (lower ppq range,  $\sim 10^{-14}$  mol/L) for transuranium elements (Pu,



Fig. 1: Element XR SF-ICP-MS setup.

Np, Am) with almost zero backgrounds. In combination with advanced sample introduction (i.e. desolvation) systems even detection limits in the sub ppq ( $10^{-15}$  mol/L) range have been reported [2]. In addition to superior sensitivity sector field instruments also provide an improved mass resolution up to  $\sim 10.000$  which strongly enhances the selectivity and, therefore, the accuracy of measurements. This is especially beneficial for isotopes in the medium mass range that suffer from molecular interferences (e.g.  $^{40}\text{Ar}^{16}\text{O}$  interfering on  $^{56}\text{Fe}$ , or  $^{40}\text{Ar}^{38}\text{Ar}$  on  $^{78}\text{Se}$ ). The Element XR (Thermo Fisher Scientific, Bremen) at the INE radioactive laboratories is adapted to a glove box system for handling of active material (Figure 1).

Combined with species selective techniques such as capillary electrophoresis (CE)-SF-ICP-MS can be also used for speciation and complexation studies of actinides in solution taking advantage of the high sensitivity of modern SF-ICP-MS instruments. Studies using CE-SF-ICP-MS have reported species detection limits of  $\sim 10^{-12}$  mol/L for Pu [3] which is also confirmed by investigations recently conducted at INE.

#### ***SF-ICP-MS – Exploiting high Sensitivity and Selectivity for the Detection of Actinides and Lanthanides***

One of the main tasks of the mass spectrometer is the detection and quantification of elements especially actinides at very low concentrations (i.e. in the ng/L and pg/L range).

Figure 2 shows the results obtained for the detection of  $^{242}\text{Pu}$  and  $^{237}\text{Np}$  in samples from a radionuclide migration experiment conducted at the underground Grimsel Test Site in 2012 (run 12-02). Both radionuclides together with  $^{243}\text{Am}$ , Ni doped montmorillonite and several other radionuclides were injected into a shear zone at the beginning of the migration test.

The concentrations that were obtained for  $^{237}\text{Np}$  and  $^{242}\text{Pu}$  lie in range of several  $10^{\text{ths}}$  of ppq up to 3 ppt for  $^{242}\text{Pu}$  with detection limits of  $\sim 10\text{-}20$  ppq. The results demonstrate the excellent sensitivity of SF-ICP-MS for transuranium elements.

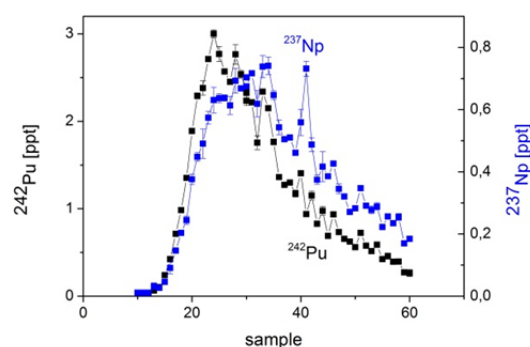


Fig. 2: Breakthrough curves of  $^{237}\text{Np}$  and  $^{242}\text{Pu}$  obtained from a radionuclide migration experiment conducted at the Swiss Grimsel Test Site (GTS, run 12-02, cf. chapter 6.3).

An important feature of the SF-ICP-MS technique is the adjustment of medium and high mass resolution whereby polyatomic mass interferences can be reduced very efficiently. Lanthanides which are often used as homologues for trivalent actinides such as Cm exhibit distinct mass interferences at low mass resolution (commonly available in quadrupole instruments). Most of these interferences can be strongly reduced to an analytical acceptable level using medium or high mass resolution combined with proper plasma tuning conditions. Figure 3 depicts lanthanide concentrations that were obtained for a certified river water reference material (SLRS-4) compared to the elemental concentrations published for this specific reference material [4]. Both data sets show excellent agreements for all lanthanides within the experimental error.

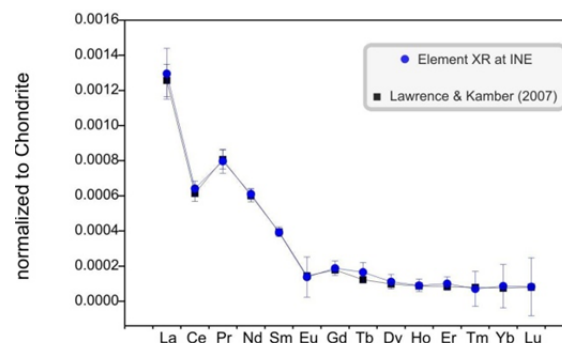


Fig. 3: Relative elemental concentrations of lanthanides in a river water standard reference material (SLRS-4) determined by SF-ICP-MS at medium mass resolution; comparison between published [4] and own data (normalized to Chondrite meteorite concentrations).

### CE-SF-ICP-MS – Hyphenated Technique for the Determination of Actinide and Iron Redox Species

At INE special attention is currently drawn to the development of hyphenated techniques in order to determine the distribution of redox species in aqueous solution with special emphasis on actinides (Pu, Np), fission products (Se, Tc), and also Fe. Iron is of particular interest because a variety of actual studies are focusing on sorption of actinides on Fe mineral phases (especially Fe-oxides and Fe-hydroxides).

The redox state is a key property which determines not only the solubility of elements in aquatic systems but also the sorption on mineral surfaces. Both solubility and retention due to sorption have a strong impact on the potential mobility of elements. In order to trace and quantify redox species in aqueous solution at very low concentrations (which is required for the study of processes below the solubility limit) we chose capillary electrophoresis coupled to the SF-ICP-MS. Several studies have already demonstrated that CE-SF-ICP-MS is a very suitable tool for speciation studies at concentrations  $< 10^{-10}$  mol/L [2,5] particularly for transuranium elements such as Pu.

At INE we applied a CE method similar to the approach of Kuczewski et al. [6] to separate different Pu redox species using 1 M acetic acid as background electrolyte. All separations were carried out with bare fused silica capillaries (50  $\mu\text{m}$  ID, 70-75 cm length), with hydrodynamic sample injection, a separation voltage of 30 kV, and at various Pu concentrations. Integrated peak areas show a linear relationship over several orders of magnitude and detection limits between  $10^{11}$  to  $10^{13}$  mol/L for the higher valence states Pu(VI) and Pu(V). These results are consistent with measured CE detection limits for pentavalent Np of  $\sim 10^{-12}$  mol/L and published values [3]. However, detection limits determined for Pu(IV) are in analogy to Th(IV) significantly higher ( $\sim 10^{-9}$  mol/L). So far this has been explained by possible sorption of tetravalent actinides at the surface of silica fused capillaries.

Although the CE method allows the separation of different Pu valence states (Pu(III), Pu(IV), Pu(V) and Pu(VI)) at concentrations lower than  $10^{-10}$  mol/L (if all Pu redox species are considered) there still remains the challenge to overcome the limited stability of the different Pu redox states during the course of the measurements. In order to avoid any oxidation/reduction reactions taking place during the separation we are planning to modify our method by using different ligands to stabilize the different valence states.

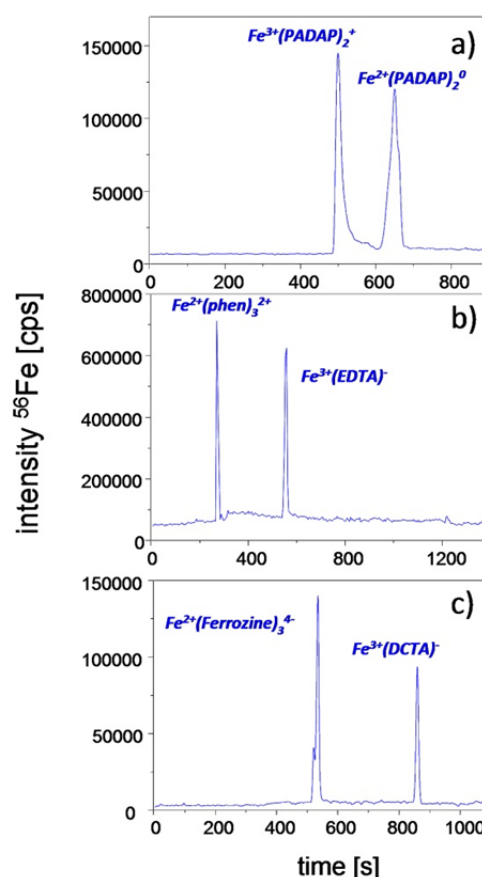


Fig. 4: Electropherograms of Fe(II)/Fe(III) capillary electrophoresis separations. **a)** sample: Fe(II) and Fe(III) (each  $1.6 \times 10^{-5}$  mol/L) plus PADAP ( $1.2 \times 10^{-4}$  mol/L), BGE: 12.5 mM HAc, 12.5 mM KAC, hydrodynamic sample injection for 10 s at 2 psi, separation at 30 kV. **b)** sample: Fe(II) and Fe(III) (each  $2.5 \times 10^{-5}$  mol/L) plus EDTA and o-phen (each  $2.5 \times 10^{-4}$  mol/L), hydrodynamic sample injection for 10 s at 2 psi, BGE: 5.0 mM  $\text{K}_3\text{PO}_4$ , pH = 12.3, separation at 25 kV **c)** sample: Fe(II) and Fe(III) (each  $0.6 \times 10^{-6}$  mol/L) plus DCTA and ferrozine (each  $5 \times 10^{-5}$  mol/L), BGE: 100 mM HAc plus DCTA ( $0.5 \times 10^{-3}$  mol/L) and ferrozine ( $0.9 \times 10^{-3}$  mol/L), hydrodynamic sample injection for 10 s at 1 psi, separation at -30 kV.

A similar approach has been already used for the determination of Fe(II)/Fe(III). So far we tested several potential ligands to complex and stabilize the two Fe redox species. Among those are o-phenanthroline, disodium 4-[3-(2-pyridinyl)-6-(4-sulfophenyl)-1,2,4-triazin-5-yl] (ferrozine), EDTA, DCTA, 2-(5-bromo-2-pyridylazo)-5-diethylaminophenol (PADAP), 4-(2-pyridylazo)resorcinol (PAR), and 1,2-Dihydroxybenzene-3,5-disulfonic acid (Tiron). Figure 4 depicts the electrochromatograms of 3 different separations which were conducted with various background electrolytes (acetic acid,  $K_3PO_4$ ,  $NaH_2PO_4$ ) and ligands (o-phenanthroline, ferrozine, PADAP, DCTA, EDTA). Applying hydrodynamic sample injection both Fe redox species are successfully separated by all three methods with detection limits around  $10^{-7}$  mol/L.

Using electrokinetic injection of samples containing 40 vol% methanol even a detection limit of  $\sim 10^{-9}$  mol/L was achieved for Fe(II) using o-phen as complexing agent and  $NaH_2PO_4$  as background electrolyte. The advantage of organic solvents is based on the reduced electroosmotic flow and the lower conductivity of the sample zone, both leading to stronger focusing of ions during separation.

Further improvements and developments are in progress, particularly related to 1) improved detection limits of the CE separations and 2) the determination of redox species in solutions with elevated ionic strength ( $>100$  mM salt content) which are prerequisites for our fundamental research objectives.

## References

- [1] Doubleva, G. et al., The COMET-L1 experiment on long-term MCCI and late melt surface flooding, Forschungszentrum Karlsruhe (2006).
- [2] Becker, J. S. and Dietze, H.-J., *J. of Anal. At. Spec.*, 14: 1493 (1999).
- [3] Topin, S. et al., *Anal. Chem.*, 81: 5354 (2009).
- [4] Lawrence, M. G., Kamber, B. S., *Geostandards and Geoanalytical Research*, 31: 1 (2007).
- [5] Ambard, C. et al., *Radiochim. Acta*, 93: 665 (2005).
- [6] Kuczewski, B. et al., *Anal. Chem.*, 75: 6769 (2003).



## 11 Radiation Protection Research

*B. Breustedt, P. Panak, F. Becker, A. Benzler, C. Blunck, J. S. Eberhardt, C. Figuera, M. A. Harrendorf, B. Heide, T. Keck, W. Klein, S. Laubersheimer, D. Leone, O. Marzocchi, S. Pölz*

### Introduction

Radiation Protection Research at INE is focusing on assessing radiation exposures by estimation of doses either from external radiation fields or from intakes of radionuclides. Besides measurements, the modeling and simulation of radiation fields and their interaction with tissues of the human body or detectors measuring the field are the techniques applied in the work of the group. Basic vision of the work is to provide techniques and models for an individualized dosimetry, which goes beyond the current approach of applying reference models in the dose assessments. The exposed individual with his or her anatomical and physiological properties as well as the radiation fields – properly characterized – are taken into account in an individualized dosimetry. In 2012 we again focused on the three main topics

- Dosimetry in external radiation fields
- Dosimetry after intakes of radionuclides
- Modeling and Simulation of Radiation Protection Scenarios

The ASF group is collaborating with national and international partners in several research projects funded by BmBF (e.g. Projects “Strahlung und Umwelt” in Competence Alliance Radiation Research KVSF) or EC (e.g. Project “BOOSTER” in FP7Sec). Our group is also engaged in the European Radiation Dosimetry Group (EURADOS e.V., <http://www.eurados.org>), which promotes and develops research and European Collaboration in radiation dosimetry.

Selected results from the 2012 work of the radiation protection research group at INE are presented in this chapter.

### Dosimetry for CT fluoroscopy staff

Simulation supported dosimetry is mainly employed for cases where measurements are difficult or not feasible. This includes research on CT fluoroscopy staff dosimetry, which is currently investigated in one of the task groups of EURADOS WG12 [1]. Analyses of measurements performed at CT devices at the Coimbra hospital and at the Klinikum Karlsruhe, as well as corresponding feasibility studies of simulations were finalized

In figure 1 simulated dose values at different positions (red spots) on a hand phantom are illustrated. The cross line indicates the beam position and the rotation axis of the CT scanner with the thick and thin line, respectively. A strong dose gradient is observed; within a few mm away from the beam spot the dose is reduced by at least an order of magnitude. The benchmark for simulations with the two different simulation programs MCNPX [2] and GMctdospp [3] were completed [4,5]. Henceforth it is planned to compare accomplished and ongoing measurements of handling scenarios with simulations.

Two studies on CT-fluoroscopy have been finished in 2012. A collaboration between ITN and KIT comprised measurements at Coimbra hospital and Klinikum Karlsruhe and the according MCNPX simulations [4], as well as a three month research stay at KIT (Visiting Researcher Scholarship of the Karlsruhe House of Young Scientists (KHYS)). The second study [5] applied the Monte Carlo code GMctdospp to simulate measurements taken at Klinikum Karlsruhe. The two studies showed that Monte Carlo codes are useful tools to investigate the complex radiation field for exposure scenarios in CT fluoroscopy. It is confirmed that CT fluoroscopy is among the highest exposure scenarios for medical staff – in the considered scenarios, the annual skin dose limit would be

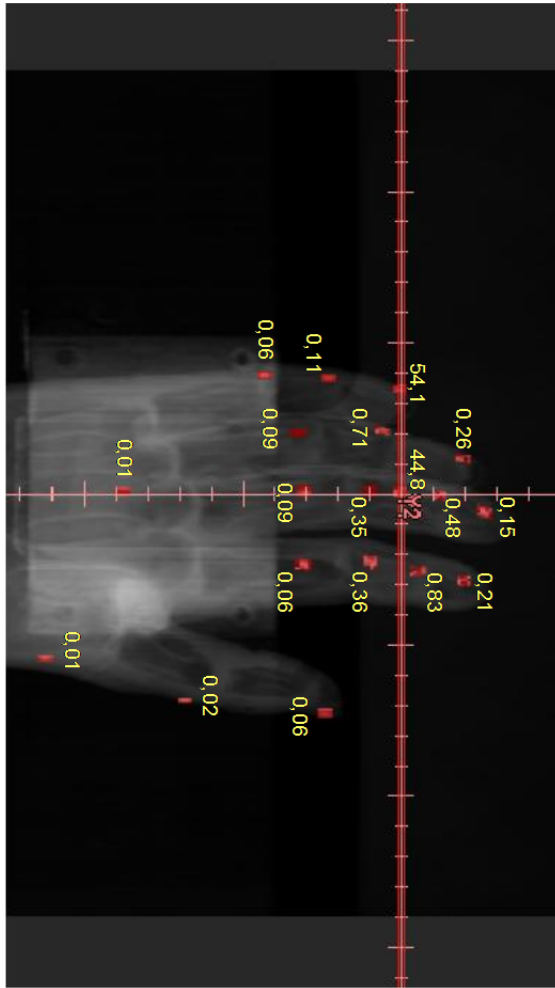


Fig. 1: DICOM-File of a CT scanned hand phantom with  $H_p(0,07)$  dose values in mSv as obtained from simulations with GMctdospp.

exceeded within a few tens of identical irradiations.

### Monte Carlo Simulation of electron transport in thin layers of tissue

The simulation of classical radiation transport has become an important method for analysing absorbed doses or detector response functions among others. In the following, we applied the Monte Carlo Nuclear-Particle transport code (MCNP) and simulated absorbed doses in layers of tissue-equivalent materials. The layers were so thin that their thicknesses were comparable with the average diameter of human cells (i. e. 0.001 cm). Determining the dose in such thin layers is at the border of the scope of MCNP, since smaller cells do not encompass enough collisions so

that the underlying multiple-scattering theory is still applicable. The explicit scenario consisted of a Sr-90/Y-90 area source, implemented in the Beta Secondary Standard BSS2 [6], and a cuboid phantom made of tissue-equivalent material. A pike of lead was located inside the phantom. The slabs of the scoring cell were subdivided into rings or, to be more precise, hollow cylinders. A drawing of the simulation scenario is given in figure 2. This task formulation is part of the more comprehensive work of Ref. [7] and described in more detail therein as well.

The dose amplification factor referring to depths between 0.001 cm and 0.007 cm has been calculated. Looking at the curve for the tiny slab (radius: 0.03 cm), a distinct amplification over all depths is obvious. The bump of this curve is due to the build-up factor. The build-up factor also causes the curve to rise considerably for the first hollow cylinder (radii: 0.03 cm – 0.06 cm) and for the second one (radii: 0.06 cm – 0.09 cm). Dose enhancement is most obvious for the tiny slab and the first two hollow cylinders. The tiny slab and the first two hollow cylinders together form a slab with radius of 0.09 cm which has a cross-sectional area of about 1/40 of 1 cm<sup>2</sup>. For this slab, dose enhancement ranges between 68% and 88%, whereas hardly any dose enhancement results for the big slab (radius: 0.6 cm) with a cross-sectional area of about 1 cm<sup>2</sup>. The maximum dose enhancement of about 113% is reached for the first

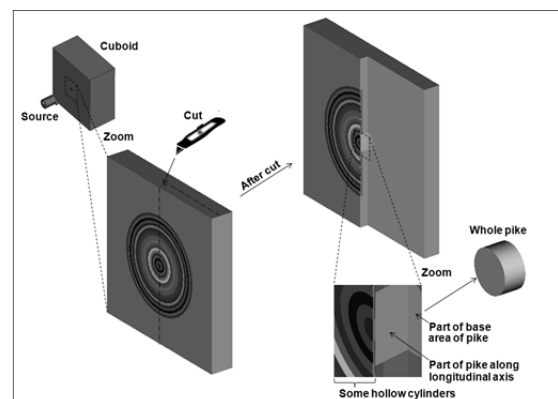


Fig. 2: Simulation scenario. Left: rings of the cuboid are presented enlarged. Right: Cut-out of the enlarged representation of the cuboid. Some hollow cylinders and parts of the cylindrical pike are displayed at the bottom as well.

hollow cylinder at a depth of 0.007 cm. Hardly any dose enhancement is obvious for the curve which refers to the big slab (radius: 0.6 cm) having an area of about 1 cm<sup>2</sup>, while it is the case for the slab with a radius of 0.09 cm. The almost lacking dose enhancement of the big slab is remarkable, since the dose is normally related to an area of 1 cm<sup>2</sup> in operational radiation protection.

### **Partial body counter calibration using Voxel2MCNP and the JAERI phantom**

Modelling for radiation transport simulation is an essential task for prospective and retrospective evaluation of radiation protection scenarios. This task can be quite complex and time-consuming when confronted with large amounts of data from various sources that may be frequently updated or are provided in different file formats. One common scenario is body counter calibration for the detection of incorporated activity, where detector models may change, new phantoms become available, and large simulation series have to be created, managed, and evaluated.

Voxel2MCNP [8] was enhanced to provide a unified framework supporting users in modelling radiation transport scenarios using voxel phantoms and other geometric models, generating corresponding input for the Monte Carlo code MCNPX, and evaluating simulation output. It offers a common interface for modelling, visualization, and evaluation of data and is compatible with several file formats, such as Evaluated Nuclear Structure Data File (ENSDF) [9] for nuclear structure properties and radioactive decay data, SimpleGeo [10] for solid geometry models, and MCNPX's MCTAL for simulation results. The foundation of Voxel2MCNP is formed by a generic, modular data model describing radiation transport scenarios. It defines several independent data structures for geometry, materials, sources, simulation results, etc., which are linked via cross-references. The data model is also available in an XML-based file format to facilitate data exchange with other researchers or different software tools.

For body counter calibration, a special module implements the detector kinematics of KIT's partial body counter and allows detector positioning using its parameters. Voxel2MCNP can automatically generate the according MCNPX input for a scenario model, and also process simulation results (e.g. detector spectra) after computation. Simulation series can be produced with Voxel2MCNP by creating a template common for all scenarios and then adding or replacing certain features (e.g. different detectors, phantoms, or sources).

A JAERI phantom [11] provided by the International Atomic Energy Agency [12] has been used as a test case. A voxel model of the phantom has been created by KIT in 2010. Three HPGe detectors were used in the measurements and positioned according to routine measurements at KIT, i.e. at left lung, right lung, and liver (see figure 3). In total, 21 measurements were taken, including two background measurements with blank lungs.

After finishing the measurement setup, a corresponding scenario template was created (see figure 3). It consists of three main components: three HPGe detectors annotated with individual tallies, the voxel model of the basic JAERI phantom annotated with a designated source location (lungs), and an empty source representing the inactive lung set. All components were modelled individually and then combined with the scenario template for each overlay and lung set. Detector positions were reproduced according to the records. Simulation input was created, simulations

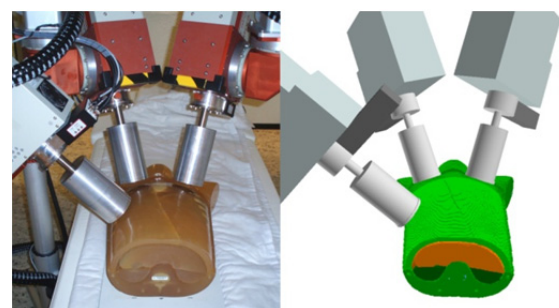


Fig. 3: Comparison of the real measurement scenario (left) and its virtual representation in voxel2MCNP (right).

were performed with MCNPX, and results were evaluated using standard methods for peak area estimation.

In general, the measurements could be reproduced. However, differences in counting efficiencies between simulations and measurements are up to 20%. Due to the systematic over- or underestimation for certain radionuclides, it is suspected that the main causes are high uncertainties in the certified activities and possible inhomogeneous distributions inside the lungs. Also, imprecise detector positioning due to tolerances in mechanics and measurements, and missing details in detector and phantom models (e.g. air inclusions in the lung material of the active lung set) may have an effect.

The framework presented here has proven to be capable of handling modelling and evaluation tasks related to body counter calibration efficiently. Updating simulation data and detector models or adding new phantoms is straightforward and intuitive. Development is ongoing, and support for other applications related to radiation transport will be added in the future.

### Evaluation of dose conversion factors using Voxel2MCNP

Since Voxel2MCNP is built as a tool for radiation protection, the calculation of dose conversion factors will be soon implemented in the code. The dose conversion factors allow assessing effective dose. In case of body irradiation from outside dose conversion factors are given in terms of absorbed dose normalized to air kerma, while in the case of internal contamination one speaks about specific absorbed fraction SAF, defined as the fraction of energy emitted from the source organ absorbed from the target organ, normalized to the mass of the target organ. Those coefficients depend on the anatomy of the phantoms, on the kind and the energy of the radiation, on the direction of the radiation in case of external irradiation. They can be calculated only making use of Monte Carlo simulations and of voxel model phantoms. The reference ICRP adult male has been used; the values of

the conversion factors have been compared with the published ones [13] in several scenarios both for external and internal contamination. The values have been correctly reproduced in order to validate our methods. This latter will be implemented in the software in order to automatize the calculations. Once this step will be concluded, it will be possible to automatically calculate the dose conversion factors for any voxel phantom available in Voxel2MCNP.

### Implementation and quality assurance of recent ICRP biokinetic models

Within the biokinetic task group of EURADOS WG7 [14] test calculations have been performed with the new biokinetic models of ICRP. These models represent the biokinetic behaviour of radionuclides and are applied in interpretation of bioassay measurements and dose assessments after incorporation of radionuclides. ICRP recently published a draft of their new document "Occupational Intakes of Radionuclides" [15] for consultation. Here the new models of several radionuclides are described. In the task group several nuclides and scenarios have been selected for comparison. These tests by independent users are performed to test if the description of the models shows ambiguities and might be refined. They also show the ability of the users to apply the models. At KIT the new models for the radionuclides H-3, Fe-59, Co-60, Sr-90, I-131 and Cs-137 have been implemented in the in-house developed SABiM Code [16]. The reten-

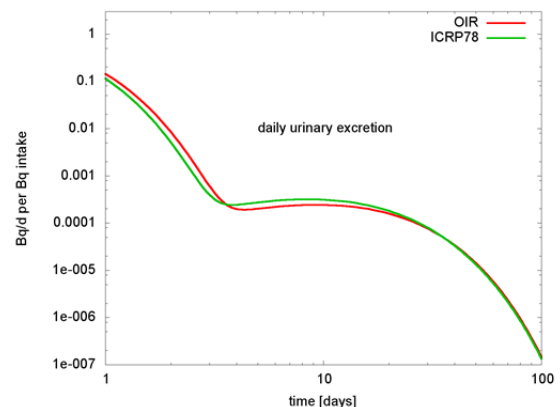


Fig. 4: Comparison of the daily urinary excretion of I-131 predicted by the draft OIR document (OIR) and the recent ICRP models (ICRP78) taken from [5].

tion for blood, the main retention organs and total body as well as daily excretion values for urine and faeces have been calculated. Figure 4 shows exemplary the daily urinary excretion of I-131 calculated with the new models (OIR) and the existing models (ICRP78) taken from [17]. The slight difference between the predictions of the new and the recent models can be seen. The next step will be to study the influence on the predicted doses.

A comparison with first calculations from other groups showed that all descriptions have been interpreted the same and only minor numerical discrepancies whose sources are recently under investigation were observed. The analyses of the whole set of calculations of all partners is still to follow.

## References

- [1] EURADOS (2012) European Radiation Dosimetry Group, WG12 – European Medical ALARA Network, website <http://www.eurados.org/>, March 2013.
- [2] Pelowitz, D. B., MCNPX USER'S MANUAL, Version 2.6.0, LA-CP-07-1473, Los Alamos Laboratory, USA (2008).
- [3] GMctdospp - Version 0.2.5.04, website <http://www.thm.de/imps/programme/95-gmctdospp>, May 2012.
- [4] Figueira, C. et al., Medical staff extremity dosimetry in CT Fluoroscopy: an anthropomorphic hand voxel phantom study, *Phys. Med. Biol.*, (2012) submitted.
- [5] Göpfert, F., Einsatz der Simulationssoftware GMctdospp zur Untersuchung der Exposition des Personals bei der CT-Fluoroskopie, Bachelor-Arbeit, DHBW Karlsruhe (2012).
- [6] Ambrosi, P. et al., The PTB Beta Secondary Standard BSS 2 for Radiation Protection. *JINST*, 2 : P11002 (2007).
- [7] Heide, B., Assessment of doses caused by electrons in thin layers of tissue equivalent materials using MCNP MCNP. *Radiation Protection Dosimetry*, (2013) accepted.
- [8] Hegenbart, L. et al., *Health Phys.* 102(2): 221 (2012).
- [9] Tuli, J. K., BNL-NCS-51655-01/02-Rev (2001).
- [10] Theis, C. et al., *Nucl. Instrum. Meth. A* 562(2): 827 (2006).
- [11] Shirotani, T., *J. Nucl. Sci. Technol.* 25(11): 875 (1988).
- [12] International Atomic Energy Agency, IAEA-TECDOC-1334 (2003).
- [13] ICRP Publication 110, October 2008
- [14] EURADOS European Radiation Dosimetry Group, Website – Working groups. [http://www.eurados.org/en/Working\\_groups](http://www.eurados.org/en/Working_groups), March 2013.
- [15] ICRP. Website – Consultations of reports: [http://www.icrp.org/consultation\\_page.asp](http://www.icrp.org/consultation_page.asp), March 2013.
- [16] Klein, W., Stochastische Aspekte der internen Dosimetrie, Dissertation, KIT Karlsruhe (2011).
- [17] ICRP Publication 78, *Ann. ICRP* 27 (3-4), (1997).



## 12 Publications

### „Peer reviewed“ contributions in Journals, Conference Proceedings, Books

BECKER, F.; BLUNCK, CH.; FIGUEIRA, C.; ESTEVES, B.; DI MARIA, S.; PAULO, G.; SANTOS, J.; TELES, P.; VAZ, P.

Radiation exposure of medical staff: application of hand phantoms in experiments and simulations  
Safety Engineering Vol 2, No. 2 (2012), 99-102.

BEELE, B. B.; MÜLLICH, U.; SCHWÖRER, F.; GEIST, A.; PANAK, P. J.

Systematic modifications of BTP-type ligands and effects on the separation of trivalent lanthanides and actinides.

Procedia Chemistry 7 (2012), 146–151.

BELL, K.; GEIST, A.; MCLACHLAN, F.; MODOLO, G.; TAYLOR, R.; WILDEN, A.

Nitric acid extraction into TODGA.

Procedia Chemistry 7 (2012), 152–159.

BELL, K.; CARPENTIER, C.; CARROTT, M.; GEIST, A.; GREGSON, C.; HÉRÈS, X.; MAGNUSSON, D.; MALMBECK, R.; MCLACHLAN, F.; MODOLO, G.; MÜLLICH, U.; SYPULA, M.; TAYLOR, R.; WILDEN, A.

Progress towards the development of a new GANEX process.

Procedia Chemistry 7 (2012), 392–397.

BESBES, R.; NOUREDDINE, O.; ABDERABBA, M.; LINDQVIST-REIS, P.; LATROUS, H.

Investigation of the self-diffusion coefficients of trivalent Gd(III) in aqueous solutions: The effect of hydrolysis and nitrate ion

Mediterr. J. Chem., 1 (2012), 334-346.

BOUBY, M.; FINCK, N.; GECKEIS, H.

Flow field-flow fractionation (FIFFF) coupled to sensitive detection techniques: a way to get insight into the radionuclide interaction with colloidal systems

Mineralogical Magazine, 76 (2012), 2709-2722.

BOURG, S.; POINSSOT, C.; GEIST, A.; CASSAYRE, L.; RHODES, C.; EKBERG, C.

Advanced reprocessing developments in Europe: Status on European projects ACSEPT and ACTINET-13.

Procedia Chemistry 7 (2012), 166–171.

BRANDT, F.; SCHÄFER, T.; CLARET, F.; BOSBACH, D.

Heterogeneous formation of ferric oxide nanoparticles on chlorite surfaces studied by x-ray absorption spectromicroscopy (STXM),

Chem. Geol. 329 (2012), 42-52.

BREMER, A., RUFF, C.M., GIRNT, D., MÜLLICH, U., ROTHE, J., ROESKY, P. W., PANAK, P.J., KARPOV, A., MÜLLER, T. J. J., DENECKE, M. A., GEIST, A.

2,6-Bis-(5-(2,2-dimethylpropyl)-1H-pyrazol-3-yl)-pyridine as ligand for the efficient actinide(III) / lanthanide(III) separation.

Inorg. Chem. 51 (2012), 5199–5207.

BREMER, A., GEIST, A., PANAK, P.J.  
Complexation of Cm(III) with 6-(5,6-dipentyl-1,2,4-triazin-3-yl)-2,2'-bipyridine studied by time resolved laser fluorescence spectroscopy.  
Dalton Trans. 41 (2012), 7582–7589.

D. BROGGIO ET AL.

Monte Carlo modelling for the in vivo lung monitoring of enriched uranium: Results of an international comparison.  
Rad. Meas. 47 (7) (2012), 492–500.

BRUGGEMAN, C.; MAES, N.; CHRISTIANSEN, B. C.; STIPP, S. L. S.; BREYNAERT, E.; MAES, A.; REGENSPURG, S.; MALSTRÖM, M. E.; LIU, X.; GRAMBOW, B.; SCHÄFER, T.  
Redox-active phases and radionuclide equilibrium valence state in subsurface environments – New insights from 6th EC FP IP FUNMIG,  
Appl. Geochem., 27 (2012), 404-413.

BUBE, C.; METZ, V.; BOHNERT, E.; GARBEV, K.; SCHILD, D.; KIENZLER, B.  
Long-term cement corrosion in chloride-rich solutions relevant to radioactive waste disposal in rock salt - leaching experiments and thermodynamic simulations.  
Physics and Chemistry of the Earth (2012), <http://dx.doi.org/10.1016/j.pce.2012.11.001>.

CARVAJAL-NUNEZ, U.; PRIEUR, D.; VITTOVA, T.; SOMERS, J.  
Charge Distribution and Local Structure of Americium-Bearing Thorium Oxide Solid Solutions.  
Inorg. Chem, (2012) DOI: 10.1021/ic301709d.

DARBHA, G. K.; FISCHER, C.; LUETZENKIRCHEN, J.; SCHÄFER, T.  
Site-specific retention of colloid at rough rock surfaces  
Environmental Science and Technology, 46 (2012), 9379-9384.

DARBHA, G. K.; FISCHER, C.; MICHLER, A.; LUETZENKIRCHEN, J.; SCHÄFER, T.; HEBERLING, F.; SCHILD, D.  
Deposition of latex colloid at rough mineral surfaces: An analogue study using nanopatterned surfaces  
Langmuir, 28 (2012), 6606-6617.

DENECKE, M. A.; BORCHERT, M.; DENNING, R. G.; DE NOLF, W.; FALKENBERG, G.; HÖNIG, S.; KLINKENBERG, M.; KVASHNINA, K.; NEUMEIER, S.; PATOMMEL, J.; PETERSMANN, T.; PRUESSMANN, T.; RITTER, S.; SCHROER, CH. G.; STEPHAN, S.; VILLANOVA, J.; VITTOVA, T.; WELLENREUTHER, G.  
Highly resolved synchrotron-based investigations related to nuclear waste disposal  
MRS proceedings 2012, 1444, mrs12-1444-y01-05 (2012). doi:10.1557/opl.2012.1159.

DIENER, A.; NEUMANN, T.; KRAMAR, U.; SCHILD, D.  
Structure of selenium incorporated in pyrite and mackinawite as determined by XAFS analyses.  
J. Contaminant Hydrology, 133 (2012), 30-39.

ELANIQUE, A.; MARZOCCHI, O.; LEONE, D.; HEGENBART, L.; BREUSTEDT, B.; OUFNI, L.  
Dead layer thickness characterization of an HPGe detector by measurements and Monte Carlo simulations.  
Appl. Radiat. Isotopes, 70 (2012), 538-542.

- FILBY, A.; PLASCHKE, M.; GECKEIS, H.  
AFM force spectroscopy study of carboxylated latex colloids interacting with mineral surfaces.  
Colloids and Surfaces A: Physicochem. Eng. Aspects, 414 (2012), 400–414.
- FINCK, N.; BOUBY, M.; DARDENNE, K.; GECKEIS, H.  
Characterization of Eu(III) coprecipitated with and adsorbed on hectorite: from macroscopic crystallites to nanoparticles  
Mineralogical Magazine, 76(7) (2012), 2723-2740.
- FINCK, N.; DARDENNE, K.; BOSBACH, D.; GECKEIS, H.  
Selenide retention by mackinawite  
Environ. Sci. Technol., 46(18) (2012), 3845-3851.
- FISCHER, C.; MICHLER, A.; DARBHA, G. K.; KANBACH, M.; SCHÄEFER, T.  
Deposition of mineral colloids on rough rock surfaces  
American Journal of Science, 312 (2012), 885-906.
- GAONA, X.; TITS, J.; DARDENNE, K.; LIU, X.; ROTHE, J.; DENECKE, M. A.; WIELAND, E.; ALTMAIER, M.  
Spectroscopic investigations of Np(V/VI) redox speciation in hyperalkaline TMA-(OH,Cl) solutions  
Radiochim. Acta, 100 (2012), 759-770.
- GECKEIS, H.; KIENZLER, B.; GOMPPER, K.,  
Nuklearchemische Grundlagenforschung: Bausteine für eine sichere Entsorgung radioaktiver Abfälle,  
atw 57, Jg. (2012) Heft 7, pp. 457 – 466.
- GECKEIS, H.; RÖHLIG, K.-J.; MENGEL, K.  
Chemie im Endlagersystem: Endlagerung radioaktiver Abfälle  
Chem. Unserer Zeit, 46 (2012), 282–293.
- GEIST, A.; MÜLLICH, U.; MAGNUSSON, D.; KADEN, P.; MODOLO, G.; WILDEN, A.; ZEVACO, T.  
Actinide(III)/lanthanide(III) separation via selective aqueous complexation of actinides(III) using a hydrophilic 2,6-bis(1,2,4-triazin-3-yl)-pyridine in nitric acid.  
Solvent Extr. Ion Exch., 30 (2012), 433–444.
- HEGENBART, L.; PÖLZ, S.; BENZLER, A.; URBAN, M.  
Voxel2MCNP: Software for handling voxel models for Monte Carlo radiation transport calculations.  
Health Physics, 102 (2) (2012), 221-229.
- HOLLIDAY, K.; BABELOT, C.; WALTHER, C.; BOSBACH, D.; STUMPF, T.  
Site-selective time resolved laser fluorescence spectroscopy of Eu and Cm doped LaPO<sub>4</sub>.  
Radiochim. Acta, 100 (2012), 189-194.
- HOLLIDAY, K.; CHAGNEAU, A.; SCHMIDT, M.; CLARET, F.; SCHÄFER, T.; STUMPF, T.  
Discriminating factors affecting incorporation: comparison of the fate of Eu<sup>3+</sup>-Cm<sup>3+</sup> in the Sr carbonate-sulfate system.  
Dalton Transactions, 41 (2012), 3642-3647.
- HOLLIDAY, K.; HANDLEY-SIDHU, S.; DARDENNE, K.; RENSHAW, J.; MACASKIE, L.; WALTHER, C.; STUMPF, T.  
A New Incorporation Mechanism for Trivalent Actinides into Bioapatite: A TRIFS and EXAFS Study.  
Langmuir, 28(8) (2012), 3845-3851.

- HU, J.; POHL, A.; WANG, S.; ROTHE, J.; FICHTNER, M.  
Additive Effects of  $\text{LiBH}_4$  and  $\text{ZrCoH}_3$  on the Hydrogen Sorption of the Li-Mg-N-H Hydrogen Storage System.  
*J. Phys. Chem., C*, 116 (2012), 20246–20253.
- HUBER, F.; ENZMANN, F.; WENKA, A.; BOUBY, M.; DENTZ, M.; SCHÄFER, T.  
Natural micro-scale heterogeneity induced solute and nanoparticle retardation in fractured crystalline rock.  
*J. Cont. Hydrol.*, 133 (2012), 40-52.
- HUBER, F.; SCHILD, D.; VITOVA, T.; ROTHE, J.; KIRSCH, R.; SCHÄFER, T.  
U(VI) removal kinetics in presence of synthetic magnetite nanoparticles.  
*Geochim. Cosmochim. Acta*, 96 (2012), 154–173.
- HUITTINEN, N.; RABUNG, TH.; SCHNURR, A.; HAKANEN, M.; LEHTO, J.; GECKEIS, H.  
New insight into Cm(III) interaction with kaolinite - influence of mineral dissolution.  
*Geochim Cosmochim Acta*, 99 (2012), 100-109.
- KADEN, P.; FREUDENBERGER, J.; LUY, B.  
Non-covalent and covalent cross-linked polyurethane gels as alignment medium and the suppression of residual polymer signals using diffusion filtered spectroscopy.  
*Magn. Reson. Chem.*, 50 (2012), S22–S28.
- KALLAY, N.; PREOCANIN, T.; SUPLJIKA, F.; LÜTZENKIRCHEN, J.; LOVKOVIC, M.  
Influence of interfacial water layer on surface properties of silver halides: Effect of pH on the isoelectric point.  
*J. Coll. Int. Sci.*, 375 (2012), 167-171.
- KOSOG, B.; DENECKE, M. A.; HEINEMANN, F. W.; MEYER, K.  
Oxidation State Delineation via U LIII Edge XANES in a Series of Isostructural Uranium Coordination Complexes.  
*Inorg. Chem.*, 51 (2012), 7940–7944.
- LANSON, B.; LANTENOIS, S.; VAN AKEN, P. A.; BAUER, A.; PLANÇON, A.  
Experimental investigation of smectite interaction with metal iron at 80°C: Structural characterization of newly formed Fe-rich phyllosilicates.  
*American Mineralogist*, 97 (2012), 864–871.
- LÉON, A.; ROTHE, J.; HAHN, H.; GLEITER, H.  
Short range order around Sc atoms in  $\text{Fe}_{90}\text{Sc}_{10}$  nanoglasses using fluorescence X-ray absorption spectroscopy.  
*Revue de Métallurgie*, 109 (2012), 35-39.
- LOIDA, A.; GENS, R.; LEMMENS, K.; CACHOIR, C.; MENNECART, T.; KIENZLER, B.  
Corrosion Behaviour of Spent Nuclear Fuel in High pH Solutions – Effect of Hydrogen.  
*Material Research Society Symposium Proceedings*, 1475 (2012), 119–124.
- LÜTZENKIRCHEN, J.  
Summary of studies on (ad)sorption as a "well-established" process within FUNMIG activities.  
*Applied Geochemistry*, 27 (2012), 427-443.

- LÜTZENKIRCHEN, J.; PREOČANIN, T.; BAUER, A.; METZ, V.; SJÖBERG, S.  
Net surface proton excess of smectites obtained from a combination of potentiometric acid-base, mass and electrolyte titrations.  
Coll. Surf. A-Physicochem. Eng. Aspects, 412 (2012), 11-19.
- LÜTZENKIRCHEN, J.; PREOČANIN, T.; KOVAČEVIĆ, D.; TOMIŠIĆ, V.; LÖVGREN, L.; KALLAY, N.  
Potentiometric Titrations as a Tool for Surface Charge Determination.  
Croatica Chemica Acta, 85 (2012), 391-417.
- MAGNUSSON, D.; GEIST, A.; MALMBECK, R.; MODOLO, G.; WILDEN, A.  
Flow-sheet design for an innovative SANEX process using TODGA and SO<sub>3</sub>-Ph-BTP.  
Procedia Chemistry 7 (2012), 245-250.
- MARTIN CABANAS, B.; LÜTZENKIRCHEN, J.; LECLERCQ, S.; BARBOUX, P.; LEFÈVRE, G.  
Surface charging patterns of stainless alloys - Effect of ageing in conditions of primary cooling circuit of pressurized water reactors.  
J. Nucl. Mat., 430 (2012), 150-155.
- MENGEL, K.; RÖHLIG, K.J.; GECKEIS, H.  
Endlagerung radioaktiver Abfälle. Die Wirtsgesteine: Tonstein, Granit, Steinsalz.  
Chemie in unserer Zeit, 46 (2012), 208-217.
- METZ, V.; GECKEIS, H.; GONZÁLEZ-ROBLES, E.; LOIDA, A.; BUBE, C.; KIENZLER, B.  
Radionuclide behaviour in the near-field of a geological repository for spent nuclear fuel.  
Radiochim. Acta, 100 (2012), 699-713.
- MODOLO, G.; WILDEN, A.; GEIST, A.; MAGNUSSON, D.; MALMBECK, R.  
A review of the demonstration of innovative solvent extraction processes for the recovery of trivalent minor actinides from PUREX raffinate.  
Radiochim. Acta, 100 (2012), 715-725
- MONTAVON, G.; LE DU, A.; CHAMPION, J.; RABUNG, T.; MORGENSTERN, A.  
DTPA complexation of Bi in human blood serum.  
Dalton Trans., 41 (2012), 8615-8623.
- NOSECK, U.; TULLBORG, E.L.; SUKSI, J.; LAAKSOHARJU, M.; HAVLOVA, V.; DENECKE, M. A.; BUCKAU, G.  
Real system analyses/natural analogues.  
Applied Geochemistry, 27 (2012), 490-500.
- PEKOV, I. V.; CHUKANOV, N. V.; FILINCHUK, Y. E.; ZADOV, A. E.; KONONKOVA, N. N.; EPANCHINTSEV, S. G.; KADEN, P.; KUTZER, A.; GÖTTLICHER, J.  
Kasatkinite, Ba<sub>2</sub>Ca<sub>8</sub>B<sub>5</sub>Si<sub>8</sub>O<sub>32</sub>(OH)<sub>3</sub>·6H<sub>2</sub>O, a new mineral from the Bazhenovskoe deposit (Middle Urals, Russia).  
Zapiski RMO, 3 (2012), 39-49.
- PREOČANIN, T.; SELMANI, A.; LINDQVIST-REIS, P.; HEBERLING, F.; KALLAY, N.; LÜTZENKIRCHEN, J.  
Surface charge at Teflon/aqueous solution of potassium chloride interfaces.  
Colloids and Surfaces A-Physicochemical and Engineering Aspects, 412 (2012), 120-128.

- RÖHLIG, K. J.; GECKEIS, H.; MENGEL, K.  
Endlagerung radioaktiver Abfälle. Fakten und Konzepte.  
Chemie in unserer Zeit, 46 (2012), 140-149.
- ROTHER, J.; BUTORIN, S.; DARDENNE, K.; DENECKE, M. A. ; KIENZLER, B.; LÖBLE, M.; METZ, V.; SEIBERT, A.; STEPPERT, M.; VITOVA, T.; WALTHER, C.; GECKEIS, H.  
The INE-Beamline for actinide science at ANKA.  
Review of Scientific Instruments, 83(4) (2012), 043-105.
- RUFF, C. M.; MÜLLICH, U.; GEIST, A.; PANAK, P. J.  
Complexation of Cm(III) and Eu(III) with a hydrophilic 2,6-bis(1,2,4-triazin-3-yl)-pyridine studied by time-resolved laser fluorescence spectroscopy.  
Dalton Trans. 41 (2012), 14594–14602.
- RUFF, C. M.; MÜLLICH, U.; GEIST, A.; PANAK, P. J.  
Neue Strategien in der Actinidenabtrennung – wasserlösliche Komplexbildner für den innovativen SANEX-Prozess.  
Energiewirtschaftliche Tagesfragen, 62(3) (2012), 86-88.
- SCHÄFER, T.; HUBER, F.; SEHER, H.; MISSANA, T.; ALONSO, U.; KUMKE, M.; EIDNER, S.; CLARET, F.; ENZMANN, F.  
Nanoparticles and their influence on radionuclide mobility in deep geological formations.  
Appl. Geochem., 27 (2012), 390-403.
- SCHMIDT, M.; WILSON, R. E.; LEE, S. S.; SODERHOLM, L.; FENTER, P.  
Adsorption of Plutonium-Oxide Nanoparticles on Muscovite.  
Langmuir, 28 (2012), 2620-2627.
- SCHMIDT, M.; LEE, S.S.; WILSON, R. E.; SODERHOLM, L.; FENTER, P.  
Sorption of tetravalent Thorium on Muscovite.  
Geochim. Cosmochim. Acta, 88 (2012), 66-76.
- SERRANO-PURROY, D.; CLARENS, F.; GONZÁLEZ-ROBLES, E.; GLATZ, J. P.; WEGEN, D. H.; DE PABLO, J.; CASAS, I.; GIMÉNEZ, J.; MARTINEZ-ESPARZA, A.  
Instant release fraction and matrix release of high burn-up UO<sub>2</sub> spent nuclear fuel: Effect of high burn-up structure and leaching solution composition.  
J. Nucl. Mat., 427 (2012), 249-258.
- STEPPERT, M.; ČÍSAŘOVÁ, I.; FANGHÄNEL, TH.; GEIST, A.; LINDQVIST-REIS, P.; PANAK, P. J.; ŠTĚPNIČKA, P.; TRUMM, S.; WALTHER, C.  
Complexation of europium(III) by bis(dialkyltriazinyl)bipyridines in 1-octanol.  
Inorg. Chem., 51 (2012), 591-600.
- STEPPERT, M.; WALTHER, C.; FUSS, M.; BÜCHNER, S.  
On the Hydrolysis of Hexavalent Uranium. An Electrospray Mass-Spectrometry Study.  
Rapid Commun. Mass Spectrom., 26 (2012), 583–591.
- SYPUŁA, M.; WILDEN, A.; SCHREINEMACHERS, C.; MALMBECK, R.; GEIST, A.; TAYLOR, R.; MODOLO, G.  
Use of polyaminocarboxylic acids as hydrophilic masking agents for fission products in actinide partitioning processes.  
Solvent Extr. Ion Exch., 30 (2012), 748–764.

TRUMM, M.; GUERRERO MARTINEZ, Y. O.; REAL, F.; MASELLA, M.; VALLET, V.; SCHIMMELPFENNIG, B.  
Modeling the hydration of mono-atomic anions from the gas phase to the bulk phase: the case of the  
halide ions F<sup>-</sup>, Cl<sup>-</sup> and Br<sup>-</sup>.  
J. Chem. Phys., 136 (2012), 044509.

VESPA, M.; RINI, M.; SPINO, J.; VITOVA, T.; SOMERS, J.  
Fabrication and characterization of (U, Am)O<sub>2-x</sub> transmutation targets.  
J. Nucl. Mat., 421 (2012), 80-88.

WALTHER, C.; ROTHE, J.; SCHIMMELPFENNIG, B.; FUSS, M.  
Thorium nanochemistry: the solution structure of the Th(IV)-hydroxo pentamer.  
Dalton Trans., 41(36) (2012), 10941-10947.

WILDEN, A.; MODOLO, G.; SYPULA, M.; GEIST, A.; MAGNUSSON, D.  
The recovery of An(III) in an innovative-SANEX process using a TODGA-based solvent and selective  
stripping with a hydrophilic BTP.  
Procedia Chemistry 7 (2012), 418-424.

### **Book chapter**

ALTMAYER, M.; VERCOUTER, TH.  
Aquatic chemistry of the actinides.  
Radionuclide behaviour in the natural environment; H. Geckeis, Ch. Poinssot (eds.), Woodhead  
Publishing, 2012.

LEFÈVRE, G.; PREOČANIN, T.; LÜTZENKIRCHEN, J.  
Attenuated Total Reflection - Infrared Spectroscopy Applied to the Study of Mineral - Aqueous  
Electrolyte Solution Interfaces: A General Overview and a Case Study.  
Infrared Spectroscopy - Materials Science, Engineering and Technology. T. Theophanides (editor),  
InTech, 2012, pp. 97-122.

## Reports

ALTMAIER, M.; BUBE, C.; KIENZLER, B.; METZ, V.; REED, D.T. (EDS.)  
Proceedings of the International Workshops ABC-Salt(II) and HiTAC 2011.  
KIT Scientific Reports 7625 (2012).

GECKEIS, H.; STUMPF, T. (EDS)  
Annual Report 2011: Institute for Nuclear Waste Disposal.  
KIT Scientific Reports 7617, (2012).

KIENZLER, B.; ALTMAIER, M.; BUBE, C.; METZ, V.  
Radionuclide Source Term for HLW Glass, Spent Nuclear Fuel, and Compacted Hulls and End Pieces  
(CSD-C Waste).  
KIT Scientific Reports 7624, Karlsruhe, ISBN 978-3-86644-907-7, S. 92, (2012).

KIENZLER, B.; SCHLIEKER, M.; HILPP, S.; FINCK, N.; GEYER, F.; HECK, S.; KISELY, T.; LAGOS, M.; METZ,  
V.; MOISEI-RABUNG, S.; PLASCHKE, M.; SEITHER, A.; SOBALLA, E.  
Sorptionseigenschaften von technischen Sorel-basierten Baustoffen. Ergebnisse der Vorversuche.  
Rahmenvertrag SCHACHTANLAGE ASSE II. Studien zur Entwicklung des geochemischen Milieus und  
den daraus resultierenden Radionuklidkonzentrationen“.  
PSP-Nr. 9A 242; BfS Bst. Nr.: 8759-0, (2012).

METZ, V.; BOHNERT, E.; BUBE, C.; GONZÁLEZ-ROBLES, E.; KIENZLER, B.; LOIDA, A.; MÜLLER, N.;  
CARBOL, P.; GLATZ, J. P.; NASYROW, R.; PAPAIOANNOU, D.; RONDINELLA, V. V.; SERRANO PURROY,  
D.; WEGEN, D.; CURTIUS, H.; KLINKENBERG, H.; GÜNTHER-LEOPOLD, I.; CACHOIR, C.; LEMMENS, K.;  
MENNECART, T.; VANDENBORRE, J.; CASAS, I.; CLARENS, F.; DE PABLO, J.; SUREDA PASTOR, R.;  
HÓZER, Z.; SLONSKI, E.; EKEROTH, E.; ROTH, O.  
Fast / Instant Release of Safety Relevant Radionuclides from Spent Nuclear Fuel (FIRST-Nuclides):  
Characterisation of spent nuclear fuel samples to be used in FIRST-Nuclides – relevance of samples  
for the Safety Case.  
Deliverable No 1.1. European Commission, Brussels (2012).

RABUNG, T.; MOLINERO, J.; GARCIA, D.; MONTOYA V. (EDS.)  
1st Workshop Proceedings of the Collaborative Project “Crystalline Rock Retention Processes” (7th  
EC FP CP CROCK).  
KIT Scientific Report 7629 (2012).

WOLF, J.; BEHLAU, J.; BEUTH, T.; BRACKE, G.; BUBE, C.; BUHMANN, D.; DRESBACH, C.; HAMMER, J.;  
KELLER, S.; KIENZLER, B.; KLINGE, H.; KRONE, J.; LOMMERZHEIM, A.; METZ, V.; MÖNIG, J.;  
MRUGALLA, S.; POPP, T.; RÜBEL, A.; WEBER, J.R.  
Erstellung eines FEP-Kataloges für die vorläufige Sicherheitsanalyse Gorleben. Bericht für  
Arbeitspaket 7 „FEP-Katalog“.  
GRS, Gesellschaft für Anlagen- und Reaktorsicherheit, GRS-293, (2012).

## **Internal reports**

LOIDA, A.

Rückblick auf das INE-Vorhaben „Verfestigung aktinidenhaltiger Abfälle in keramischer Matrix“.  
KIT-INE 003/12 (2012).

KIENZLER, B.; KUPCIK, T.; LÜTZENKIRCHEN, J.; METZ, V.; RABUNG, T.; SCHÄFER, T.

Abschätzung von Sorptionskoeffizienten im Deckgebirge der Schachanlage Asse II - Ableitung von oberen und unteren Grenzwerten der Sorptionskoeffizienten für nicht untersuchte Nuklide.  
KIT-INE 05/2012, 38 S, (2012).

## Reports and Proceedings of Workshops and Conferences

ALTMAIER, M.

Investigation of radionuclide solubility and speciation in concentrated salt brine solutions.  
Book of Abstracts, 15th International Symposium on Solubility Phenomena and Related equilibrium Processes, Xining, China, July 23-27, 2012.

ALTMAIER, M.

Aquatic Chemistry and Thermodynamics of Actinides.  
Book of Abstracts, ATALANTE 2012 – Nuclear Chemistry for Sustainable Fuel Cycles, September 2-7 2012, Montpellier, France.

ALTMAIER, M.

“THEREDA Database Project”  
Book of Abstracts, International Conference on Nuclear and Radiochemistry (NRC-8), Como, Italy, 2012 Sep 16-21.

ALTMAIER, M.; GAONA, X.; FELLHAUER, D.; BUCKAU, G.

Recosy Intercomparison Exercise on Redox Determination Methods – Final Report on main Conclusions and Recommendations.  
Abstract in the Proceedings of the Plutonium Futures “The Science” 2012, Cambridge (UK), July 15-20, 2012.

ALTMAIER, M.; KIENZLER, B.; DURO, L.; GRIVE, M.; MONTOYA, V. (EDS.)

4th Annual Workshop Proceedings of the Collaborative Project “Redox Phenomena Controlling Systems” (7th EC FP CP RECOSY).  
KIT Scientific Report 7625, 2012, Karlsruhe Institute of Technology, KIT Scientific Publishing, Karlsruhe, Germany.

ALTMAIER, M.; METZ, V.; BUBE, C.; SKERENCAK, A.; KIENZLER, B. (EDS.)

Proceedings of the ABC-Salt(II) and HiTAC Workshops.  
KIT Scientific Report 7625, 2012, Karlsruhe Institute of Technology, KIT Scientific Publishing, Karlsruhe, Germany.

BANIK, N. L.; MARQUARDT, C.; SCHILD, D.; ROTHE, J.; GECKEIS, H.; SCHÄFER, T.

The behaviour of neptunium and plutonium in the Opalinus clay / Callovo Oxfordian argillite – pore water system, Plutonium Futures, 15-20 July 2012, University of Cambridge, UK, Book of Abstracts, p. 87.

BANIK, N. L.; WALZ, S.; MARQUARDT, C. M.; PANAK, P.; SKERENCAK, A.

Complexation studies of Np(V)-Lactate at elevated temperature.  
Proceedings of the International Workshop ABC-Salt (II) and HiTAC 2011. Ed.: M. Altmaier Verlag: KIT Scientific Publishing, Karlsruhe (2012) KIT Scientific reports 7625.

BECKER, F.; BLUNCK, CH.; FIGUEIRA, C.; ESTEVES, B.; DI MARIA, S.; PAULO, G.; SANTOS, J.; TELES, P.; VAZ, P.

Radiation exposure of medical staff: application of hand phantoms in experiments and simulations.  
Proceedings / the first international conference on radiation and dosimetry in various fields of research (RAD 2012) - ISBN 978-86-6125-063-7.

BOUBY, M.; GECKEIS, H.; BUCKAU, G.  
Humic acid agglomeration study as a function of ionic strength and metal ion loading.  
Proceedings of the International Workshop ABC-Salt (II) and HiTAC 2011. Ed.: M. Altmaier  
Verlag: KIT Scientific Publishing, Karlsruhe (2012) KIT Scientific reports 7625.

BECKER, F., ZHANG, G., URBAN, M.  
Determination of the Radiation Field in an Interim Storage Facility  
Online Publication on IRPA13 Downloads Page:  
<http://www.irpa13glasgow.com/information/downloads/>.

BEELE, B. B.; MÜLLICH, U.; GEIST, A.; PANAK, P. J.  
Partitioning and Transmutation - BTP-Type N-Donor ligands in the SANEX Process, Proceedings of the  
7<sup>th</sup> European Summer School on Supramolecular, intermolecular, interaggregate interactions and  
separation chemistry, Eds.: K. E. German, L. B. Boinovich, A. Yu. Tsivadze, Verlag: Publishing House ID  
Granica, Moscow (2012).

BELL, K.; CARPENTIER, C.; CARROTT, M.; GEIST, A.; GREGSON, C.; HÉRÈS, X.; MAGNUSSON, D.;  
MALMBECK, R.; MODOLO, G.; MÜLLICH, U.; SYPULA, M.; TAYLOR, R.; WILDEN, A.  
Towards a new GANEX 2nd cycle process for the co-separation of TRU.  
Nuclear Fuel Cycle Conference 2012, Manchester, UK, 23.–25. 4. 2012.

BOURG, S.; BOUVET, S.; CASSAYRE, L.; DE ANGELIS, G.; EKBERG, C.; ESPARTERO, A. G.; GEIST, A.;  
GUILBAUD, P.; HARRISON, M.; MALMBECK, R.; MODOLO, G.; OUVRIER, N.; RHODES, C.; TAYLOR, R.  
ACSEPT – reprocessing for advanced fuel cycles.  
Nuclear Fuel Cycle Conference 2012, Manchester, UK, 23.–25. 4. 2012.

BUBE, C.; ALTMAIER, M.; METZ, V.; NECK, V.; SCHILD, D.; KIENZLER, B.  
Thermodynamics of long-term metastable magnesium (chloro) hydroxo carbonates at 25 °C.  
Proceedings of the International Workshops ABC-Salt(II) and HiTAC 2011 (eds. M. Altmaier et al.). KIT  
Scientific Report 7625, Karlsruhe, (2012) 31-32.

BUBE, C.; METZ, V.; SCHILD, D.; BOHNERT, E.; KIENZLER, B.  
Long-term cement-corrosion in chloride-rich solutions - a thermodynamic interpretation. *European  
Geosciences Union General Assembly 2012 (EGU2012)*, 22-27 April 2012, Vienna, Austria.

BUBE, C.; ALTMAIER, M.; METZ, V.; SCHILD, D.; KIENZLER, B.; NECK, V.  
Thermodynamics of magnesium carbonate phases in dilute to concentrated magnesium chloride  
solutions at 25°C. 15th International Symposium on Solubility Phenomena and Related Equilibrium  
Processes, Qinghai Institute of Salt Lakes, Xining (PR China), July 23-27, 2012, Book of Abstracts.

CHAGNEAU, A.; CLARET, F.; MADÉ, B.; TUCKERMANN, J.; ENZMANN, F.; SCHÄFER, T.  
Applicability of a geometrical model coupled to computed tomography to characterize the transport  
properties of porous materials: comparison with through diffusion experiments.  
5th International Meeting “Clays in Natural and Engineered Barriers for Radioactive Waste  
Confinement” Montpellier - October 22-25, 2012, Book of Abstracts, p. 865-866.

DARBHA, G. K.; FISCHER, C.; LUETZENKIRCHEN, J.; SCHÄFER, T.  
Understanding the deposition behavior of colloids at mineral and rock surfaces as a function of  
surface roughness and topography.  
GeoHannover 2012 „GeoRohstoffe für das 21. Jahrhundert“ / “GeoResources for the 21st Century”,  
1–3. Oktober 2012, Leibniz Universität Hannover, Germany, Book of Abstracts.

DENECKE, M. A.; PETERSMANN, T.; MARSAC, R.; DARDENNE, K.; VITOVA, T.; PRÜßMANN, T.; BORCHERT, M.; BÖSENBERG, U.; FALKENBERG, G.; WELLENREUTHER, G.  
XANES characterization of UO<sub>2</sub>/Mo(Pd) thin films as models for ε-particles in spent nuclear fuel  
XAFS-XV Conference Proceedings, Beijing, PR China, July 22-28, 2012 (in print).

DENECKE, M. A.; PETERSMANN, T.; DE NOLF, W.; KLINKENBERG, M.; NEUMEIER, S.; VILLANOVA, J.; PRÜßMANN, T.  
Characterization of UO<sub>2</sub>/Mo(Pd) thin films as models for ε-particles in spent nuclear fuel using XANES, XRF and tomographic techniques  
XAFS-XV Conference Proceedings, Beijing, PR China, July 22-28, 2012 (in print).

FELLHAUER, D.; ALTMAIER, M.; NECK, V.; RUNKE, J.; LÜTZENKIRCHEN, J.; GAONA, X.; FANGHÄNEL, TH.  
Solubility and speciation of Np in dilute to concentrated CaCl<sub>2</sub> solutions under different redox conditions.  
Proceedings of the International Workshop ABC-Salt (II) and HiTAC 2011. Ed.: M. Altmaier Verlag: KIT Scientific Publishing, Karlsruhe (2012) KIT Scientific reports 7625, 49-50.

FELLHAUER, D.; ALTMAIER, M.; ROTHE, J.; NECK, V.; RUNKE, J.; FANGHÄNEL, TH.  
Speciation and Solubility of Np(V) in alkaline CaCl<sub>2</sub> Solutions.  
Abstract in the Proceedings of the Plutonium Futures "The Science" 2012, Cambridge (UK), July 15-20, 2012.

FINCK, N.; DARDENNE, K.  
Am(III) coprecipitation with and adsorption to hectorite: powder and polarized XAS insights  
ANKA Experimental Report, Annual Report 2010-2011 (2012) 345 – 346.

GAONA, X.; ALTMAIER, M.; PETROV, V.; FELLHAUER, D.; TITS, J.; WIELAND, E.; DARDENNE, K.; FANGHÄNEL, TH.  
Aqueous speciation of Np(V/VI) in hyperalkaline systems.  
ANKA Experimental Report, Annual Report 2010-2011 (2012) 304 -306.

GAONA, X.; FELLHAUER, D.; DARDENNE, K.; ROTHE, J.; ALTMAIER, M.  
Redox chemistry of Np(V/VI) under hyperalkaline conditions: aqueous speciation, solubility and chemical analogies with Pu.  
Proceedings of the International Workshop ABC-Salt (II) and HiTAC 2011. Ed.: M. Altmaier Verlag: KIT Scientific Publishing, Karlsruhe (2012) KIT Scientific reports 7625 43-44.

GAONA, X.; FELLHAUER, D.; ROTHE, J.; ALTMAIER, M.  
Investigations on Np(VI) in alkaline NaCl solutions: aqueous chemistry and solid phase characterization  
S&T contribution in the ReCosy 4th annual workshop, Karlsruhe (Germany), January 23-27, 2012.

GAONA, X.; FELLHAUER, D.; ROTHE, J.; ALTMAIER, M.  
Solubility of Np(VI) in dilute to concentrated alkaline NaCl solutions  
Abstract in Proceedings of the ReCosy 4th annual workshop, Karlsruhe (Germany), January 23-27, 2012.

GAONA, X.; FELLHAUER, D.; ROTHE, J.; FANGHÄNEL, T.; ALTMAIER, M.  
Thermodynamics of Np(VI) in alkaline NaCl solutions – comparison with Pu(VI).  
Abstract in the Proceedings of the Plutonium Futures "The Science" 2012, Cambridge (UK), July 15-20, 2012.

GECKEIS, H.; STUMPF, T. (EDS.)  
Institute for Nuclear Waste Disposal - Annual Report 2011.  
KIT Scientific Reports 7617.

GONZÁLEZ-ROBLES, E.; LOIDA, A.; MÜLLER, N.; SCHILD, D.; METZ, V.; BOHNERT, E.; KIENZLER, B.  
Corrosion of spent nuclear fuel segment in presence of Fe (II)/Fe(III) oxide.  
Book of Abstracts (CD-ROM) European Materials Research Society, E-MRS 2012 Spring Meeting,  
Strasbourg (France) 14-18 May 2012.

GRANGEON, S.; TOURNASSAT, C.; LEROUGE, C.; GIFFAUT, E.; SCHÄFER, T.  
Prediction of Nickel mobility in a clayey formation requires accurate knowledge of the mineralogical  
assemblage.  
5th International Meeting "Clays in Natural and Engineered Barriers for Radioactive Waste  
Confinement" Montpellier - October 22-25, 2012, Book of Abstracts, p. 891-892.

GRÜNEWALD, W.; PLASCHKE, M.; ROTH, G.; TOBIE, W.; WEISS, K. H.; WEISENBURGER, S.;  
STOLLENWERK, A.; GAUTHIER, R.; EISSLER, A.  
Process control and glass product quality assessment applied in the VEK plant. GLOBAL 2011: Toward  
and Over the Fukushima Daiichi Accident, Makuhari Messe, Chiba, J, December 11-16, 2011 Proc.on  
CD-ROM Paper 392621 Tokyo : Atomic Energy Society of Japan, 2012.

HAMPEL, A.; SALZER, K.; GÜNTHER, R.-M.; MINKLEY, W.; PUDEWILLS, A.; LEUGER, B.; ZAPF D.;  
ROKAHR, R.; HERCHEN, K.; WOLTERS, R.; DÜSTERLOH, U.  
Joint Projects on the Comparison of Constitutive Models for the Mechanical Behavior of Rock Salt - II.  
Overview of the models and results of 3-D benchmark calculations.  
In: Proc. of the 7th Conference on Mechanical Behavior of Salt, P. Bérest, M. Ghoreychi, F. Hadj-  
Hassen & M. Tijani (Hrsg.): Proc. 7th Conf. on the Mechanical Behavior of Salt, Paris, 16.-19. April  
2012. CRC Press A Balkema, Leiden, NL, ISBN 978-0-415-62122-9, 2012, pp 231-240.

HEBERLING, F.; ENG, P.; LÜTZENKIRCHEN, J.; STUBBS, J.; SCHÄFER, T.; GECKEIS, H.  
Ion specific effects at the calcite(104) - water interface. Goldschmidt 2012, June 24-29, 2012,  
Montréal, Canada, Session 08g "Structure and dynamics of ions and water at mineral-water  
interfaces: insights from experimental and computational studies", Book of Abstracts.

HEBERLING, F.; ROTHE, J.; DARDENNE, K.; HECK, S.  
Selenium (IV) and (VI) interactions with calcite.  
ANKA Experimental Report, Annual Report 2010-2011 (2012) 333–335.

HEIDE, B.  
Dose Enhancement in Thin Layers of Skin-Equivalent Material Caused by Photons and Electrons: A  
Monte-Carlo Study Using MCNP. Poster, 13th International Congress of the International Radiation  
Protection Association (IRPA), Glasgow, United Kingdom, 13–18 May 2012, No. 2429500.

HINZ, K.; ALTMAIER, M.; RABUNG, T.; GECKEIS, H.  
Complexation of Nd(III)/Cm(III) with borate in dilute to concentrated alkaline NaCl and CaCl<sub>2</sub>  
solutions.  
Proceedings of the International Workshop ABC-Salt (II) and HiTAC 2011. Ed.: M. Altmaier  
Verlag: KIT Scientific Publishing, Karlsruhe (2012) KIT Scientific reports 7625.

HINZ, K.; ALTMAIER, M.; RABUNG, T.; RICHMANN, M.; BORKOWSKI, M.; REED, D.; GECKEIS, H.  
Solubility and Speciation of Cm(III) and Nd(III) in borate rich NaCl and CaCl<sub>2</sub> solutions.  
Plutonium Futures 2012, Cambridge, England; Book of Abstracts.

HOLLIDAY, K.; CHAGNEAU, A.; SCHMIDT, M.; CLARET, F.; SCHÄFER, T.; STUMPF, T.  
Discriminating factors affecting incorporation: Comparison of the fate of Eu<sup>3+</sup>/Cm<sup>3+</sup> in the Sr carbonate/sulfate system. Goldschmidt 2012, June 24-29, 2012, Montréal, Canada, Session 08c  
*“Structural incorporation of heavy metals/ radionuclides into mineral phases in aqueous environment”*, Book of Abstracts.

HUBER, F.; HECK, S.; HÖSS, P.; TRUCHE, L.; BOUBY, M.; BRENDLÉ, J.; SCHÄFER, T.  
The use of synthetic Zn-/Ni-labeled montmorillonite colloids as a natural bentonite marker.  
5th International Meeting *“Clays in Natural and Engineered Barriers for Radioactive Waste Confinement”* Montpellier - October 22-25, 2012, Book of Abstracts, p. 838-839.

HUBER, F.; SCHILD, D.; VITOVA, T.; ROTHE, J.; KIRSCH, R.; SCHÄFER, T.  
U removal kinetics in the presence of magnetite and maghemite nanoparticles.  
4th Annual Workshop Proceedings, 7th EC FP Recosy CP.

KIENZLER, B.; METZ, V.; MONTOYA, V.  
Fast / Instant Release of Safety Relevant Radionuclides from Spent Nuclear Fuel (FIRST-Nuclides).  
Proceedings of the International Workshop ABC-Salt (II) and HiTAC 2011. Ed.: M. Altmaier et al.  
KIT Scientific Publishing, Karlsruhe (2012) KIT Scientific reports 7625, pp. 67-68.

KIRSCH, R.; FELLHAUER, D.; ALTMAIER, M.; CHARLET, L.; FANGHÄNEL, TH.; SCHEINOST, A. C.  
Plutonium redox chemistry under anoxic conditions in the presence of iron(II) bearing minerals.  
Goldschmidt 2012, Montréal (Canada), June 24-29, 2012.

KOBAYASHI, T.; YALCINTAS, E.; ALTMAIER, M.  
Solubility of TcO<sub>2</sub>(s)·xH<sub>2</sub>O in dilute to concentrated NaCl, CaCl<sub>2</sub>, and BaCl<sub>2</sub> solutions.  
Proceedings of ABC-Salt II workshop *“Actinide Brine Chemistry in a Salt-Based Repository”*, Karlsruhe (Germany), November 7-8, 2011. KIT Scientific Report 7625, 2012, Karlsruhe Institute of Technology, KIT Scientific Publishing, Karlsruhe, Germany.

KLEIN, W.  
Fehlerquellen in der internen Dosimetrie – Analyse biokinetischer Modelle, Abschlussbericht  
Verbundprojekt Strahlung und Umwelt, Radionuklide in der Umwelt, ihr Transport in Nahrungsketten  
zum und im Menschen, March, 2012.

KUPCIK, T.; KERN, R.; RABUNG, T.; EIDNER, S.; KUMKE, M.; SCHÄFER, T.  
Sr<sup>2+</sup>/Eu<sup>3+</sup> - illite interaction: sorption and diffusion studies.  
5th International Meeting *“Clays in Natural and Engineered Barriers for Radioactive Waste Confinement”* Montpellier - October 22-25, 2012, Book of Abstracts, p. 62-63.

LI, B.; DARDENNE, K.; VITOVA, T.; ROTHER, J.; FOERSTENDORF, N.; RAFF, J.  
P and S k-edge XANES investigation of U(VI) complexes with several organic model compounds  
ANKA Experimental Report, Annual Report 2010-2011 (2012) 379.

LINDQVIST-REIS, P.; KLENZE, R.; FANGHÄNEL, TH.  
Octa- and nonahydrated Cm(III) in aqueous solution from 20 to 200 °C  
Proceedings of the International Workshop ABC-Salt (II) and HiTAC 2011 (eds. M. Altmaier et al.).  
KIT Scientific Reports 7625, Karlsruhe, (2012) pp. 169-170.

LINDQVIST-REIS, P.; KLENZE, R., SCHIMMELPFENNIG, B.  
Spectroscopic evidence of ion-association in aqueous  $\text{Ln}^{3+}$  and  $\text{An}^{3+}$  perchlorate solutions at low water activity  
Proceedings of the International Workshop ABC-Salt (II) and HiTAC 2011 (eds. M. Altmaier et al.).  
KIT Scientific Reports 7625, Karlsruhe, (2012) pp. 95-96.

LÖBLE, M.; VITOVA, T.; BRENEBACH, B.; ROTHE, J.; DARDENNE, K.; DENECKE, M. A.; BREHER, F.  
New insights in electronic properties of f-element coordination compounds  
ANKA Experimental Report, Annual Report 2010-2011 (2012) 337 – 338.

LÖBLE, M.; VITOVA, T.; BRENEBACH, B.; ROTHE, J.; DARDENNE, K.; DENECKE, M. A.; BREHER, F.  
P and S K edge XANES investigations of lanthanide complexes consisting of a  $\kappa^6\text{N}$ -donor ligand with podand topology.  
ANKA Experimental Report, Annual Report 2010-2011 (2012) 307 -309.

MARQUARDT, C.M. (ED.)  
Interaction and Transport of Actinides in Natural Clay Rock with Consideration of Humic Substances and Clay Organic Compounds, Executive Summary of a BMWi joint project, KIT-Scientific Report, in preparation (2012).

MARZOCCHI, O.; BREUSTEDT, B.; MOSTACCI, D.; URBAN, M.  
A New HPGE-Detector Based Body Counter Capable of Detecting Also Low Energy Emitters  
Strahlenschutz Praxis, 18(1), 42-47, 2012.

METZ, V.; KIENZLER, B.; MONTOYA, V.  
EURATOM FP7 Collaborative Project FIRST-Nuclides.  
European Materials Research Society E-MRS 2012 Spring Meeting, 14.-18. May 2012, Strasbourg, France, Book of Abstracts (CD-ROM).

METZ, V.; BUBE, C.; SCHILD, D.; LAGOS, M.; BOHNERT, E.; GARBEV, K.; ALTMAIER, M.; KIENZLER, B.  
Interactions of U(VI) with cement alteration products at high ionic strength.  
Proceedings of the International Workshops ABC-Salt(II) and HiTAC 2011 (eds. M. Altmaier et al.).  
KIT Scientific Reports 7625, Karlsruhe, (2012) pp. 51-52.

NORRFORS, K. K.; BOUBY, M.; WOLD, S.; SCHÄFER, T.; GECKEIS, H.  
Influence of montmorillonite colloid size heterogeneity on their stability and radionuclide sorption/desorption properties.  
5th International Meeting "Clays in Natural and Engineered Barriers for Radioactive Waste Confinement" Montpellier - October 22-25, 2012, Book of Abstracts, p. 840-841.

NOSECK, U.; FLÜGGE, J.; SCHÄFER, T.; BLECHSCHMIDT, I.  
Impact of bentonite colloids on radionuclide transport in fractured systems – results from field experiments and modeling.  
EUROSAFE Forum "Towards Enhanced Robustness in Nuclear Safety", Brussels, 5<sup>th</sup> and 6<sup>th</sup> November 2012, Book of Abstracts, 12 pages.

PETROV, V. G.; DARDENNE, K.; GAONA, X.; FELLHAUER, D.; KALMYKOV, S. N.; ALTMAIER, M.  
Solubility limiting Np(V) solid phases in NaCl solutions  
ANKA Experimental Report, Annual Report 2012.

PETROV, V.G.; GAONA, X.; FELLHAUER, D.; DARDENNE, K.; KALMYKOV, S. N.; ZADORIN, A. A.;  
ALTMAIER, M.  
Pentavalent neptunium solubility and sorption behaviour in solutions of different ionic strengths.  
7th Russian Conference on Radiochemistry "Radiochemistry-2012", October 15-19, 2012.

PETROV, V.G.; GAONA, X.; FELLHAUER, D.; DARDENNE, K.; KALMYKOV, S.N.; ALTMAIER, M.  
Pentavalent neptunium solubility and solid phase transformation in solutions of different ionic  
strengths.  
ReCosy 4th Annual Workshop, January, 2012, Germany.

PETROV, V.G.; GAONA, X.; FELLHAUER, D.; DARDENNE, K.; KALMYKOV, S. N.; ZADORIN, A. A.;  
ALTMAIER, M.  
Np(V) solubility and sorption onto magnetite in aqueous NaCl solutions of different ionic strengths. "  
"Pu Futures: The Science 2012", Cambridge (UK), July 15-20, 2012.

PETROV, V. G.; GAONA, X.; FELLHAUER, D.; DARDENNE, K.; KALMYKOV, S. N.; ALTMAIER, M.  
Pentavalent Neptunium Solubility and Solid Phase Transformation at high ionic strengths.  
Proceedings of the International Workshop ABC-Salt (II) and HiTAC 2011.  
Ed.: M. Altmaier Verlag: KIT Scientific Publishing, Karlsruhe, KIT Scientific reports 7625 (2012).

PETROV, V. G.; ROTHE, J.; DARDENNE, K.; GAONA, X.; FELLHAUER, D.; KALMYKOV, S. N.;  
ALTMAIER, M.  
Solid phase transformation of Np(V) hydroxide in NaCl solutions  
ANKA Experimental Report, Annual Report 2010-2011 (2012) 343–344.

PLASCHKE, M.; ROTHE, J.; SCHÄFER, T.; DARDENNE, K.; DENECKE, M.A.; GECKEIS, H.  
Soft X-Ray Spectromicroscopy of Natural Organics affecting Actinide Mobility – an Overview.  
Eurosoil 2012, Bari, Italy, 2-6 July 2012, Abstract on CD-ROM, S04.07-5 217.

PÖLZ, S.; SCHNEIDER, T.; HEGENBART, L.; URBAN, M.; GECKEIS, H.  
Quantification of the effect of respiratory motion on efficiency calibration for internal dosimetry.  
The 13th International Congress of the International Radiation Protection Association. Glasgow,  
Scotland, May 13-18, 2012.

PUDEWILLS, A.  
Numerical Simulation of Coupled Thermo- Hydro- Mechanical Processes in Rock Salt, In Proc. of  
Mechanical Behavior of Salt VII, Paris, France, 16-19 April 2012, P. Berest, M. Ghoreychi, F.Hadj-  
Hassen& M.Tijani (eds), CRC Press A Balkema, Leiden, NL, ISBN 978-0-415-62122-9, 2012, pp. 115-  
122.

PUDEWILLS, A.  
Simulation of Long-term Behaviour of an Underground Structure in Rock Salt,  
The Eighth Int. Conf. on Engineering Computational Technology, 4-7 Sep, Dubrovnik, Croatia, Civil-  
Comp Press, Stirlingshire, UK, 2012, pp.110 and USB-Stick ISBN 978-1-905088-55-3,  
<http://www.civil-comp.com/conf/ect2012.htm> .

RABUNG, TH.; BAUER, A.; CLARET, F.; SCHÄFER, T.; BUCKAU, G.; FANGHÄNEL, TH.  
Influence of temperature on sorption of europium onto smectite: the role of organic contaminants  
International workshop on High Temperature Aqueous Chemistry – HITAC, Karlsruhe, 9<sup>th</sup> November  
2011, KIT Scientific Publishing 2012.

RABUNG, TH.; SCHNURR, A.; PETROV, V., LÜTZENKIRCHEN, J., GECKEIS, H.  
Sorption processes under high ionic strength conditions  
ABC-Salt Proceedings, KIT Scientific Publishing 2012.

ROBINET, J.C.; MICHAU, N.; SCHÄFER, T.  
Imaging techniques in clay Sciences: A key tool to go a step further. 5th International Meeting "Clays in Natural and Engineered Barriers for Radioactive Waste Confinement" Montpellier - October 22-25, 2012, Book of Abstracts, p. 49-50.

ROJO, H.; GAONA, H.; RABUNG, TH.; GARCIA, M.; MISSANA, T.; ALTMAIER, M.  
Complexation of Nd(III)/Cm(III) and Np(IV) with Gluconate in dilute to concentrated alkaline NaCl and CaCl<sub>2</sub> solutions  
ABC-Salt Proceedings, KIT Scientific Publishing 2012.

ROSENBERG, Y.O., METZ, V., GANOR, J.  
Thermodynamic properties of the Na-Ra-Cl-SO<sub>4</sub>-H<sub>2</sub>O system – estimating Pitzer parameters for RaCl<sub>2</sub>.  
Proceedings of the International Workshops ABC-Salt(II) and HiTAC 2011 (eds. M. Altmaier et al.).  
KIT Scientific Reports 7625, Karlsruhe, (2012) p. 35-36.

ROSENBERG, Y. O.; METZ, V.; GANOR, J.  
Ra-Ba co-precipitation in a large scale evaporitic system.  
in Proceedings of the International Workshops ABC-Salt(II) and HiTAC 2011 (eds. M. Altmaier et al.).  
KIT Scientific Reports 7625, Karlsruhe, (2012) pp. 79-80.

ROTHMEIER, M.; PETROV, V.; RABUNG, T.; LÜTZENKIRCHEN, J.; FINCK, N.; ALTMAIER, M.  
Surface charging of (oxyhydr)oxide minerals to high ionic strength  
Proceedings of the International Workshop ABC-Salt (II) and HiTAC 2011. Ed.: M. Altmaier  
Verlag: KIT Scientific Publishing, Karlsruhe (2012) KIT Scientific reports 7625.

RUFF, C.M.; MÜLLICH, U.; GEIST, A.; PANAK, P.J.  
Neue Strategien in der Actinidenabtrennung – wasserlösliche Komplexbildner für den innovativen SANEX-Prozess.  
Energiewirtschaftliche Tagesfragen 62 (2012), 86–88.

SALZER, K.; GÜNTHER, R.-M.; MINKLEY, W.; POPP, T.; WIEDEMANN, M.; HAMPEL, A.; PUDEWILLS, A.; LEUGER, B.; ZAPF, D.; ROKAHR, R.; HERCHEN, K.; WOLTERS, R.; DÜSTERLOH, U.  
Joint projects on the comparison of constitutive models – I. Overview of the projects, reference mine for 3-D benchmark calculations, in-situ measurements and laboratory tests.  
In: Proceedings of the 7th Conference on Mechanical Behavior of Salt, In Proc. of Mechanical Behavior of Salt VII, Paris, France, 16-19 April 2012, P. Berest, M. Ghoreychi, F.Hadj-Hassen& M.Tijani (eds), CRC Press A Balkema, Leiden, NL, ISBN 978-0-415-62122-9, 2012, pp. 221-230.

SCHÄFER, T.; STAGE, E.; BÜCHNER, S.; HUBER, F.; DRAKE, H.  
Characterization of new crystalline material for investigations within CP CROCK. In: Rabung, T., Molinero, J., García, D., and Montoya, V. (Eds.) 1st Workshop Proceedings of the Collaborative Project "Crystalline Rock Retention Processes" (7th EC FP CP CROCK), KIT Scientific Report 7629, p.63-72.

SCHMIDT, M.; FENTER, P.; LEE, S. S.; WILSON, R. E.; KNOPE, K. E.; SODERHOLM, L.  
Actinide Sorption at the Muscovite-Electrolyte Interface.  
Goldschmidt 2012, Montréal, QC, Canada, June 24 – 29, 2012.

SCHMIDT, M.; LEE, S. S.; WILSON, R. E.; KNOPE, K. E.; FENTER, P.; SODERHOLM, L.  
Actinide Sorption and Reactivity at the Muscovite-Aqueous Interface.  
Plutonium Futures 2012, Cambridge, UK, July 15 – 20, 2012.

SCHMIDT, M.; BOSBACH, D.; STUMPF, T.; WALTHER, C.  
Guest ion speciation in a homogeneous solid solution by polarisation-dependent TRIFS.  
1st European Mineralogical Conference, Frankfurt/Main, Germany, September 2- 6, 2012.

SCHMIDT, M.; LEE, S. S.; WILSON, R. E.; KNOPE, K. E.; FENTER, P.; SODERHOLM, L.  
X-ray Reflectivity Investigations on the Interfacial Reactivity of Actinides.  
Advanced Techniques in Actinide Spectroscopy Workshop, Helmholtz-Zentrum Dresden Rossendorf,  
Dresden, Germany, November 3–7, 2012.

SELLIN, P.; SUNDMAN, D.; BAILEY, L.; MISSANA, T.; SCHÄFER, T.; CERVINKA, R.; KOSKINEN, K.  
Bentonite erosion: effects on the long term performance of the engineered barrier and radionuclide  
transport- the BELBaR project.  
5th International Meeting *“Clays in Natural and Engineered Barriers for Radioactive Waste  
Confinement”* Montpellier - October 22-25, 2012, Book of Abstracts, p. 851-852.

SHARRAD, C.; GOFF, G.; MAY, I.; RUNDE, W.; BANIK, N. L.; BRENEBACH, B.; DARDENNE, K.;  
DENECKE, M. A.; MARQUARDT, C. M.  
U L3 edge XAFS investigation on U(VI) monomer species  
ANKA Experimental Report, Annual Report 2010-2011 (2012) 315-318.

SHARRAD, C.; GOFF, G.; MAY, I.; RUNDE, W.; BANIK, N. L.; BRENEBACH, B.; DARDENNE, K.;  
DENECKE, M. A.; MARQUARDT, C. M.  
U L3 edge XAFS investigation on U(VI) dimer species  
ANKA Experimental Report, Annual Report 2010-2011 (2012) 319-320.

SHARRAD, C.; GOFF, G.; MAY, I.; RUNDE, W.; BANIK, N. L.; BRENEBACH, B.; DARDENNE, K.;  
DENECKE, M. A.; MARQUARDT, C. M.  
Pu L3 edge XAFS investigation on Pu(IV) pentacarbonate species  
ANKA Experimental Report, Annual Report 2010-2011 (2012) 321-322.

STAGE, E.; HUBER, F.; SCHÄFER, T.  
Sorption/Desorption of  $^{137}\text{Cs(I)}$ ,  $^{152}\text{Eu(III)}$  and  $^{233}\text{U(VI)}$  onto new CROCK derived Äspö diorite - A Batch  
type study. In: Rabung, T., Molinero, J., García, D., and Montoya, V. (Eds.) 1st Workshop Proceedings  
of the Collaborative Project *“Crystalline Rock Retention Processes”* (7th EC FP CP CROCK), KIT  
Scientific Report 7629, p.53-62.

TOTSKIY, Y.; GECKEIS, H.; SCHÄFER, T.  
Sorption of Tc(VII) on Äspö Diorite (ÄD).  
In: (Rabung, T., Molinero, J., García, D., and Montoya, V. Eds.) 1<sup>st</sup> Workshop Proceedings of the  
Collaborative Project *“Crystalline Rock Retention Processes”* (7th EC FP CP CROCK) KIT Scientific  
Report 7629 (2012), pp. 97-106.

TOTSKIY, Y.; GECKEIS, H.; SCHÄFER, T.  
Sorption of Tc(VII) on crystalline rock material from Äspö (Sweden).  
Joint ITU-INE Research Fellow's Day, JRC-KIT, Karlsruhe, 22 June 2012, pp. 118-119.

TOTSKIY, Y.; STAGE, E.; GECKEIS, H.; SCHÄFER, T.; KALMYKOV, S.  
Sorption of Tc(VII), Cs(I), Eu(III), U(VI) and Am(III) on crystalline rock material from Äspö (Sweden) and Nizhnekansk massif (Russia).  
Proceedings of the 7th Russian Conference on Radiochemistry "Radiochemistry-2012", Dimitrovgrad, Russia, 15-19 October, 2012, p. 350.

VITOVA, T.; DARDENNE, K.; DENECKE, M. A.; ERNST, H.; ROTHE, J.  
The latest development and optimization of the high-resolution X-ray emission spectrometer at the INE-Beamline.  
ANKA Experimental Report, Annual Report 2010-2011 (2012) 326.

VITOVA, T.; HUBER, F.; ROTHE, J.; DARDENNE, K.; SCHÄFER, T.  
Interaction of uranium(VI) with synthetic magnetite nanoparticles.  
ANKA Experimental Report, Annual Report 2010-2011 (2012) 329-330.

VITOVA, T.; BUTORIN, S. M.; SEIBERT, A.; ROTHE, J.; DARDENNE, K.; VEGELIUS, J.; CACIUFFO, R.; DENECKE, M. A.  
High-resolution X-ray absorption spectroscopy study of plutonium dioxide in contact with water.  
ANKA Experimental Report, Annual Report 2010-2011 (2012) 394-395.

VITOVA, T.; CACIUFFO, R.; DENECKE, M. A.; HUBER, F.; PRÜSSMANN, T.; ROTHE, J.; SCHÄFER, T.; GECKEIS, H.  
Actinide speciation with high-energy resolution x-ray absorption spectroscopy and inelastic x-ray scattering.  
Atas workshop, Dresden, November 5-11, 2012.

VITOVA, T.; CACIUFFO, R.; DENECKE, M. A.; HUBER, F.; GÖTTLICHER, J.; KOSOG, B.; KVASHNINA, K.; MEYER, K.; PRÜßMANN, T.; ROTHE, J.; SCHÄFER, T.; GECKEIS, H.  
Actinide speciation with high-energy resolution X-ray absorption spectroscopy and inelastic X-ray scattering.  
XAFS-XV Conference Proceedings, Beijing, PR China, July 22-28, 2012 (in print).

WEGEN, D. H.; CARBOL, P.; SEIBERT, A.; GOUDER, T.; PETERSMANN, T.; PEHRMAN, R.; TRUMMER, M.; LOUSADA, C.; JONSSON, M.; LOIDA, A.; MÜLLER, N.; METZ, V.; BOHNERT, E.; KIENZLER, B.; CUI, D.; SPAHIU, K.; DOBREV, D.; ČERVINKA, R.; VOKÁL, A.  
Redox Reactions Affecting the Spent Fuel Source-Term. ReCosy WP6 Final Report. Contract No. FP7-212287 ReCosy, JRC Scientific and Policy Reports (2012).

WERSIN, P.; LÜTZENKIRCHEN, J.  
The influence of temperature on sorption: A preliminary assessment for Uranium(VI) sorption to bentonite.  
Proceedings of the International Workshop ABC-Salt (II) and HiTAC 2011. Ed.: M. Altmaier  
Verlag: KIT Scientific Publishing, Karlsruhe (2012) KIT Scientific reports 7625.

WILDEN, A.; SCHREINEMACHERS, C.; SADOWSKI, F.; GÜLLAND, S.; SYPULA, M.; MODOLO, G.; MAGNUSSON, D.; GEIST, A.; LEWIS, F. W.; HARWOOD, L. M.; HUDSON, M. J.  
Demonstration of a 1-cycle SANEX process for the selective recovery of trivalent actinides from PUREX raffinate using a CyMe4-BTBP/TODGA solvent.  
Nuclear Fuel Cycle Conference 2012, Manchester, UK, 23.-25. 4. 2012.

YALCINTAS, E.; KOBAYASHI, T.; ALTMAIER, M.; GECKEIS, H.  
Redox Behavior of the Tc(VII)/Tc(IV) Couple in Dilute to Concentrated NaCl Solutions.  
Proceedings of the International Workshop ABC-Salt (II) and HiTAC 2011. Ed.: M. Altmaier  
Verlag: KIT Scientific Publishing, Karlsruhe (2012) KIT Scientific reports 7625.

YALCINTAS, E.; KOBAYASHI, T.; ALTMAIER, M.; GECKEIS, H.  
Technetium redox chemistry in dilute to concentrated aqueous systems  
Book of Abstracts; International Conference on Nuclear and Radiochemistry (NRC-8), Como, Italy,  
2012 Sep 16-21.

## Invited oral presentations

ALTMAIER, M.

Investigation of radionuclide solubility and speciation in concentrated salt brine solutions.  
15th International Symposium on Solubility Phenomena and Related equilibrium Processes, Xining, China, July 23-27, 2012.

ALTMAIER, M.

Aquatic Chemistry and Thermodynamics of Actinides.  
ATALANTE 2012 – Nuclear Chemistry for Sustainable Fuel Cycles, September 2-7 2012, Montpellier, France.

ALTMAIER, M.

ReCosy (Redox Phenomena Controlling Systems).  
EURADISS; EURATOM disposal program dissemination workshop (October 25th-26th, 2012), Montpellier, France.

DARDENNE, K.

Introduction à la spectroscopie d'absorption des rayons X.  
First Workshop on „Surfaces et Nucléaire“ Méjannes-le-Clap, France 16-18 October 2012.

DENECKE, M. A.

Actinide and lanthanide Speciation with X-ray Spectroscopy: micro- to nano- and other dimensions.  
4th EuCheMS Chemistry Congress, 26-30 August 2012, Prague, Czech Republic (PLENARY).

DENECKE, M. A.

Highly resolved synchrotron-based investigations for investigations related to nuclear waste disposal.  
MRS Spring Meeting, San Francisco, 9.-13. April 2012.

GAONA, X.; FELLHAUER, D.; ALTMAIER, M.

Actinide speciation and thermodynamics in aqueous solutions.  
Speciation Seminar, Montpellier (France), May 29-31, 2012.

GECKEIS, H.

Actinide environmental behavior - role of nanoparticle formation.  
7th European summer school on supramolecular, intermolecular, interaggregate interactions and separation chemistry (ESSSIISC-2012), A.N. Frumkin Institute of physical chemistry and electrochemistry, Russian Academy of Sciences (IPCE RAS), Moscow, Russia, July 20-23, 2012.

GECKEIS, H.

Endlagerung radioaktiver Abfälle: Konzepte, Kontroversen, Konflikte, Konfusionen, Konstruktive Forschung?  
Festkolloquium zu Ehren von Prof. Dr. Rolf Michel, Institut für Radioökologie und Strahlenschutz, Leibniz Universität Hannover, 11.07.2012.

GECKEIS, H.

Einstieg in die Energiewende – Ausstieg aus der nuklearen Sicherheitsforschung?, Chancen der Energiewende.  
Jahrestagung des KIT-Zentrums Energie, 19. Juni 2012.

GECKEIS, H.

Das Problem der nuklearen Entsorgung aus der Sicht des Chemikers.

Seminar des Mainzer Jungchemiker Forums: Probleme der nuklearen Entsorgung und Lösungsansätze aus der Chemie und Physik, 26.04.2012.

GECKEIS, H.; GOMPPER, K.

Forschung zur Nuklearen Entsorgung am KIT.

Ministerium für Umwelt, Klima und Energiewirtschaft, Referat 36, Stuttgart, 19.04.2012.

GECKEIS, H.

Radionuclide reactions at the solid/liquid interface: all mechanisms understood?

Seminar talk, Nano-Science Center, Kobenhavns Universitet, 19.04.2012.

GECKEIS, H.; KIENZLER, B.; GOMPPER, K.

Geologische Endlagerung radioaktiver Abfälle - Tragfähiges Konzept oder Selbstbetrug?

Seminarvortrag, Universität Stuttgart, Institut für Kernenergetik und Energiesysteme, 07.02.2012.

GECKEIS, H.

Das Problem der nuklearen Entsorgung - aus der Sicht des Chemikers.

GDCH Jungchemikerforum, Uni Gießen, 07.02.2012.

GECKEIS, H.

Radionuclide reactions at the solid/liquid interface, Research activities at KIT-INE.

Seminaire, Institute of Earth Science (ISTerre-OSUG UMR 5275), University of Grenoble I, 17.01.2012.

GEIST, A.

Abtrennung von Actiniden aus bestrahlten Kernbrennstoffen.

TRAKULA Workshop: Radiochemistry of the Actinides, Mainz, 21.–23.05.2012.

GEIST, A.; BEELE, B. B.; BREMER, A.; DENECKE, M. A.; MÜLLICH, U.; PANAK, P. J.; ROTHE, J.; RUFF, C. M.

Actinide Separations Using N Donor Compounds.

ACTINET-13 Theoretical User Lab (ThUL), Karlsruhe, 26.–29.3.2012.

HUBER, F.; SCHILD, D.; VITOVA, T.; ROTHE, J.; KIRSCH, R.; SCHÄFER, T.

U removal kinetics in the presence of magnetite and maghemite nanoparticles.

4<sup>th</sup> Annual Workshop, 7<sup>th</sup> EC FP Recosy CP. (2012).

KADEN, P.

NMR at KIT-INE and ideas for G-NMR.

TU München, München, 21.09.2012.

KADEN, P.; ADAM, C.; BEELE, B. B.; MÜLLICH, U.; TRUMM, S.; GEIST, A.; PANAK, P. J.; DENECKE, M. A.

NMR-investigations on Paramagnetic Effects in  $(n\text{PrBTP})_3$  complexes of Lanthanides(III) and Americium(III).

School of Chemistry Energy Mini Symposium, Manchester, UK, 24.10.2012.

KIENZLER, B.; METZ, V.; VALLS, A.

Euratom 7<sup>th</sup> Framework Programme: Collaborative Project "Fast / Instant Release of Safety Relevant Radionuclides from Spent Nuclear Fuel" (FIRST-Nuclides).

EURADISS 2012, EURATOM disposal program dissemination workshop, 25<sup>th</sup>–26<sup>th</sup> October 2012, Montpellier, France.

LINDQVIST-REIS, P.; SKRIPKIN, M.; SCHIMMELPFENNIG, B.; KLENZE, R.; MINK, J.; POLLY, R.  
TRLFS studies of Cm<sup>3+</sup> aqua complexes in solution and in solid hydrates.  
Mendeleev 2012, Saint-Petersburg, Russia, April 3-6, 2012.

LÜTZENKIRCHEN, J.  
Bimodal behavior of some solid – electrolyte interfaces.  
ACS conference, Symposium 'Atmospheric and geochemical interfaces' organized by Dennis Hore and Franz Geiger, San Diego (USA), March, 2012.

LÜTZENKIRCHEN, J.  
Interactions de solutes et colloïdes avec des surfaces – relevance dans les études sur le stockage des déchets nucléaires.  
ENSCP, Paris (France) 26.04.2012.

LÜTZENKIRCHEN, J.  
Advanced concepts: CD-MUSIC  
FIMIN – Workshop, Modelling of surface reactions of ferric (hydr)oxides, Bayreuth (Germany), 8.–12. October 2012.

LÜTZENKIRCHEN, J.  
Surface complexation models - Towards high ionic strength.  
GRS, Braunschweig (Germany) 06.12.2012.

METZ, V.  
Ra-Ba precipitation in a large scale evaporitic system and in laboratory systems.  
Salt Club Workshop on Natural Analogues for Safety Cases of Repositories in Rock Salt,  
5. September 2012, Braunschweig.

PANAK, P. J.; RUFF, C. M.; MÜLLICH, U.; GEIST, A.  
A novel path in partitioning – Water-soluble BTP ligands for the innovative SANEX process.  
International Conference on Methods and Application of Radioanalytical Chemistry (MARX IX), March 25-30, Kailua-Kona, Hawaii, USA (2012).

POLLY, R.; SCHIMMELPFENNIG, B.; JANECEK, J.; FLOERSHEIMER, M.; RABUNG, T.; KUPCIK, T.; KLENZE, R.; NETZ, R. R.; GECKEIS, H.  
Theoretical investigation of the sorption of trivalent f-elements and the structure of hydrated water at the corundum surface.  
Conference title: Accurate Methods for Accurate Properties, June 4-6, 2012, Zurich, Switzerland.

RABUNG, T.; MOLINERO, J.; GARCIA, D.; MONTOYA, V.  
CROCK: Crystalline Rock Retention Processes, A 7<sup>th</sup> Framework Programme Collaborative Project (2011-2013).  
Euratom Disposal Programme Dissemination Workshop, 25.-26. October 2012, Montpellier, France.

SCHÄFER, T.  
Application of synchrotron techniques to resolve interfacial processes retarding pollutants.  
7<sup>th</sup> International Conference 'Interfaces Against Pollution' (IAP2012), 11th-14th June 2012, Nancy, France, invited by Laurent Michot.

SCHÄFER, T.  
Geochemische Aspekte der Hydrogeologie: Benötigen wir nanoskalige Informationen?  
TU München Berufungskommission W3 Professur „Hydrogeologie“, 11.1.2012.

SCHÄFER, T.

The Role of Natural Occurring Nanoparticles on Metal Mobility in the Environment.  
IWC-Seminar, 20.02.2012, München, Germany, invited by Reinhard Nießner.

SCHÄFER, T.

Monitoring of radionuclide transport and retardation behaviour – the CRR, CFM and LTD projects – IAEA Training course: “Monitoring in argillaceous and crystalline rocks in the context of repository development –The role and contribution of URL programmes”.  
15.-19. Oct. 2012, Mont Terri/Grimsel (CH), hosted by Nagra/Swisstopo.

SCHÄFER, T.

Radionuclide transport in crystalline formations: laboratory and field experiments.  
2<sup>nd</sup> Chinese-German Workshop on Radioactive Waste Disposal, Karlsruhe, Oct. 15-16, 2012.

SCHÄFER, T.

Vorschlag für ein Rundgespräch: Anthropogen induzierte geochemische Gradienten in niedrig-permeablen tiefengeologischen Formationen.

4. Sitzung der Senatskommission für Zukunftsaufgaben der Geowissenschaften der Deutschen Forschungsgemeinschaft (Geokommission) am 22./23. Oktober 2012 im Parkhotel Hitzacker.

SCHMIDT, M.; FENTER, P.; LEE, S. S.; WILSON, R. E.; KNOPE, K. E.; SODERHOLM, L.

Actinide Sorption at the Muscovite-Electrolyte Interface.

APS/CNM/EMC User Meeting, Argonne National Laboratory, Argonne, IL, USA, .May 7 – 10, 2012.

STEPPERT, M.; WALTHER, C.

Nano-Electrospray Massenspektrometrie: Eine direkte Speziationsmethode für Actinid-Ionen in Lösung.

IRS Institutsseminar, Loccum, 02.-03.02.2012.

STUMPF, T.

Solid Solutions: Spectroscopic Evidence.

Workshop “From atomistic calculations to thermodynamic modeling”, Frankfurt, Germany, February 19, 2013.

STUMPF, T.

ImmoRad Langzeitsicherheit durch Immobilisierung langlebiger Radionuklide; Erste Ergebnisse.

Projektstatusgespräch des BMBF 2012, Karlsruhe, Germany, November 14, 2012.

STUMPF, T.

Prozessverständnis auf molekularer Ebene ein wesentlicher Beitrag zur Endlagerforschung im Hinblick auf die Sicherheit von Mensch und Umwelt.

Gemeinsames Kolloquium des Helmholtz-Zentrums Dresden Rossendorf und der Technischen Universität Dresden, Dresden, Germany, July 23, 2012.

## Presentations at conferences and workshops

ADAM, C.; KADEN, P.; SCHIMMELPFENNIG, B.; GEIST, A.; PANAK, P. J.; DENECKE, M. A.  
NMR investigations on partitioning-relevant complexes of americium (III) nitrate and n-Propyl-BTP.  
ThUL Spring School 2012, Karlsruhe, 26.03.-30.03.2012.

ADAM, C.; GEIST, A.; PANAK, P. J.; DENECKE, M. A.; KADEN, P.;  
Evaluation of Different Strategies to Discriminate Covalent and Dipolar Metal-ligand Interactions in  
Trivalent Lanthanide and Actinide BTP-complexes by NMR Investigations.  
INE-ITU Research Fellows Day 2012, Karlsruhe, 22.06.2012.

ADAM, C.; KADEN, P.; GEIST, A.; DENECKE, M. A.; PANAK, P. J.  
Evaluation of different strategies to discriminate covalent and dipolar metal-ligand interactions in  
trivalent Lanthanide and Actinide BTP-complexes by NMR investigations.  
Euromar 2012, Dublin, Ireland, 01.-06.07.2012.

ADAM, C.; KADEN, P.; GEIST, A.; DENECKE, M. A.; PANAK, P. J.  
Evaluation of different strategies to discriminate covalent and dipolar metal-ligand interactions in  
trivalent Lanthanide and Actinide BTP-complexes by NMR investigations.  
ATALANTE 2012, Montpellier, Frankreich, 02.-07.09.2012.

ALTMAIER, M.  
"THEREDA Database Project".  
International Conference on Nuclear and Radiochemistry (NRC-8), Como, Italy, 2012 Sep 16-21.

ALTMAIER, M.; FELLHAUER, D.; GAONA, X.; KOBAYASHI, T.; NECK, V.; PETROV, V.  
Np and Tc redox processes and solubility in aqueous media.  
ReCoty 4th annual workshop, Karlsruhe (Germany), January 23-27, 2012.

ALTMAIER, M.; GAONA, X.; FELLHAUER, D.; BUCKAU, G.  
Recoty Intercomparison Exercise on Redox Determination Methods – Final Report on main  
Conclusions and Recommendations.  
ReCoty 4th Annual Workshop, Karlsruhe (Germany), January 23-27, 2012.

ALTMAIER, M.; GAONA, X.; FELLHAUER, D.; BUCKAU, G.  
Recoty Intercomparison Exercise on Redox Determination Methods – Final Report on main  
Conclusions and Recommendations.  
Plutonium Futures "The Science" 2012, Cambridge (UK), July 15-20, 2012.

BANIK, N. L.; MARSAC, R.; MARQUARDT, C. M.; SCHILD, D.; ROTHE, J.; LÜTZENKIRCHEN, J.; SCHÄFER,  
T.; GECKEIS, H.  
The behaviour of neptunium and plutonium in the Opalinus Clay / Callovo-Oxfordian argillite – pore  
water system.  
Plutonium Futures—The Science 2012, 15.-21. July, 2012, Cambridge, England.

BAUER, N.; PANAK, P. J.  
Interaction of Cm(III) with human serum transferrin studied by time-resolved laser fluorescence  
spectroscopy (TRLFS).  
NRC-8, EuCheMS International Conference on Nuclear and Radiochemistry, September 16-21, 2012,  
Como, Italy.

BECKER, F.; ZHANG, G.; URBAN, M.

Determination of the Radiation Field in an Interim Storage Facility.

13th International. Congress of the International Radiation Protection Association, 13-18 May 2012, Glasgow, Scotland.

BECKER, F.

Group Leader Presentations for EURADOS WG 12 European Medical ALARA Network - SG1: CT-Fluoroscopy staff dosimetry.

EURADOS Annual Meeting AM2012, Vienna, 6-10th Feb 2012.

BECKER, F.

Strahlenexposition des Personals bei der CT-Fluoroskopie: Einsatz des LPS-Handphantoms.

76. Sitzung des FS-Arbeitskreises Dosimetrie externer Strahlung (AKD) in der Landesstelle für Personendosimetrie und Strahlenschutz Ausbildung (LPS) in Berlin am 12. und 13. April 2012.

BECKER, F.; BLUNCK, C.; FIGUEIRA, C.; ESTEVES, B.; DI MARIA, S.; PAULO, G.; SANTOS, J.; TELES, P.; VAZ, P.

Radiation exposure of medical staff: application of hand phantoms in experiments and simulations.

The First International Conference on Radiation and Dosimetry in Various Fields of Research (RAD 2012), at the Faculty of Electronic Engineering in Niš, Serbia, from April 25th to 27th, 2012.

BECKER, F.; ZHANG, G.

Monte-Carlo-calculations for the determination of the radiation field in an interim storage facility.

12th International Conference on Radiation Shielding (ICRS-12) & 17th Topical Meeting of the Radiation Protection & Shielding Division of ANS (RPSD-2012), Nara Prefectural New Public Hall in Nara (Japan), 2nd to 7th Sept. 2012.

BECKER, F.; BLUNCK, C.; FIGUEIRA, C.; GÖPFERT, F.

Application of hand phantoms in simulations to determine the radiation exposure of medical staff.

Workshop on Computational Medical Physics September, 2, 2012 at Nara Prefectural New Public Hall, Nara, Japan.

BECKER, F.; ZHANG, G.

Monte-Carlo Simulationen zum Einsatz von Albedo-Dosimetern in einem Zwischenlager.

77. Sitzung des FS-Arbeitskreises Dosimetrie externer Strahlung (AKD), 20.9.2012, am KIT.

BECKER, F.

Group Leader Presentations for EURADOS WG 12 European Medical ALARA Network - SG1: CT-Fluoroscopy staff dosimetry.

WG12 meeting: Ruder Boskivich Institute, Zagreb, Croatia, 4-5 October 2012.

BEELE, B.

N-Donor ligands in the partitioning strategy.

Trilateral Cooperation, 7th European Summer School on Supramolecular, intermolecular, interaggregate interactions and separation chemistry, 20.-23.07.2012, Moscow, Russland.

BEELE, B. B.; MÜLLICH, U.; SCHWÖRER, F.; GEIST, A.; PANAK, P. J.

Systematic Modifications of BTP-type Ligands and Effects on the Separation of Trivalent Lanthanides and Actinides.

ATALANTE 2012 – Nuclear Chemistry for Sustainable Fuel Cycles, 02.-07.09.2012, Montpellier, Frankreich.

BEELE, B.; MÜLLICH, U.; SCHWÖRER, F.; GEIST, A.; PANAK, P. J.  
Separation of Trivalent Lanthanides and Actinides in Nitric Acid by Modified BTP-type Ligands).  
Joint ITU-INE Research Fellows' Day, 22.06.2012.

BEELE, B. B.; MÜLLICH, U.; SCHWÖRER, F.; GEIST, A.; PANAK, P. J.  
Characterization of BTP-Type Ligands with TRLFS and Liquid-liquid Extraction.  
Workshop AG Chemie und Energie Energietransformationen - Die Rolle der Chemie, 15.11.2012.

BELL, K.; CARPENTIER, C.; CARROTT, M.; GEIST, A.; GREGSON, C.; HÉRÈS, X.; MAGNUSSON, D.;  
MALMBECK, R.; MODOLO, G.; MÜLLICH, U.; SYPULA, M.; TAYLOR, R.; WILDEN, A.  
Towards a new GANEX 2<sup>nd</sup> cycle process for the co-separation of TRU.  
Nuclear Fuel Cycle Conference 2012, Manchester, UK, 23.–25. 4. 2012.

BLUNCK, C.; BECKER, F.; URBAN, M.  
Simulation of <sup>90</sup>Y Hand Exposure of Staff in Nuclear Medicine.  
Jahrestagung des Kit-Zentrums Energie, Karlsruhe 19.06.2012.

BOURG, S.; BOUVET, S.; CASSAYRE, L.; DE ANGELIS, G.; EKBERG, C.; ESPARTERO, A. G.; GEIST, A.;  
GUILBAUD, P.; HARRISON, M.; MALMBECK, R.; MODOLO, G.; OUVRIER, N.; RHODES, C.; TAYLOR, R.  
ACSEPT – reprocessing for advanced fuel cycles.  
Nuclear Fuel Cycle Conference 2012, Manchester, UK, 23.–25. 4. 2012.

BREMER, A.; GEIST, A.; PANAK, P. J.  
Complexation of Cm(III) with 2,6-bis(5-(2,2-dimethylpropyl)-1H-pyrazol-3-yl)pyridine (C5-BPP) studied  
by time-resolved laser fluorescence spectroscopy.  
NRC-8, EuCheMS International Conference on Nuclear and Radiochemistry, September 16-21, 2012,  
Como, Italy.

BREMER, A.; GEIST, A.; PANAK, P. J.  
Complexation of Cm(III) with the partitioning relevant ligand C5-BPP studied by TRLFS.  
Joint ITU-INE Research Fellows' Day, 22 June 2012, Karlsruhe.

BREMER, A.; GEIST, A.; PANAK, P. J.  
Complexation of Cm(III) with the partitioning relevant ligand C5-BPP studied by TRLFS.  
7th ESSSMIISC (Seventh European Summer School on Supramolecular, Intramolecular, Interaggregate  
Interactions and Separation Chemistry, July 20-23, 2012, Moscow, Russia.

BREUSTEDT, B.; BLANCHARDON, E.; BERARD, P.; GREMY, O.; GUISSANI, A.; LOPEZ, M. A.  
Modeling of DTPA decorporation therapy - still puzzling after all these years.  
13th Internat. Congress of the International Radiation Protection Association (IRPA 13), Glasgow, GB,  
May 13-18, 2012, Download unter (<http://www.irpa13glasgow.com/information/downloads/>), 2012.

BREUSTEDT, B.; MOHR, U.; MARZOCCHI, O.; BIEGARD, N.; CORDES, G.; FRANK, G.  
In-vivo Messungen inkorporierter Radionuklide nach der Reaktorkatastrophe in Fukushima.  
Jahrestagung Kerntechnik 2012, Stuttgart, 22.-24. Mai 2012.

BREUSTEDT, B.; ESCHNER, W.; NOSSKE, D.  
Wahre Dosis kommt von Innen – Rechenmodelle für die Interne Dosimetrie.  
Jahrestagung 2012 des Fachverbandes Strahlenschutz e.V., KIT Karlsruhe, 17.-20. September 2012.

BREUSTEDT, B.; MCCORD, S.; TOLMACHEV, S. Y.

Biokinetic modeling of chelation therapy for Am-241 – USTUR Case 0846.

57th Annual Meeting of the Health Physics Society, Sacramento, CA, July 22-26, 2012.

BUBE, C.; ALTMAIER, M.; METZ, V.; SCHILD, D.; KIENZLER, B.; NECK, V.

Thermodynamics of magnesium carbonate phases in dilute to concentrated magnesium chloride solutions at 25°C.

15th International Symposium on Solubility Phenomena and Related Equilibrium Processes, Qinghai Institute of Salt Lakes, Xining, China, July 2012.

BUBE, C.; METZ, V.; SCHILD, D.; BOHNERT, E.; KIENZLER, B.

Long-term cement-corrosion in chloride-rich solutions - a thermodynamic interpretation.

EGU General Assembly 2012, Vienna (Austria), April 23-27 2012.

BUBE, C.; DARDENNE, K.; DENECKE, M. A.; KIENZLER, B.; METZ, V.; PRUESSMANN, T.; ROTHE, J.;

SCHILD, D.; SOBALLA, E.; VITTOVA, T.

Characterization of U(VI)-phases in corroded cement products by micro( $\mu$ )-spectroscopic methods.

XAFS-XV - 15th International Conference on X-Ray Absorption Fine Structure, Beijing, China, July 22-28, 2012.

BUBE, C.; DARDENNE, K.; DENECKE, M. A.; KIENZLER, B.; METZ, V.; PRÜßMANN, T.; ROTHE, J.; SCHILD, D.; SOBALLA, E.; VITTOVA, T.

Characterization of U(VI)-phases in corroded cement products by micro( $\mu$ )-spectroscopic methods.

ANKA / KNMF Joint Users Meeting, Ettlingen, Germany, October 10-11, 2012.

CHAGNEAU, A.; CLARET, F.; MADÉ, B.; TUCKERMANN, J.; ENZMANN, F.; SCHÄFER, T.

Applicability of a geometrical model coupled to computed tomography to characterize the transport properties of porous materials: comparison with through diffusion experiments.

5th International Meeting "Clays in Natural and Engineered Barriers for Radioactive Waste Confinement" Montpellier - October 22-25, 2012.

DARBHA, G. K.; FISCHER, C.; MICHLER, A.; LUETZENKIRCHEN, J.; SCHÄFER, T.

Understanding the deposition behavior of colloids at mineral and rock surfaces as a function of surface roughness and topography.

GeoHannover 2012 „GeoRohstoffe für das 21. Jahrhundert“ / “GeoResources for the 21st Century”, Leibniz Universität Hannover, Germany, October 1-3, 2012.

DARDENNE, K.; DENECKE, M. A.; GRUNWALDT, J.-D.; HUTTEL, E.; LICHTENBERG, H.; MANGOLD, S.;

PRUESSMANN, T.; ROTHE, J.; STEININGER, R.; VITTOVA, T.

The CAT-ACT Beamline at ANKA: a new high energy X-ray spectroscopy facility for CATalysis and ACTinide research.

XAFS-XV Conference, Beijing, China, July 22-28, 2012.

FELLHAUER, D.; ALTMAIER, M.; FÄNGHÄNEL, TH.; GECKEIS, H.

Verhalten von Actiniden unter endlagerrelevanten Bedingungen.

KIT-Zentrum Energie, 1. Jahrestagung, Karlsruhe (Germany), June 19, 2012.

FELLHAUER, D.; ALTMAIER, M.; ROTHE, J.; NECK, V.; RUNKE, J.; FANGHÄNEL, TH.

Speciation and Solubility of Np(V) in alkaline CaCl<sub>2</sub> Solutions.

Plutonium Futures "The Science" 2012, Cambridge (UK), July 15-20, 2012.

FINCK, N.; DARDENNE, K.  
Clay mineral coprecipitation with Zr(IV).  
ANKA / KNMF Joint Users Meeting, October 10 – 11 2012, Schloss Ettlingen, Germany.

FINCK, N.; DARDENNE, K.  
Americium coprecipitation with and adsorption on hectorite  
E-MRS Conference, May 15-17 2012, Strasbourg, France.

FINCK, N.; DARDENNE, K.  
Americium retention by the smectite hectorite.  
5<sup>th</sup> International Meeting „Clays in Natural and Engineered barriers for Radioactive Waste Confinement“, Montpellier. (France, 22<sup>nd</sup> – 25<sup>th</sup> October 2012).

FINCK, N.; DARDENNE, K.; BOSBACH, D.; GECKEIS, H.  
Selenide retention by mackinawite.  
„Selen2012“, Karlsruhe, Germany, 8<sup>th</sup> – 9<sup>th</sup> October 2012.

FRITSCH, P. F.; BREUSTEDT, B. B.; BLANCHARDON, E. B.; BLANCHIN, N. B.; BERARD, P. B.; HURTMEN, C. H.; GREMY, O. G.  
MADORTools for management of internal contamination by actinides and DTPA therapy.  
13th International Congress of the International Radiation Protection Association (IRPA 13), Glasgow, GB, May 13-18, 2012, Download unter (<http://www.irpa13glasgow.com/information/downloads/>), 2012.

FRÖHLICH, D. R.; SKERENCAK, A.; ROTHE, J.; DARDENNE, K.; GÖTZ, R.; HAUSER, W.; PANAK, P. J.  
A new experimental setup to study the complexation behaviour of actinides in aqueous solution by EXAFS spectroscopy up to 200°C.  
ANKA / KNMF Joint Users Meeting, October 10 – 11 2012, Schloss Ettlingen, Germany.

GAONA, X.; FELLHAUER, D.; ROTHE, J.; ALTMAIER, M.  
Solubility of Np(VI) in dilute to concentrated alkaline NaCl solutions.  
ReCosy 4th annual workshop, Karlsruhe (Germany), January 23-27, 2012.

GAONA, X.; FELLHAUER, D.; ROTHE, J.; FANGHÄNEL, T.; ALTMAIER, M.  
Thermodynamics of Np(VI) in alkaline NaCl solutions – comparison with Pu(VI).  
Plutonium Futures “, The Science” 2012, Cambridge (UK), July 15-20, 2012.

GARCIA, C. C.; VAN WINCKEL, S.; HOLLAS, S.; SERRANO-PURROY, D.; GLATZ, J.-P.  
Localized analysis of fission products and actinides in irradiated nuclear fuels by LA-ICP-MS.  
11th European Workshop on Laser Ablation & II Spanish Workshop on LA, Gijon (Spain), June 19-22, 2012.

GERSTMAN, U. C.; FISCHER, P.; BREUSTEDT, B.; LOHNERT, D.; BARTENSTEIN, P.; SONNENSCHN, W.; NIGGEMANN, G.; MESTER, J.; KRIENS, M.; LÖSCHER, S.; LEISNER, S.; ESCHNER, W.; GEWORSKI, L.; KELLER, K. D.; NEUDERT, N.; SPROSS, T.; LASSMANN, M.; KIRCHNER, U.; LIEBERZ, W.; HILL, P.  
In-vivo measurements at German Competent Incorporation Measuring Bodies in the wake of Fukushima.  
13th International Congress of the International Radiation Protection Association 2012, May 13-18, Glasgow, Scotland, Download unter (<http://www.irpa13glasgow.com/information/downloads/>), 2012.

GONZÁLEZ-ROBLES, E.; BOHNERT, E.; PLASCHKE, M.; LAGOS, M.  
INE Contribution to WP2.  
FIRST-Nuclides kick-off meeting, Barcelona (Spain), 9. February 2012.

GONZÁLEZ-ROBLES, E.  
Chemical and mineralogical properties of spent nuclear fuel.  
INEPT Nuclear Fuel Training Course KIT-Campus North - INE, Karlsruhe (Germany), 8th March 2012.

GONZÁLEZ-ROBLES, E.; LOIDA, A.; MÜLLER, N.; METZ, V.; KIENZLER, B.; BOHNERT, E.  
Corrosion of cladged spent nuclear fuel segment in NaCl brine in presence of Fe(II)/(III) oxide powder.  
International Spent Nuclear Fuel Workshop 2012, Avignon (France), April 18-19, 2012.

GONZÁLEZ-ROBLES, E.; LOIDA, A.; MÜLLER, N.; SCHILD, D.; METZ, V.; BOHNERT, E.; KIENZLER, B.  
Corrosion of spent nuclear fuel segment in presence of Fe (II)/Fe(III) oxide.  
European Materials Research Society E-MRS 2012 Spring Meeting, Strasbourg (France), 14.-18. May 2012.

GONZÁLEZ-ROBLES, E.; BOHNERT, E.; LOIDA, A.; MÜLLER, N.; METZ, V.; KIENZLER, B.  
Characterisation of 50.4 GWd/t<sub>HM</sub> PWR fuel and set-up of dissolution experiments.  
FIRST Nuclides- 1<sup>st</sup> Annual Workshop, Budapest (Hungary), 11<sup>th</sup> October 2012.

GRANGEON, S.; TOURNASSAT, C.; LEROUGE, C.; GIFFAUT, E.; SCHÄFER, T.  
Prediction of Nickel mobility in a clayey formation requires accurate knowledge of the mineralogical assemblage.  
5th International Meeting "Clays in Natural and Engineered Barriers for Radioactive Waste Confinement" Montpellier - October 22-25, 2012.

HEBERLING, F.; ENG, P.; LÜTZENKIRCHEN, J.; STUBBS, J.; SCHÄFER, T.; GECKEIS, H.  
Ion specific effects at the calcite(104) - water interface.  
Goldschmidt Conference 2012, Montréal (Canada), June 24-29, 2012.

HEIDE, B.  
Assessment of doses caused by electrons in thin layers of tissue-equivalent materials using mcnp.  
Technical University Dresden, Institute of Nuclear and Particle Physics, 20. December 2012.

HINZ, K.; ALTMAIER, M.; RABUNG, T.; RICHMANN, M.; BORKOWSKI, M.; REED, D.; GECKEIS, H.  
Solubility and Speciation of Cm(III) and Nd(III) in borate rich NaCl and CaCl<sub>2</sub> solutions.  
Plutonium Futures 2012, Cambridge, England.

HOFMANN, S.; STUMPF, T.  
Influence of nitrate on the Eu(III) uptake by calcite: A TRLFS study.  
Goldschmidt Conference 2012, Montréal (Canada), June 24-29, 2012.

HOLLIDAY, K.; CHAGNEAU, A.; SCHMIDT, M.; CLARET, F.; SCHÄFER, T.; STUMPF, T.  
Discriminating factors affecting incorporation: Comparison of the fate of Eu<sup>3+</sup>/Cm<sup>3+</sup> in the Sr carbonate/sulfate system.  
Goldschmidt 2012, June 24-29, 2012, Montréal, Canada, Session O8c "Structural incorporation of heavy metals/ radionuclides into mineral phases in aqueous environment".

HUBER, F.; HECK, S.; HÖSS, P.; TRUCHE, L.; BOUBY, M.; BRENDLÉ, J.; SCHÄFER, T.  
The use of synthetic Zn-/Ni-labeled montmorillonite colloids as a natural bentonite marker.  
5th International Meeting "Clays in Natural and Engineered Barriers for Radioactive Waste Confinement" Montpellier - October 22-25, 2012.

HUBER, F.; SCHILD, D.; VITOVA, T.; ROTHE, J.; KIRSCH, R.; SCHÄFER, T.  
U removal kinetics in the presence of magnetite and maghemite nanoparticles.  
4th Annual Workshop, 7th EC FP Recosy CP(2012).

KADEN, P.  
NMR investigations at KIT-INE.  
ACTINET-13 Thul Spring School in Actinide Chemistry, Karlsruhe, 26.-30.03.2012.

KADEN, P.; ADAM, C.; GEIST, A.; PANAK, P. J.; DENECKE, M. A.  
NMR investigations on N-donor complexes of americium (III) nitrate and n-Propyl-BTP.  
Jahrestagung KIT-Zentrum Energie, Karlsruhe, 19.06.2012.

KADEN, P.; ADAM, C.; BEELE, B.; MÜLLICH, U.; GEIST, A.; PANAK, P. J.; DENECKE, M. A.  
NMR investigations on Paramagnetic Effects in (nPrBTP)<sub>3</sub> complexes of Lanthanides(III) and Americium(III).  
ATALANTE 2012, Montpellier, Frankreich, 02.-07.09.2012.

KADEN, P.; ADAM, C.; SCHIMMELPFENNIG, B.; GEIST, A.; PANAK, P. J.; DENECKE, M. A.  
NMR-investigations on paramagnetic and anionic effects in nPrBTP complexes of trivalent Lanthanides and Americium.  
Euromar 2012, Dublin, Ireland, 01.-06.07.2012.

KADEN, P.; ADAM, C.; BEELE, B. B.; MÜLLICH, U.; TRUMM, S.; GEIST, A.; PANAK, P. J.; DENECKE, M. A.  
NMR investigations at KIT-INE on radioactive samples – towards NMR on <sup>3</sup>T containing samples.  
Jahrestagung KIT-Zentrum Erde und Umwelt, Karlsruhe, 19.10.2012.

KADEN, P.; ADAM, C.; BEELE, B. B.; MÜLLICH, U.; TRUMM, S.; GEIST, A.; PANAK, P. J.; DENECKE, M. A.  
NMR-investigations on Paramagnetic Effects in nPrBTP Complexes of Trivalent Lanthanides and Americium.  
ATAS Workshop, Dresden, 05.-07.11.2012.

KIENZLER, B.  
European Project "FIRST-Nuclides".  
International Spent Nuclear Fuel Workshop 2012, Avignon (F), April 18-19, 2012.

KIENZLER, B.; METZ, V.; VALLS, A.  
Euratom 7<sup>th</sup> Framework Programme Collaborative Project "Fast / Instant Release of Safety Relevant Radionuclides from Spent Nuclear Fuel" (FIRST-Nuclides).  
ATALANTE 2012 – Nuclear Chemistry for Sustainable Fuel Cycles, September 2-7 2012, Montpellier, France.

KIRSCH, R.; FELLHAUER, D.; ALTMAIER, M.; CHARLET, L.; FANGHÄNEL, TH.; SCHEINOST, A.C.  
Plutonium redox chemistry under anoxic conditions in the presence of iron(II) bearing minerals.  
Goldschmidt 2012, Montréal (Canada), June 24-29, 2012.

KLEIN, W.

Implementation and QA of biokinetic models.

EURADOS WG7 "Internal Dosimetry" meeting, Budapest, 1-3 October 2012.

KUPCIK, T.; HARTMANN, E.; SCHNURR, A.; RABUNG, T.; SCHAEFER, TH.; GECKEIS, H.

Aspekte der Radionuklid/Ton- und Tongesteins-Wechselwirkung im Rahmen der tiefengeologischen Endlagerung.

Jahrestagung des KIT-Zentrums Energie, Karlsruhe, Deutschland, Juni 19, 2012.

KUPCIK, T.; KERN, R.; RABUNG, TH.; EIDNER, S.; KUMKE, M.; T. SCHÄFER

Sr<sup>2+</sup>/Eu<sup>3+</sup>- illite interaction: sorption and diffusion studies.

5<sup>th</sup> meeting on Clays in Natural and Engineered Barriers for Radioactive Waste Confinement, Montpellier, France, October, 22<sup>th</sup> - 25<sup>th</sup> 2012.

KUTZER, A.; VITOVA, T.; KADEN, P.; SOBALLA, E.; DENECKE, M.A.; ROTH, G.; WEISENBURGER, S.;

GECKEIS, H.

Structural investigations of Mo-rich model nuclear waste glass compositions.

4th ANKA/KNMF Joint Users' Meeting 2012, Ettlingen, 10.-11.10.2012.

LAGOS, M.; BANIK, N.; MARQUARDT, C.; GRASER, C. H.; KUCZEWSKI, B.; GECKEIS, H.

The determination of actinide redox species in solution using capillary electrophoresis and SF-ICP-MS.

18. Koordinierungsgespräch KIT/INE – PSI/LES, June 2012.

LOIDA, A.

Long-Term Corrosion Experiments of Cladded SNF samples.

INEPT Nuclear Fuel Training Course KIT-Campus North, INE, Karlsruhe (Germany), 8th March 2012.

LOIDA, A.; METZ, V.; BOHNERT, E.; KIENZLER, B.; MÜLLER, N.; SCHILD, D.; SOBALLA, E.

Trapping of Radionuclides/ Actinides onto Canister (Fe) Corrosion Products ReCosy.

4th Annual Workshop, Karlsruhe (Germany), 23rd to 26th January 2012.

LOIDA, A., METZ, V.; KIENZLER, B.; MÜLLER, N.; BOHNERT, E.; GONZÁLEZ-ROBLES, E.

Results from a 5-Years SNF corrosion Experiment in NaCl solution under H<sub>2</sub> overpressure and in presence of bromide.

International Spent Nuclear Fuel Workshop 2012, Avignon (France), April 18-19, 2012.

LOPEZ, M. A.; BREUSTEDT, B.; BLASHAZY, I.; BLANCHARDON, E.; BERARD, P.; BRAVO, G.; BROGGIO, D.;

CASTELLANI, C. M.; CRUZ-SUAREZ, R.; DAVESNE, E.; DOERFEL, H.; ETHERINGTON, G.; FOJITIK, P.;

FRANCK, D.; FRITSCH, P.; GIUSSANI, A.; GREGORATTO, D.; GUILMETTE, R.; HOFMANN, W.; HUIKARI,

J.; HURTGEN, C.; KRAMER, G. H.; LI, W. B.; MALATOVA, I.; MARSH, J. M.; MARZOCCHI, O.; MCCORD,

S.; MOLOKANOV, A.; NOGUERA, P.; NOSSKE, D.; PUNCHER, M.; OEH, U.; RUEHM, W.; SAIZU, M.;

PEIXOTO-TELES, P.; TOLMACHEV, S. Y.; VRBA, T.

EURADOS Network on Internal Dosimetry.

13th International Congress of the International Radiation Protection Association 2012, May 13-18, Glasgow, Scotland, Download unter (<http://www.irpa13glasgow.com/information/downloads/>), 2012.

LÜTZENKIRCHEN, J.; RICHTER, C.

Surface charging of some hydrophobic surfaces.

ISSHAC-8, Krakow, Poland, August/September, 2012.

MARQUARDT, C. M.; BANIK, N. L.; LÜTZENKIRCHEN, J.; ROTHE, J.; SCHÄFER, T.; SCHILD, D.  
Redox behaviour of neptunium, plutonium and technetium in Opalinus Clay / Callovo-Oxfordian argillite – pore water system.  
Final (4th Annual) Workshop of the Recosy Project EURATOM, EC FP7, Collaborative Project, 23.-26. January 2012, Karlsruhe, Germany, 2012.

MARZOCCHI, O.; BREUSTEDT, B.; MOSTACCI, D.; URBAN, M.  
Design and Setup of a New HPGe Detector Based Body Counter Capable of Detecting Also Low Energy Photon Emitters.  
13th International Congress of the International Radiation Protection Association 2012, May 13-18, Glasgow, Scotland, Download unter (<http://www.irpa13glasgow.com/information/downloads/>), 2012.

METZ, V.; LOIDA, A.; GONZÁLEZ-ROBLES, E.; BOHNERT, E.; KIENZLER, B.  
Characterization of irradiated PWR UOx fuel (50.4 GWd/tHM) used for leaching experiments.  
FIRST-Nuclides 1st Annual Workshop, 10. October 2012, Budapest, Hungary.

METZ, V.; BOHNERT, E.; GONZÁLEZ-ROBLES, E.; LOIDA, A.; KIENZLER, B.  
Determination of gaseous fission products released from 50.4 GWd/tHM fuel.  
FIRST-Nuclides 1st Annual Workshop, 10. October 2012, Budapest, Hungary.

METZ, V.  
Fast / Instant Release of Safety Relevant Radionuclides from Spent Nuclear Fuel (FIRST-Nuclides) - Overview of Activities within WP1 "Samples and Tools".  
FIRST-Nuclides 1st Annual Workshop, 10. October 2012, Budapest, Hungary.

METZ, V.  
Fast / Instant Release of Safety Relevant Radionuclides from Spent Nuclear Fuel (FIRST-Nuclides) - Objectives and Work Plan of WP1, "Samples and Tools".  
FIRST-Nuclides kick-off meeting, 9. February 2012, Barcelona, Spain.

METZ, V.; KIENZLER, B.; MONTOYA, V.  
EURATOM FP7 Collaborative Project FIRST-Nuclides.  
European Materials Research Society E-MRS 2012 Spring Meeting, 14.-18. May 2012, Strasbourg, France.

METZ, V.; LOIDA, A.; MÜLLER, N.; GONZÁLEZ-ROBLES, E.; BOHNERT, E.; BUBE, C.; KIENZLER, B.  
Radiolytic enhanced UO<sub>2</sub>(s) / SNF corrosion in chloride solutions with H<sub>2</sub> and Br.  
Spent Fuel Workshop, April 2012, Avignon, France.

MOHR, U.; BIEGARD, N.; CORDES, G.; BREUSTEDT, B.  
Cs-137 Körperaktivität - Die Karlsruher Referenzgruppe.  
44. Jahrestagung des Fachverbandes für Strahlenschutz, Karlsruhe, 17.-20. September 2012.

NEUMAIER, S.; DOMBROWSKI, H.; OTTO, T.; BECKER, F.  
Umgebungsüberwachung und Dosimetrie.  
44. Jahrestagung des Deutsch-Schweizerische Fachverband für Strahlenschutz e.V., 19.9.12, am KIT.

NORRFORS, K. K.; BOUBY, M.; HECK, S.; WOLD, S.; SCHÄFER, T.; GECKEIS, H.  
Montmorillonite colloid size heterogeneity: Impact on stability and radionuclides sorption properties.  
5th International Meeting, Clays in Natural and Engineered Barriers for Radioactive Waste  
Confinement, Montpellier, October 22-25, 2012.

NOSECK, U.; FLÜGGE, J.; SCHÄFER, T.; BLECHSCHMIDT, I.  
Impact of bentonite colloids on radionuclide transport in fractured systems – results from field  
experiments and modeling.  
EUROSAFE Forum "Towards Enhanced Robustness in Nuclear Safety", Brussels, 5<sup>th</sup> and 6<sup>th</sup> November  
2012.

PETROV, V.G.; GAONA, X.; FELLHAUER, D.; DARDENNE, K.; KALMYKOV, S. N.; ZADORIN, A. A.;  
ALTMAIER, M.  
Pentavalent neptunium solubility and sorption behaviour in solutions of different ionic strengths.  
7th Russian Conference on Radiochemistry "Radiochemistry-2012", October 15-19, 2012.

PETROV, V. G.; GAONA, X.; FELLHAUER, D.; DARDENNE, K.; KALMYKOV, S. N.; ALTMAIER, M.  
Pentavalent neptunium solubility and solid phase transformation in solutions of different ionic  
strengths.  
ReCosy 4th Annual Workshop, January, 2012, Germany.

PETROV, V. G.; GAONA, X.; FELLHAUER, D.; DARDENNE, K.; KALMYKOV, S. N.; ZADORIN, A. A.;  
ALTMAIER, M.  
Np(V) solubility and sorption onto magnetite in aqueous NaCl solutions of different ionic strengths.  
Pu Futures: The Science 2012", Cambridge (UK), July 15-20, 2012.

PLASCHKE, M.; ROTHE, J.; SCHÄFER, T.; DARDENNE, K.; DENECKE, M. A.; GECKEIS, H.  
Soft X-Ray Spectromicroscopy of Natural Organics affecting Actinide Mobility – an Overview.  
Eurosoil 2012, Bari, Italy, July 2-6, 2012.

PÖLZ, S.; URBAN, M.; GECKEIS, H.  
Numerische Effizienzkalibrierung von Teilkörperzählern mit Hilfe von anthropomorphen Phantomen.  
Jahrestagung Kerntechnik 2012, Stuttgart, Germany, May 22-24, 2012.

PÖLZ, S.; BREUSTEDT, B.; URBAN, M.  
Numerische Zähleffizienzkalibrierung von Teilkörperzählern mit probandenadaptierten  
anthropomorphen Phantomen.  
79. Sitzung des Arbeitskreises Inkorporationsüberwachung, Karlsruhe, Germany, September 17-21,  
2012.

POLLY, R.; SCHIMMELPFENNIG, B.; FLORSHEIMER, M.; HEBERLING, F.; STUMPF, TH.; KLENZE, R.;  
GECKEIS, H.  
Sorption and incorporation of radio-nuclides at mineral surfaces studied with quantum chemical  
methods.  
Goldschmidt, Montreal 2012.

PRÜßMANN, T.; DENECKE, M. A.; GEIST, A.; ROTHE, J.; LÖBLE, M.; CALIEBE, W.; BATCHELOR, D.;  
VITTOVA, T.  
Comparative investigation of N donor ligand-lanthanide complexes from the metal and ligand point  
of view.  
XAFS-XV Conference, Beijing, PR China, July 22-28, 2012.

PRÜßMANN, T.; DENECKE, M. A.; GEIST, A.; ROTHE, J.; LINDQVIST-REIS, P.; APOSTOLIDIS, C.;  
NAGEL, P.; SCHUPPLER, S.; VITOVA, T.  
Comparative investigation of N donor ligand-lanthanide complexes from the metal and ligand point  
of view.  
ANKA user meeting 2012.

PUDEWILLS, A.  
Numerical modelling of ground water flow and solute transport through a shear zone at the Grimsel  
Test Site.  
KIT-Kompetenzfelder: "Erde und Umwelt" und "Mathematische Modelle", Okt. 2012, KIT Campus  
Süd, <http://www.for.kit.edu/423.php> .

RABUNG, T.; MOLINERO, J.; GARCIA, D.; MONTOYA, V.  
CROCK: Crystalline Rock Retention Processes, A 7<sup>th</sup> Framework Programme Collaborative Project  
(2011-2013)  
Euratom Disposal Programme Dissemination Workshop, 25.-26. October 2012, Montpellier, France.

RABUNG, T.; SCHNURR, A.; GECKEIS, H.  
Trivalent actinide and lanthanide sorption onto clay minerals at higher ionic strengths.  
NRC8, Como, 16.- 21. September 2012.

RABUNG, T.; SCHNURR, A.; PETROV, V.; LÜTZENKIRCHEN, J.; GECKEIS, H.;  
MARQUARDT, C. M.  
Studies of the Eu/Cm sorption on illite.  
BMW-Workshop 3.-4. April 2012, Universität zu Köln, 2012.

RABUNG, T.; SCHNURR, A.; MARSAC, R.; KUPCIK, T.; HUITTINEN, N.; HEDDE, M.; LÜTZENKIRCHEN, J.;  
GECKEIS, H.; MARQUES, M.; BAEYENS, B.  
Sorption an Ton.  
18. Koordinierungsgespräch KIT/INE –PSI/LES, 28.-29. 6. 2012.

ROBINET, J. C.; MICHAU, N.; SCHÄFER, T.  
Imaging techniques in clay Sciences: A key tool to go a step further.  
5th International Meeting "Clays in Natural and Engineered Barriers for Radioactive Waste  
Confinement" Montpellier - October 22-25, 2012.

ROTHE, J.; PLASCHKE, M.; SCHÄFER, T.; DARDENNE, K.; DENECKE, M. A.; GECKEIS, H.  
Soft X-Ray Spectromicroscopy of Natural Organics affecting Actinide Mobility.  
International Workshop on Advanced Techniques in Actinide Spectroscopy (ATAS), Dresden,  
Germany, November 5-7, 2012.

RUFF, C. M.; MÜLLICH, U.; GEIST, A.; PANAK, P. J.  
Interaction of Cm(III) and Eu(III) with a water-soluble BTP-type ligand.  
ATALANTE 2012 – Nuclear Chemistry for Sustainable Fuel Cycles, 02.-07.09.2012, Montpellier,  
Frankreich.

RUFF, C. M.; MÜLLICH, U.; GEIST, A.; PANAK, P. J.  
Neue Strategien in der Actinidenabtrennung - Wasserlösliche Komplexbildner für den innovativen  
SANEX-Prozess.  
Debatten-Abend „ENERGY OUTLOOK 2012“, 08.02.2012, Stuttgart.

SCHILD, D.

Actinide speciation by 4f elemental lines and their satellites.

2012 PHI European User Meeting, Eibelstadt, Germany, April 18-19, 2012.

SELLIN, P.; SUNDMAN, D.; BAILEY, L.; MISSANA, T.; SCHÄFER, T.; CERVINKA, R.; KOSKINEN, K.

Bentonite erosion: effects on the long term performance of the engineered barrier and radionuclide transport- the BELBaR project.

5th International Meeting "Clays in Natural and Engineered Barriers for Radioactive Waste Confinement" Montpellier - October 22-25, 2012.

SHINONAGA, T.; LAGOS, M.; OKHURA, T.

Isotopic composition of uranium in aerosol samples collected at 120 km south-southwest of Fukushima before and after the nuclear power plant accident.

NRC-8, Como, Italy, 21 September 2012.

STEPPERT, M.; BÜCHNER, S.; FUSS, M.; WALTHER, C.

Untersuchungen von Uran und Plutonium mittels nano-ESI TOF MS.

DPG Frühjahrstagung 2012, Stuttgart, 12.-16.03.2012.

THOMAS, R.; LEHELLE, J.; MARTIN, P.; AUFORE, L.; BELIN R.; RIGLET-MARTIAL, C.; DARDENNE, K. ; ROTHE, J.; HEINTZ, J.-M.

Influence of sintering conditions on Pu homogeneity in MOX doped Cr fuel: EPMA, XRD and XAS study.

NUMAT 2012, 21-25 October 2012, Osaka, Japan.

TOTSKIY, Y.; GECKEIS, H.; SCHÄFER, T.

Sorption of Tc(VII) on crystalline rock material from Äspö (Sweden).

Joint ITU-INE Research Fellows' Day, JRC-KIT, Karlsruhe, 22 June 2012.

TOTSKIY, Y.; STAGE, E.; GECKEIS, H.; SCHÄFER, T.; KALMYKOV, S.

Sorption of Tc(VII), Cs(I), Eu(III), U(VI) and Am(III) on crystalline rock material from Äspö (Sweden) and Nizhnekansk massif (Russia).

7th Russian Conference on Radiochemistry "Radiochemistry-2012", Dimitrovgrad, Russia, 15-19 October, 2012.

VALLET, V.; REAL, F.; GUERRERO MARTINEZ, Y. O.; TRUMM, M.; SCHIMMELPFENNIG, B.; MASELLA, M.

Macroscopic modeling: insights in the ability of classical non-additive potentials to model radionuclides in aqueous solution.

14th ICQC, Boulder, Colorado, USA, 2012.

VALLET, V.; REAL, F.; GUERRERO MARTINEZ, Y. O.; TRUMM, M.; SCHIMMELPFENNIG, B.; MASELLA, M.

Development and application of a polarizable force-field for actinides in aqueous solution including cooperative charge-transfer terms.

ATAS-workshop, Dresden-Rossendorf Nov. 2012.

VITOVA, T.; DENECKE, M. A.; KVASHNINA, K. O.; HUBER, F.; CACIUFFO, R.; ROTHE, J.; SCHÄFER, T.; GECKEIS, H.

The potential of high-resolution X-ray emission and resonant inelastic X-ray scattering techniques for speciation studies of actinide materials.

EUFEN meeting, Tarragona, Spain, June 02-04 2012.

VITOVA, T.; CACIUFFO, R.; DENECKE, M. A.; HUBER, F.; GÖTTLICHER, J.; KOSOG, B.; KVASHNINA, K. O.; MEYER, K.; PRÜßMANN, T.; ROTHE, J.; SCHÄFER, T.; GECKEIS, H.  
Actinide speciation with high-energy resolution X-ray absorption spectroscopy and inelastic X-ray scattering.  
XAFS-XV Conference, Beijing, PR China, July 22-28, 2012.

VITOVA, T.; CACIUFFO, R.; DENECKE, M. A.; HUBER, F.; PRÜßMANN, T.; ROTHE, J.; SCHÄFER, T.; GECKEIS, H.  
Actinide speciation with high-energy resolution X-ray absorption spectroscopy and inelastic X-ray scattering.  
ATAS workshop, Dresden, November 5-11, 2012.

WILDEN, A.; SCHREINEMACHERS, C.; SADOWSKI, F.; GÜLLAND, S.; SYPULA, M.; MODOLO, G.; MAGNUSSON, D.; GEIST, A.; LEWIS, F. W.; HARWOOD, L. M.; HUDSON, M. J.  
Demonstration of a 1-cycle SANEX process for the selective recovery of trivalent actinides from PUREX raffinate using a CyMe<sub>4</sub>-BTBP/TODGA solvent.  
Nuclear Fuel Cycle Conference 2012, Manchester, UK, 23.-25. 4. 2012.

YALCINTAS, E.; KOBAYASHI, T.; ALTMAIER, M.; GECKEIS, H.  
Technetium redox chemistry in dilute to concentrated aqueous systems.  
International Conference on Nuclear and Radiochemistry (NRC-8), Como, Italy, 2012 Sep 16-21.

